2-P

NASA TECHNICAL NOTE

NASA TN D-6896

NASA TN D-6896

THE EFFECTS OF CONFIGURATION CHANGES ON THE AERODYNAMIC CHARACTERISTICS OF A FULL-SCALE MOCKUP OF A LIGHT TWIN-ENGINE AIRPLANE

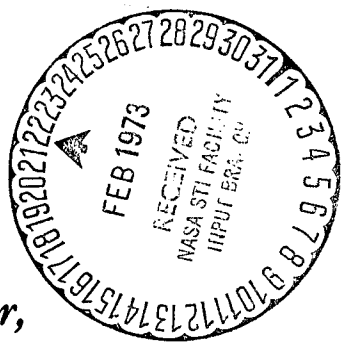

by

Marvin P. Fink, James P. Shivers, H. Douglas Greer,
Langley Research Center

and

James L. Megrail
Langley Directorate,
U.S. Army Air Mobility R&D Laboratory

NATIONAL AERONAUTICS AND SPACE ADMINISTRATION • WASHINGTON, D. C. • SEPTEMBER 1972

1. Report No.	2. Government Accession No.	3. Recipient's Catalog No.
NASA TN D-6896		

4. Title and Subtitle	5. Report Date
THE EFFECTS OF CONFIGURATION CHANGES ON THE AERODYNAMIC CHARACTERISTICS OF A FULL-SCALE MOCKUP OF A LIGHT TWIN-ENGINE AIRPLANE	September 1972
	6. Performing Organization Code

7. Author(s)	8. Performing Organization Report No.
Marvin P. Fink, James P. Shivers, H. Douglas Greer, Langley Research Center; and James L. Megrail, Langley Directorate, U.S. Army Air Mobility R & D Laboratory	L-8375
	10. Work Unit No. 760-60-01-01
9. Performing Organization Name and Address	11. Contract or Grant No.
NASA Langley Research Center Hampton, Va. 23365	
	13. Type of Report and Period Covered
12. Sponsoring Agency Name and Address	Technical Note
National Aeronautics and Space Administration Washington, D.C. 20546	14. Sponsoring Agency Code

15. Supplementary Notes

16. Abstract

The wind-tunnel model was a full-scale mockup of a light twin-engine airplane. Tests were made over an angle-of-attack range of -4° to 20° and over a sideslip range of $\pm 8^{\circ}$ at thrust coefficients of 0, 0.20, and 0.44. Tests were made with various nacelle configurations, modes of propeller rotation, orientation of the propeller thrust axis, and airfoil section at Reynolds numbers of 2.96×10^6 and 2.05×10^6.

17. Key Words (Suggested by Author(s))	18. Distribution Statement
Light twin-engine airplane Stability and control Tail downwash Nacelle configuration	Unclassified – Unlimited

19. Security Classif. (of this report)	20. Security Classif. (of this page)	21. No. of Pages	22. Price*
Unclassified	Unclassified	221	$3.00

*For sale by the National Technical Information Service, Springfield, Virginia 22151

THE EFFECTS OF CONFIGURATION CHANGES ON THE AERODYNAMIC CHARACTERISTICS OF A FULL-SCALE MOCKUP OF A LIGHT TWIN-ENGINE AIRPLANE

By Marvin P. Fink, James P. Shivers, H. Douglas Greer,
Langley Research Center

and James L. Megrail
Langley Directorate, U. S. Army Air Mobility R & D Laboratory

SUMMARY

A force-test investigation has been conducted in the Langley full-scale tunnel to determine the aerodynamic characteristics of a full-scale mockup of a light twin-engine airplane for several engine nacelle shapes, modes of propeller rotation, orientation of the thrust axis, and of a change of airfoil section of the wing. The investigation was made over an angle-of-attack range of -4° to 20° at various angles of sideslip between $\pm 8^{\circ}$ for various power and flap settings. The power conditions were a thrust coefficient of zero, which represents either a low-power or a high-speed condition (where the thrust coefficient approaches zero), 0.20 which corresponds to a climb condition, and 0.44 which corresponds to a take-off condition.

The investigation showed that major configuration changes such as nacelle shape and wing section, and lesser changes in the cowl and nacelle afterbody generally did not result in significant changes in either the longitudinal or the lateral aerodynamic characteristics. It appears from this investigation that the aerodynamic characteristics of this particular configuration are mainly a function of mode of propeller rotation, slipstream energy, and flap deflection. Certain combinations of these factors significantly affected the high lift characteristics and longitudinal stability. These same factors are also apparently very important in determining the rolling-moment characteristics, particularly at and above the stall.

INTRODUCTION

The investigations of references 1 to 3 were made to document the aerodynamic characteristics of some typical light general aviation airplanes in their basic configurations. Little or no effort was made to explore the effects of configuration changes. The present investigation was made specifically to study the effects of configuration changes

and included four nacelle shapes, four modes of propeller rotation, variation in thrust-axes orientation, and a change in wing section. In order to explore the effects of these variables, the single-engine airframe of reference 3 was outfitted with twin nacelles as a mockup of a light twin-engine model. The investigation was made with various power (up to 149 kW (200 horsepower) per engine) and flap settings over a range of angle of attack of -4° to 20° and a range of sideslip angles of $\pm 8^{\circ}$. All the tests except those at a thrust coefficient of 0.44 were made at a tunnel speed of 28.35 m/sec (93 ft/sec) and resulted in a Reynolds number of approximately 2.96×10^6 based on a mean aerodynamic chord of 1.53 m (5 ft). Tests at 0.44 thrust coefficient were made at a tunnel speed of about 19.2 m/sec (63 ft/sec) and resulted in a Reynolds number of about 2.05×10^6.

SYMBOLS

Figure 1 shows the stability-axis system used in the presentation of the data and the positive direction of forces, moments, and angles. The data are computed about the moment center shown in figure 2 which is at model longitudinal station 85 or 10.0 percent of the mean aerodynamic chord and 0.30 m (1.0 ft) below the reference line.

Measurements and calculations for this investigation were made in the U.S. Customary Units. They are presented herein in the International System of Units (SI) with the equivalent values in the U.S. Customary Units given parenthetically. Physical constants and conversion factors relating the two systems of units used in this paper may be found in reference 4.

b wing span, 10.97 m (35.98 ft)

C_D' drag coefficient, $\frac{\text{Drag}}{qS}$

C_L lift coefficient, $\frac{\text{Lift}}{qS}$

C_l rolling-moment coefficient, $\frac{\text{Rolling moment}}{qSb}$

C_m pitching-moment coefficient, $\frac{\text{Pitching moment}}{qS\bar{c}}$

C_n yawing-moment coefficient, $\frac{\text{Yawing moment}}{qSb}$

C_Y side-force coefficient, $\frac{\text{Side force}}{qS}$

c	wing chord, m (ft)
$\bar{c}$	mean geometric chord, 1.53 m (5 ft)
i_t	horizontal-tail incidence angle, deg
q	free-stream dynamic pressure, N/m^2 (lbf/ft^2)
q_t/q	ratio of dynamic pressure at the tail to free-stream dynamic pressure
S	wing area, 16.54 m^2 (178 ft^2)
T	effective thrust (at $\alpha = 0^o$), $(Drag)_{propellers\ removed} - (Drag)_{propellers\ operating}$
T_c'	thrust coefficient, $\frac{T}{qS}$
V	free-stream velocity, m/sec (ft/sec)
X_s	longitudinal axis
α	angle of attack of fuselage reference line, deg
β	angle of sideslip, positive when nose is to left, deg
δ_f	flap deflection, positive when trailing edge is down, deg
ϵ	downwash angle, deg
θ	pitch angle of thrust axis, up angles positive, deg
ϕ	toe-out angles of thrust axis of each engine, deg

MODEL

The model tested was a full-scale mockup of a light twin-engine low-wing monoplane. Figure 2 gives the principal dimensions and figure 3 shows the model mounted in the tunnel test section. The model had a wing span of 10.97 m (35.98 ft), a wing area of 16.54 m^2 (178 ft^2), and a mean geometric chord of 1.53 m (5 ft) based on projection of the outboard leading edge of the wing through the fuselage. The wing section was a modi-

fied NACA 64_2A215 airfoil. The wing was designed to have 5° dihedral, no twist, and a 2° positive incidence with respect to the fuselage reference line. Measurements of the wing after the motor installation showed that installation of the heavy electric motors in the nacelles caused no appreciable deformation of the wing. There was less than 0.5° variation in twist along the span and less than 0.5° difference in the averaged values of wing incidence between the right and left wings. The thrust axes were parallel to the fuselage reference line for most of the tests with provision for varying the thrust axes through a range of angles of -3° to 6° in pitch and 0° to 6° in toe-out. With a set of left-hand and right-hand propellers, four modes of propeller rotation (clockwise, counterclockwise, down at the center, and up at the center) were possible. The model was provided with the modifications to the cowl and nacelle afterbody as shown in figures 4 and 5, respectively. The various nacelle configurations used in the investigation are shown in figure 6. Nacelle A is a conventional nacelle used to house a horizontally opposed engine and is designated the basic configuration in this investigation. Nacelle B is the minimum size that would enclose the 149 kW (266 horsepower) electric drive motor. Nacelle C represents an inverted inline configuration. Nacelle D, a radial configuration, has as a diameter the maximum width of nacelle A.

The wing section was modified for some tests by adding a glove to the top forward 0.40c as shown in figure 7. The modification extended from the engine nacelle to the wing tip. The ordinates of the glove were those of a NACA 23015 airfoil, and gave an airfoil section which approximated a NACA 23015 airfoil.

TESTS

The tests were made in the Langley full-scale wind tunnel to determine the effects of a number of configuration changes on the aerodynamic characteristics of the model over a wide range of test conditions. The configuration changes included modifications to the cowl and the nacelle afterbody; and four nacelle shapes: a standard horizontally opposed engine nacelle; a minimum diameter cylindrical nacelle; an inverted inline nacelle; and a large cylindrical shape, which will be referred to as nacelles A, B, C, and D, respectively. Four modes of propeller rotation were tested: clockwise, counterclockwise, up at the center, and down at the center. The propeller thrust axis orientation was investigated over a pitch-angle range of -3° to 6° and for toe-out of 0°, 3°, and 6°. Nacelle A with clockwise propeller rotation and parallel thrust axes is the basic model configuration. The model was tested over an angle-of-attack range of -4° to 20°, over a sideslip range of $\pm 8^\circ$ for the clean condition $(\delta_f = 0$; gear up$)$, and for the landing condition $(\delta_f = 27^\circ$; gear down$)$. The tests were made at thrust coefficients of 0, 0.20, and 0.44, which represent flight conditions of low power or high speed (where the thrust coefficient approaches zero), climb at about 90-percent power, and climb at full power as in take-off

or wave-off conditions, respectively. Several tests were made with the horizontal tail removed. Asymmetric power tests were made to simulate an engine-out condition for either engine with the inoperative engine in a windmilling condition. The running engine had power settings of 0, 0.10, and 0.22 thrust coefficient. A propeller-blade-angle setting of 20° was used for all the tests. The thrust coefficient was set by adjusting the propeller speed to obtain the required thrust for the test condition. Tail downwash surveys using a calibrated pitch-yaw head were made along the horizontal-tail hinge axis with the horizontal tail removed and the model set at zero sideslip for flap deflections of 0° and 27°, at $T_C' = 0$, 0.20, and 0.44. All the tests, except those at a thrust coefficient of 0.44 were made at a tunnel speed of 28.35 m/sec (93 ft/sec) which resulted in a Reynolds number of approximately 2.96×10^6 based on a mean aerodynamic chord of 1.53 m (5 ft). Tests at a thrust coefficient of 0.44 were made at a tunnel speed of 19.2 m/sec (63 ft/sec) which resulted in a Reynolds number of about 2.05×10^6.

PRESENTATION OF DATA

The longitudinal data for these tests have been corrected for blockage, airstream misalinement, buoyancy effects, mounting strut tares, and wind-tunnel jet-boundary effects. The lift and drag have been corrected for the integrated average airstream misalinement. The lateral data are not corrected for the lateral variation of the stream angle. It should be pointed out, however, that most of the positive rolling moment noted at the lower angles of attack for many of the model configurations can be attributed to lateral variation of the tunnel airstream angles as shown in figure 8. Calculations of section rolling moments using the spanwise variations of stream angle of figure 8 indicated that the total measured out-of-trim rolling moment could be approximately accounted for by the airstream angularity.

The data are presented in the following figures:

RESULTS AND DISCUSSION

The basic data obtained during the wind-tunnel investigation are presented in figures 9 to 74. Summary plots have been prepared from some of the data to illustrate the effect of the various geometric changes of the model on the longitudinal and lateral characteristics. The summary plots have been presented as a function of angle of attack, and only these plots will be discussed.

Lift Characteristics

Effect of nacelle shape.- The effect of nacelle shape on the lift characteristics is presented in figures 75 and 76 for flaps up and flaps down, respectively. The only major effect of nacelle shape on the lift characteristics occurred with nacelle D where there was a reduction in lift-curve slope, an early break in the lift curve, and a reduction in maxi-

mum lift coefficient, particularly for the low power conditions. A change in nacelle design had the greatest effects with flaps down and an increase in power generally reduced the effects of the nacelle.

Effect of mode of propeller rotation.- The effect of various modes of propeller rotation on the lift characteristics with $\delta_f = 0^o$ and 27^o is presented in figures 77 and 78, respectively. The data show that with flaps up, there are no significant changes in the lift characteristics with a change in the mode of propeller rotation. With flaps down, the mode of propeller rotation had some appreciable effects on the high lift characteristics, particularly for $T_C' = 0.20$.

Effect of airfoil section.- The effect of modifying the airfoil section on the lift characteristics is shown in figure 79 for $\delta_f = 0^o$ and 27^o and the range of thrust coefficients. These data show a slight increase in the lift-curve slope and a significant increase in maximum lift over that for the basic configuration for all the conditions tested. Observations of tufts on the wing showed that the stall developed in essentially the same pattern for the modified airfoil as for the basic airfoil, but the angle of attack at which the stall appeared was several degrees higher for the modified airfoil. The part of wing stalled was not as extensive for the modified wing. These characteristics are typical of those of thicker airfoil sections.

Effect of thrust-axis orientation.- The effect of pitching the thrust axes up and down relative to the reference line of the model is presented in figure 80. These data show that tilting the thrust axes had very little effect on the lift characteristics of the model.

Pitching-Moment Characteristics

Effect of nacelle shape.- The effect of nacelle shape on the pitching-moment characteristics is presented in figure 81. The results show that the major effect of a change in nacelle shape is a large trim change. There are also some small effects on stability, but the pitching-moment curves remain fairly linear up to the stall for all configurations.

Effect of mode of propeller rotation.- The effects of the modes of propeller rotation on the pitching-moment characteristics are presented in figure 82. The data show that with power on, the mode of propeller rotation has a significant effect on the longitudinal stability, particularly with the flaps down. In general, up-at-the-center rotation is the most stable and down-at-the-center rotation is the least stable.

Effect of airfoil section.- The effect of modifying the airfoil section on the pitching-moment characteristics is presented in figure 83. These data show that changing the airfoil section had very little effect on the pitching-moment characteristics.

Effect of thrust-axes orientation.- The effect of thrust-axes orientation on pitching-moment coefficient is shown in figure 84. These data show that tilting the thrust axes

from 3° down to 6° up does cause significant changes in pitching moment with power on, and it is estimated from the data of reference 3 to be the equivalent of about 1° of elevator deflection.

Rolling-Moment Characteristics

Effect of nacelle shape.- The effect of nacelle shape on the rolling-moment coefficients are presented in figures 85 to 87. The data show that, in general, the nacelle configuration had relatively little effect on the rolling moments below the stall. The one exception was nacelle D which showed a much greater variation of rolling moment with angle of attack with power on than the other configurations. In general, all the nacelle configurations experienced an abrupt change in rolling moment at the stall with flaps down. In some of the flaps-up conditions, changing nacelles produced even larger asymmetries than those of the basic nacelle and sometimes of the opposite sign.

Effect of mode of propeller rotation.- The effects of the mode of propeller rotation on the rolling-moment coefficients are shown in figures 88 to 90. The data show that both the down-at-the-center and the up-at-the-center modes of propeller rotation had about the same effects on the rolling-moment coefficients of the model. There was generally less variation in the rolling-moment coefficient value with angle of attack below the stall, and in most cases the rolling moments at the stall were smaller than those noted for the basic configuration. Several cases were noted, however, where either up-at-the-center or down-at-the-center rotation resulted in large rolling moments at the stall which were opposite in direction to those of the basic configuration. The effects of counterclockwise rotation were generally opposite to the basic configuration and were of about the same magnitude with the flaps down.

Effect of airfoil section.- The effects of changing the airfoil section on the rolling-moment coefficients are shown in figures 91 to 93. The data of figure 91, which is for the clockwise rotation of the propellers, show no appreciable difference in the rolling-moment characteristics due to airfoil section below or above the stall, particularly for the power-on conditions. A comparison of the rolling moments in figure 92 for the modified and basic airfoils with down-at-the-center rotation shows that the airfoil had little effect. The comparison of down-at-the-center rotation with clockwise rotation in figure 93 showed that the modified airfoil behaved very much like the basic airfoil with down-at-the-center rotating propellers (fig. 88) and, therefore, the direction of propeller rotation is more significant with regard to rolling-moment characteristics than the airfoils tested.

Effect of cowl and nacelle afterbody modification.- Several tests were made to determine whether cowl or nacelle afterbody shape might have any significant influence on the wing-stall characteristics that would affect the rolling moments at the stall. These data are presented in figures 94 to 97 for the flaps-up configuration. At the stall the configura-

tion with the modified cowl (see fig. 94) had larger rolling moments at $T_c' = 0.20$ and 0.44 than was noted for the basic configuration, and the rolling moments for $T_c' = 0.44$ were in opposite direction to those with the basic cowl. Observation of tufts on the cowl and nacelles indicated turbulence on the forward part of the nacelle while those on the afterbody showed smooth flow up to an angle of attack of 20°. The cowl apparently did not trigger the wing stall which caused the roll. The configuration with the modified afterbody (fig. 95) and the configuration with both modified cowl and afterbody (fig. 96) showed no essential difference in rolling moment from those of the modified-cowl-only configuration with the exception of the small decrease in left roll and stall for $T_c' = 0.20$. At this angle of attack both configurations showed slightly less rolling moment than the basic configuration.

The modified cowl in combination with the modified airfoil approximately represents the model of reference 2 which had no roll-off tendencies at stall. Figure 97 presents the results of one test with this configuration and show that the modified configuration had larger rolling moments at stall than the basic model.

Effect of Toe-Out and Asymmetric Power on Yawing-Moment Characteristics

The condition of toe-out with asymmetric power was investigated to determine whether or not toeing out the thrust axis to shorten the moment arm of the applied thrust force would reduce the yawing moment. These data are presented in figure 98 and show that with asymmetric power, toe-out of 6° reduced the yawing moment with the left engine at full power and the right engine windmilling. The other conditions had no effect. The reduction in yawing moment at $\alpha = 0^\circ$ due to toe-out was calculated to be about one-third of the difference between $\phi = 0^\circ$ and $\phi = 6^\circ$ shown in figure 98. This reduction would indicate that other factors such as slipstream rotation may affect the pressure on the aft part of the fuselage to reduce the yawing moment for the case of the down-at-the-center rotating propeller blade.

CONCLUDING REMARKS

A full-scale wind-tunnel investigation has been made to determine the effect of engine nacelle shape, mode of propeller rotation, and orientation of the thrust axis on the longitudinal and lateral aerodynamic characteristics of a mockup of a light twin-engine airplane. It was concluded from the investigation that major configuration changes such as nacelle shape and airfoil section, and lesser changes in the cowl and nacelle afterbody generally did not result in significant changes in either the longitudinal or the lateral aerodynamic characteristics. It appears from this investigation that the aerodynamic

characteristics of this particular configuration are mainly a function of mode of propeller rotation, slipstream energy, and flap deflection. Certain combinations of these factors significantly affected the high lift characteristics and longitudinal stability. These same factors are also apparently very important in determining the rolling-moment characteristics, particularly at and above the stall.

Langley Research Center,
National Aeronautics and Space Administration,
Hampton, Va., July 18, 1972.

REFERENCES

1. Fink, Marvin P.; and Freeman, Delma C., Jr.: Full-Scale Wind-Tunnel Investigation of Static Longitudinal and Lateral Characteristics of a Light Twin-Engine Airplane. NASA TN D-4983, 1969.

2. Fink, Marvin P.; Shivers, James P.; and Smith, Charles C., Jr.: A Wind-Tunnel Investigation of Static Longitudinal and Lateral Characteristics of a Full-Scale Mockup of a Light Twin-Engine Airplane. NASA TN D-6238, 1971.

3. Fink, Marvin P.; Freeman, Delma C., Jr.; and Greer, H. Douglas: Full-Scale Wind-Tunnel Investigation of the Static Longitudinal and Lateral Characteristics of a Light Single-Engine Airplane. NASA TN D-5700, 1970.

4. Mechtly, E. A.: The International System of Units – Physical Constants and Conversion Factors (Revised). NASA SP-7012, 1969.

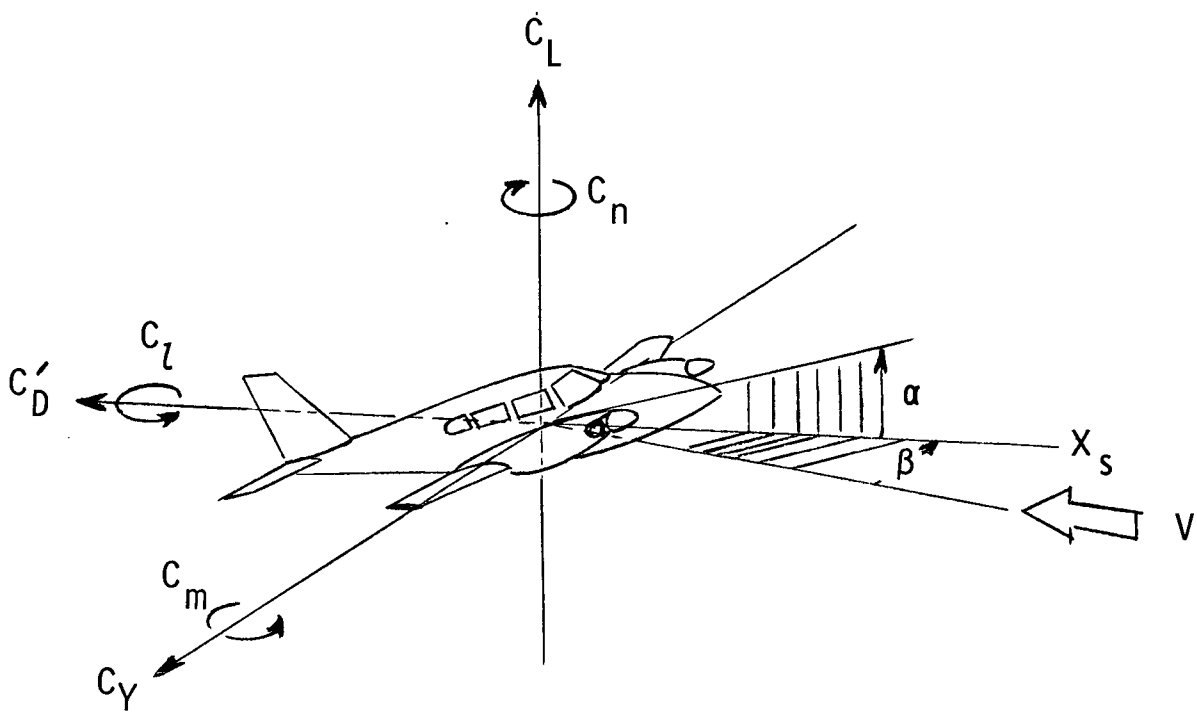

Figure 1.- System of axes and positive sense of angles, forces, and moments.

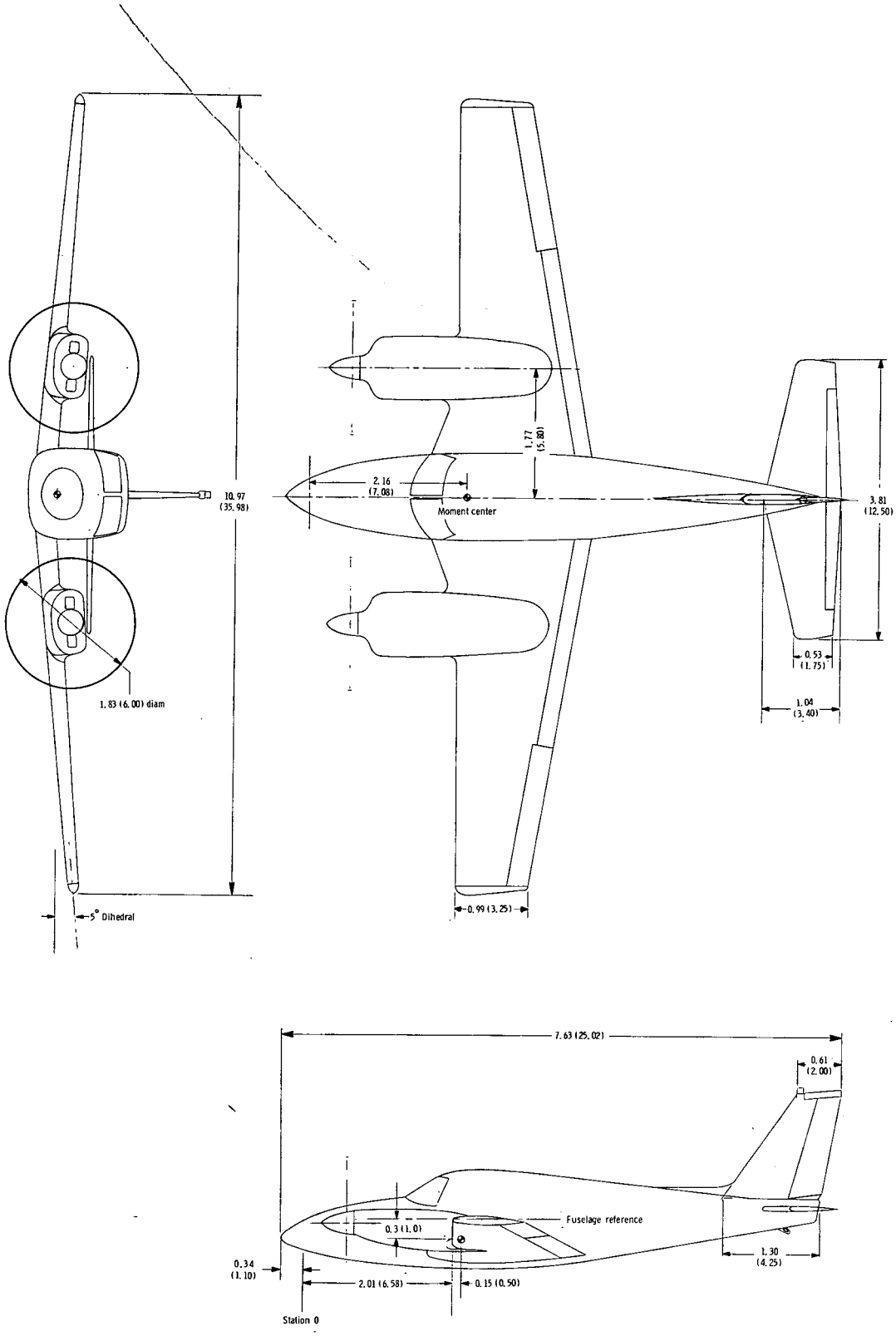

Figure 2.- Three-view drawing of the model. All dimensions are in m (ft).

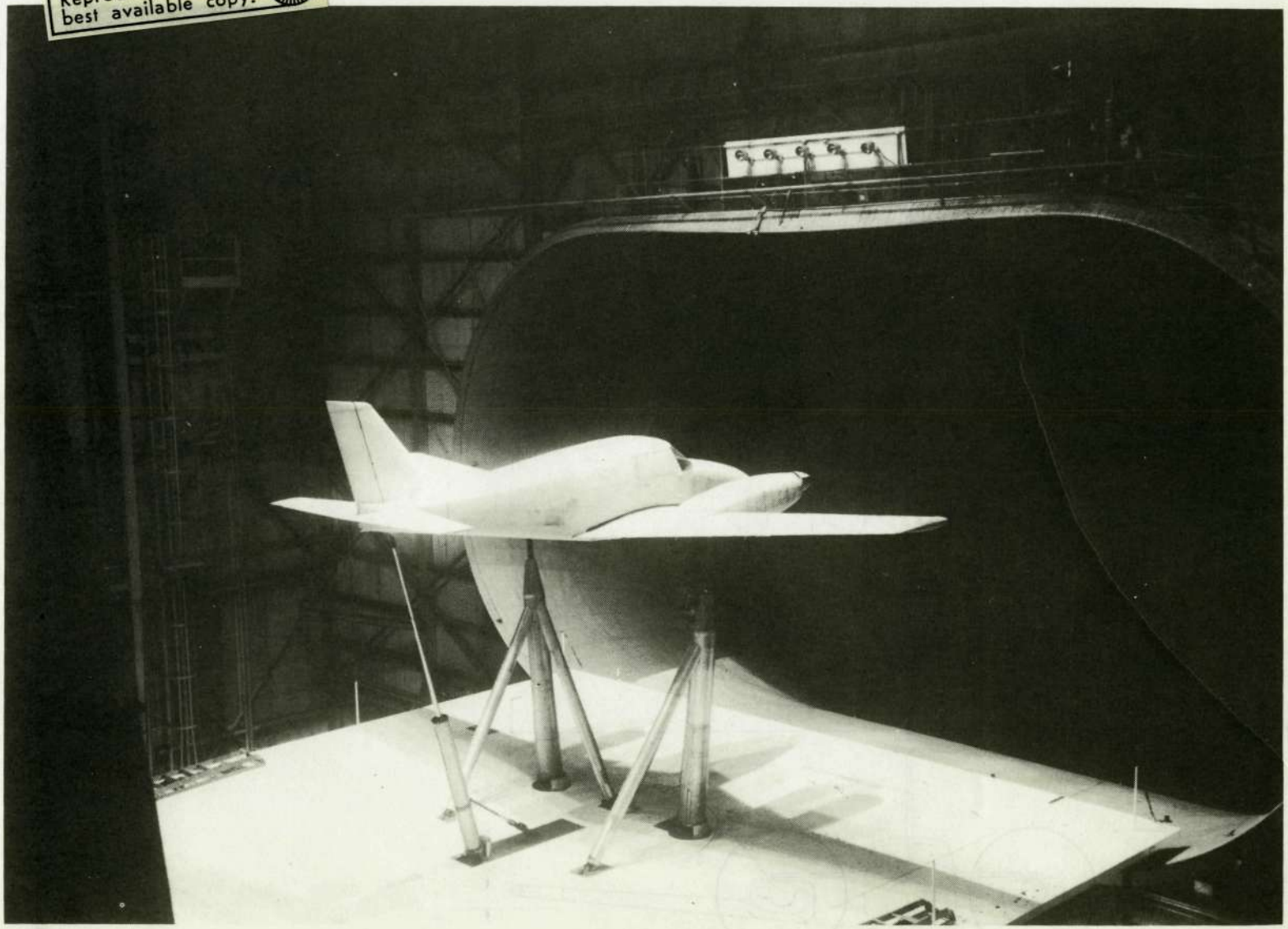

L-71-5007

Figure 3.- Photograph of model in the tunnel.

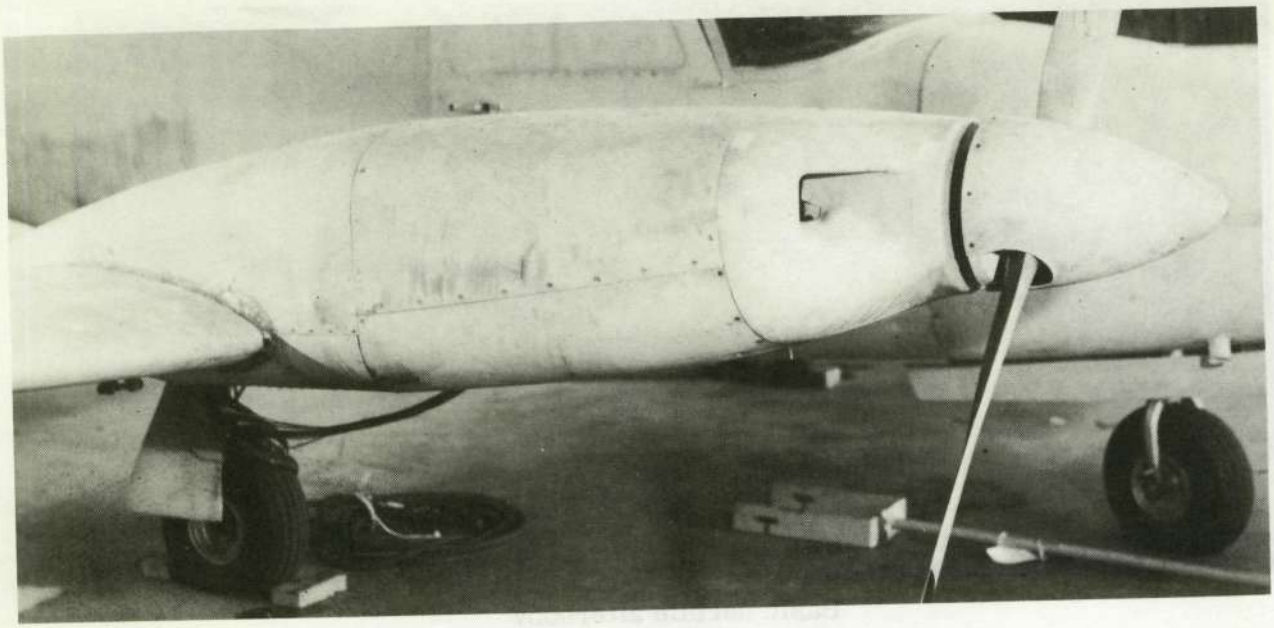

Basic cowl

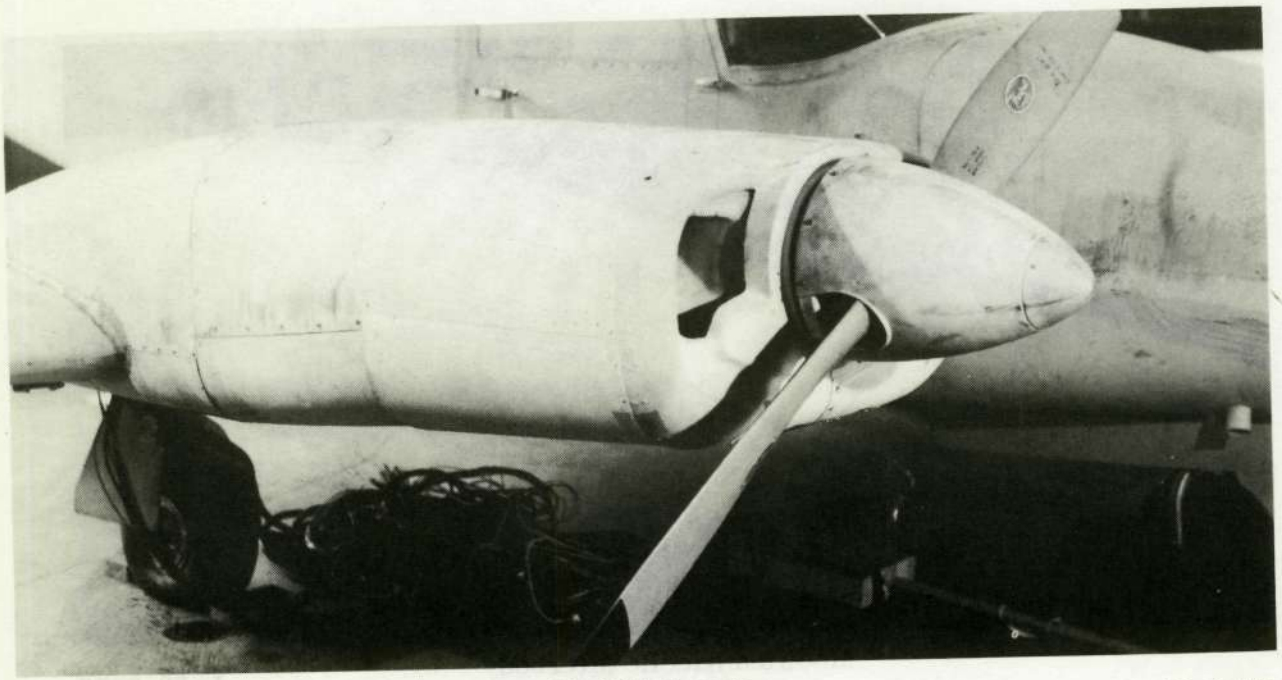

Modified cowl

L-72-2475

Figure 4.- Photograph of the basic cowl and the modified cowl.

L-8375

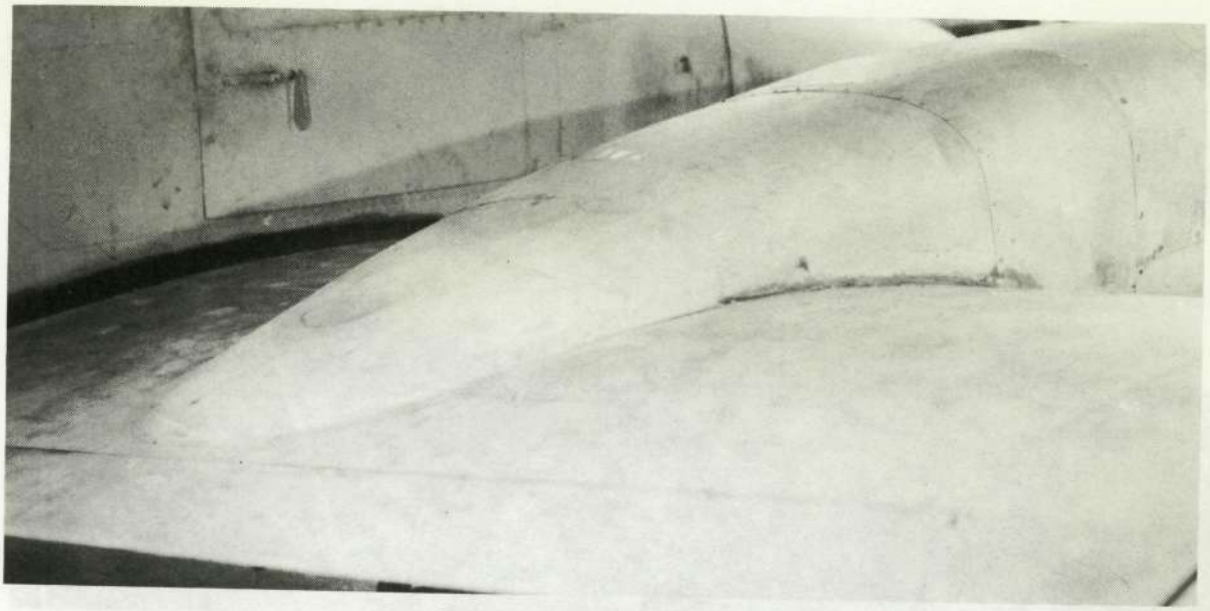

Basic nacelle afterbody

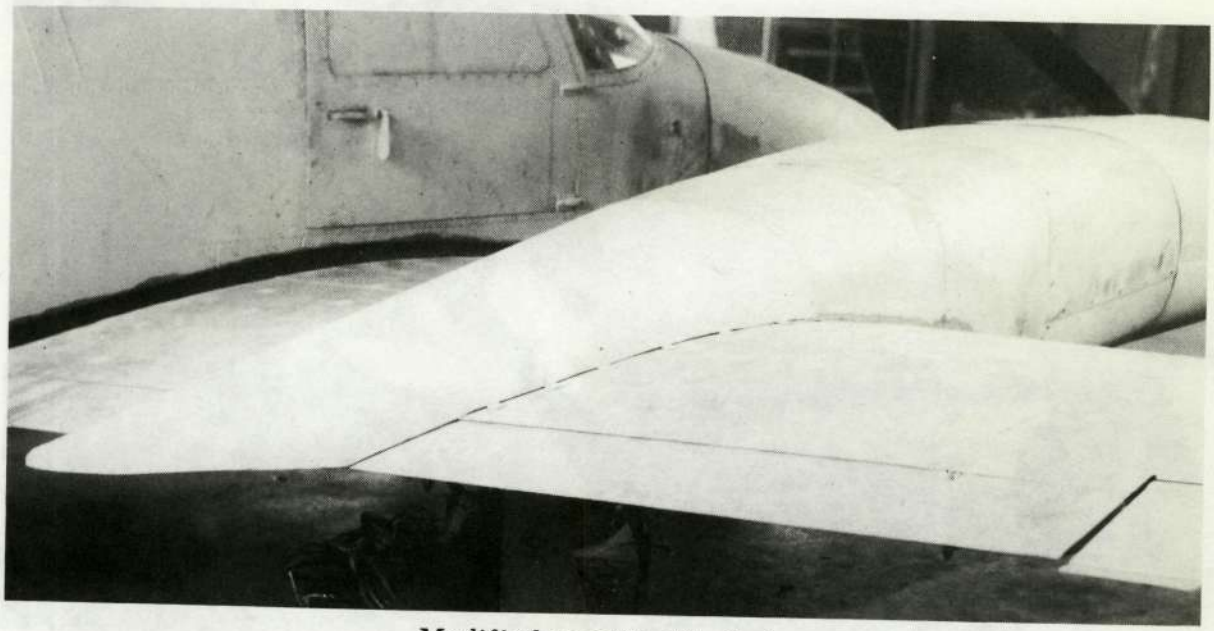

Modified nacelle afterbody

L-72-2476

Figure 5.- Photograph of the basic nacelle afterbody and the modified nacelle afterbody.

Nacelle A

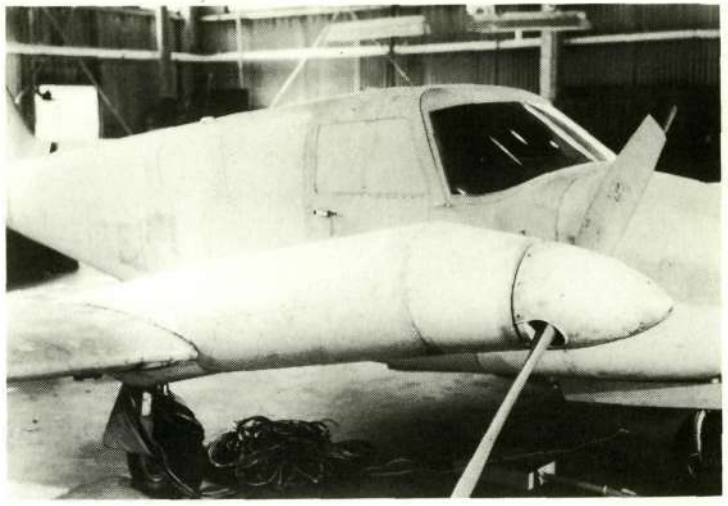

Nacelle B

Nacelle C

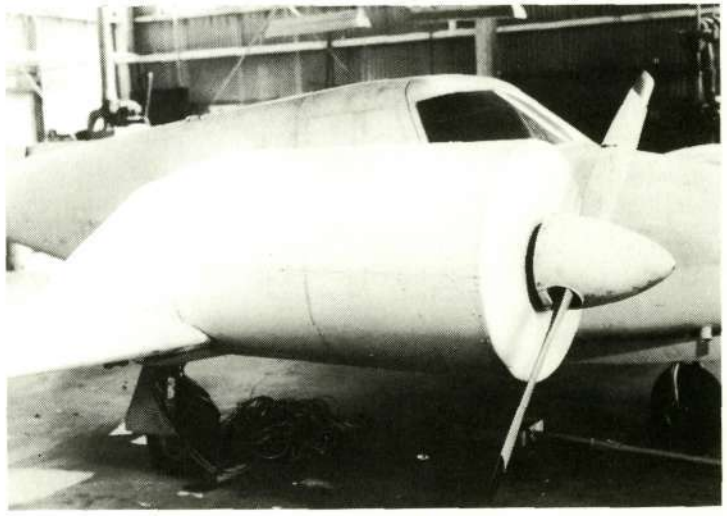

Nacelle D

L-72-2477

Figure 6.- Photographs of the nacelle configurations tested.

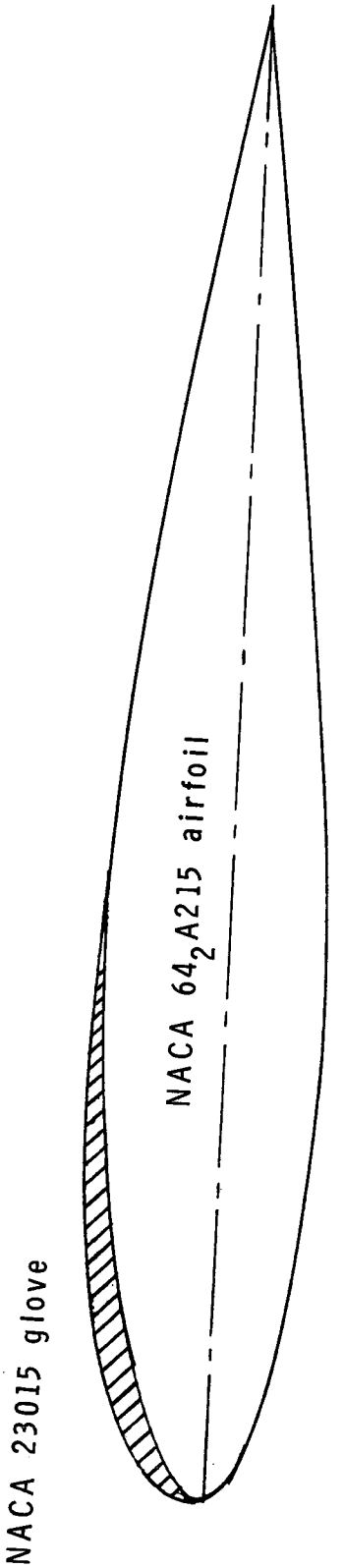

Figure 7.- Sketch of airfoil modification.

L-8375

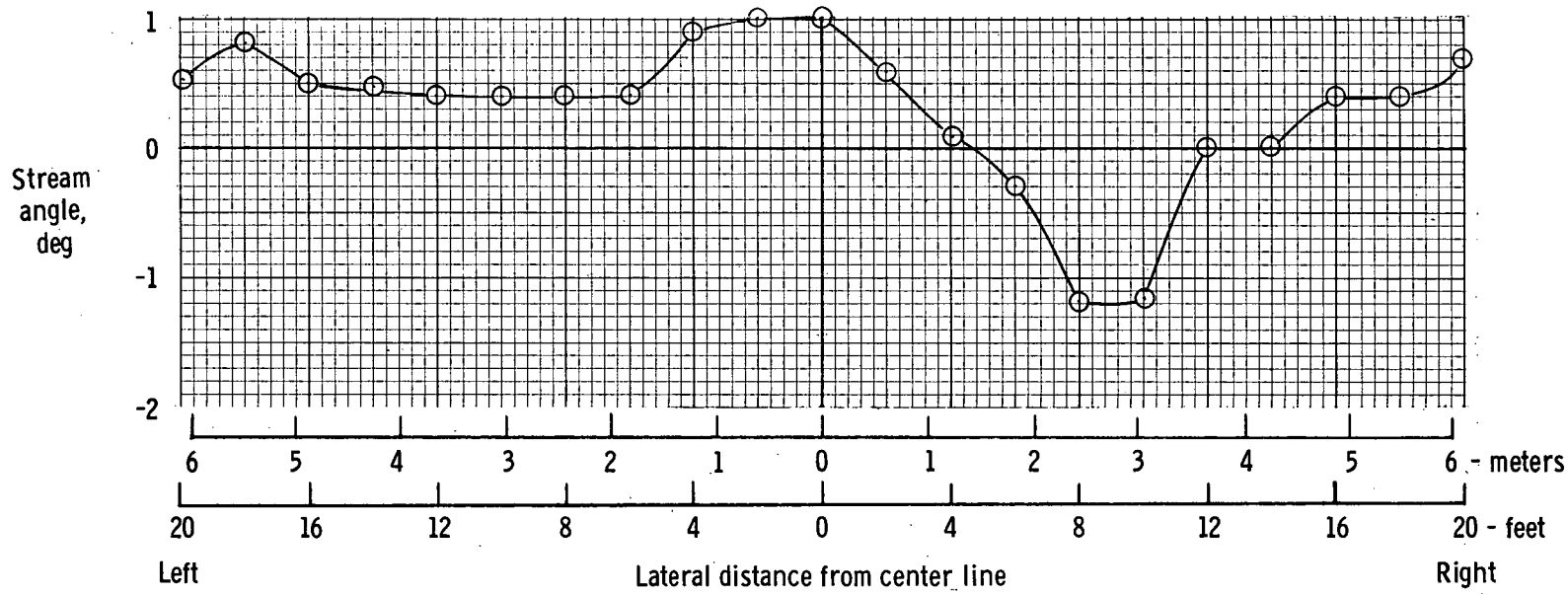

Figure 8.- Lateral variation of airstream angle at the wing location in tunnel looking upstream.

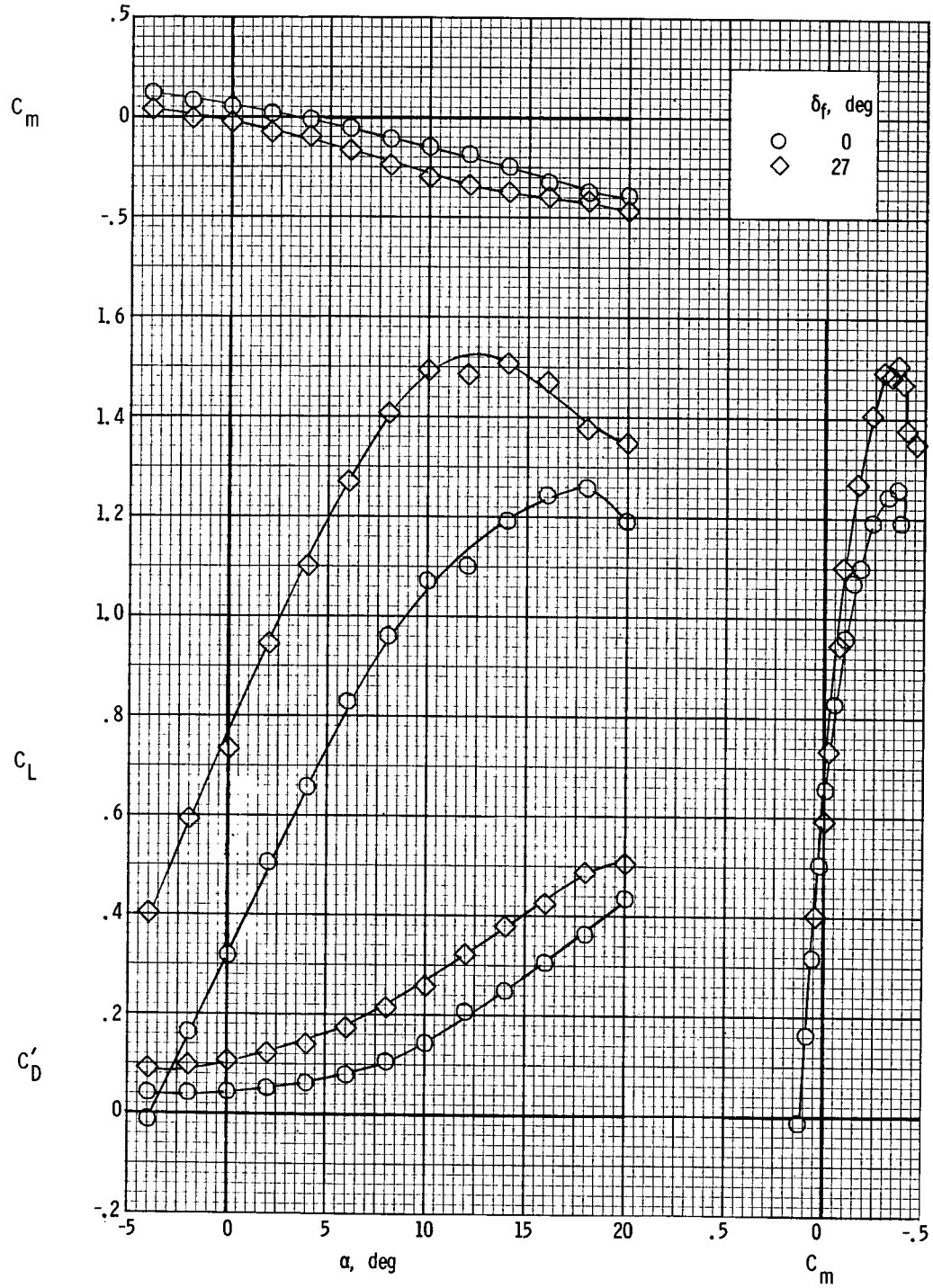

Figure 9.- Longitudinal aerodynamic characteristics of the model with the propellers removed. Nacelle A; $\beta = 0^o$.

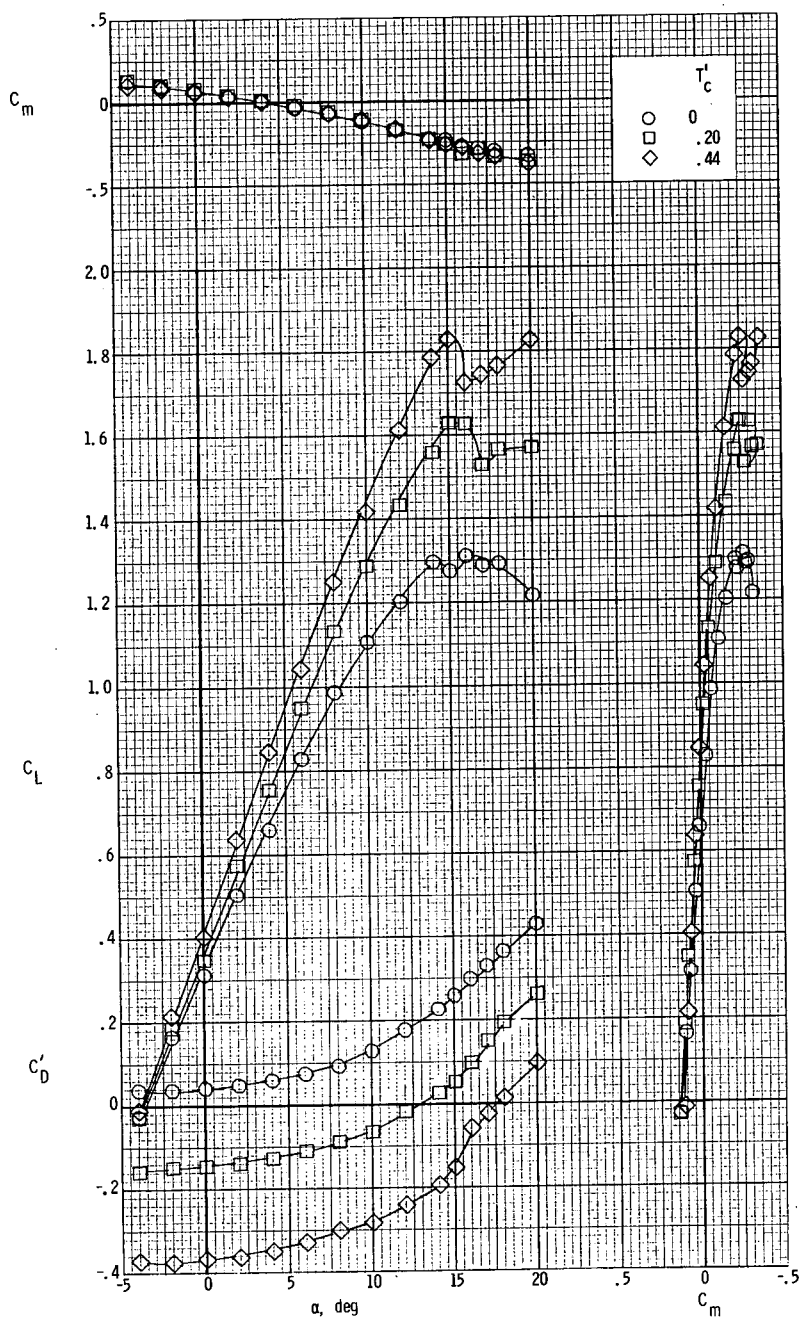

(a) $\delta_f = 0^o$.

Figure 10.- Longitudinal aerodynamic characteristics of the model with nacelle A. $\beta = 0^o$.

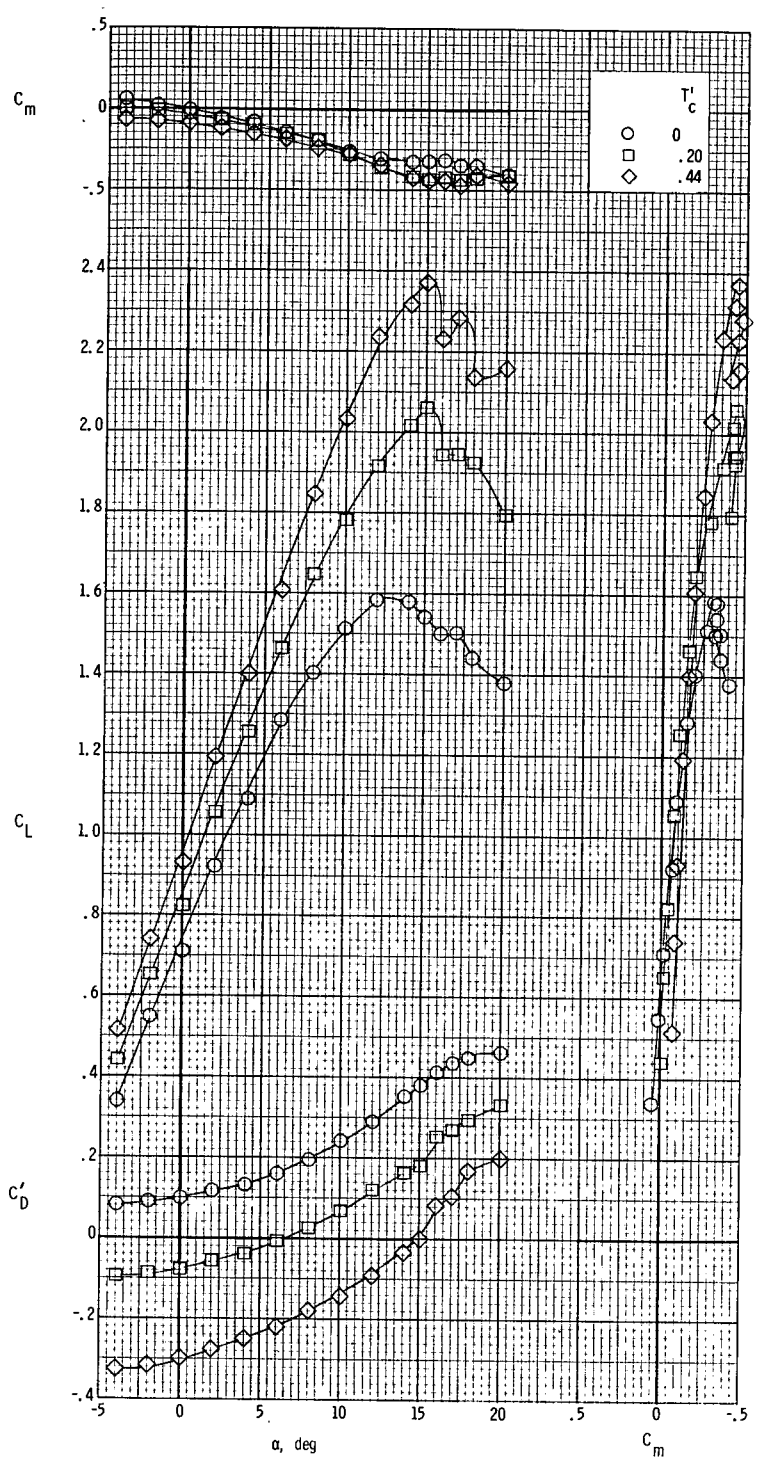

(b) $\delta_f = 27^o$.

Figure 10.- Concluded.

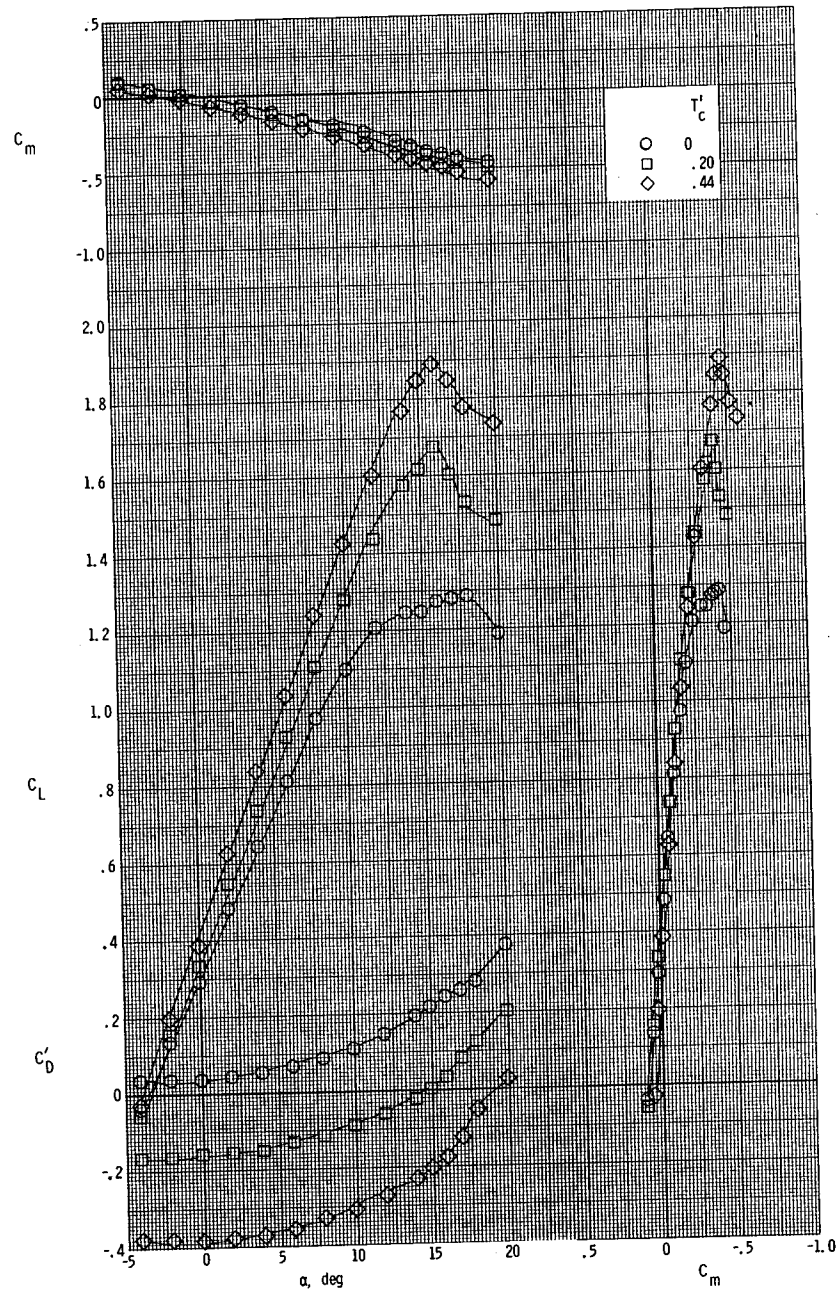

(a) $\delta_f = 0^o$.

Figure 11.- Longitudinal aerodynamic characteristics of the model with nacelle B. $\beta = 0^o$.

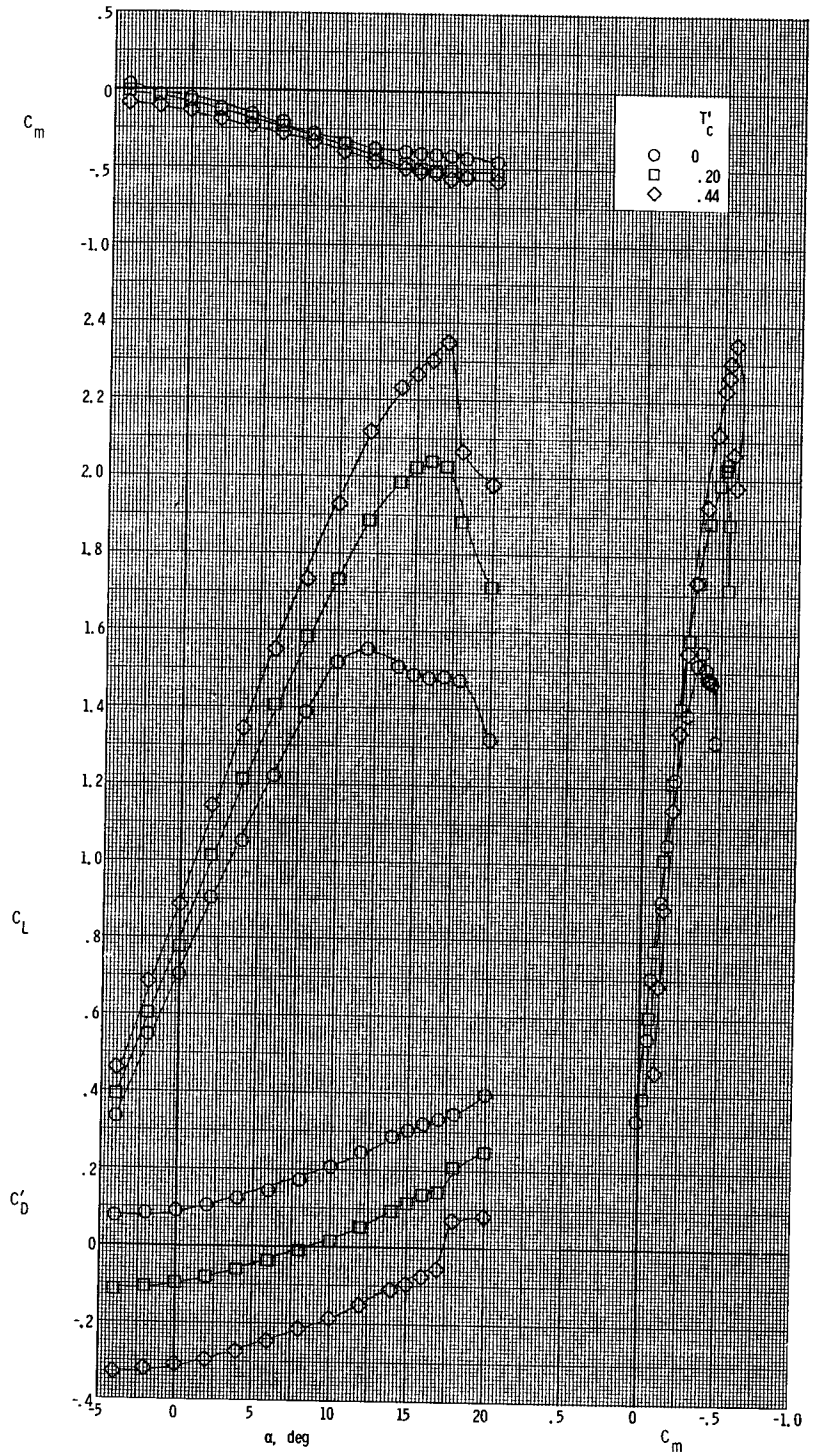

(b) $\delta_f = 27^o$.

Figure 11.- Concluded.

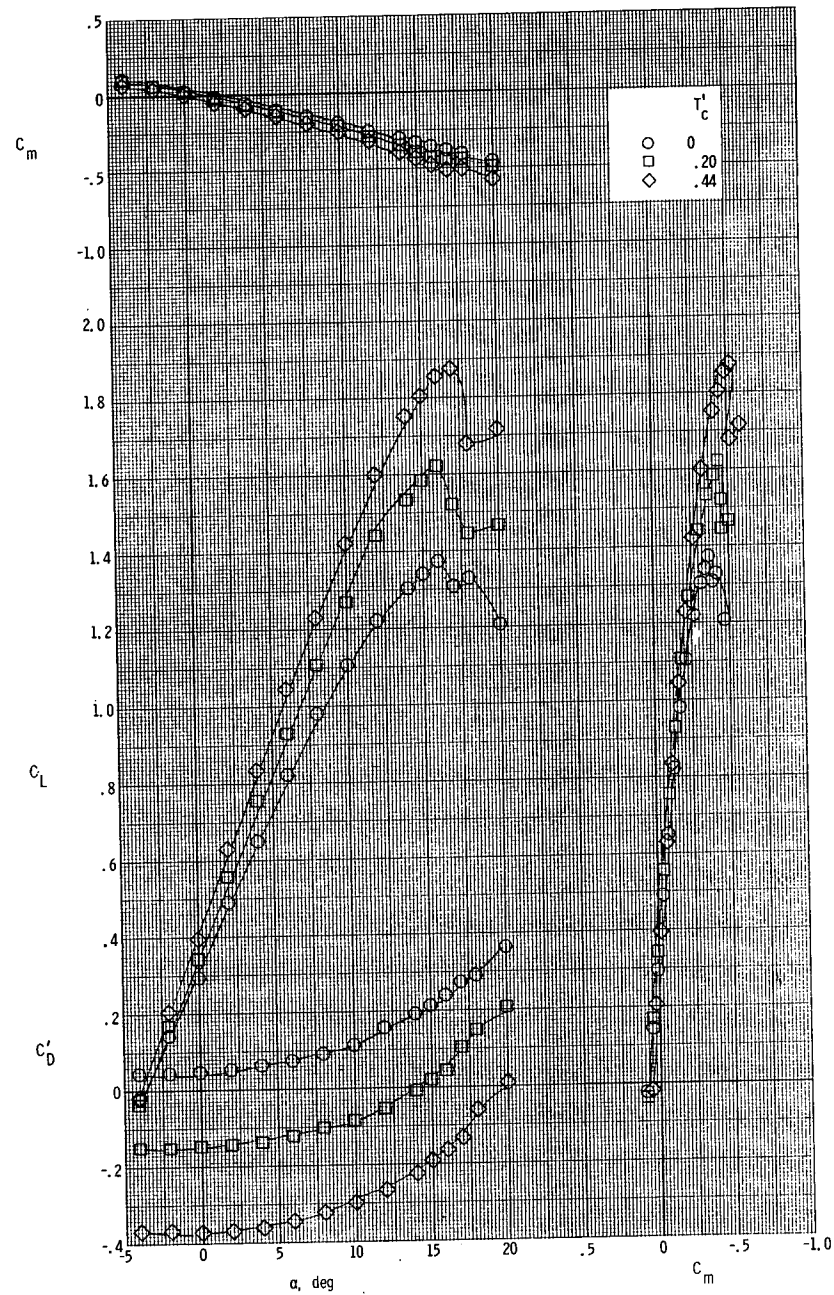

(a) $\delta_f = 0^o$.

Figure 12.- Longitudinal aerodynamic characteristics of the model with nacelle C. $\beta = 0^o$.

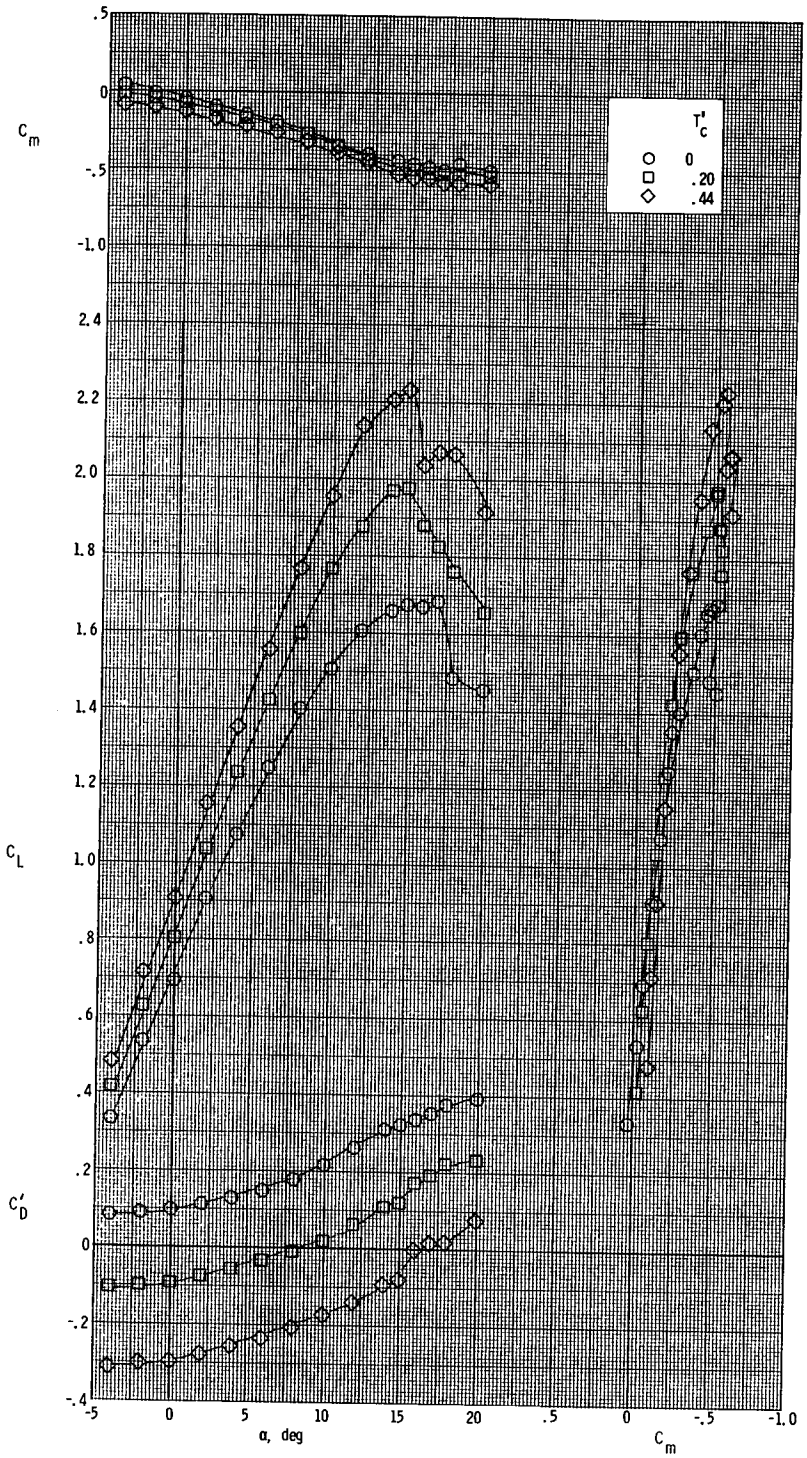

(b) $\delta_f = 27^o$.

Figure 12.- Concluded.

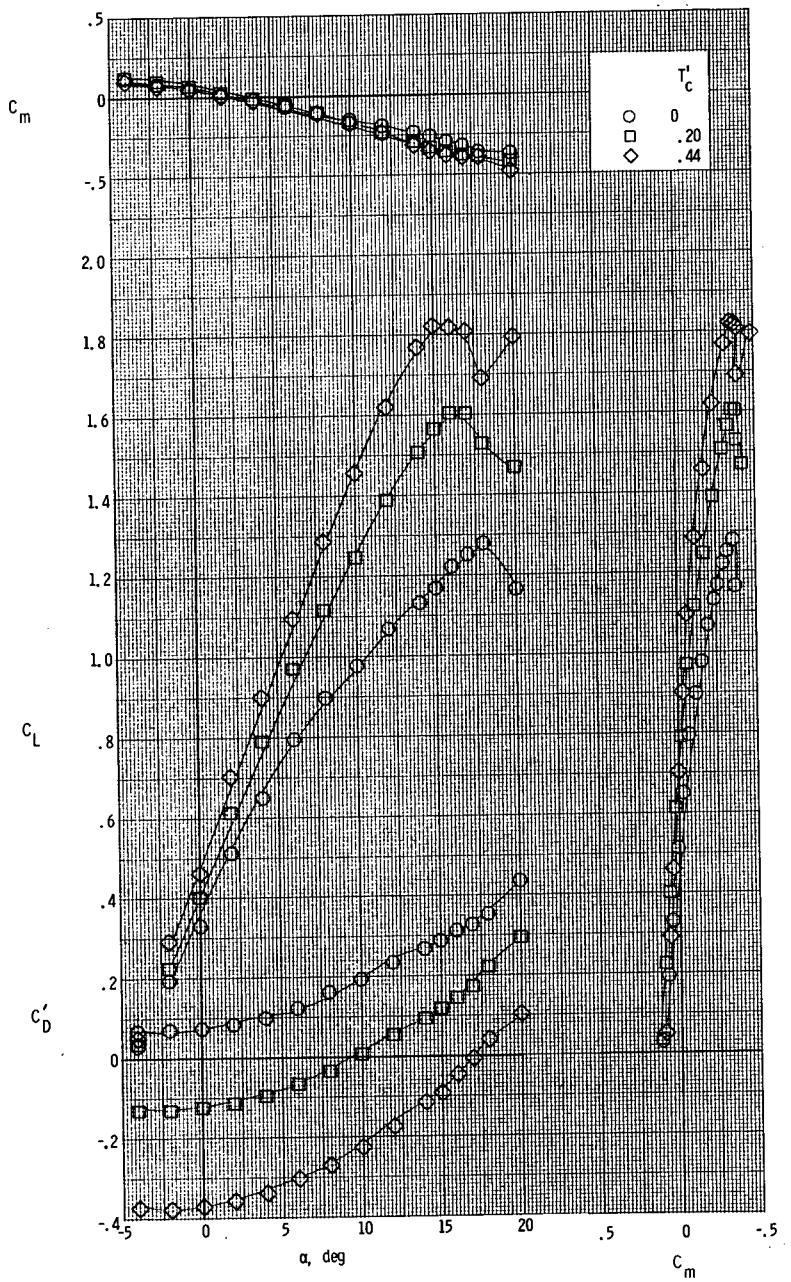

(a) $\delta_f = 0^o$.

Figure 13.- Longitudinal aerodynamic characteristics of the model with nacelle D. $\beta = 0^o$.

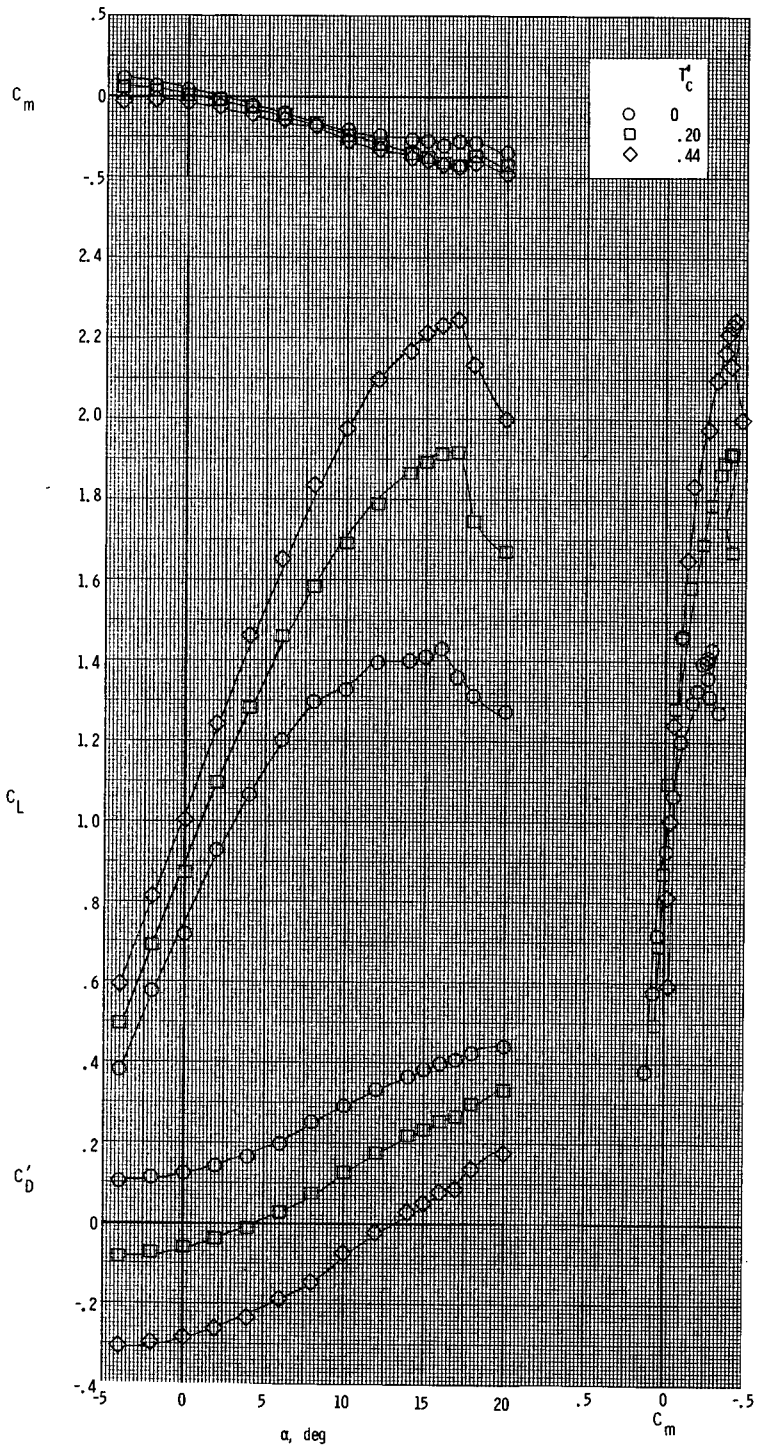

(b) $\delta_f = 27^o$.

Figure 13.- Concluded.

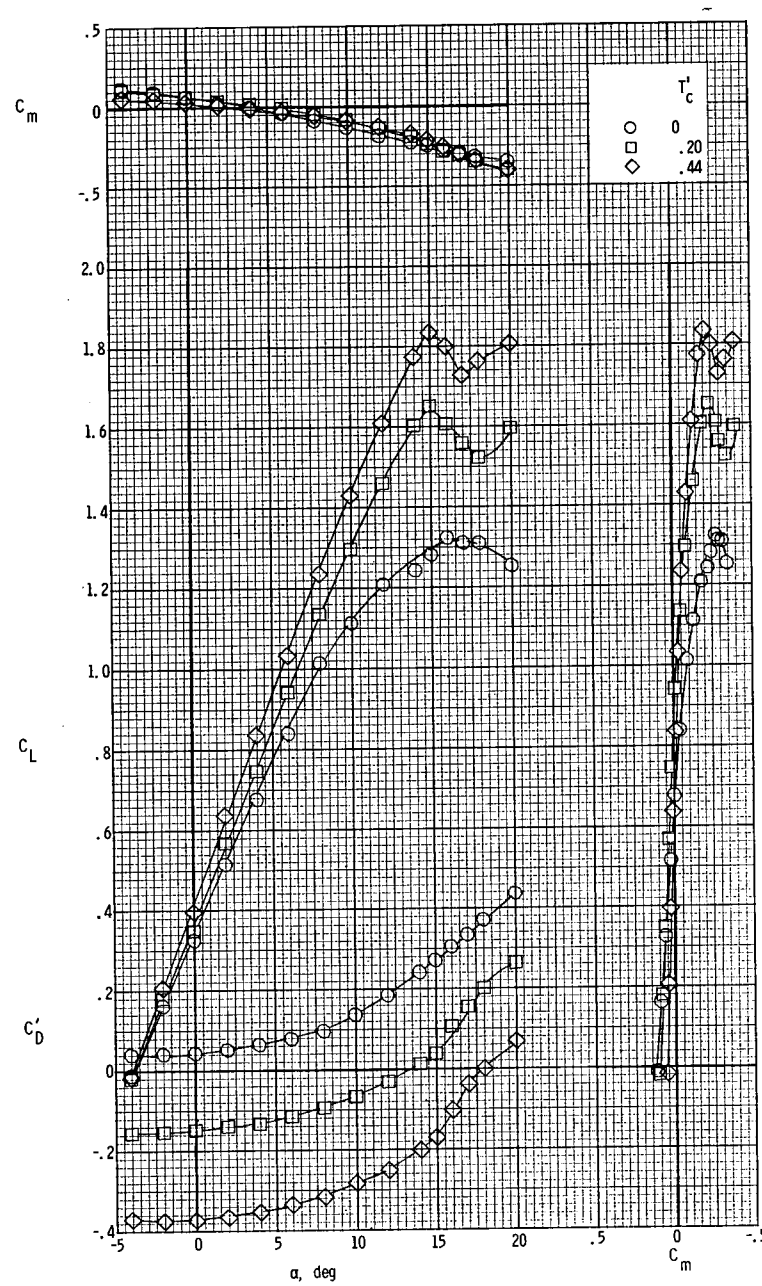

(a) $\delta_f = 0^o$.

Figure 14.- Longitudinal aerodynamic characteristics of the model with down-at-the-center propeller rotation. $\beta = 0^o$.

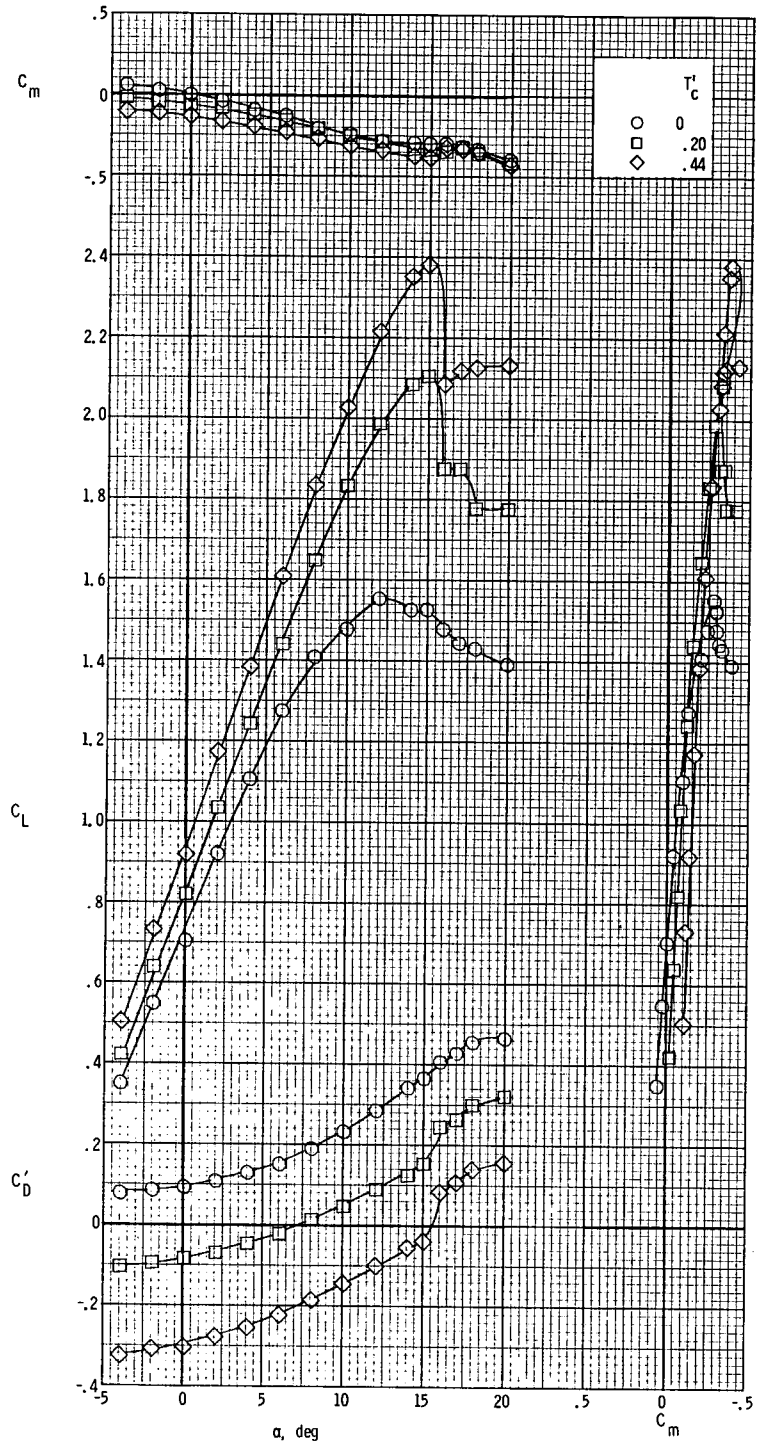

(b) $\delta_f = 27^o$.

Figure 14.- Concluded.

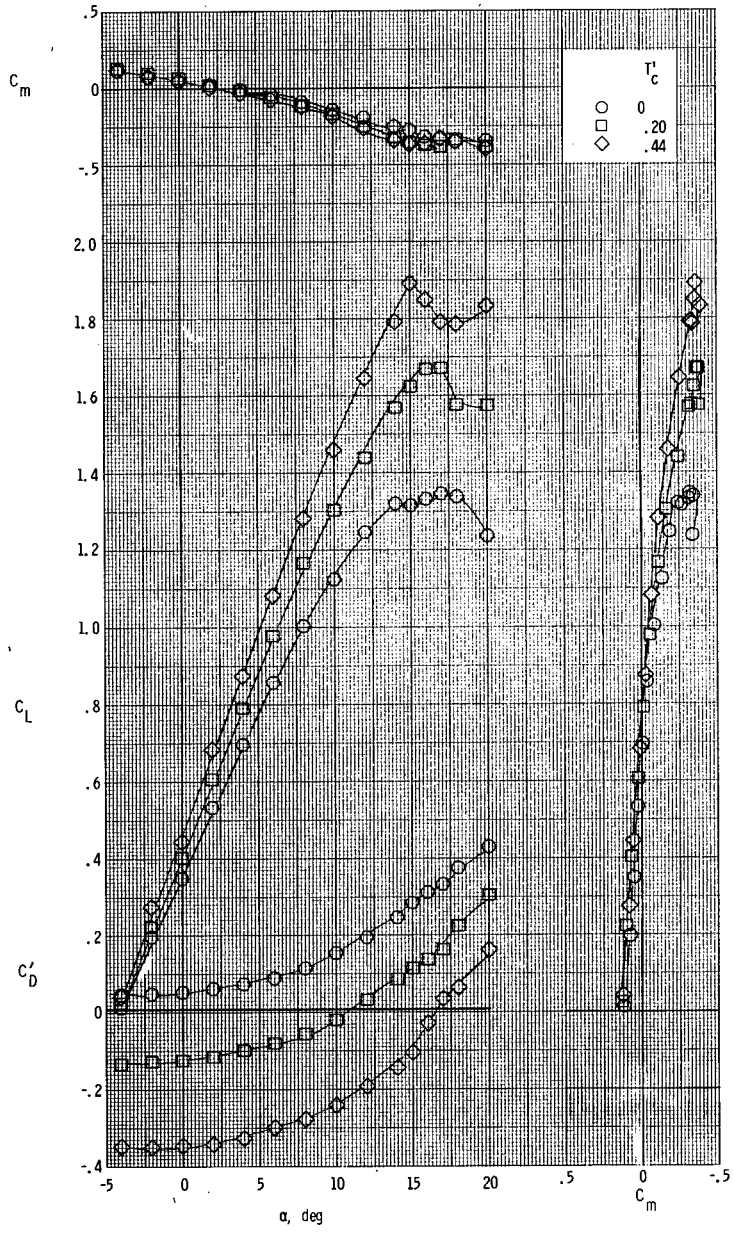

(a) $\delta_f = 0^o$.

Figure 15.- Longitudinal aerodynamic characteristics of the model with up-at-the-center propeller rotation. $\beta = 0^o$.

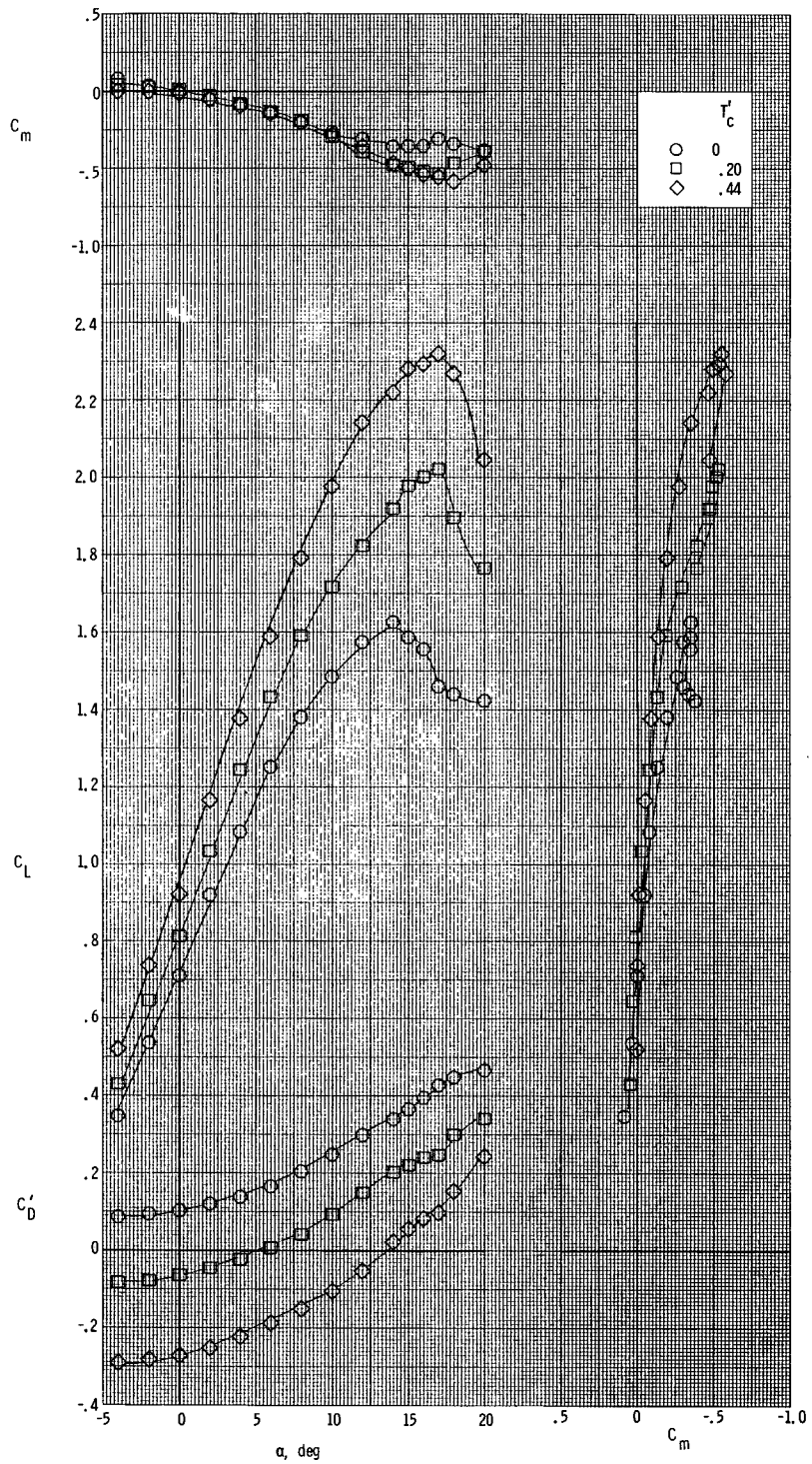

(b) $\delta_f = 27^o$.

Figure 15.- Concluded.

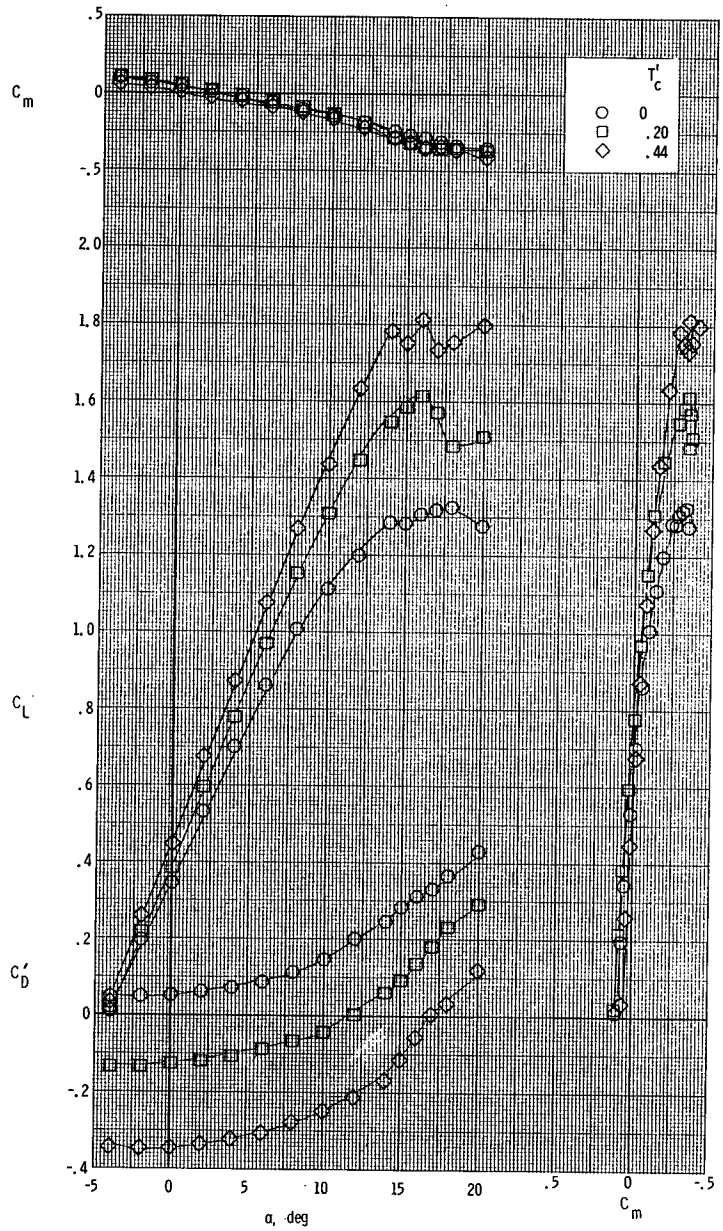

(a) $\delta_f = 0^o$.

Figure 16.- Longitudinal aerodynamic characteristics of the model with counterclockwise propeller rotation. $\beta = 0^o$.

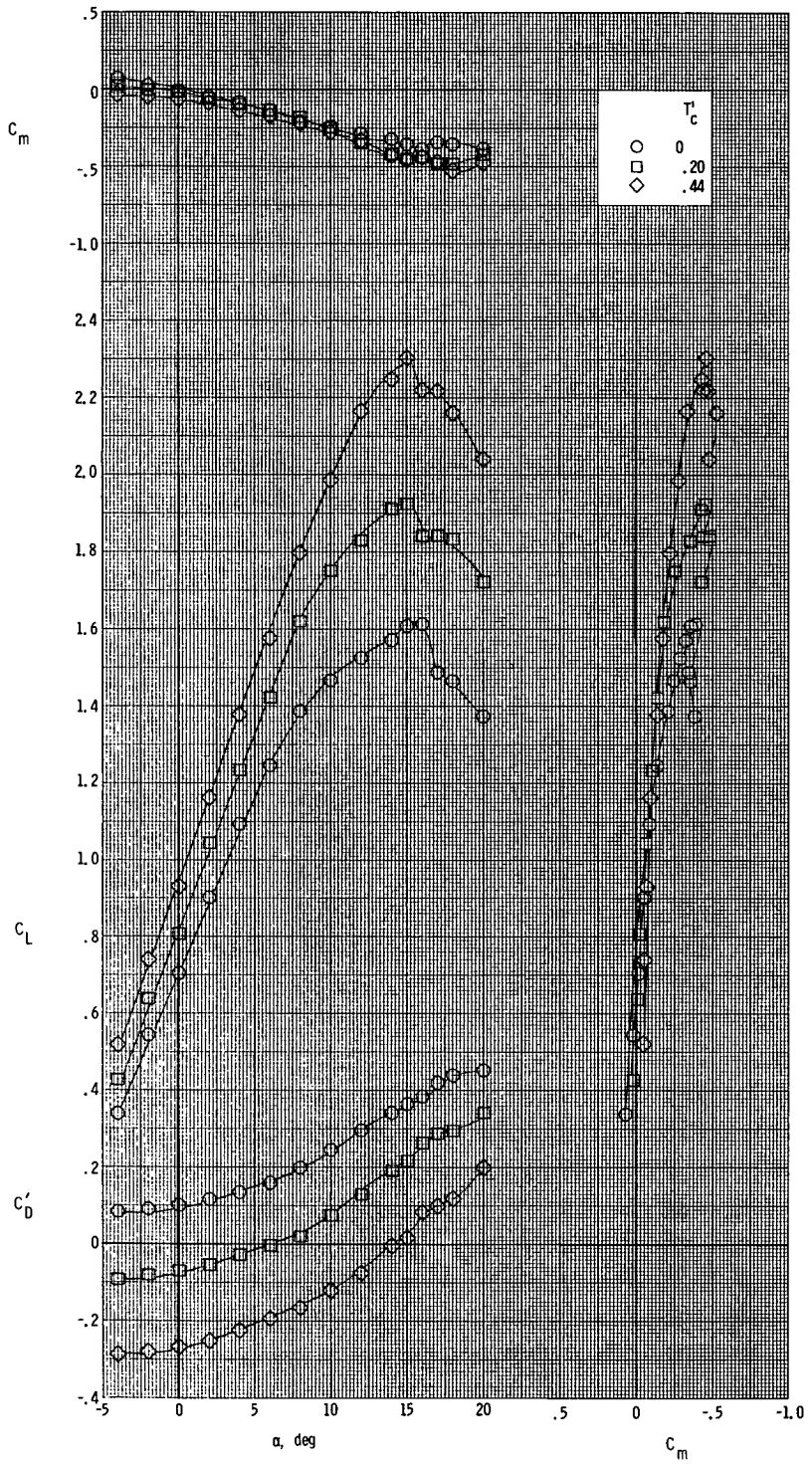

(b) $\delta_f = 27^o$.

Figure 16.- Concluded.

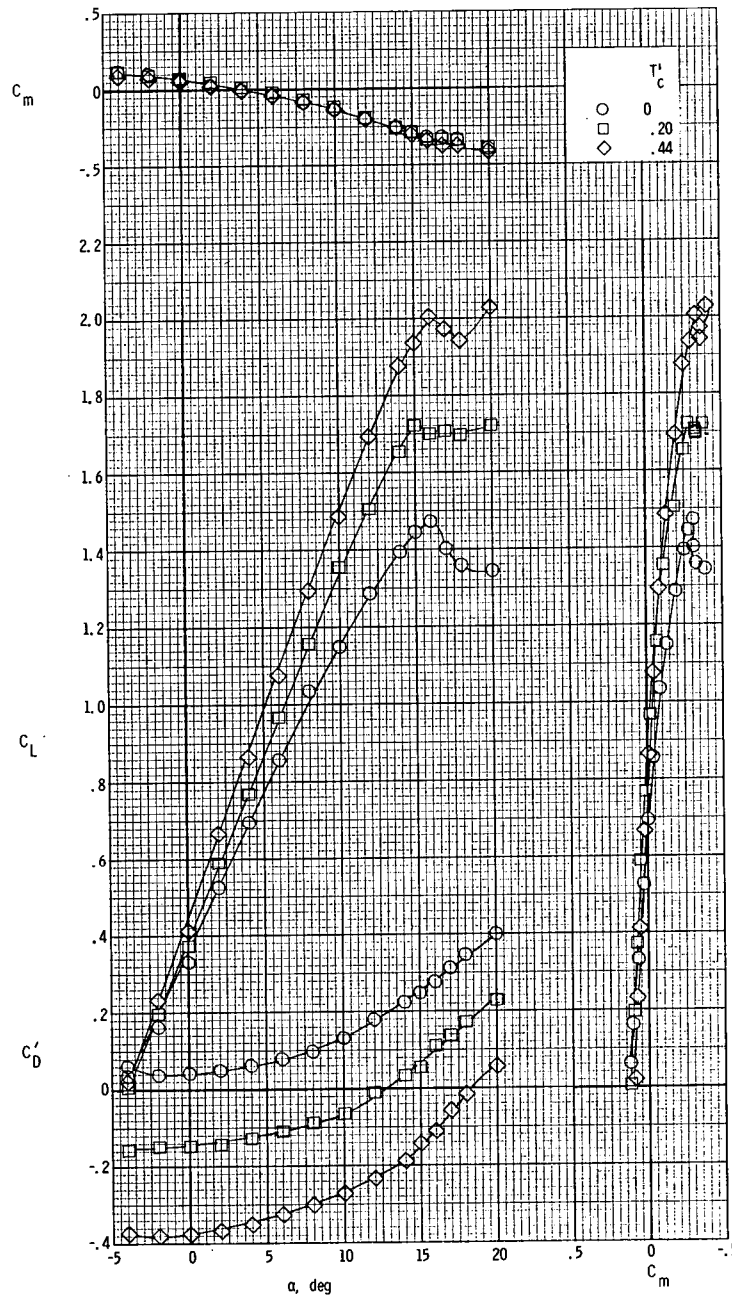

(a) $\delta_f = 0^o$.

Figure 17.- Longitudinal aerodynamic characteristics of the model with the modified airfoil. $\beta = 0^o$; clockwise rotation.

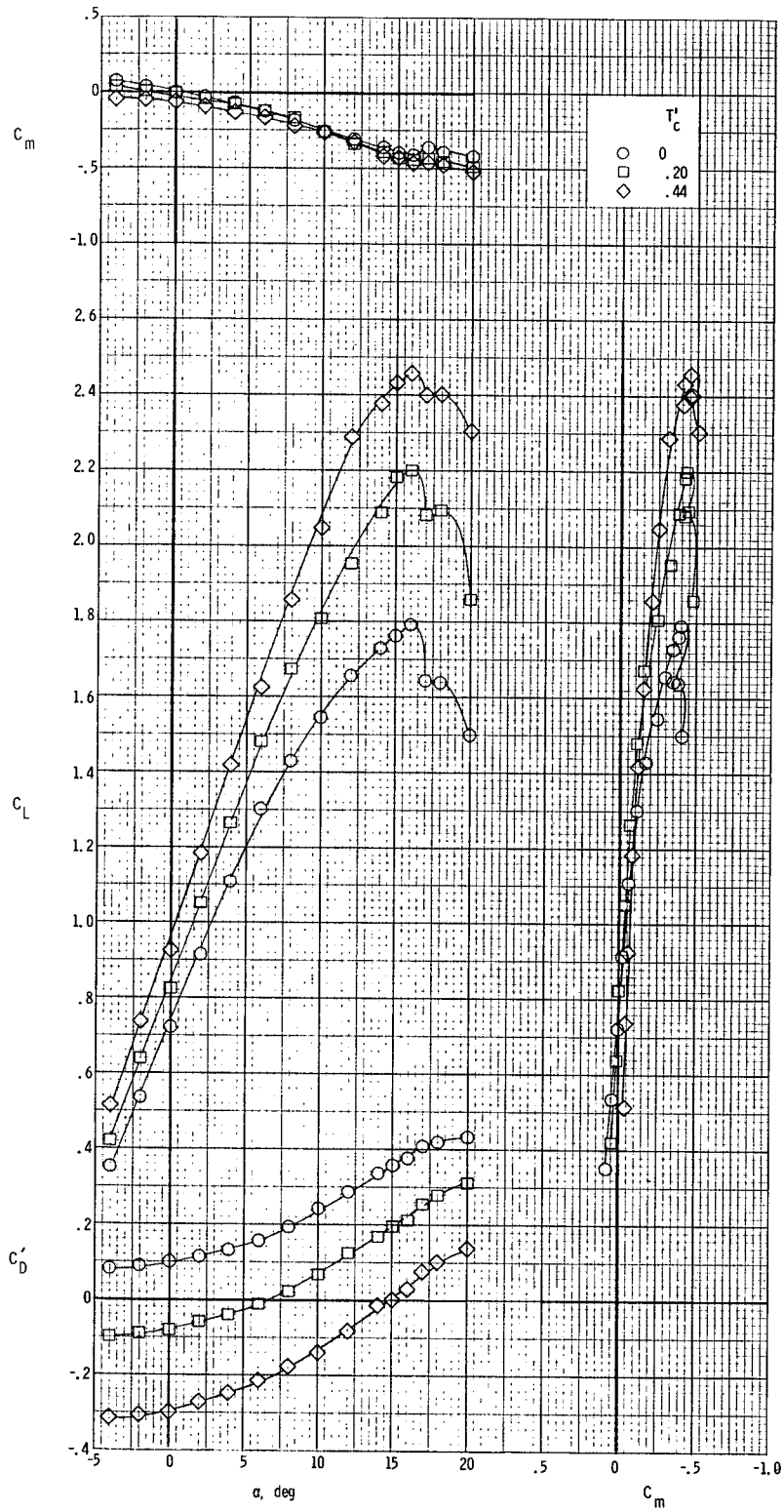

(b) $\delta_f = 27^o$.

Figure 17.- Concluded.

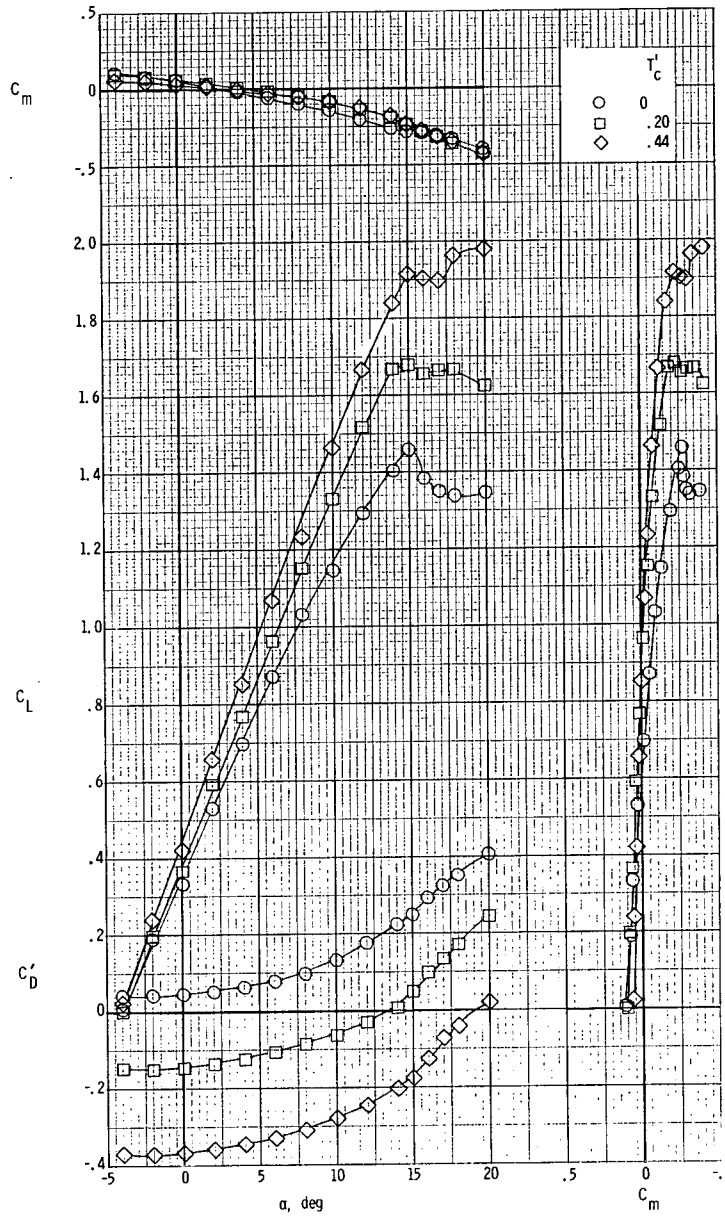

(a) $\delta_f = 0^o$.

Figure 18.- Longitudinal aerodynamic characteristics of the model with the modified airfoil and down-at-the-center propeller rotation. $\beta = 0^o$; nacelle A.

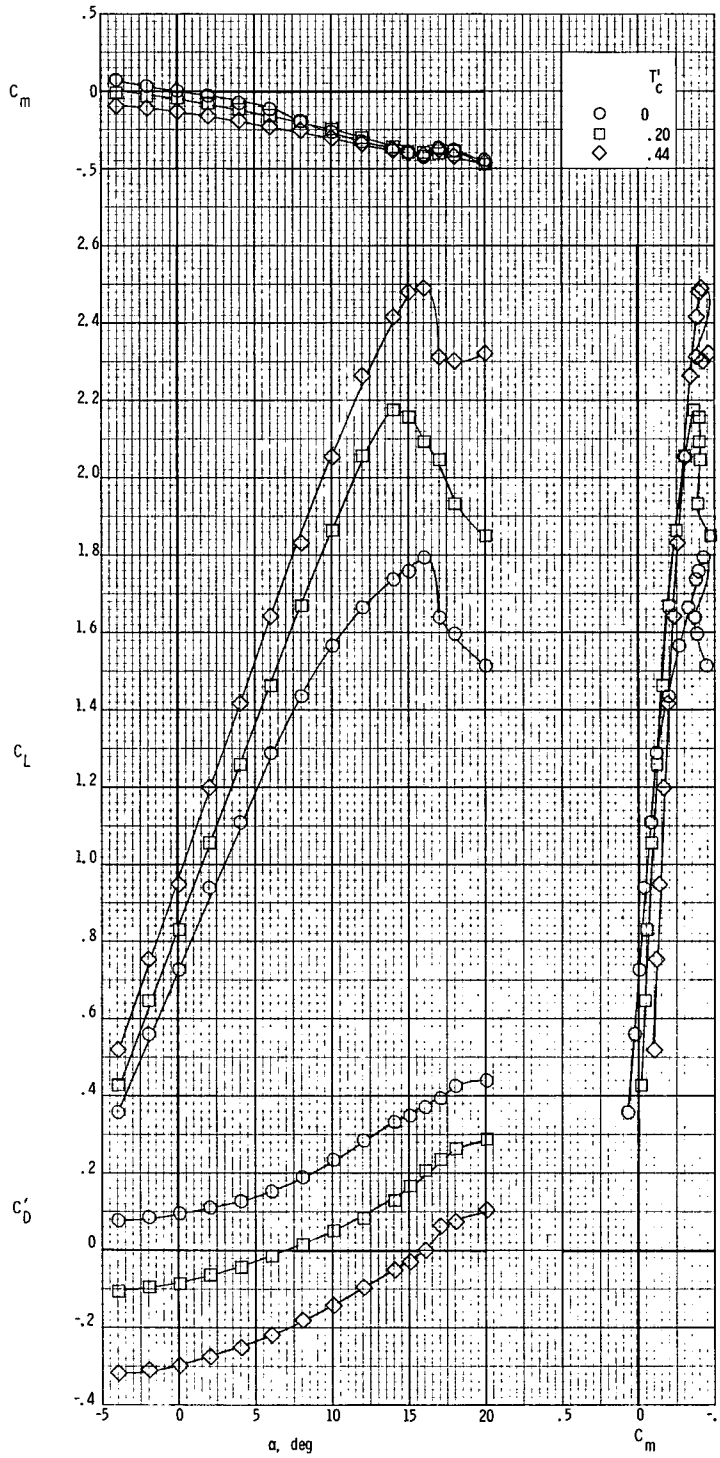

(b) $\delta_f = 27^o$.

Figure 18.- Concluded.

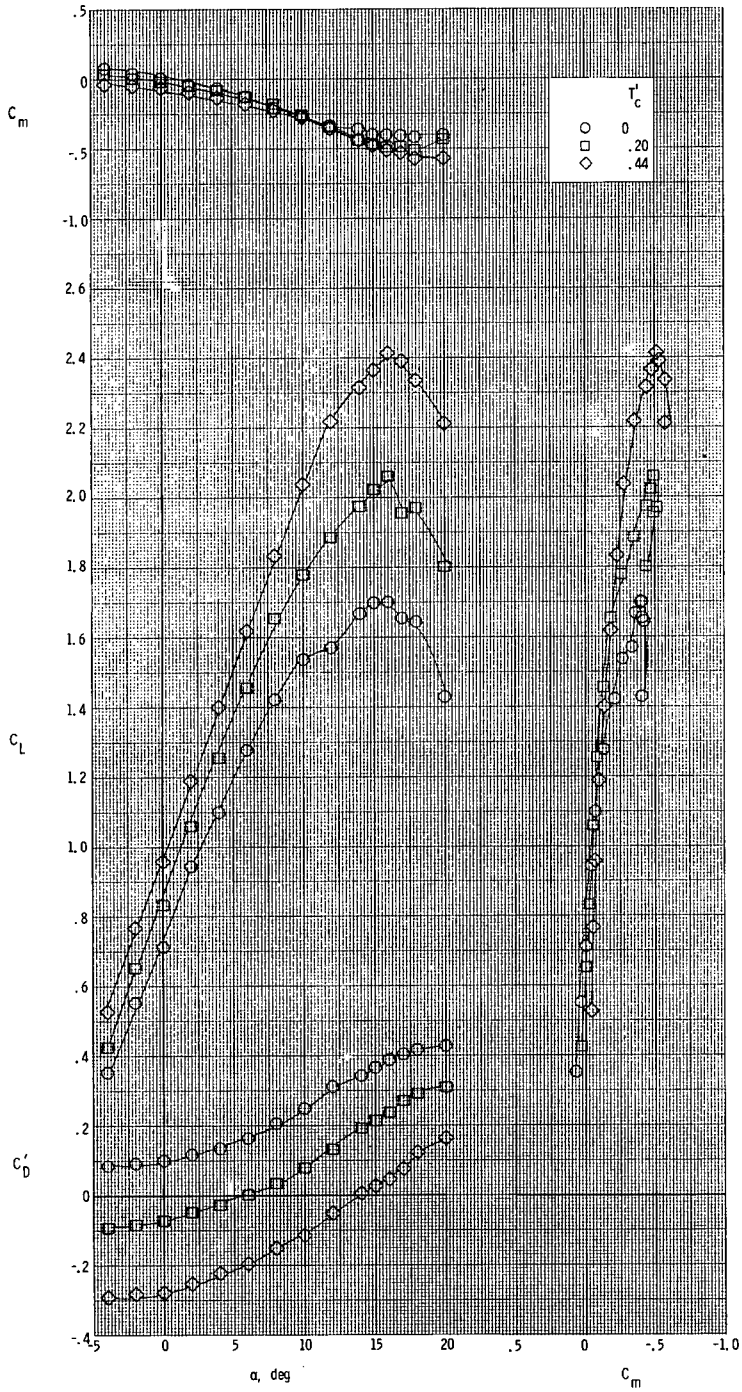

Figure 19.- Longitudinal aerodynamic characteristics of the model with the modified airfoil and counterclockwise propeller rotation. $\beta = 0^o$; $\delta_f = 27^o$; nacelle A.

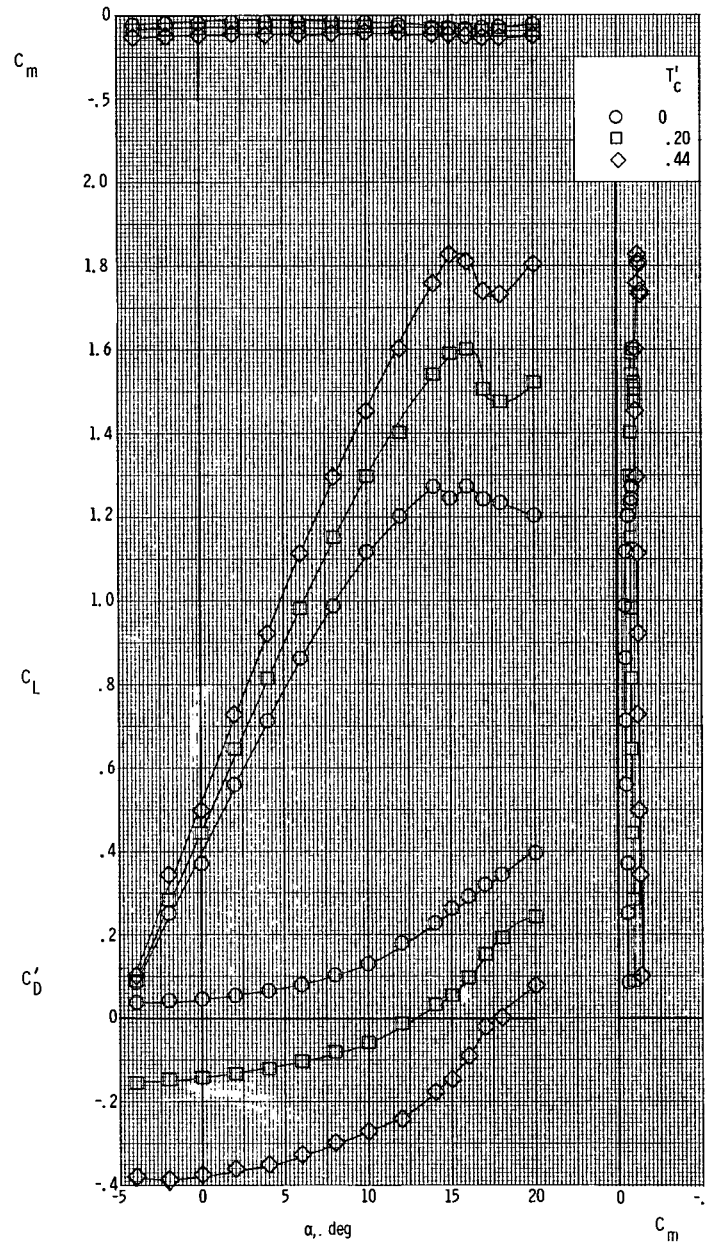

(a) $\delta_f = 0^o$.

Figure 20.- Longitudinal aerodynamic characteristics of the model with the horizontal tail removed. $\beta = 0^o$; nacelle A.

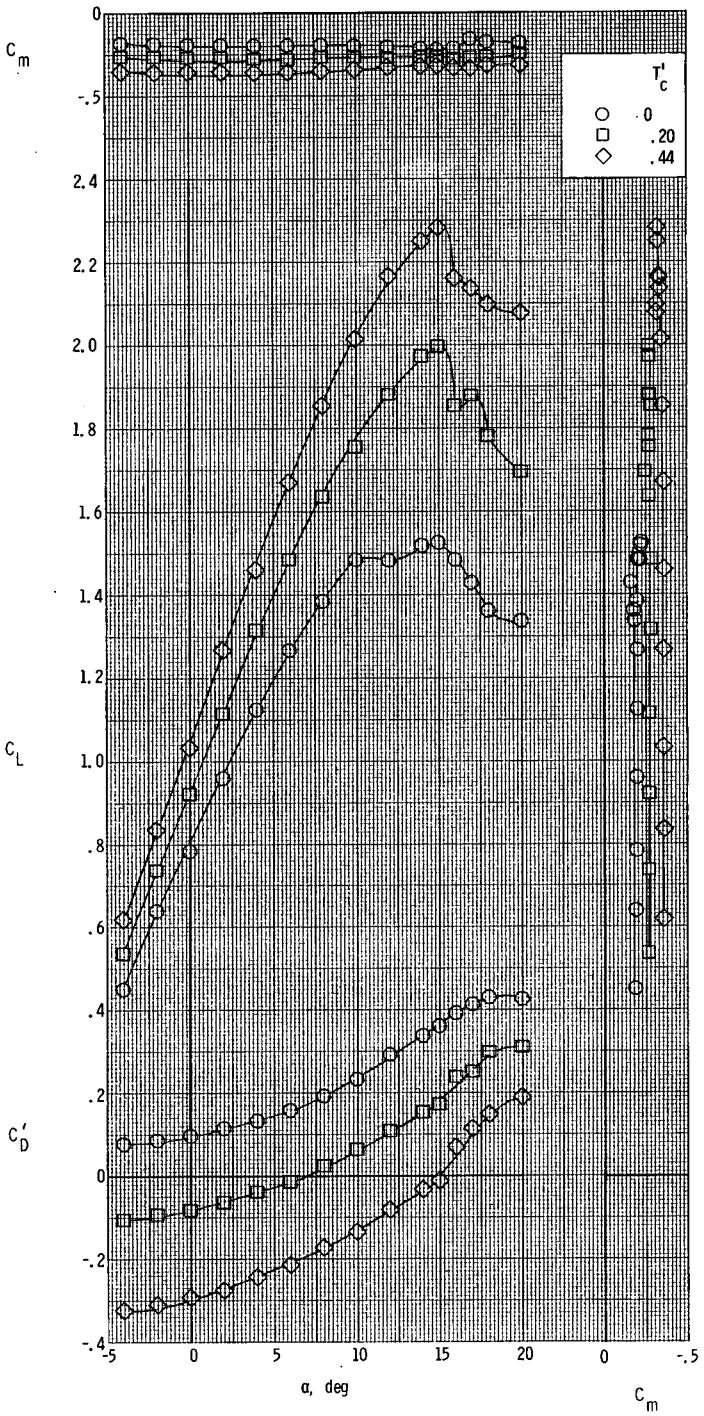

(b) $\delta_f = 27^o$.

Figure 20.- Concluded.

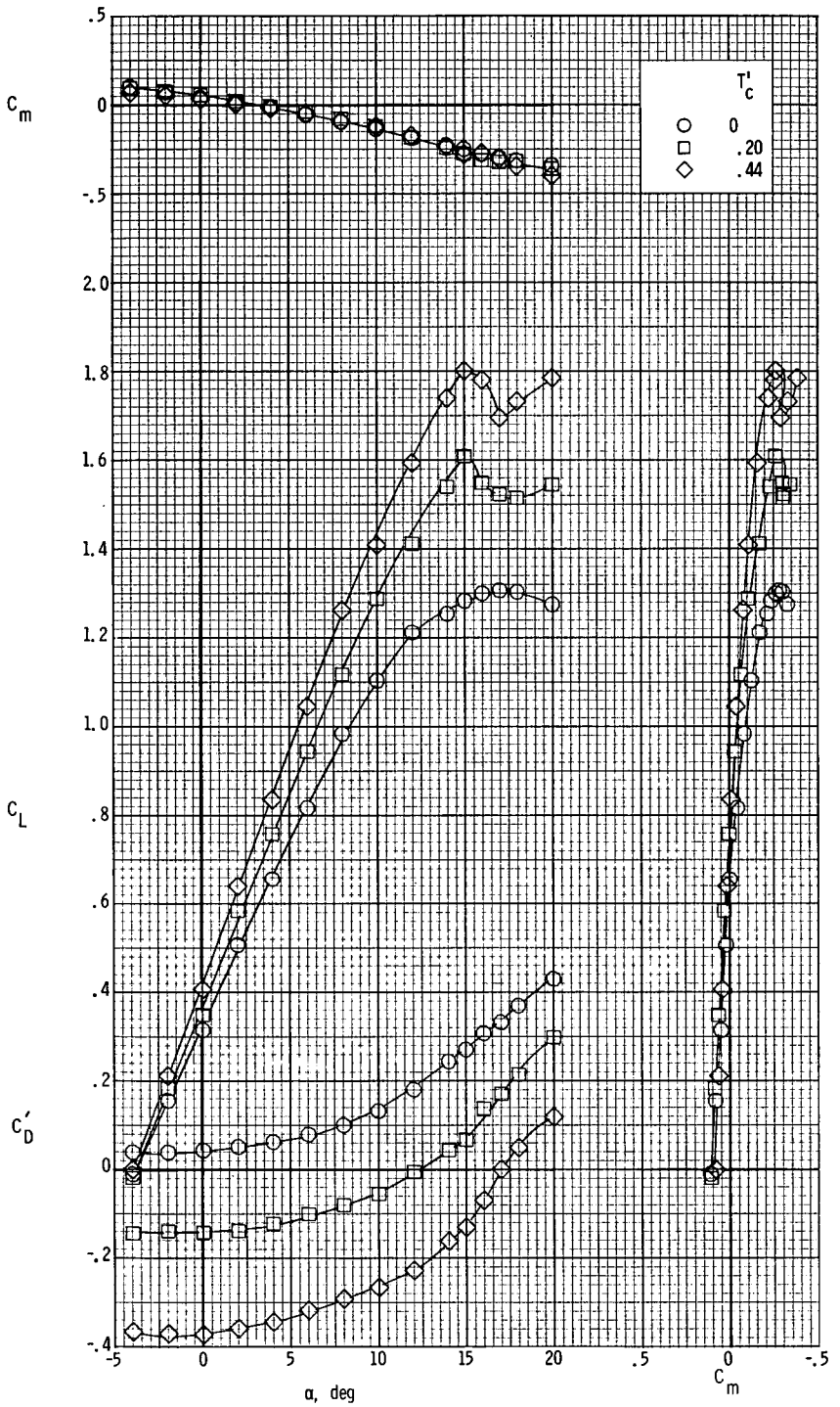

Figure 21.- Longitudinal aerodynamic characteristics of the model with the modified cowl. $\beta = 0^o$; $\delta_f = 0^o$; nacelle A.

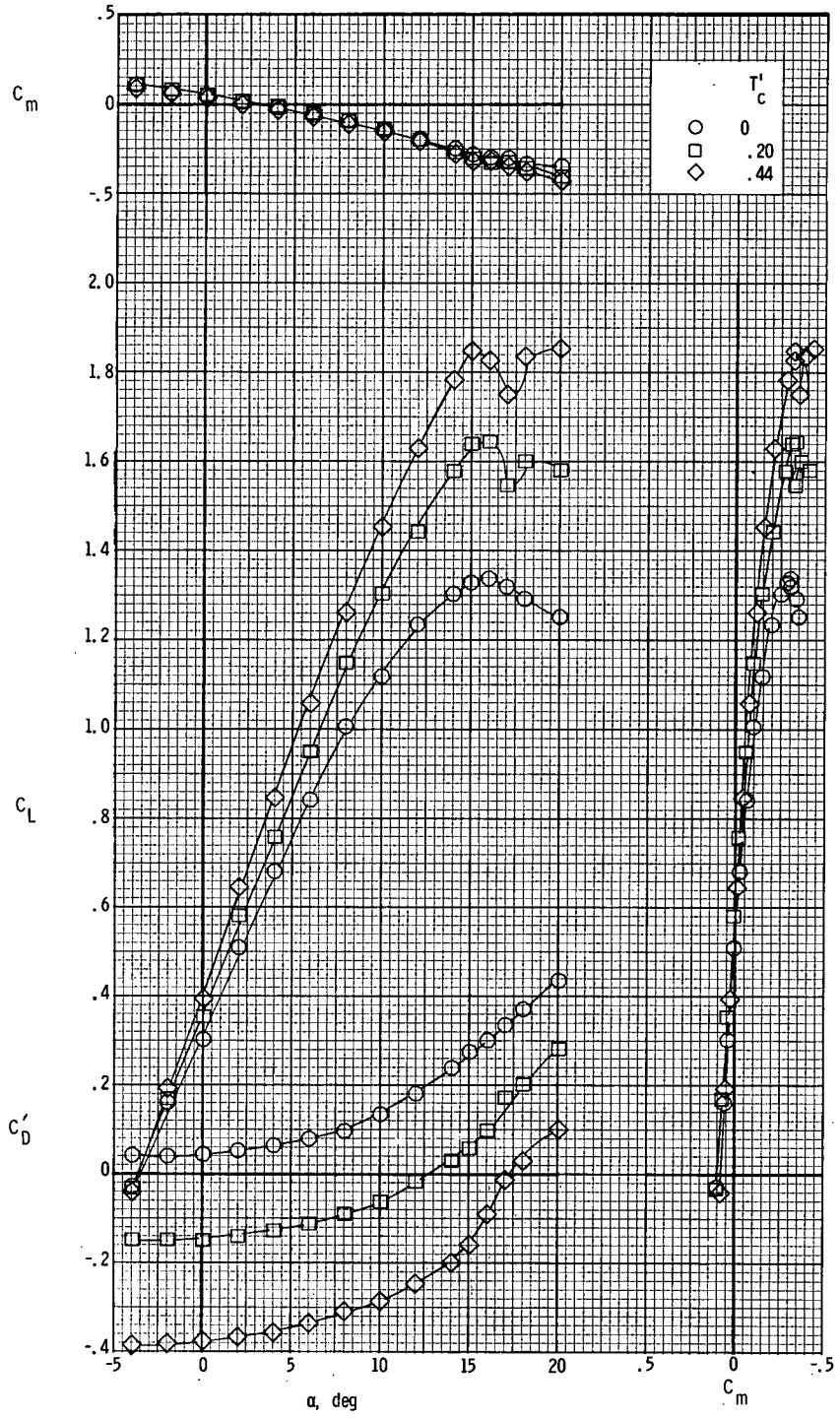

Figure 22.- Longitudinal aerodynamic characteristics of the model with the modified afterbody. $\beta = 0^o$; $\delta_f = 0^o$; nacelle A.

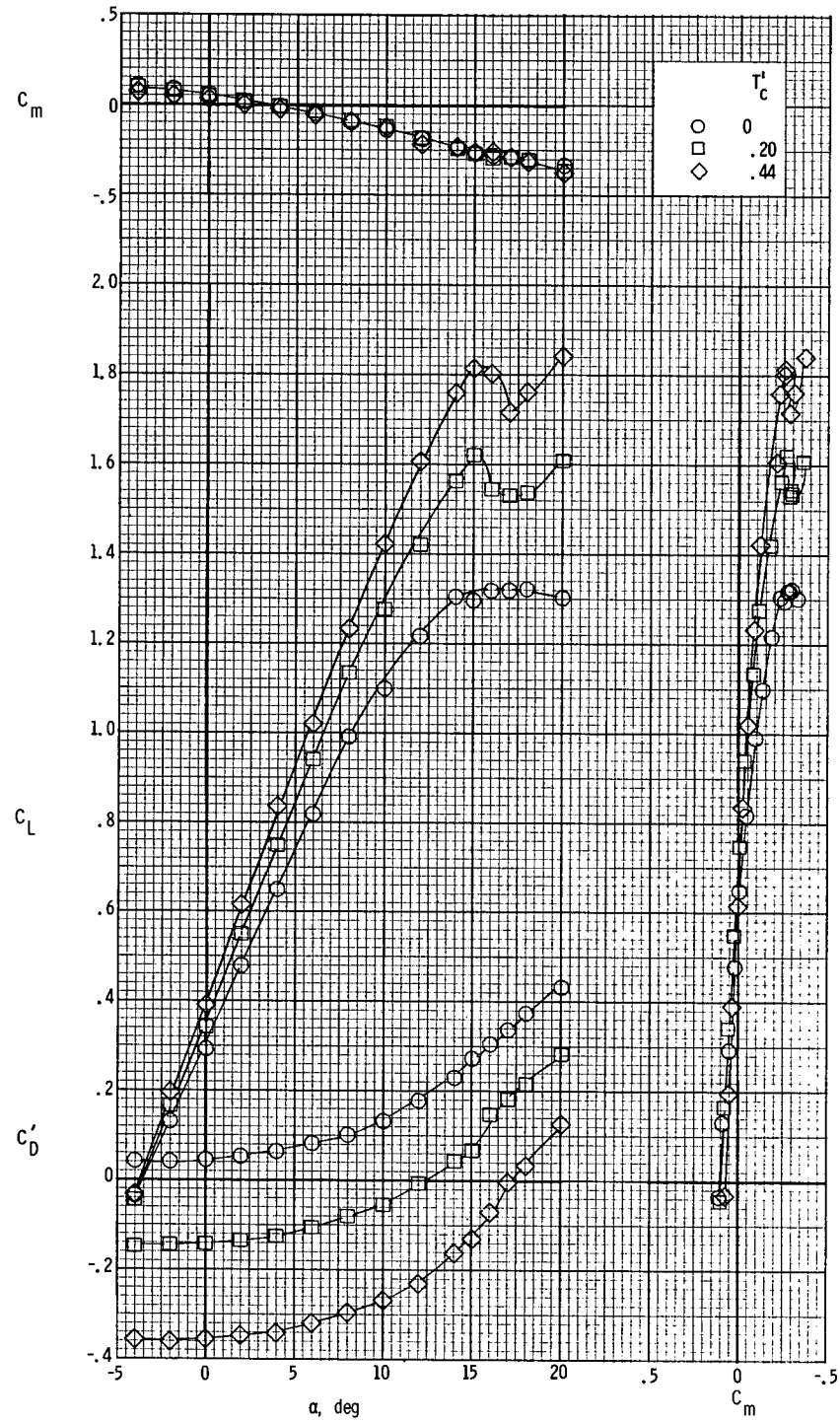

Figure 23.- Longitudinal aerodynamic characteristics of the model with the modified cowl and modified afterbody. $\beta = 0^o$; $\delta_f = 0^o$; nacelle A.

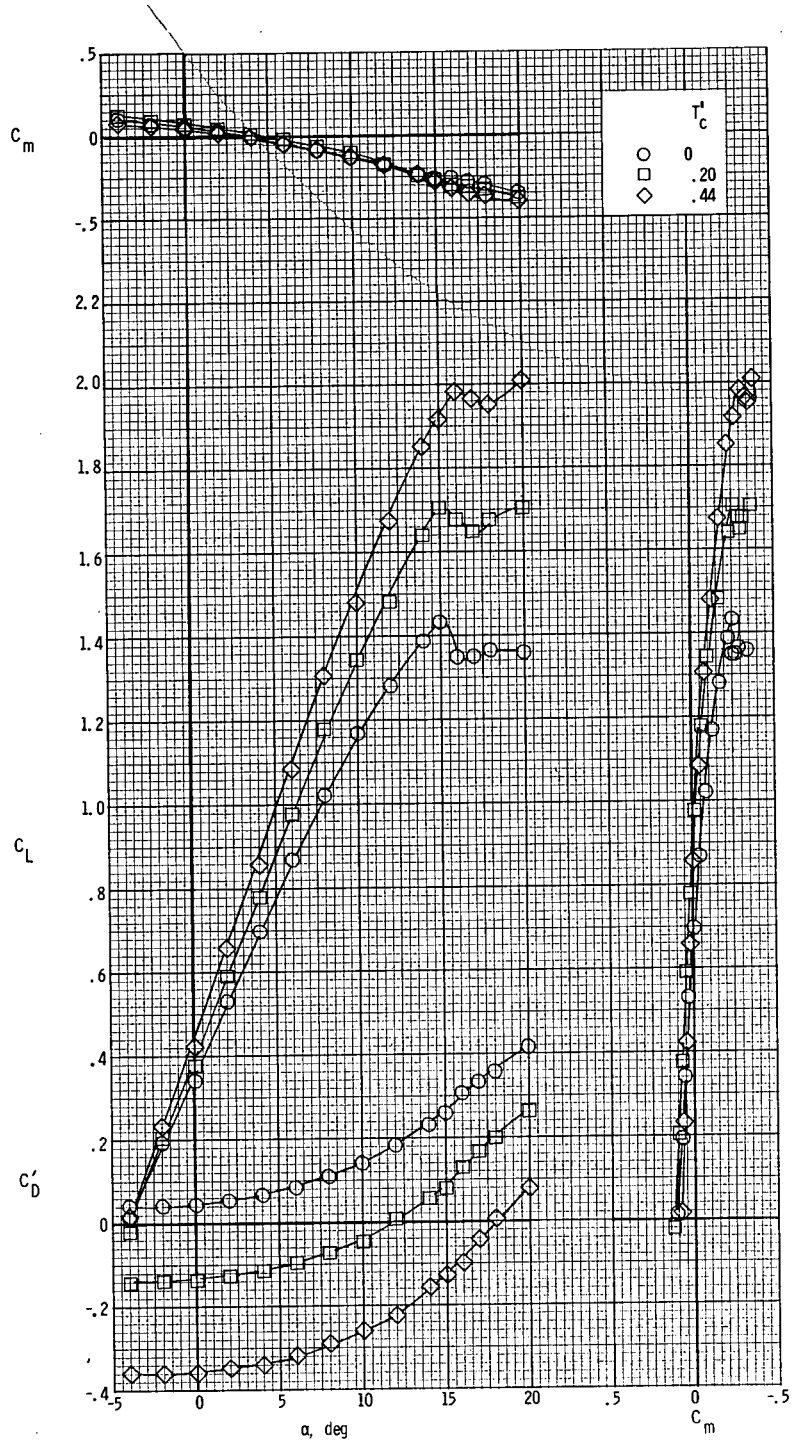

Figure 24.- Longitudinal aerodynamic characteristics of the model with the modified cowl and modified airfoil. $\beta = 0^o$; $\delta_f = 0^o$; nacelle A.

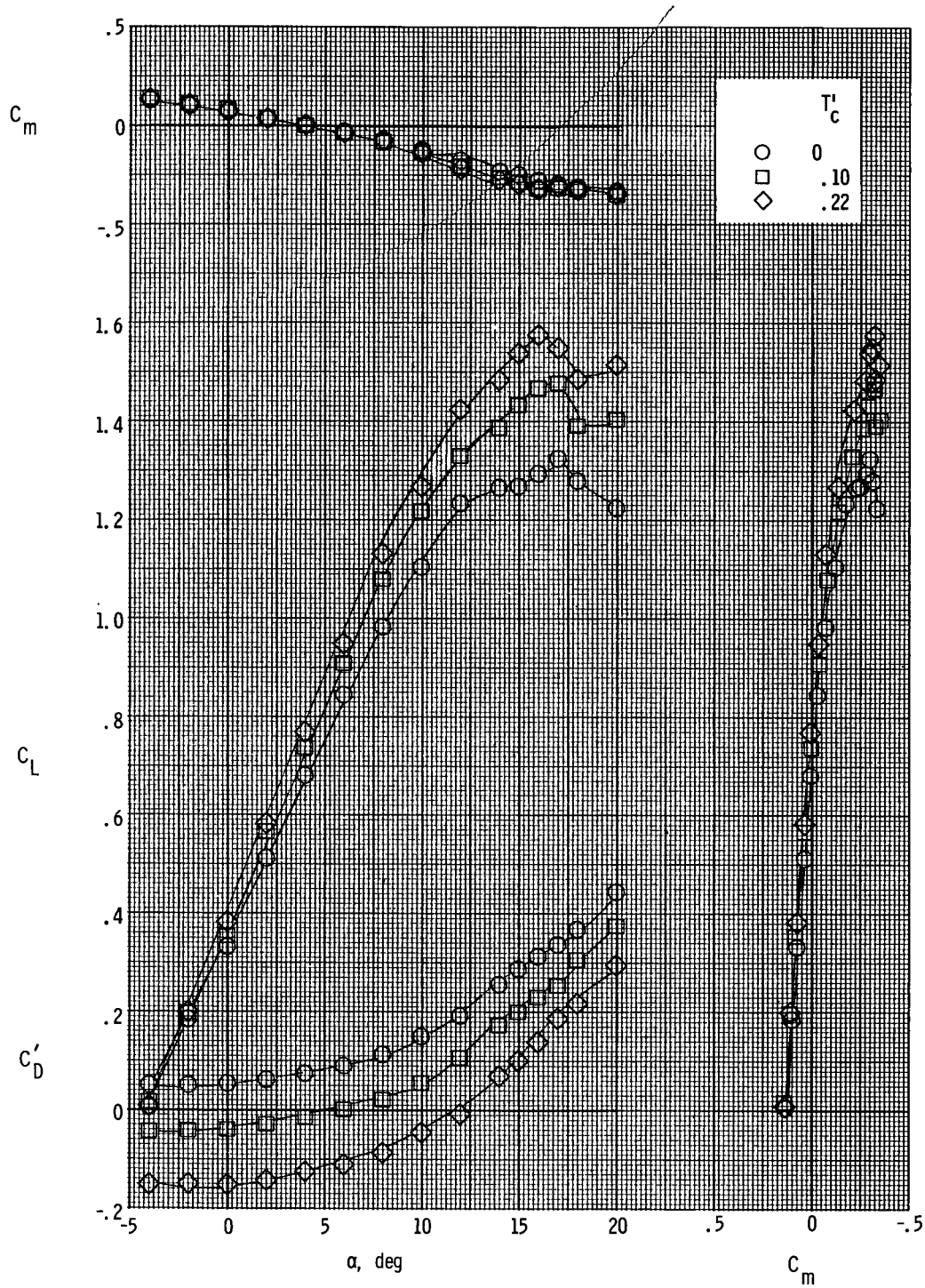

(a) Right propeller powered, left windmilling.

Figure 25.- Longitudinal aerodynamic characteristics of the model with asymmetric power. $\beta = 0^o$; $\delta_f = 0^o$.

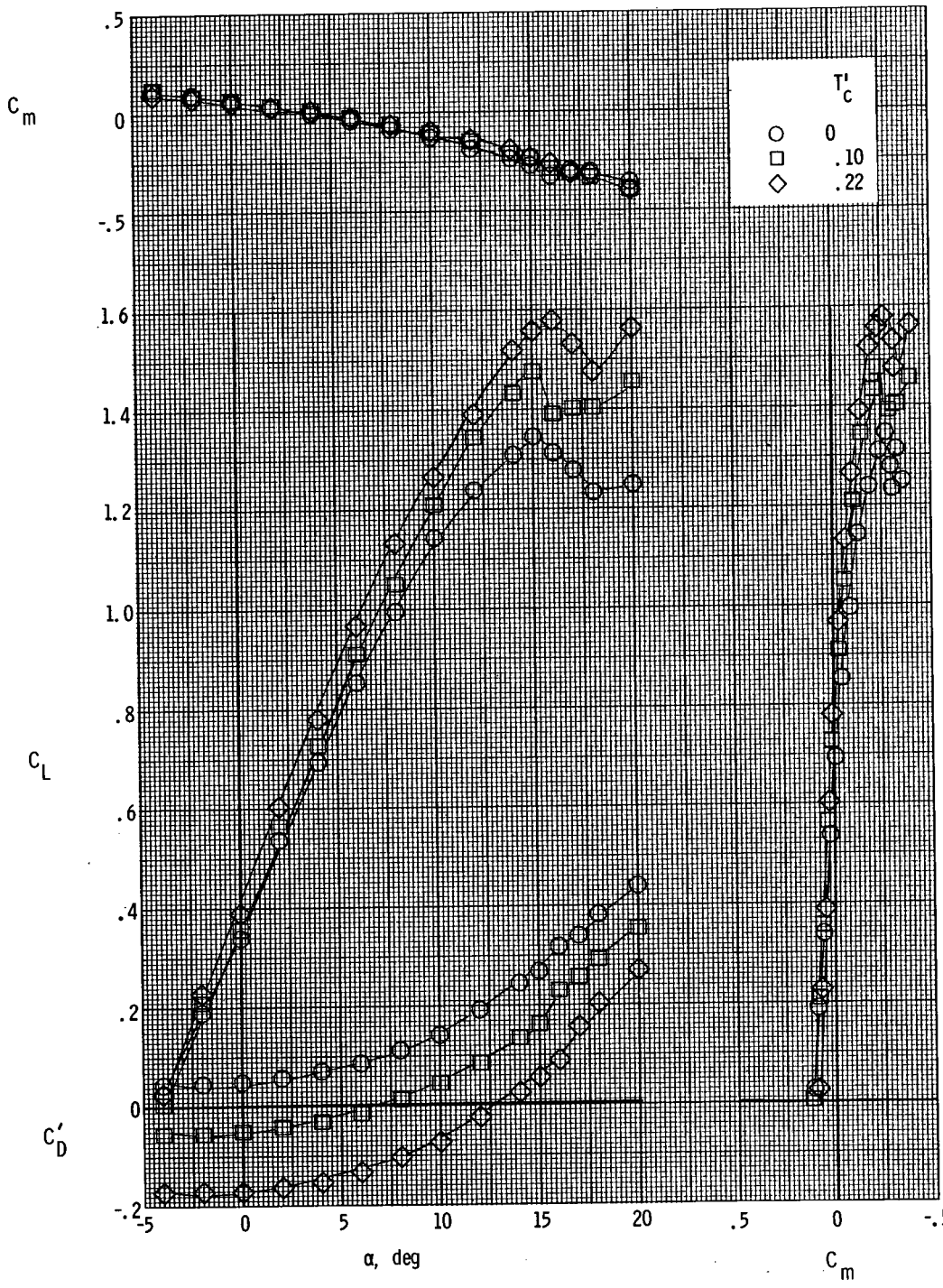

(b) Left propeller powered, right windmilling.

Figure 25.- Concluded.

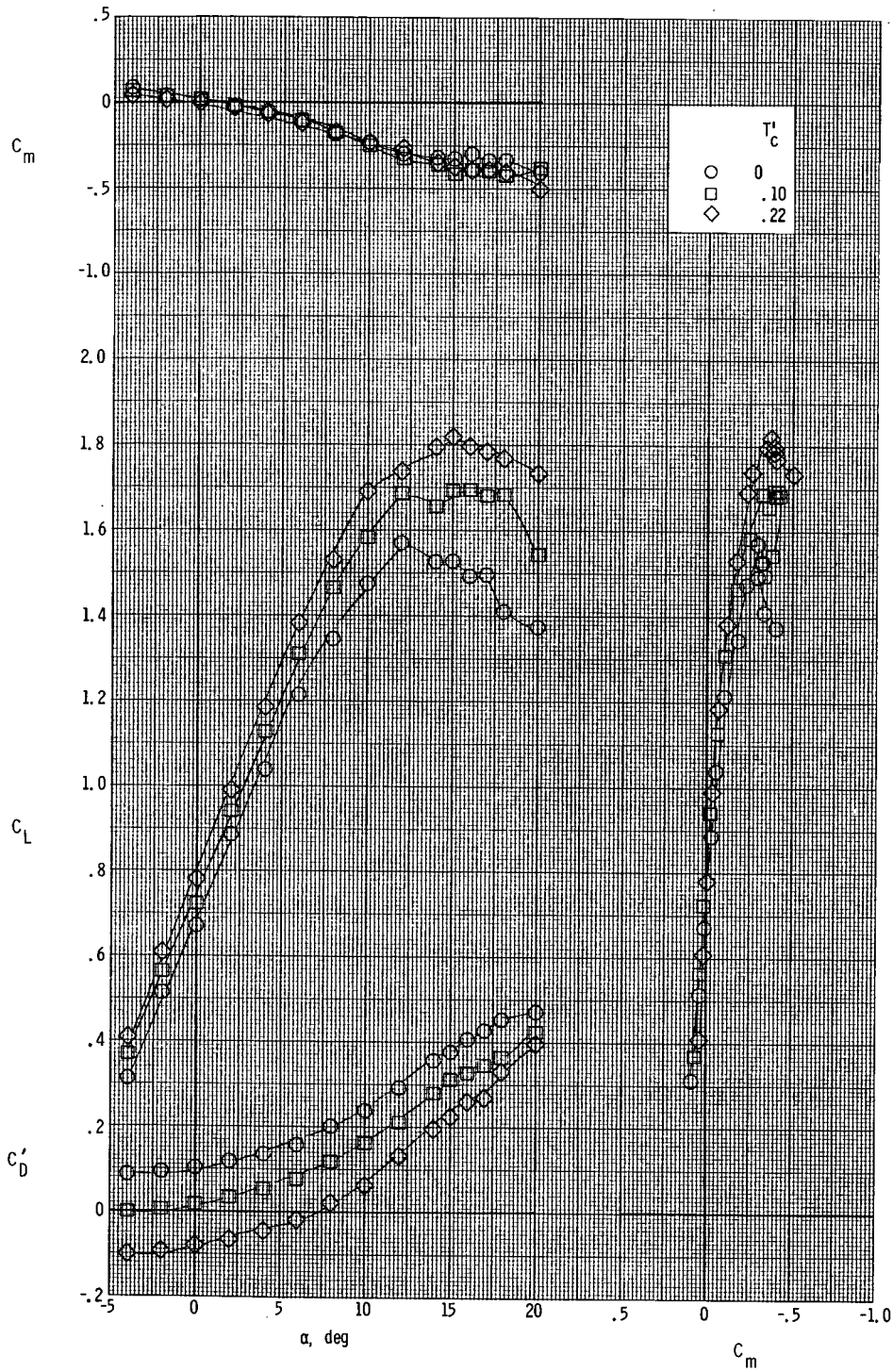

(a) Right propeller powered, left windmilling.

Figure 26.- Longitudinal aerodynamic characteristics of the model with asymmetric power. $\beta = 0^o$; $\delta_f = 27^o$.

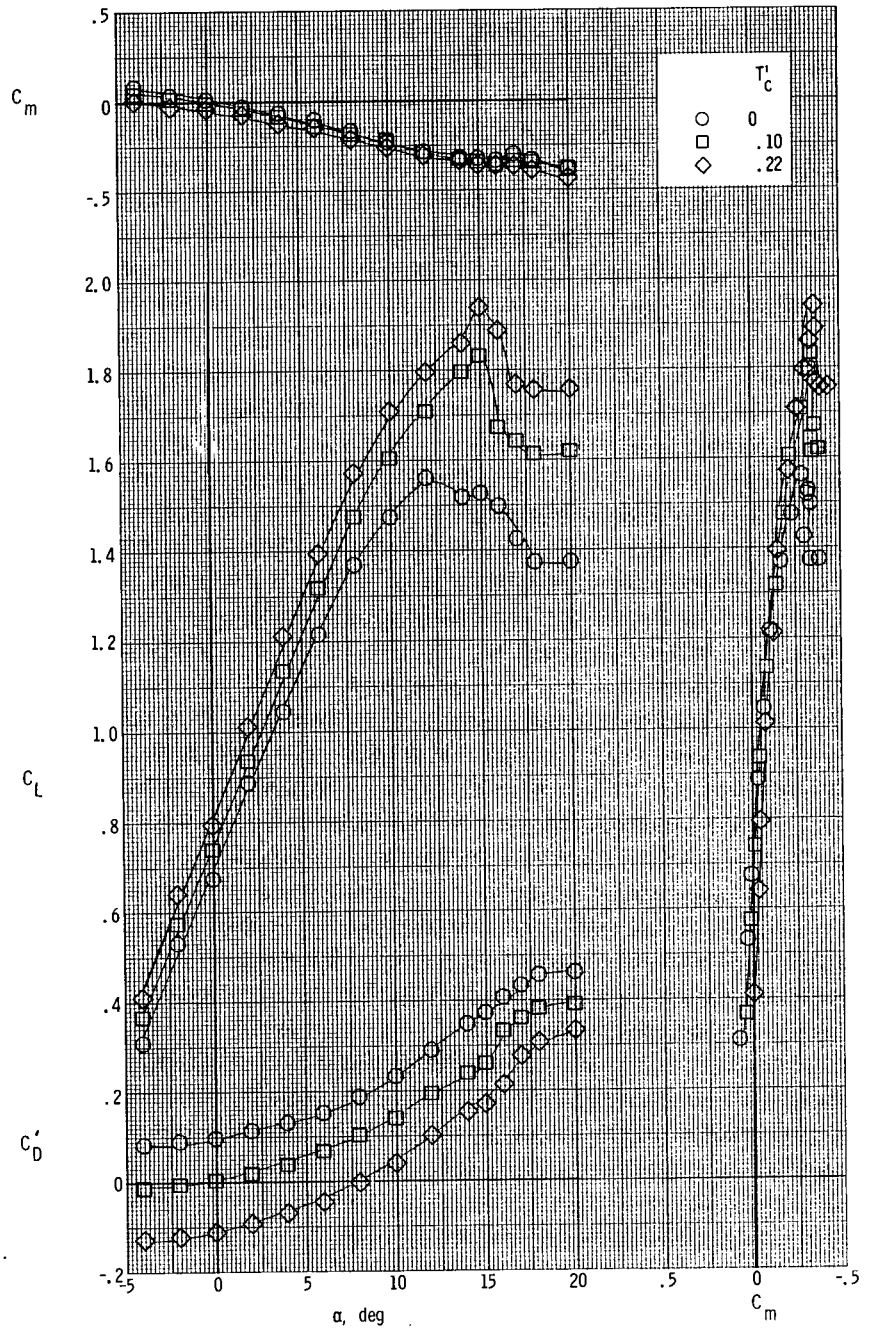

(b) Left propeller powered, right windmilling.

Figure 26.- Concluded.

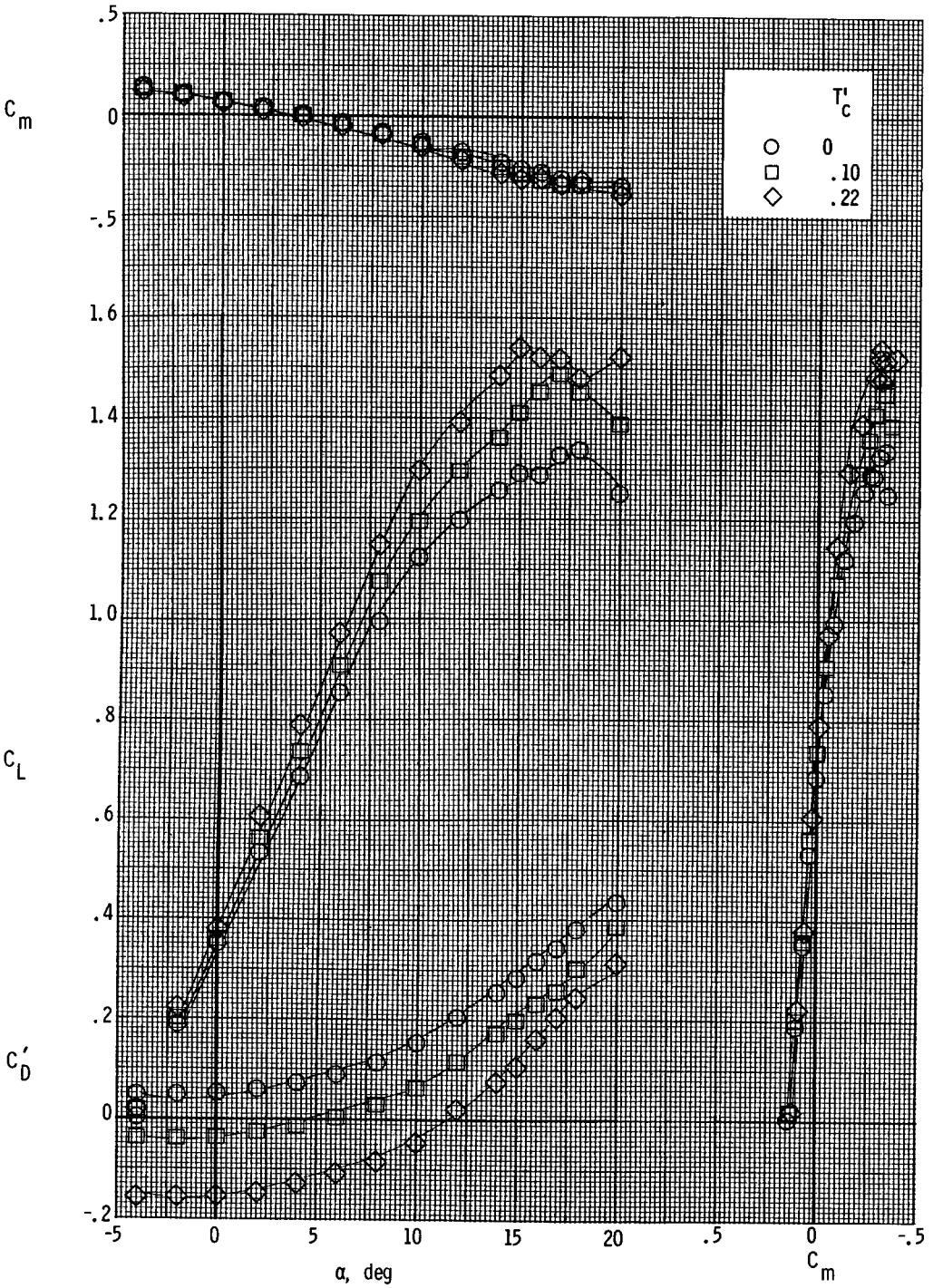

(a) Right propeller powered, left windmilling.

Figure 27.- Longitudinal aerodynamic characteristics of the model with asymmetric power and the vertical tail removed. $\beta = 0^o$; $\delta_f = 0^o$.

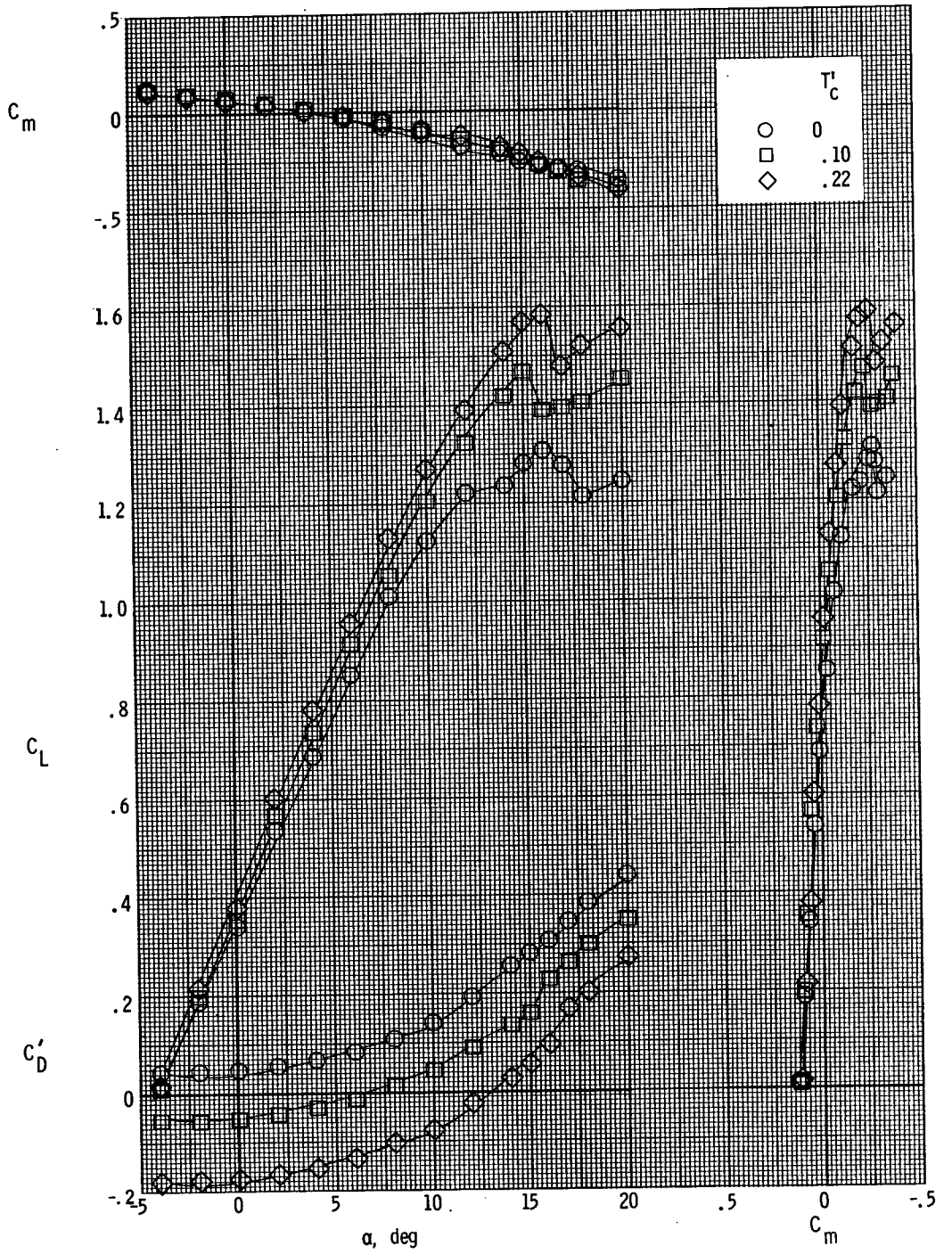

(b) Left propeller powered, right windmilling.

Figure 27.- Concluded.

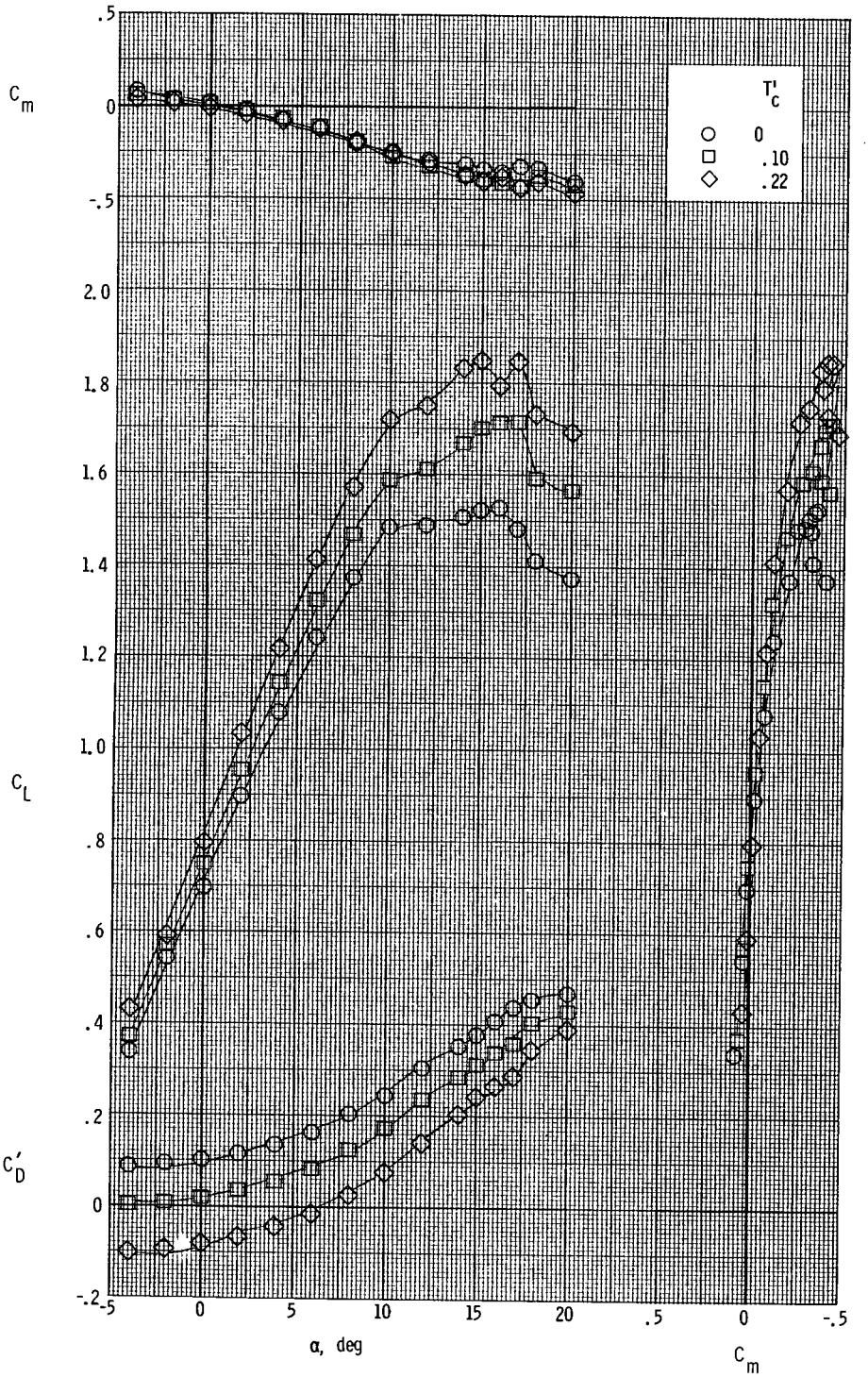

(a) Right propeller powered, left windmilling.

Figure 28.- Longitudinal aerodynamic characteristics of the model with asymmetric power and the vertical tail removed. $\beta = 0^o$; $\delta_f = 27^o$.

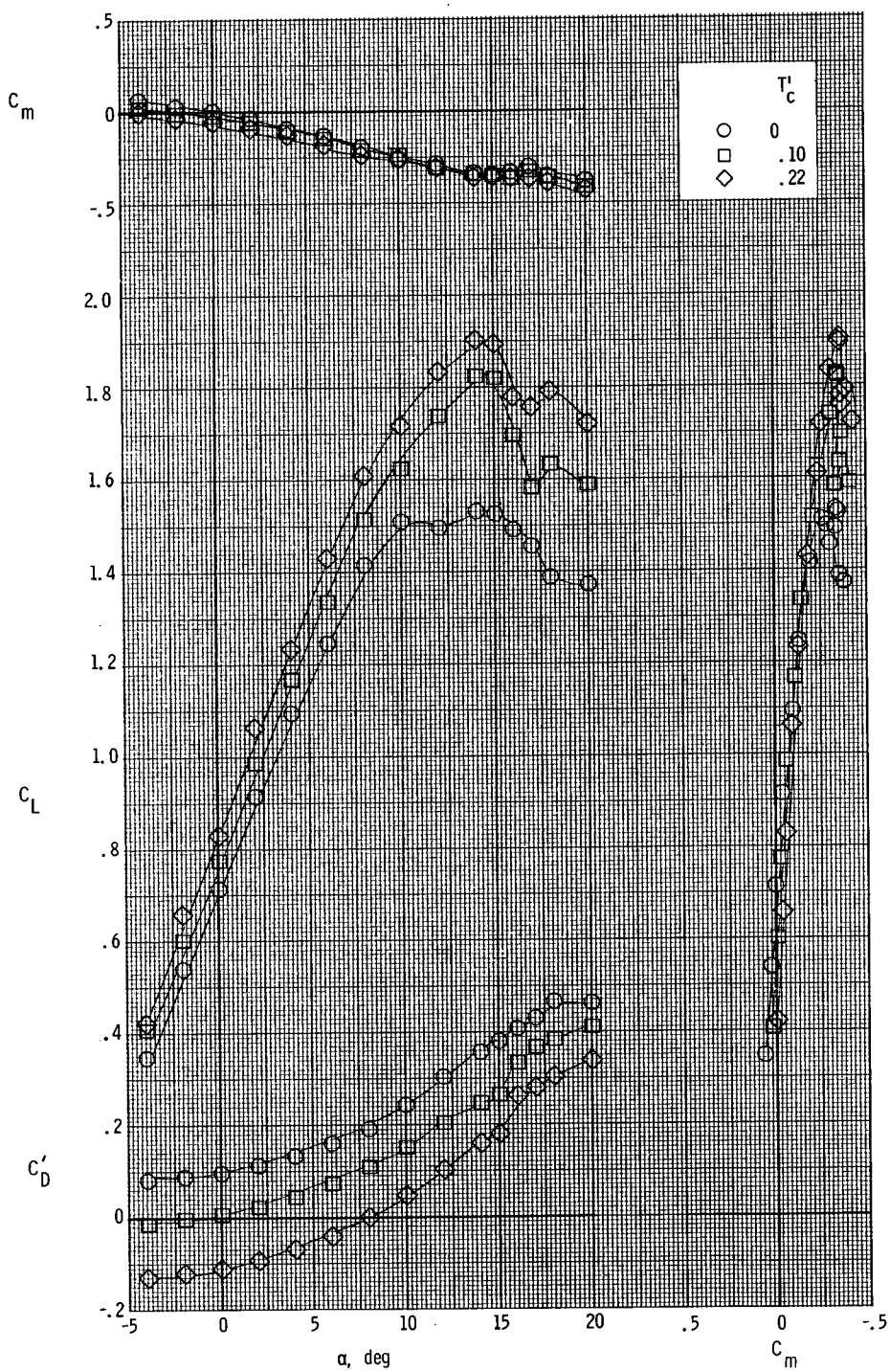

(b) Left propeller powered, right windmilling.

Figure 28.- Concluded.

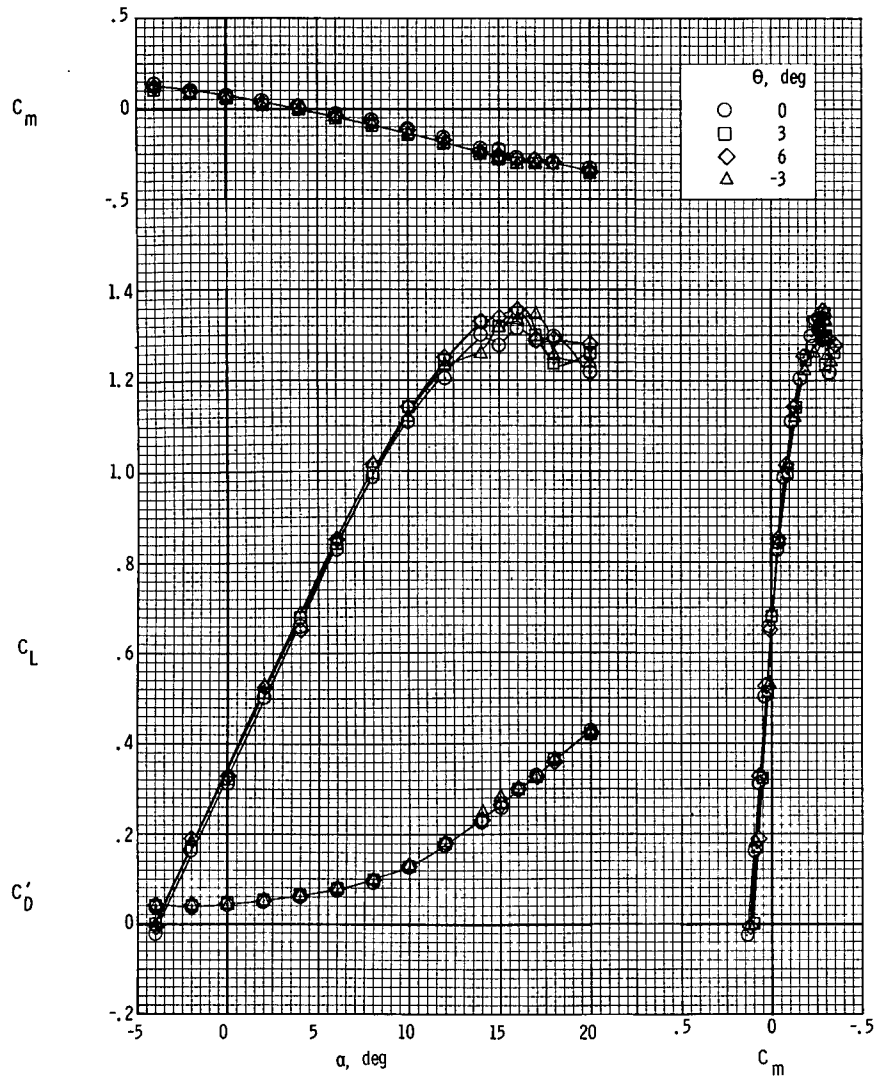

(a) $T'_C = 0$.

Figure 29.- Longitudinal aerodynamic characteristics of the model with the thrust axes pitched. $\beta = 0^o$; $\delta_f = 0^o$; nacelle A.

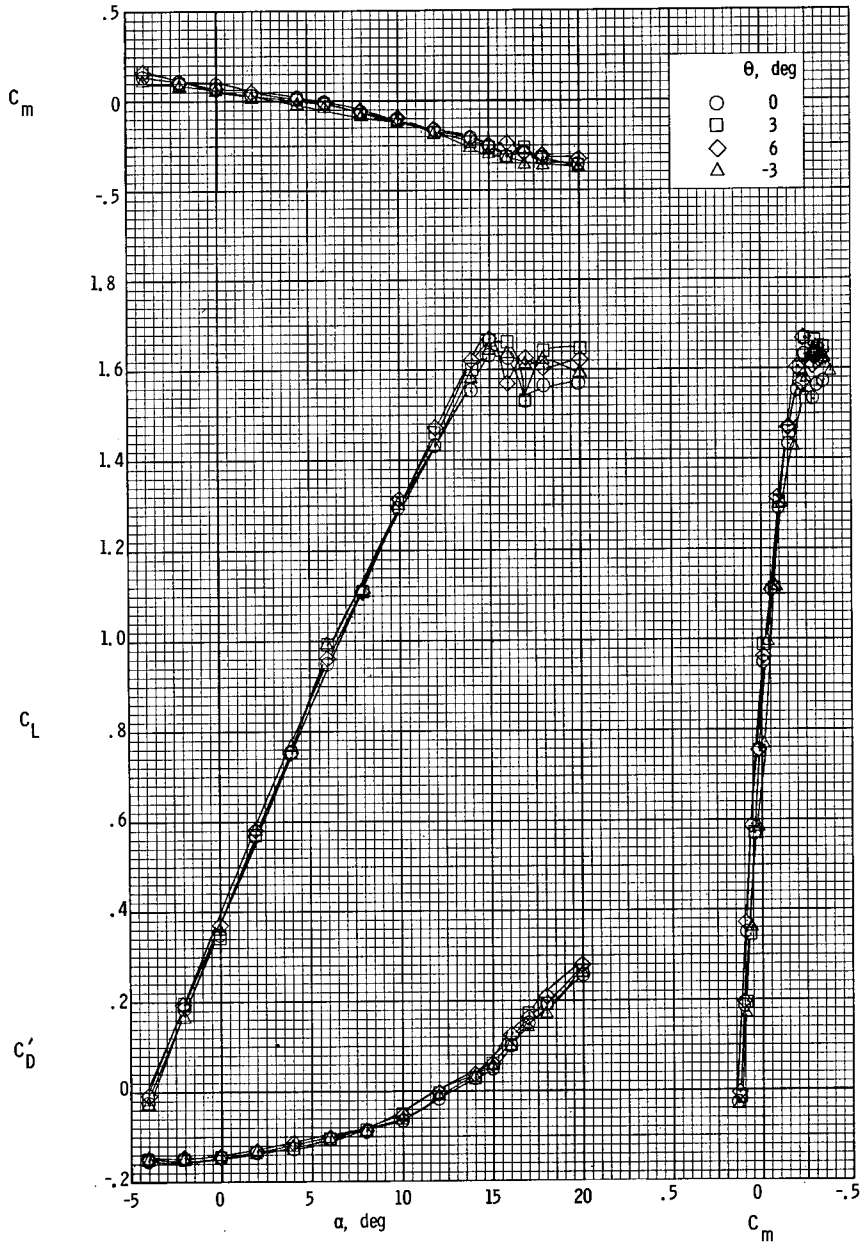

(b) $T'_c = 0.20$.

Figure 29.- Continued.

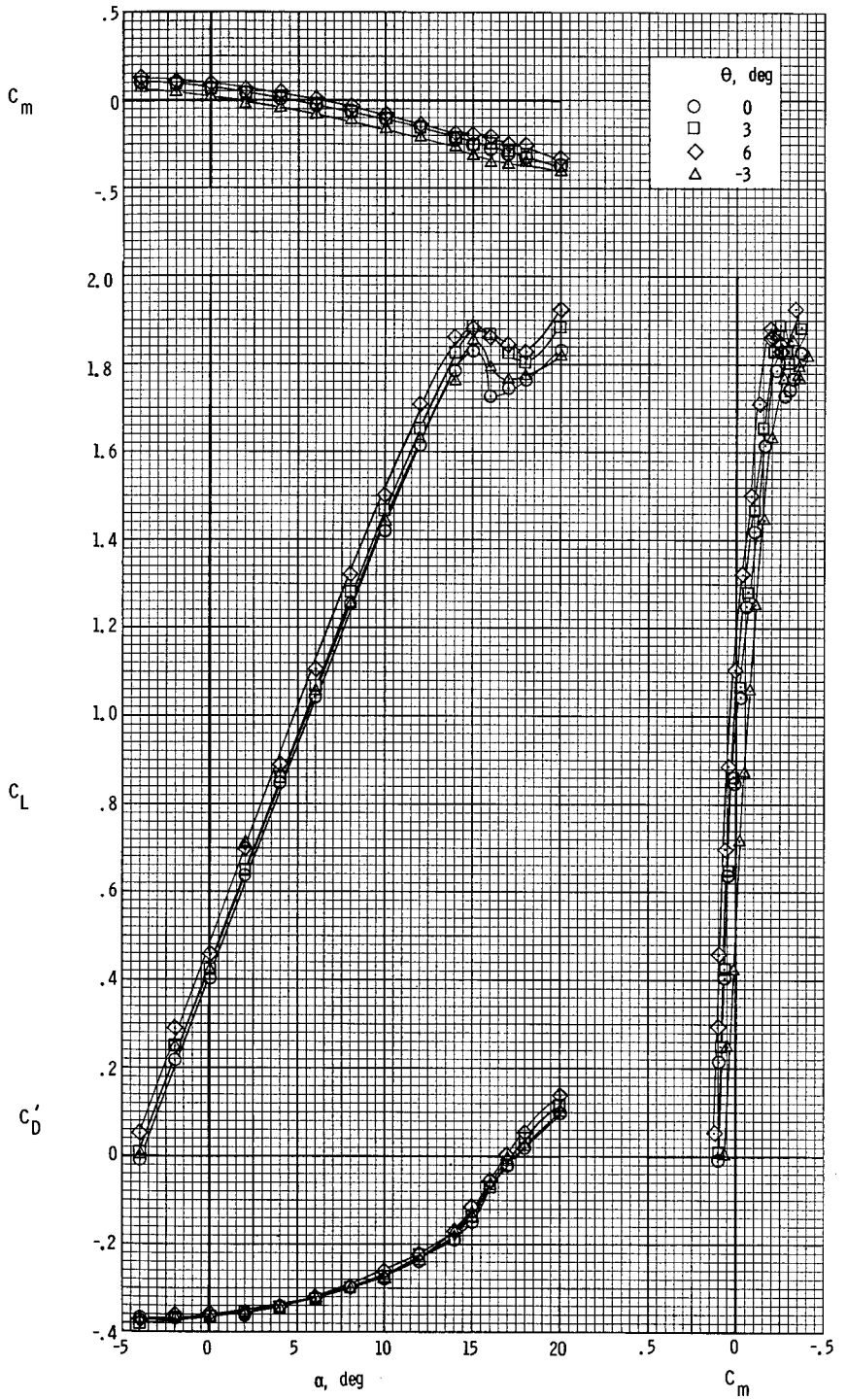

(c) $T_c' = 0.44$.

Figure 29.- Concluded.

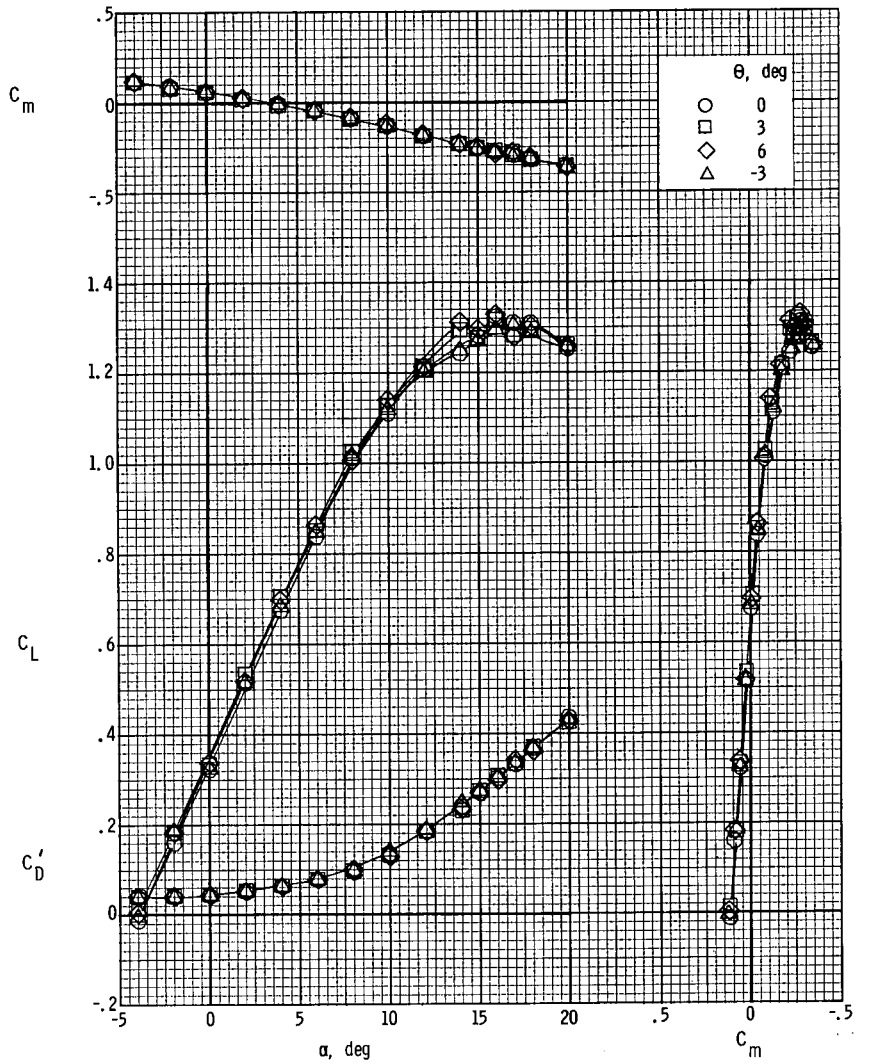

(a) $T_c' = 0$.

Figure 30.- Longitudinal aerodynamic characteristics of the model with thrust axes pitched and with down-at-the-center propeller rotation. $\beta = 0^o$; $\delta_f = 0^o$; nacelle A.

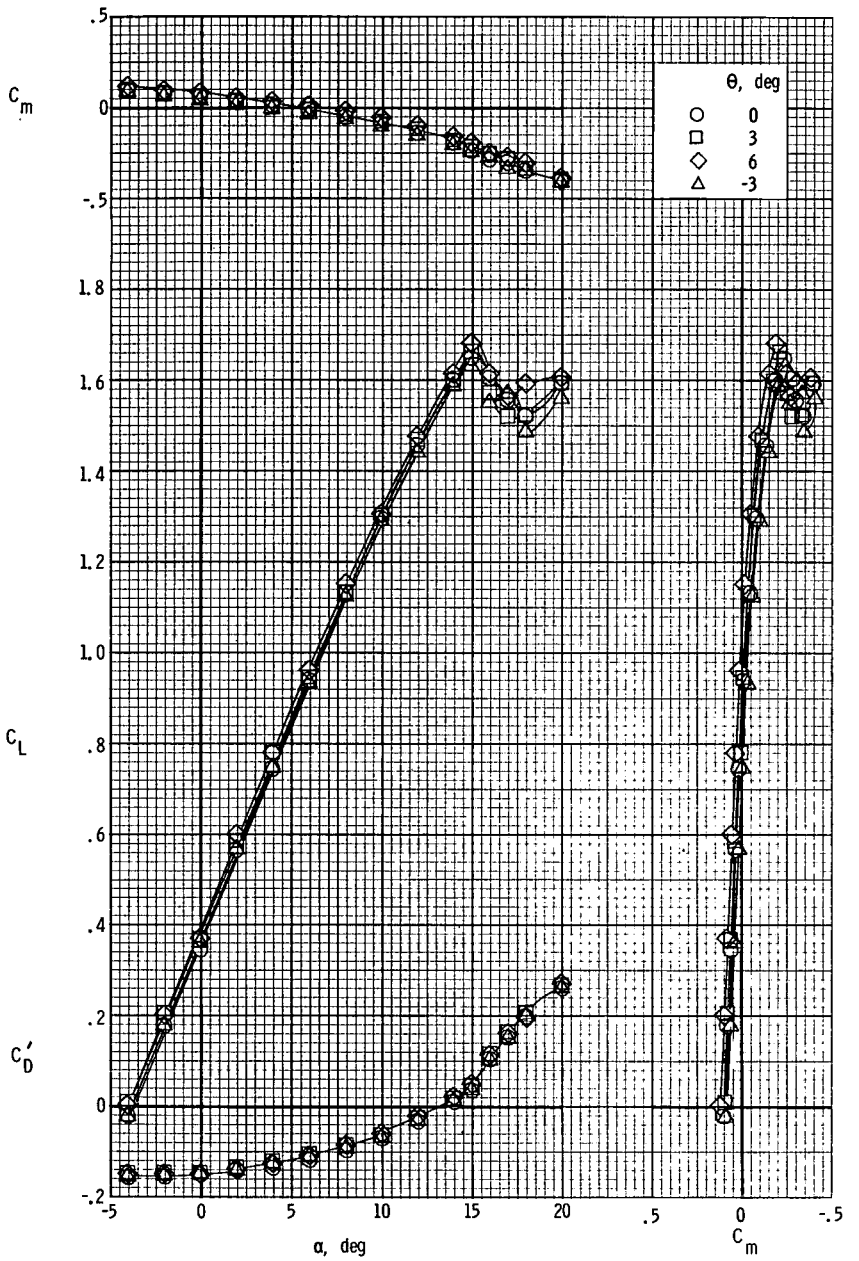

(b) $T_c' = 0.20$.

Figure 30.- Continued.

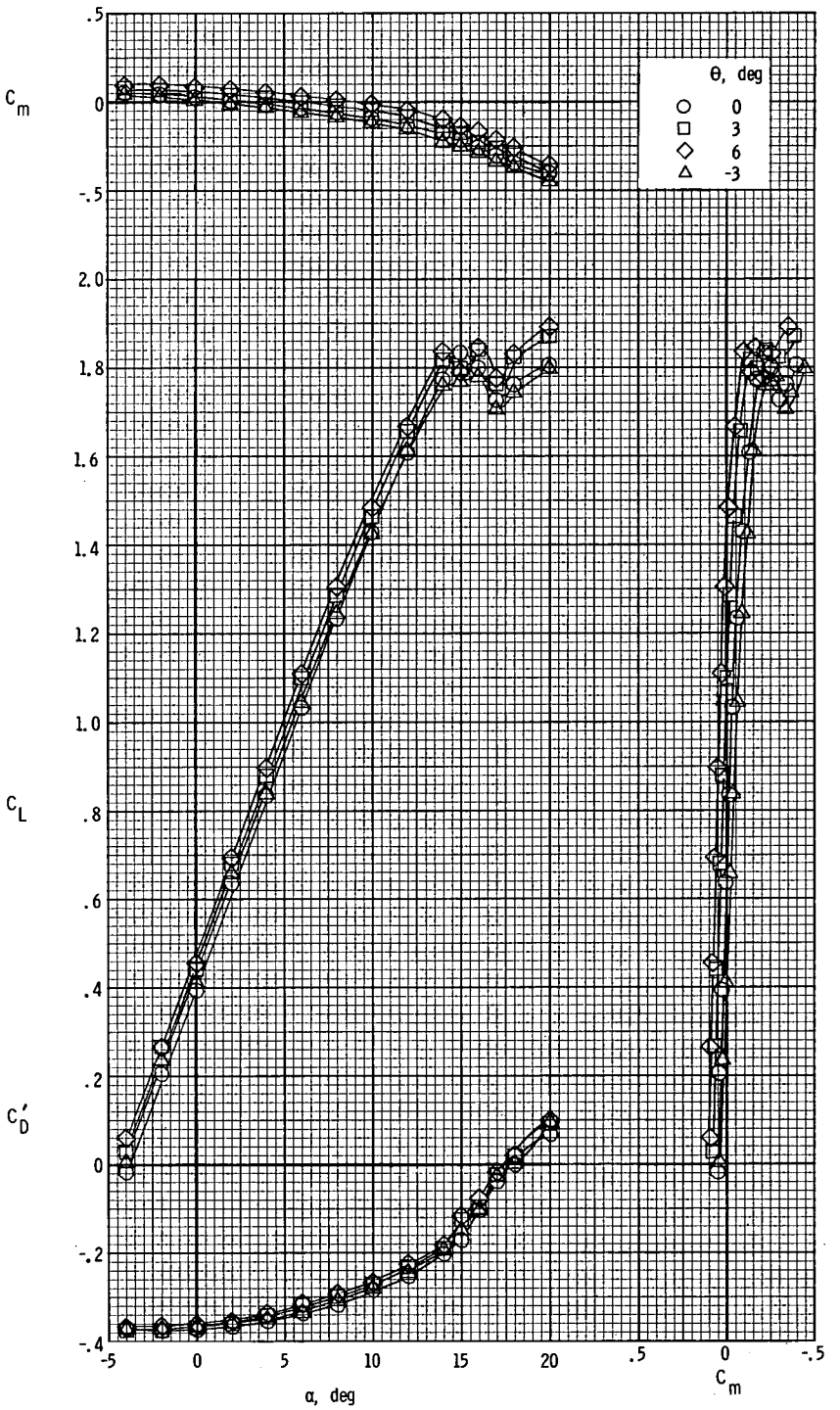

(c) $T_c' = 0.44$.

Figure 30.- Concluded.

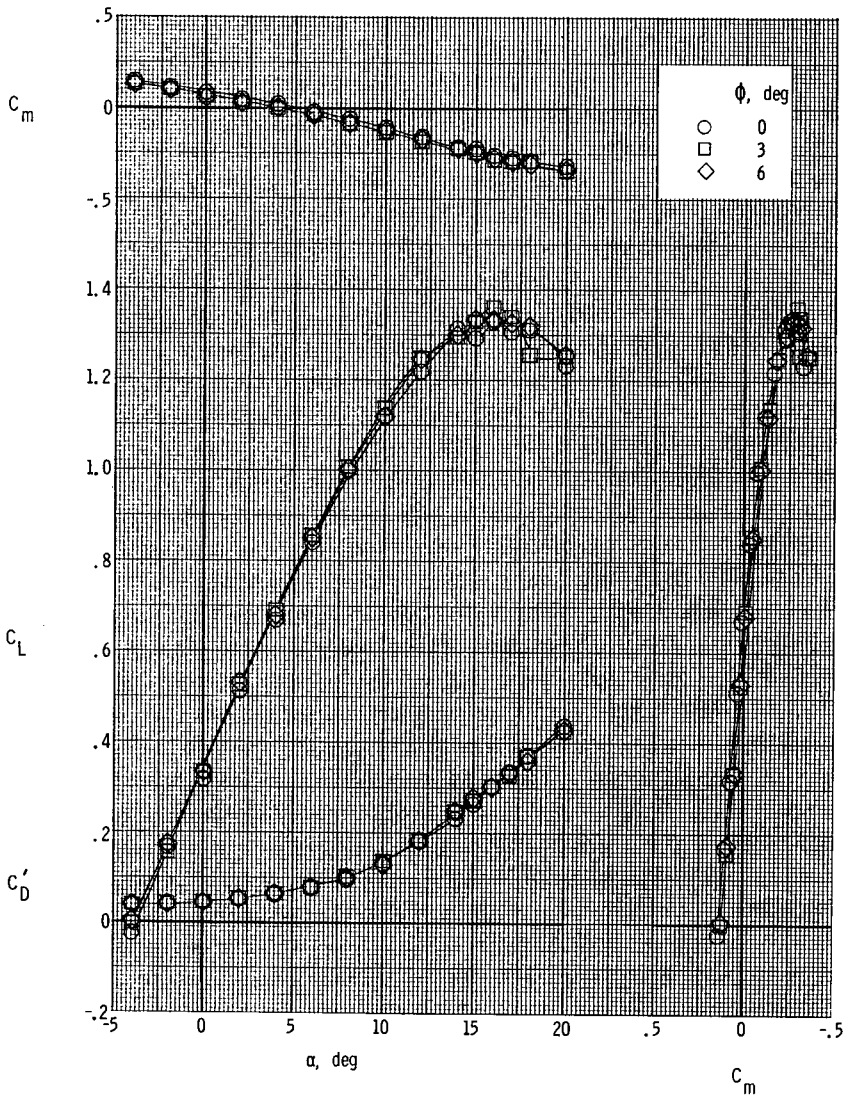

(a) $T_c' = 0$.

Figure 31.- Longitudinal aerodynamic characteristics of the basic model with toed-out thrust axes. $\beta = 0^o$; $\delta_f = 0^o$; nacelle A.

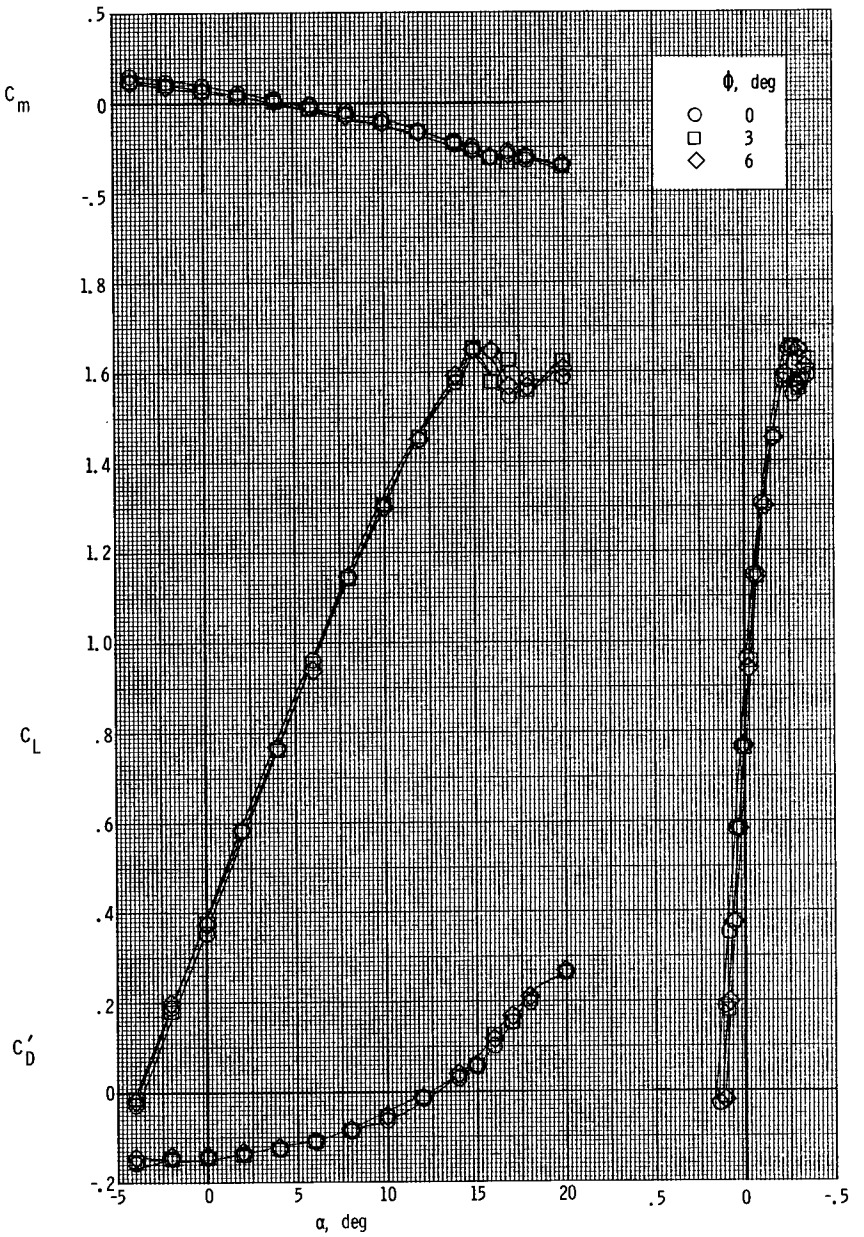

(b) $T_C' = 0.20$.

Figure 31.- Continued.

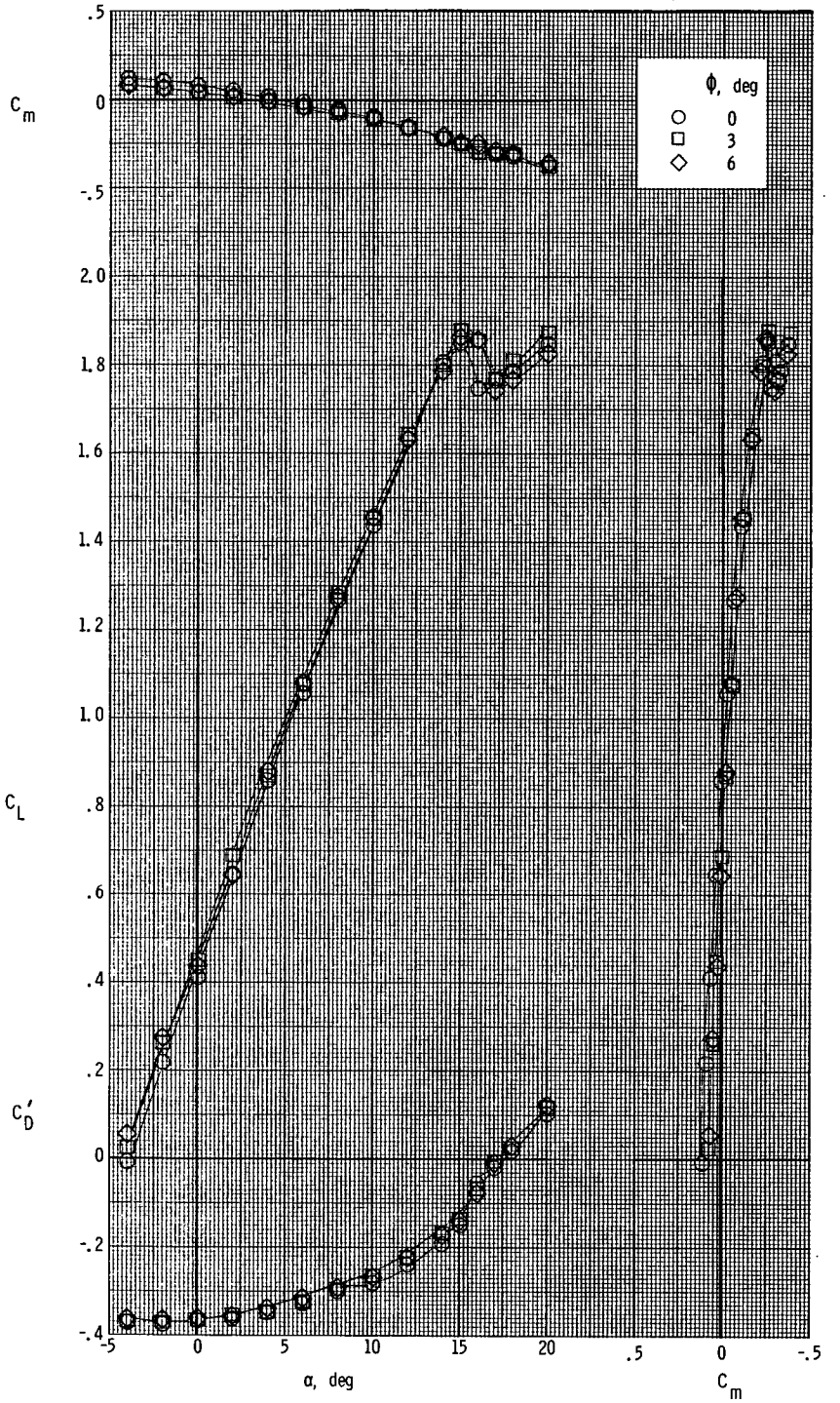

(c) $T_c' = 0.44$.

Figure 31.- Concluded.

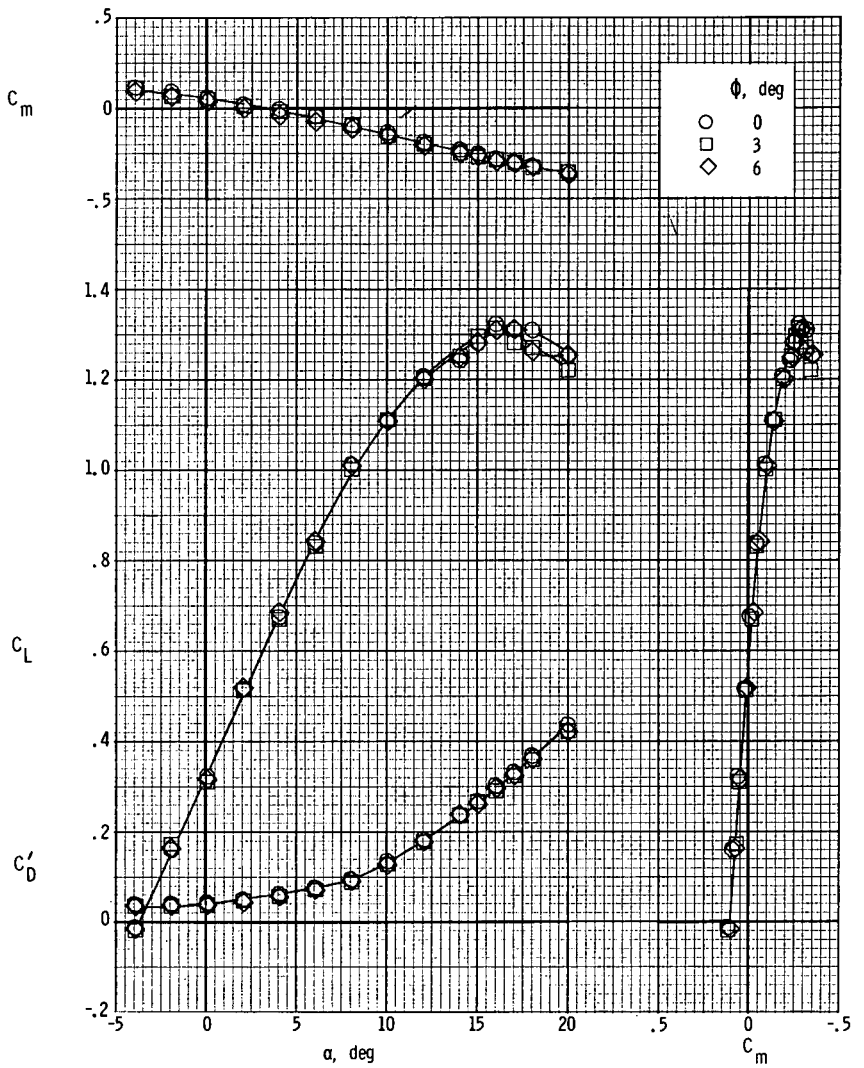

(a) $T'_c = 0$.

Figure 32.- Longitudinal aerodynamic characteristics of the model with toed-out thrust axes and down-at-the-center propeller rotation. $\beta = 0^o$; $\delta_f = 0^o$; nacelle A.

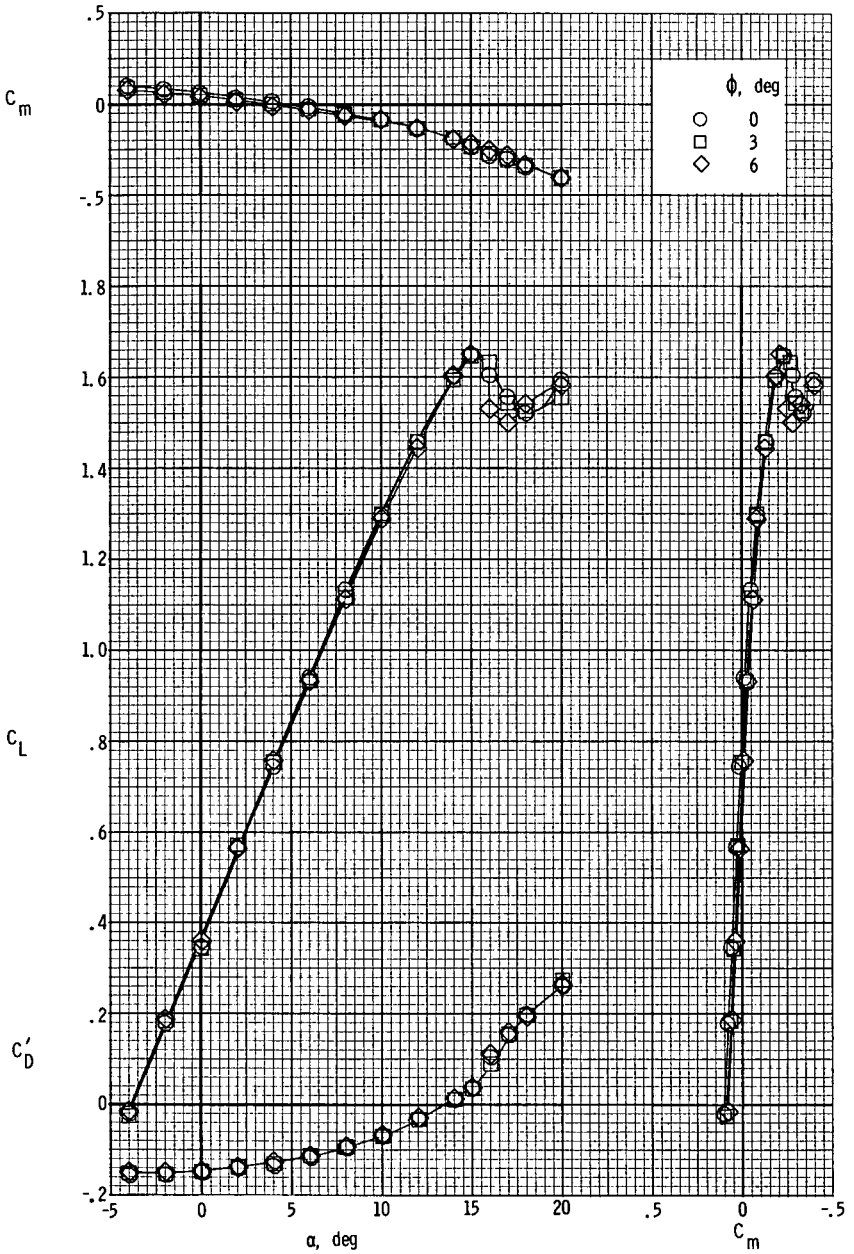

(b) $T'_c = 0.20$.

Figure 32.- Continued.

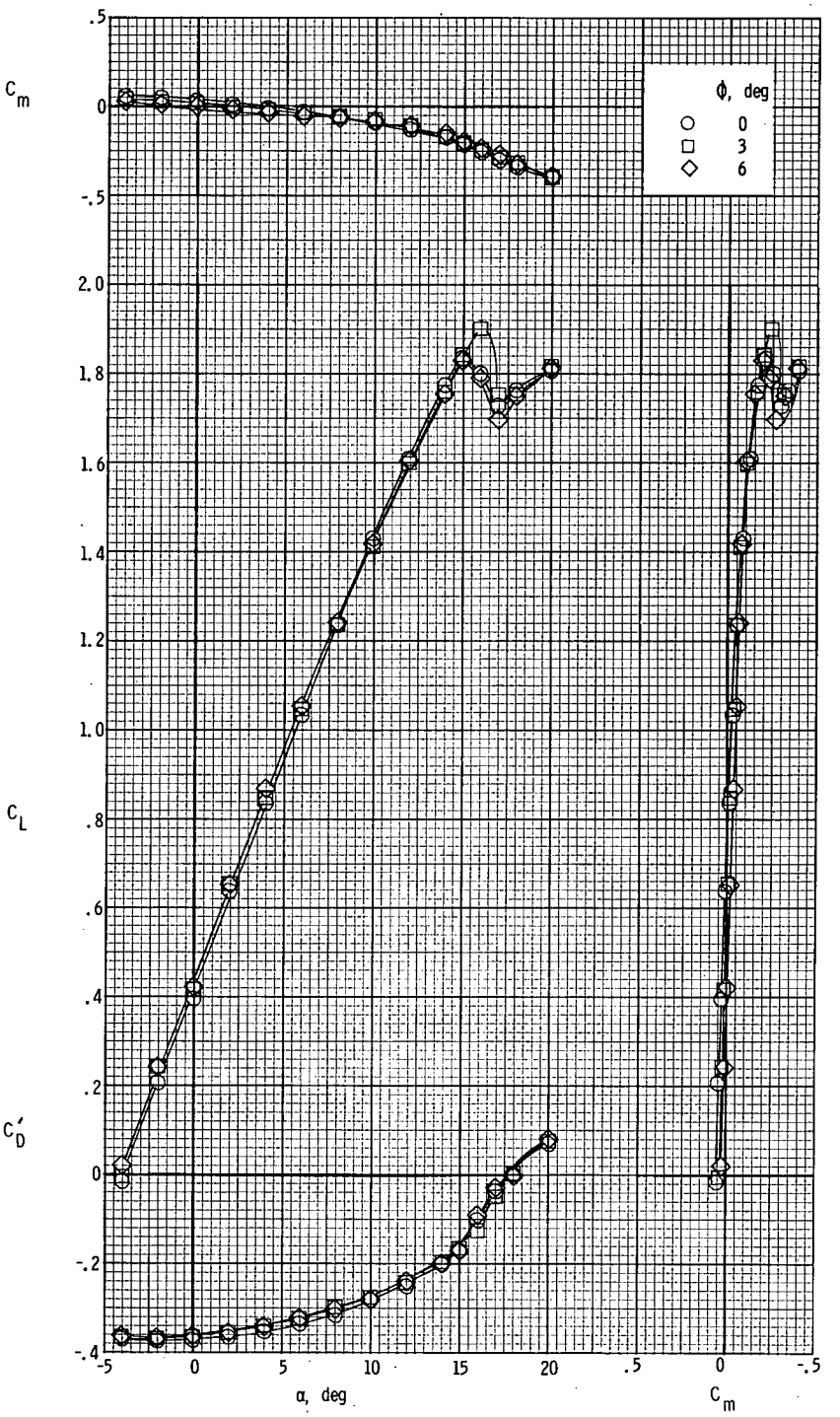

(c) $T_c' = 0.44$.

Figure 32.- Concluded.

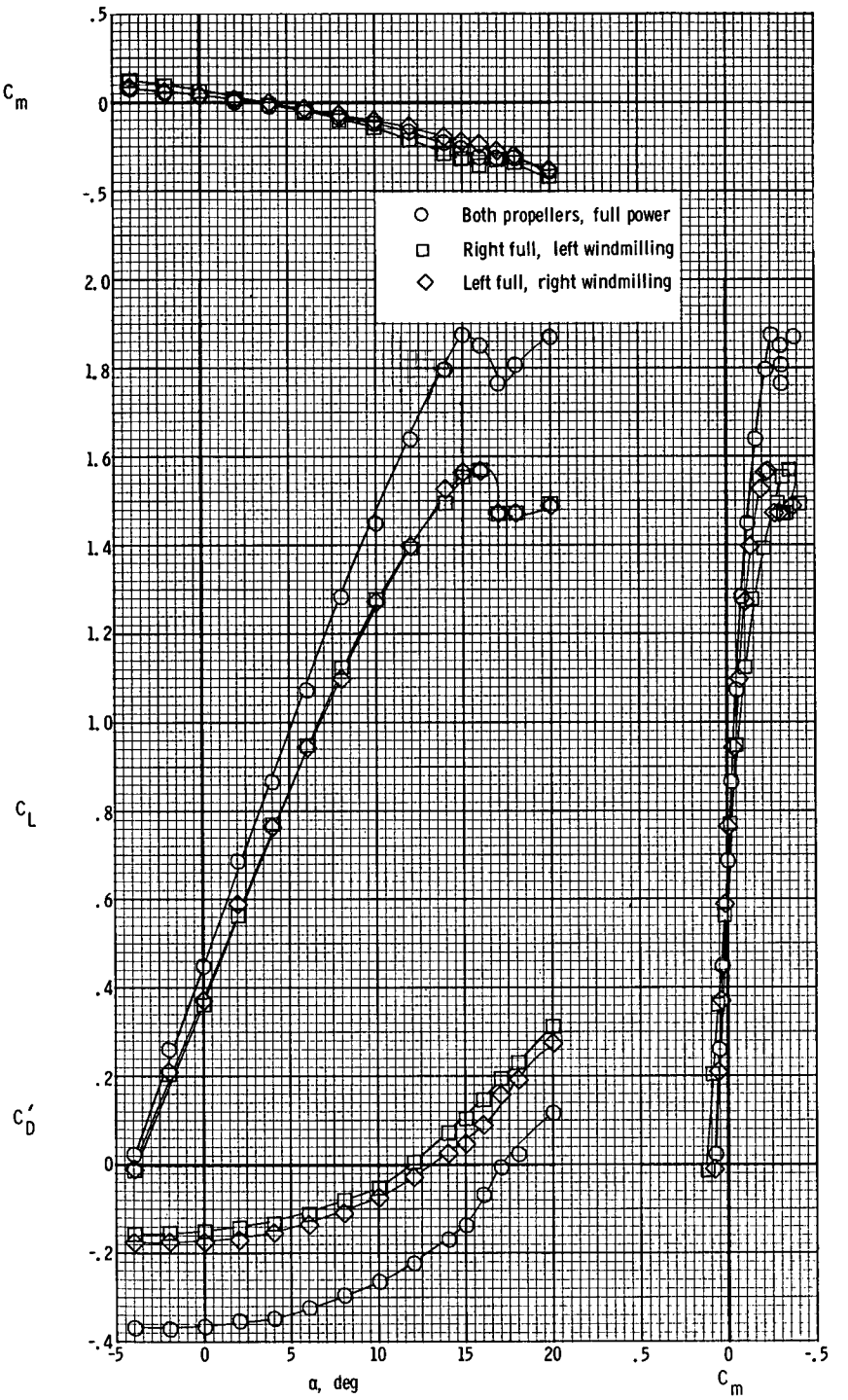

(a) $\phi = 3^{\circ}$.

Figure 33.- Longitudinal aerodynamic characteristics of the model with toed-out thrust axes and asymmetric power. $\beta = 0^{\circ}$; $\delta_f = 0^{\circ}$; nacelle A.

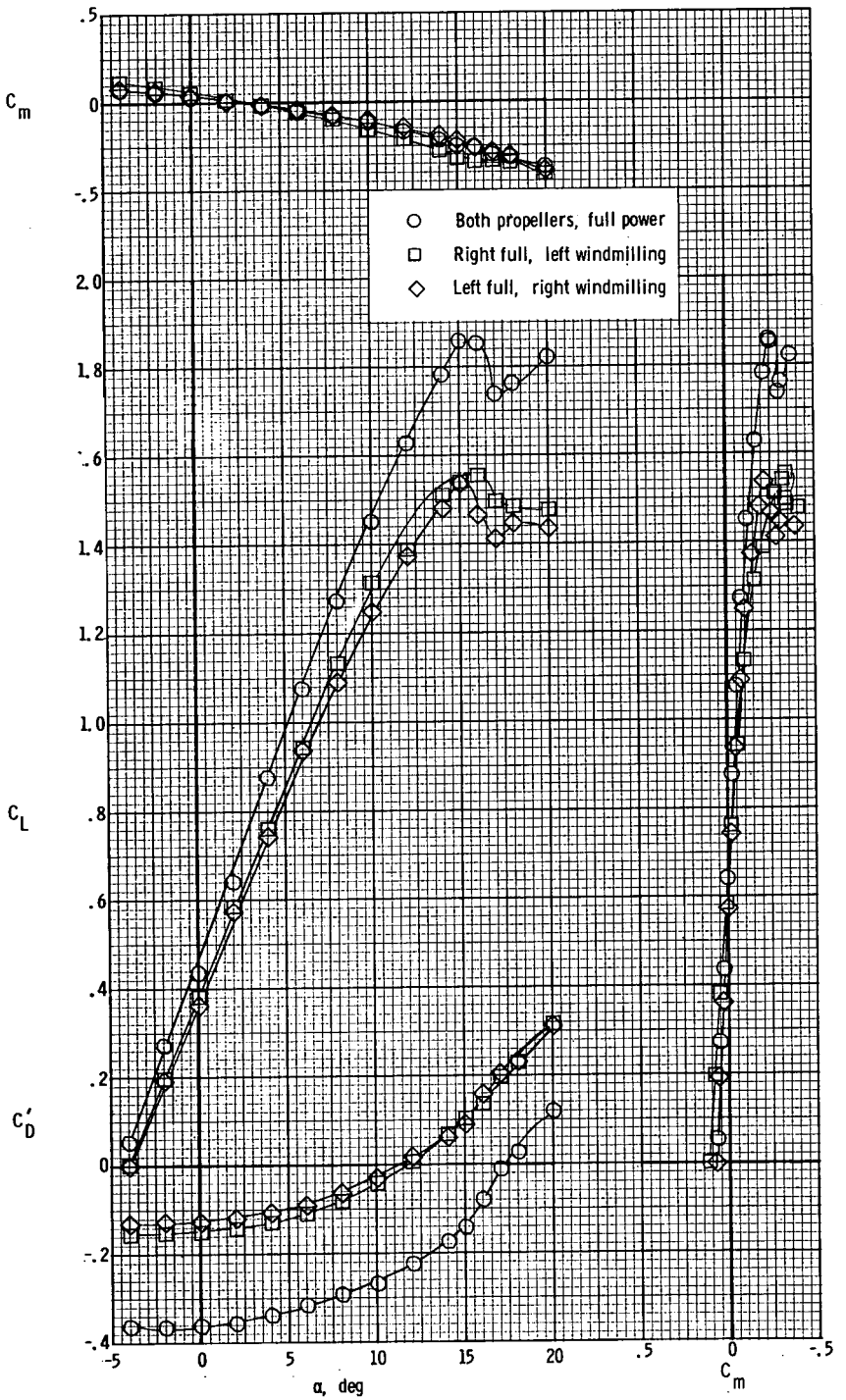

(b) $\phi = 6^{o}$.

Figure 33.- Concluded.

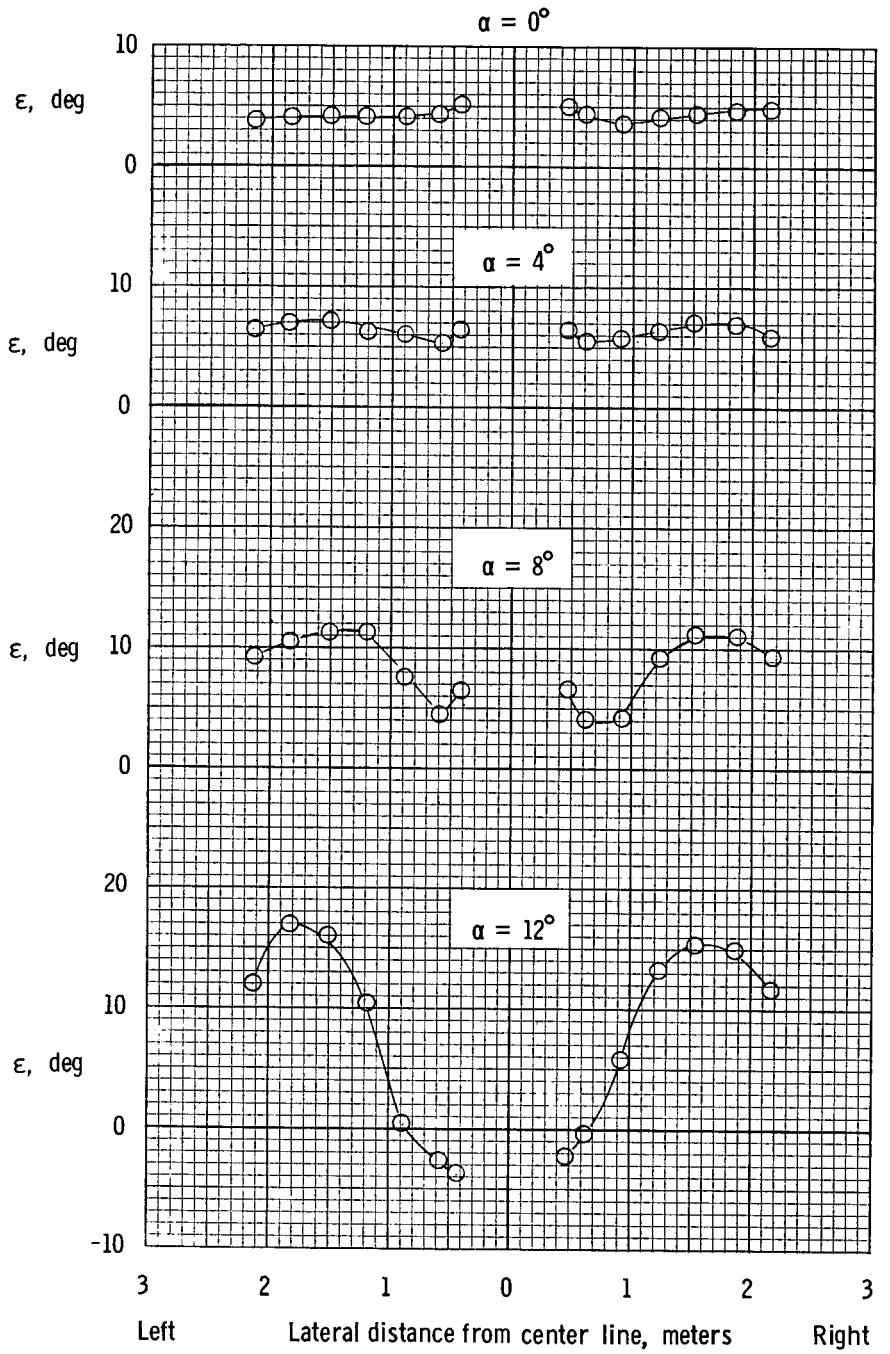

(a) $\delta_f = 0^o$.

Figure 34.- Distribution of downwash angle across span of horizontal-tail surface with propellers removed. $\beta = 0^o$.

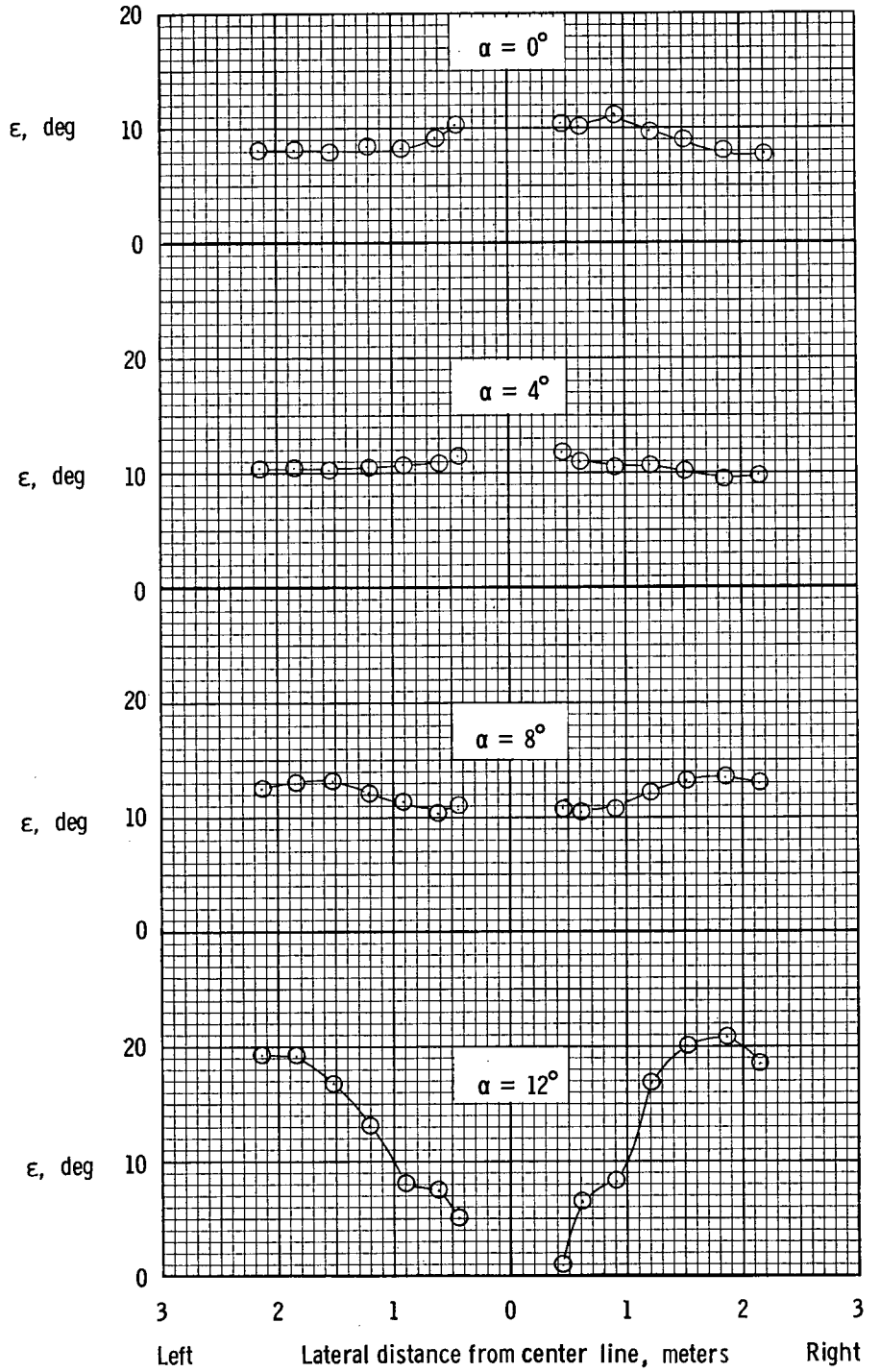

(b) $\delta_f = 27^\circ$.

Figure 34.- Concluded.

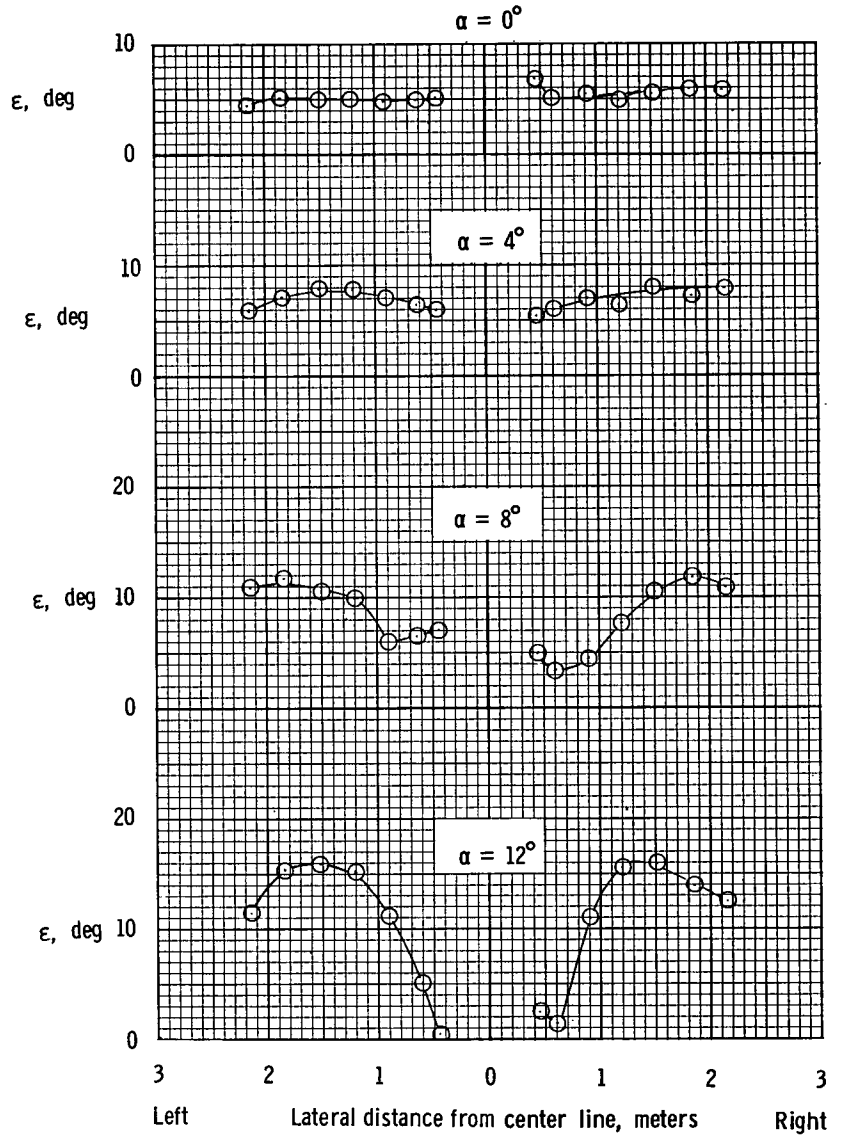

(a) $T_c' = 0$.

Figure 35.- Distribution of downwash angle across span of horizontal-tail surface. $\delta_f = 0^o$; $\beta = 0^o$; nacelle A.

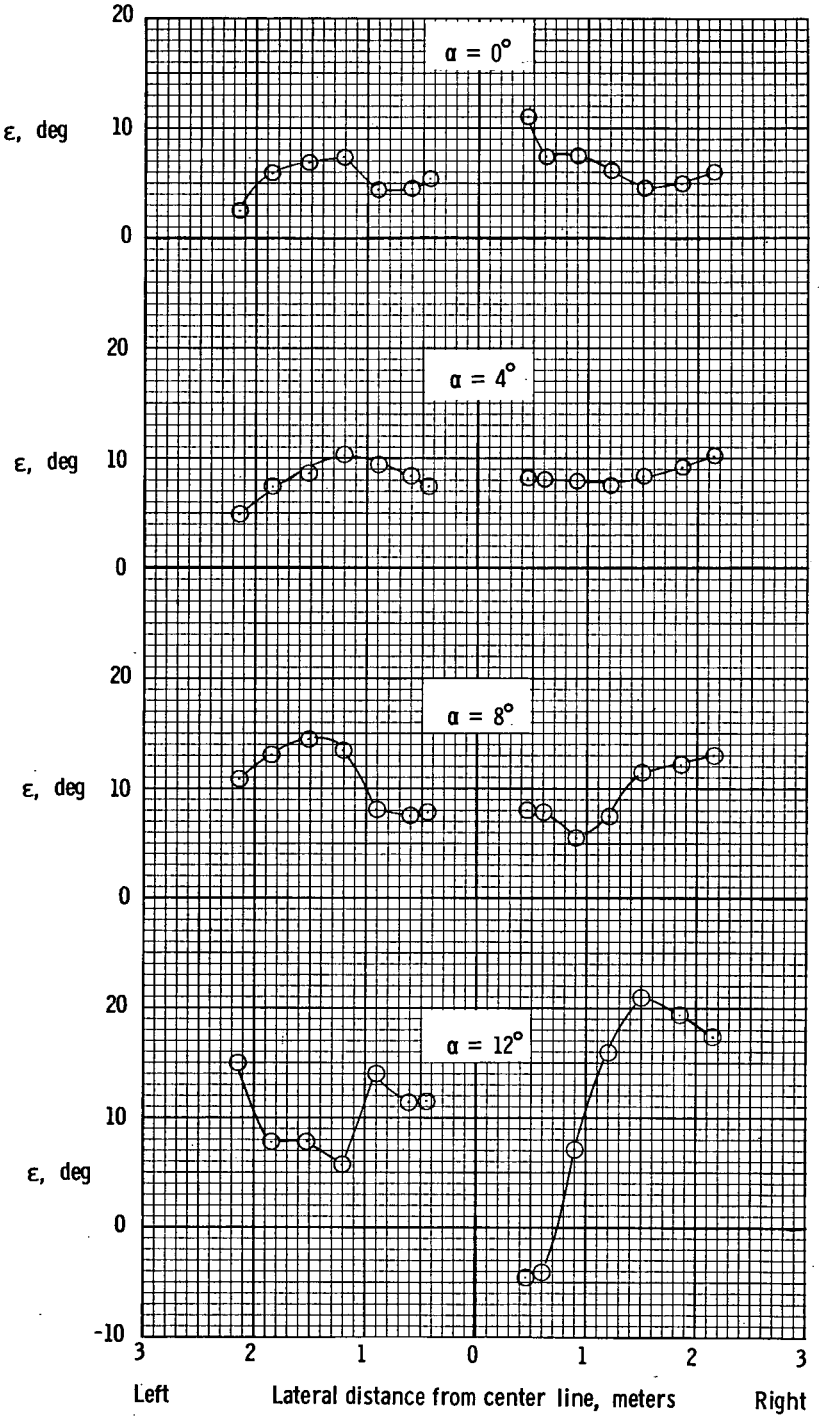

(b) $T_c' = 0.20$.

Figure 35.- Continued.

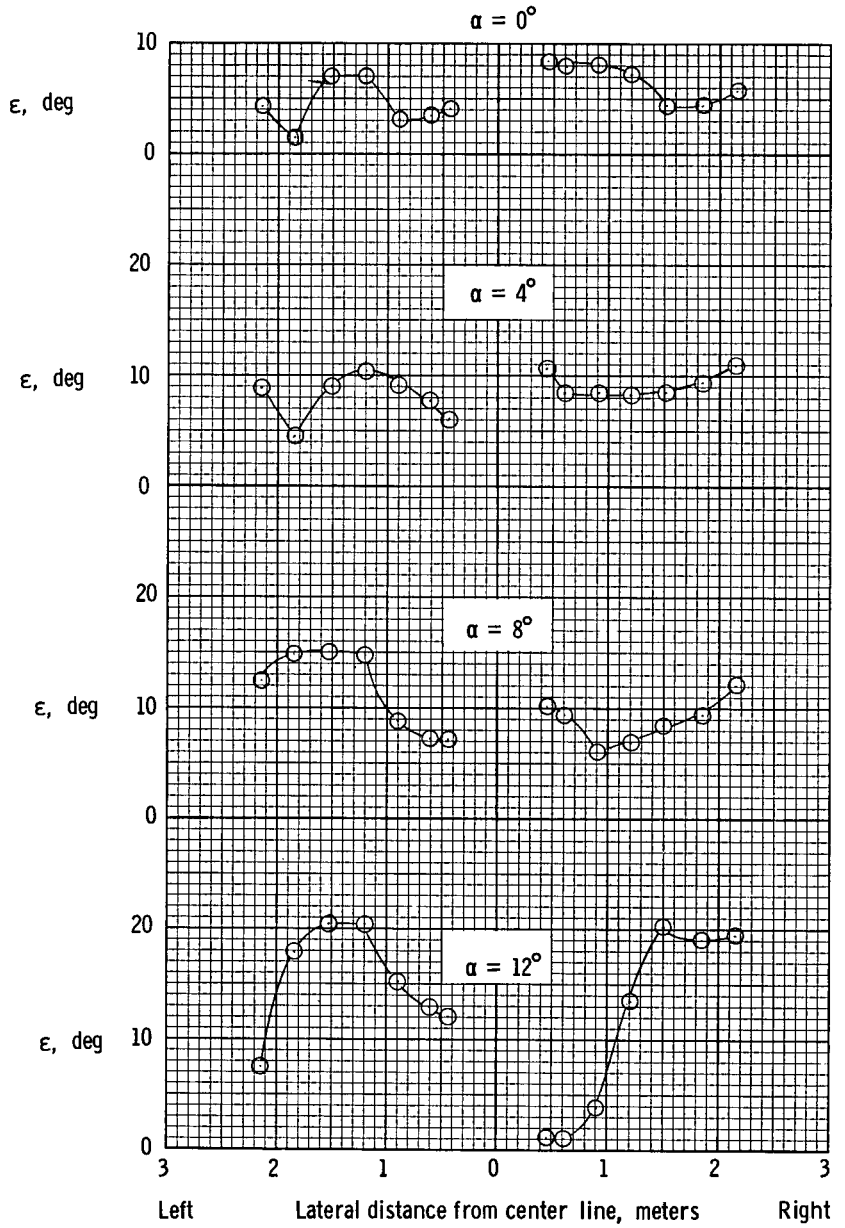

(c) $T_c' = 0.44$.

Figure 35.- Concluded.

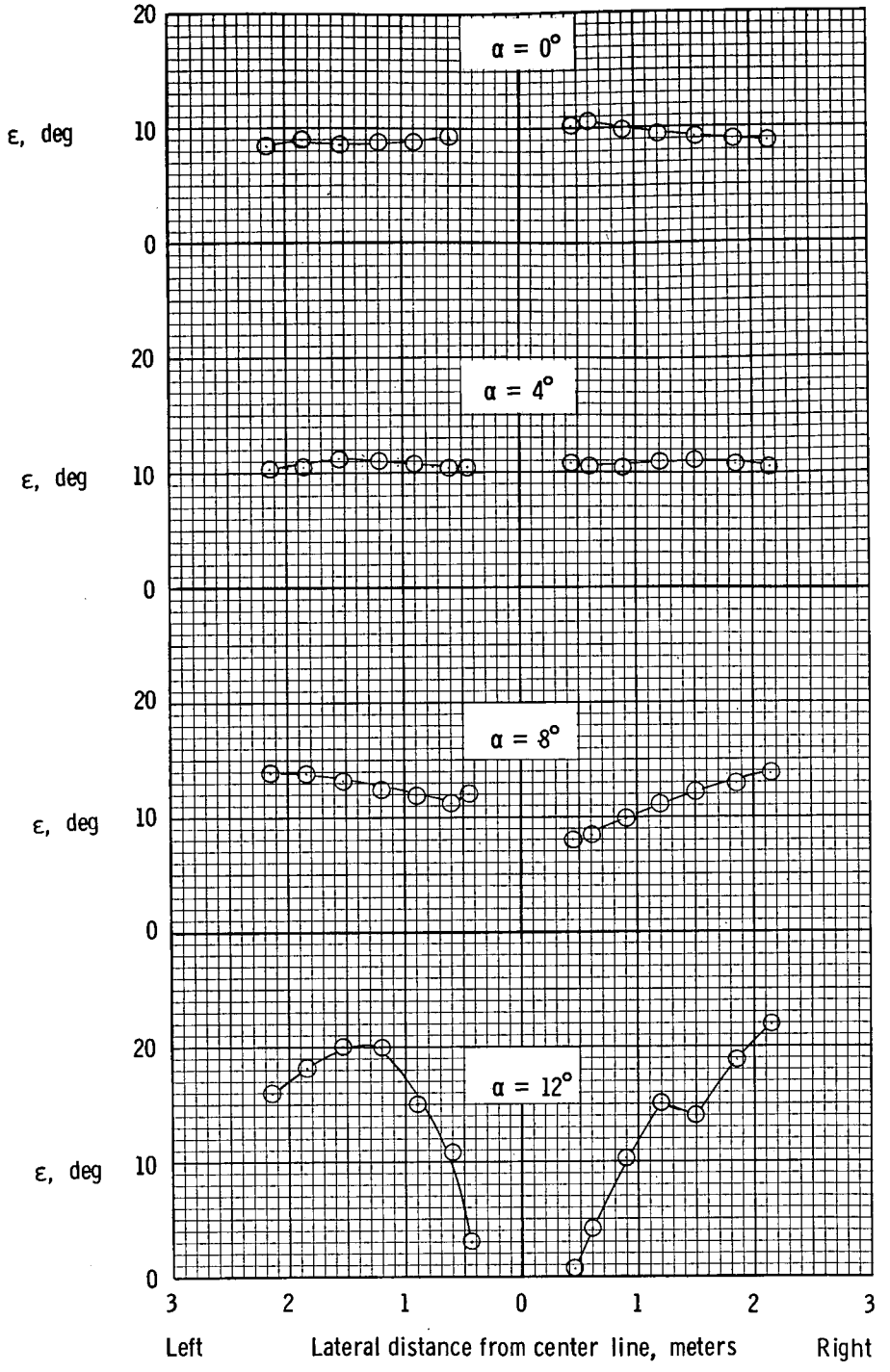

(a) $T_c' = 0$.

Figure 36.- Distribution of downwash angle across span of horizontal-tail surface. $\delta_f = 27^o$; $\beta = 0^o$; nacelle A.

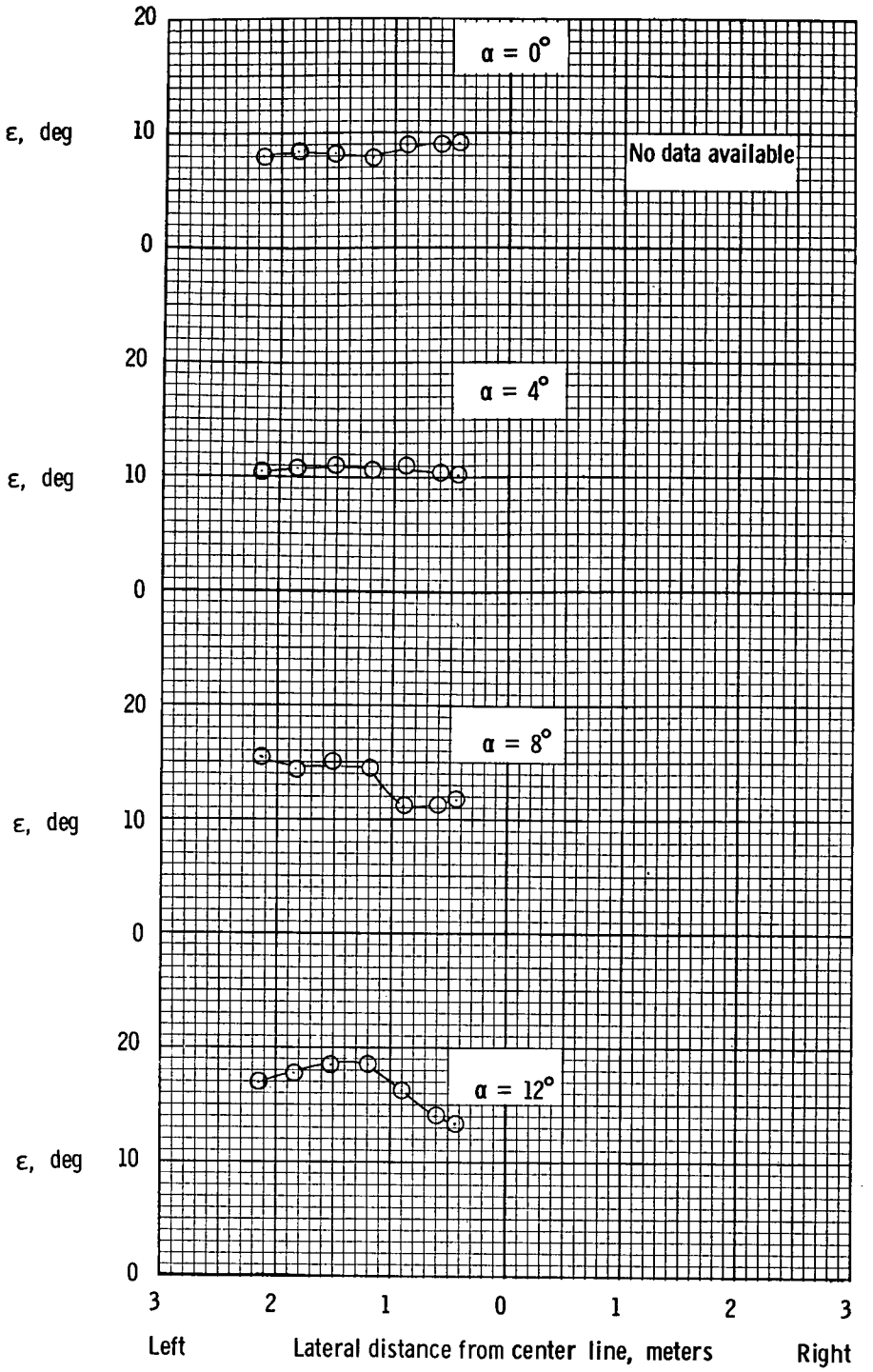

(b) $T_c' = 0.20$.

Figure 36.- Continued.

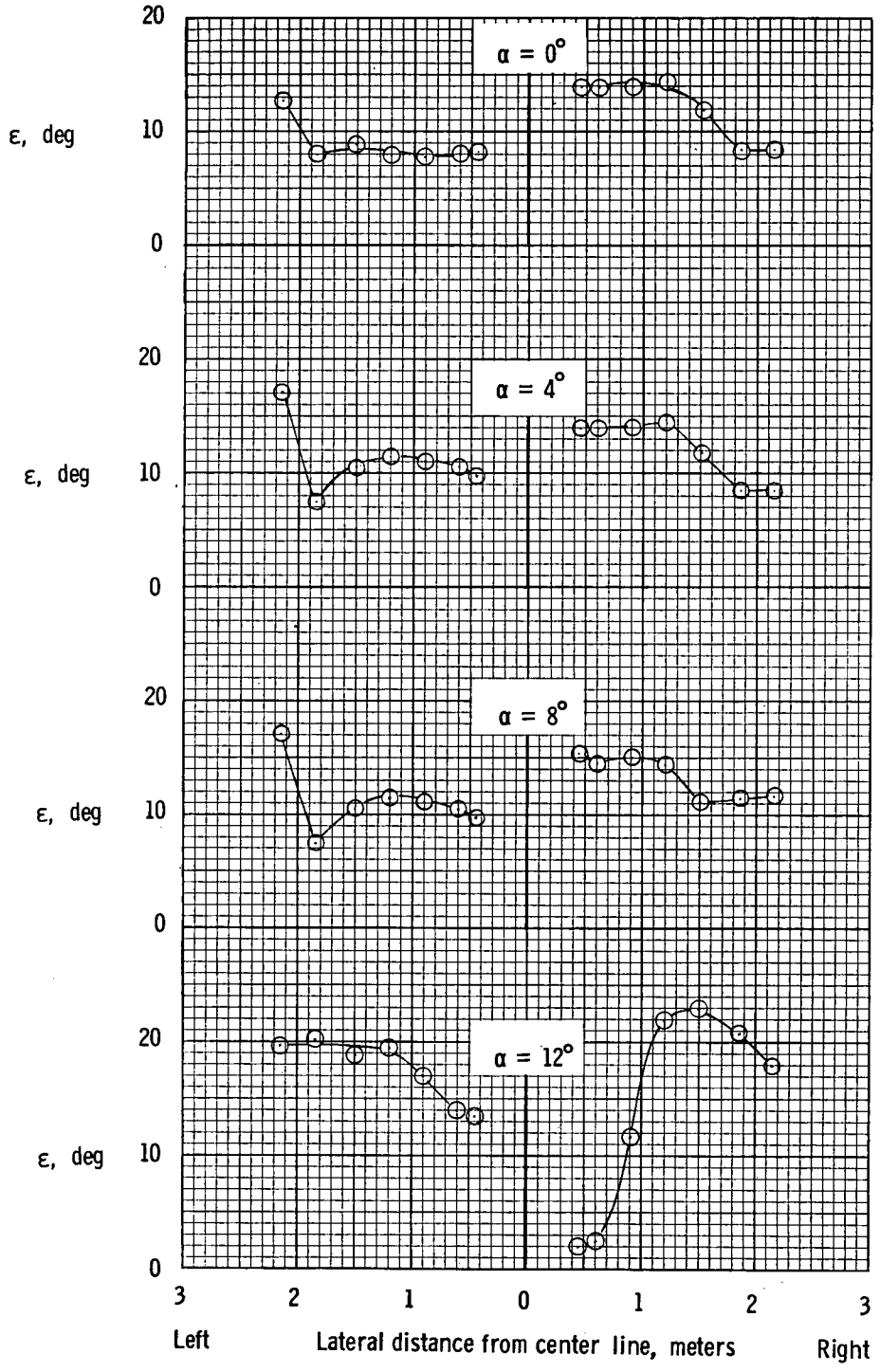

(c) $T_c' = 0.44$.

Figure 36.- Concluded.

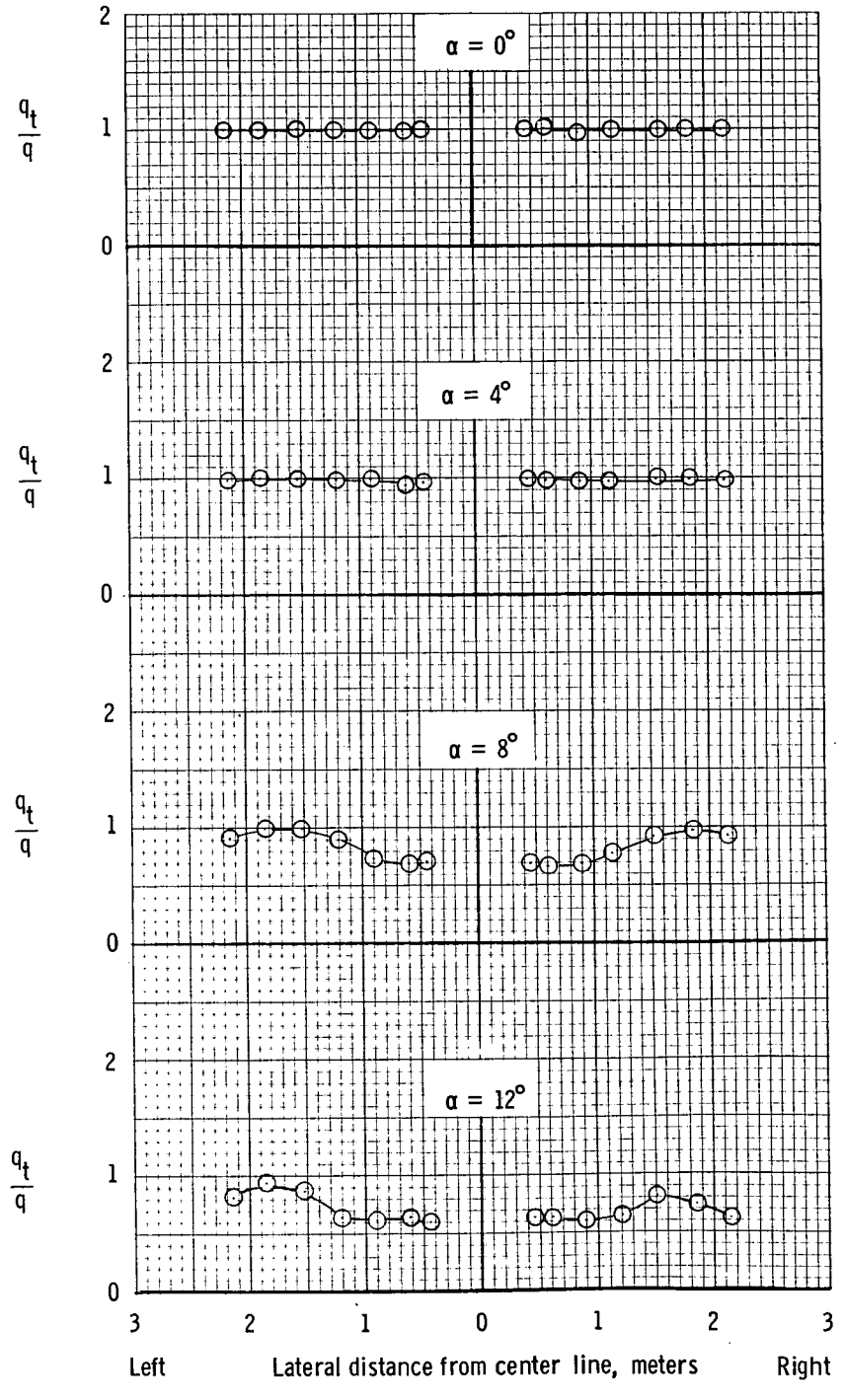

(a) $\delta_f = 0^o$.

Figure 37.- Distribution of dynamic pressure across the horizontal-tail surface with the propellers removed. Nacelle A.

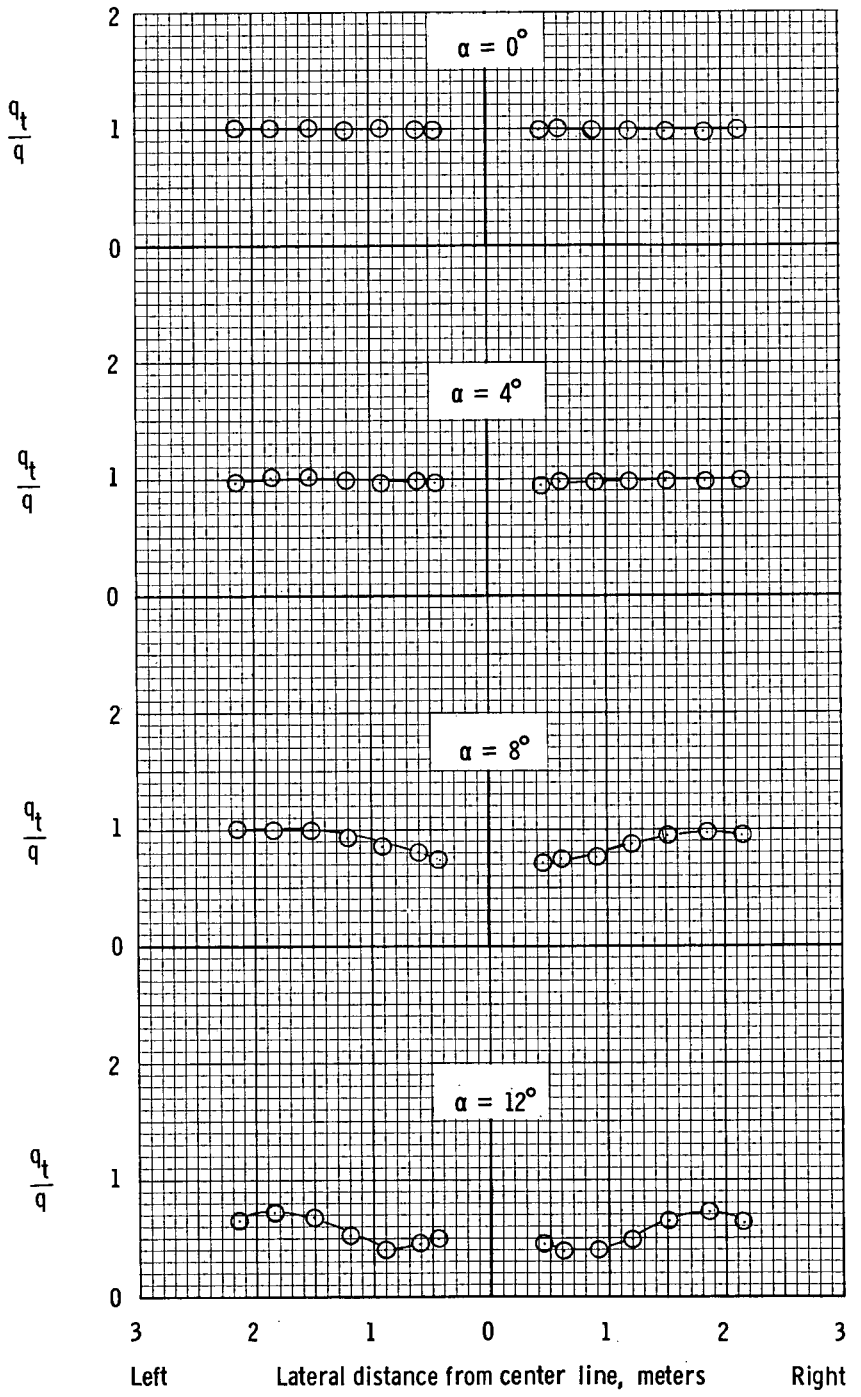

(b) $\delta_f = 27^\circ$.

Figure 37.- Concluded.

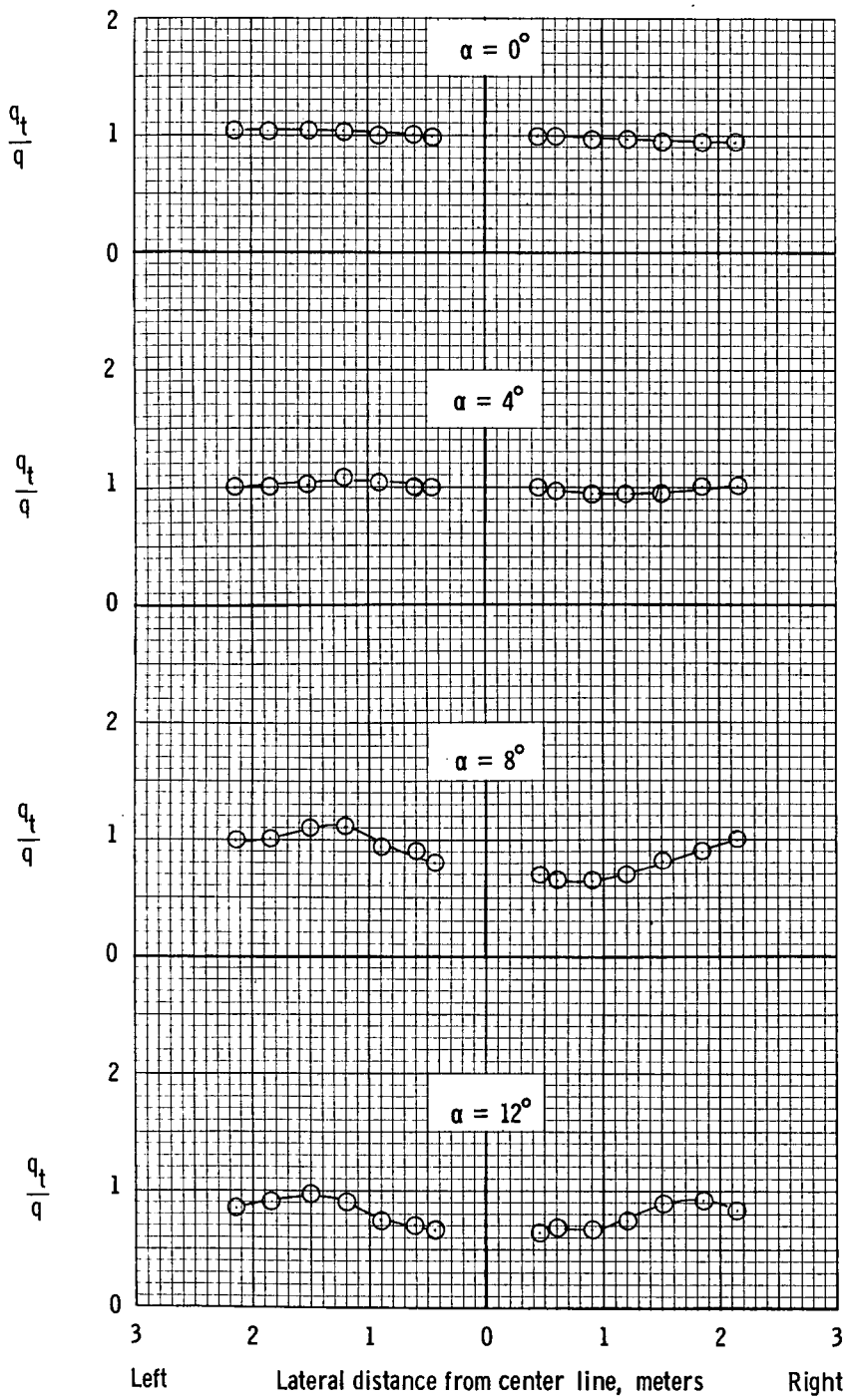

(a) $T_c' = 0$.

Figure 38.- Distribution of dynamic pressure across span of horizontal-tail surface. $\delta_f = 0^o$; $\beta = 0^o$; nacelle A.

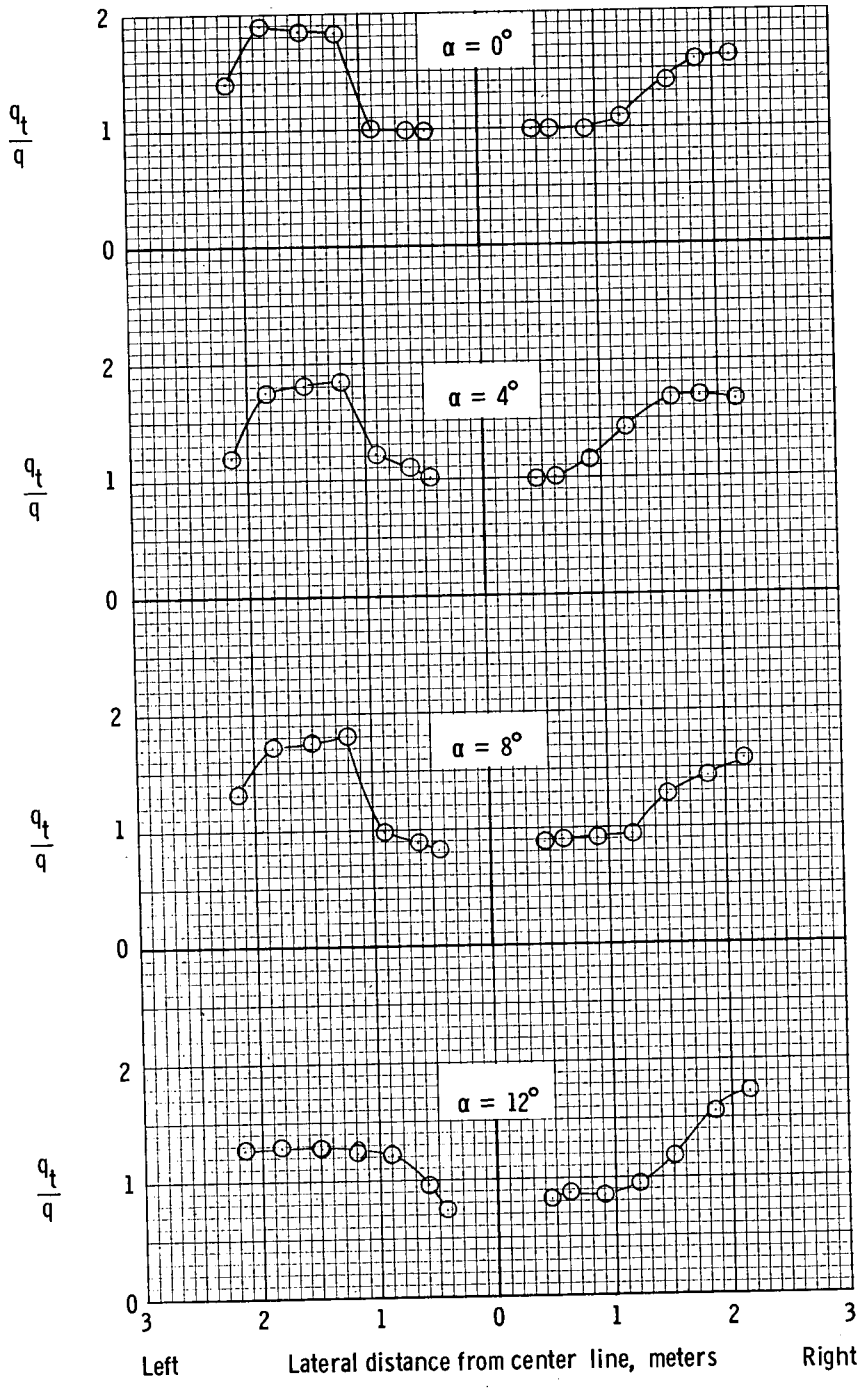

(b) $T_c' = 0.20$.

Figure 38.- Continued.

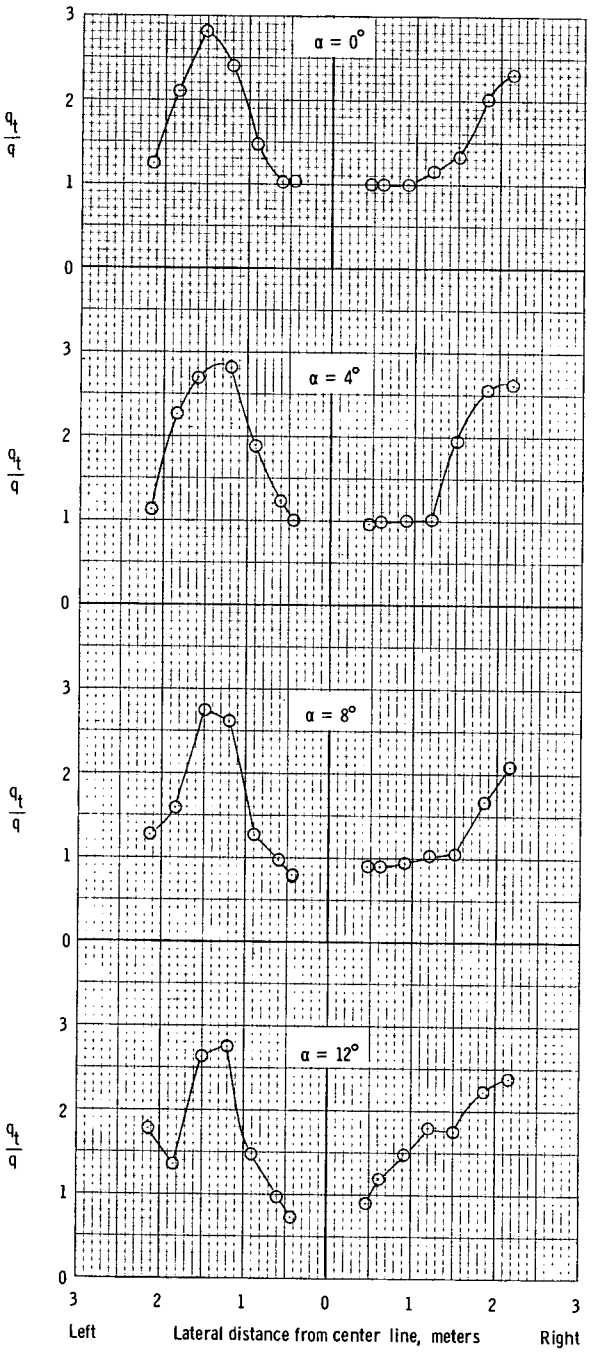

(c) $T_c' = 0.44$.

Figure 38.- Concluded.

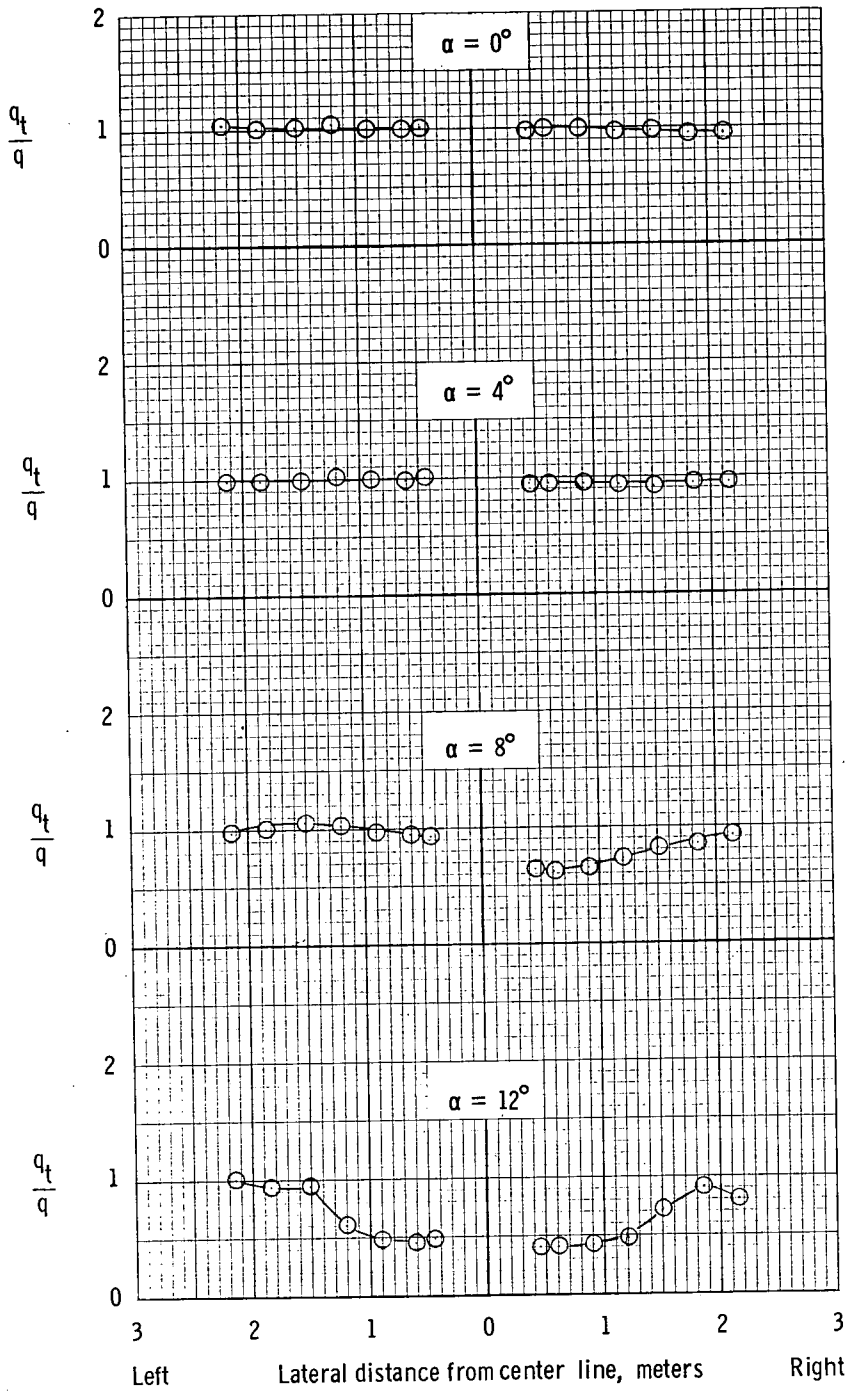

(a) $T_c' = 0$.

Figure 39.- Distribution of dynamic pressure across span of horizontal-tail surface. $\delta_f = 27^o$; $\beta = 0^o$; nacelle A.

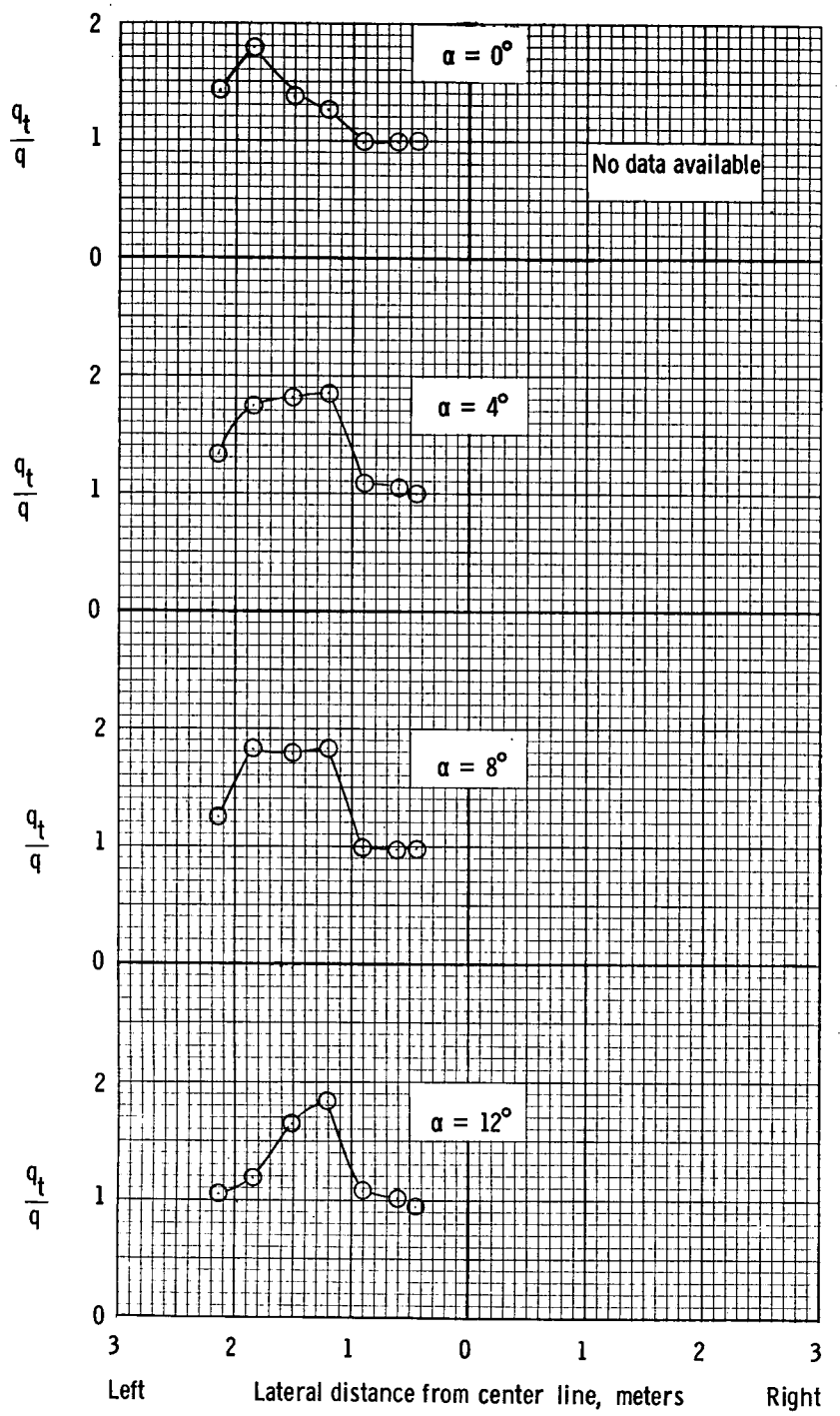

(b) $T_c' = 0.20$.

Figure 39.- Continued.

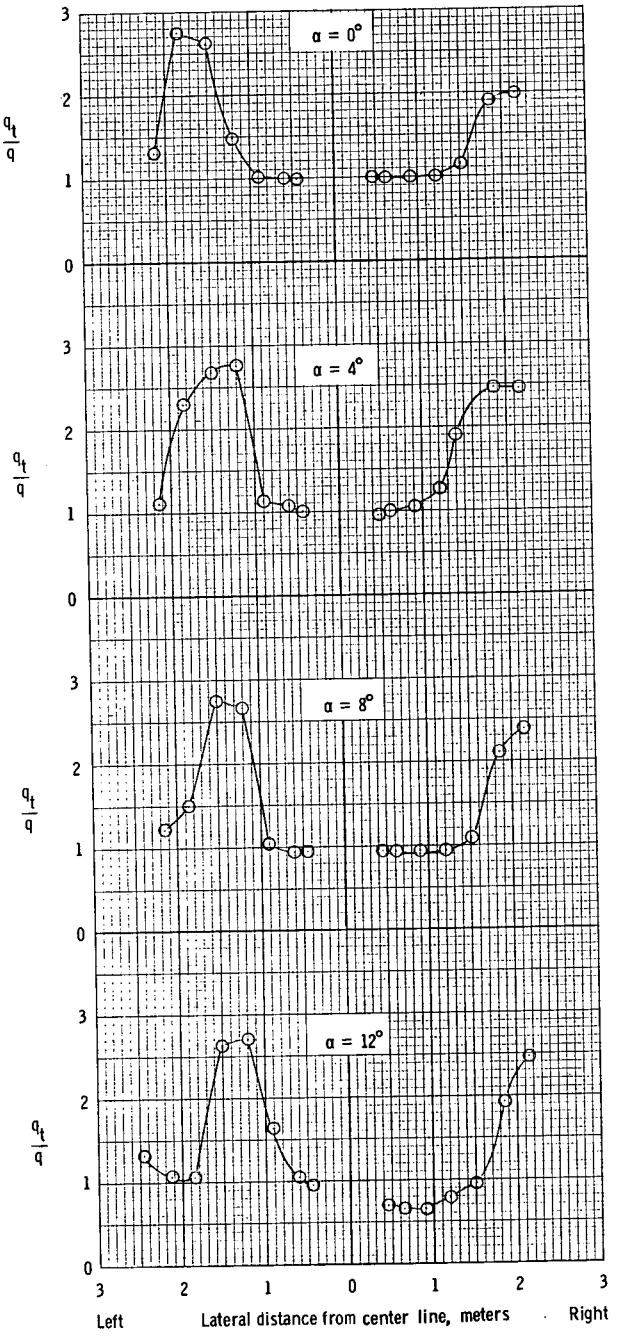

(c) $T'_C = 0.44$.

Figure 39.- Concluded.

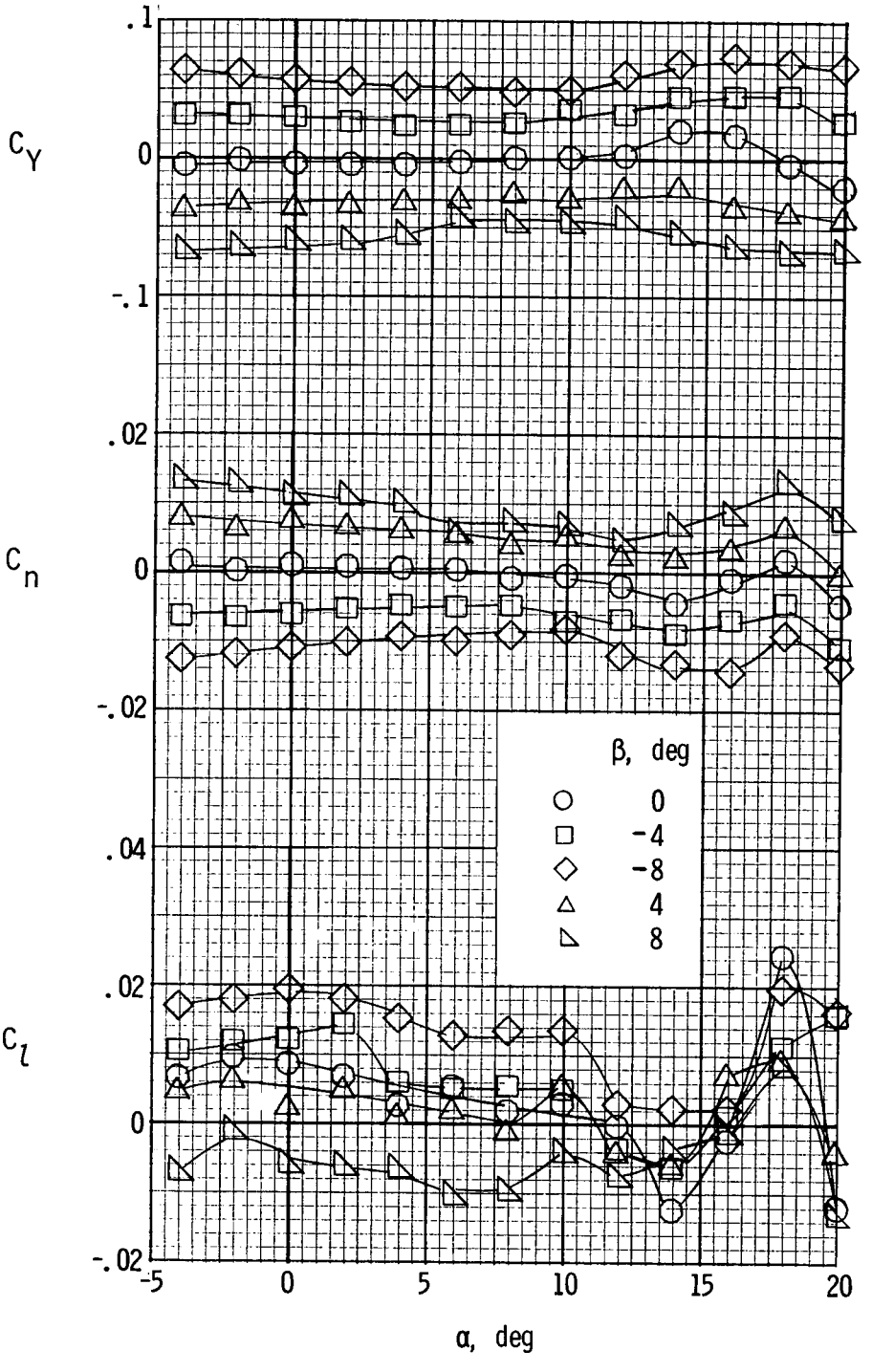

(a) $\delta_f = 0^o$.

Figure 40.- Lateral aerodynamic characteristics of the model with nacelle A. Propellers removed.

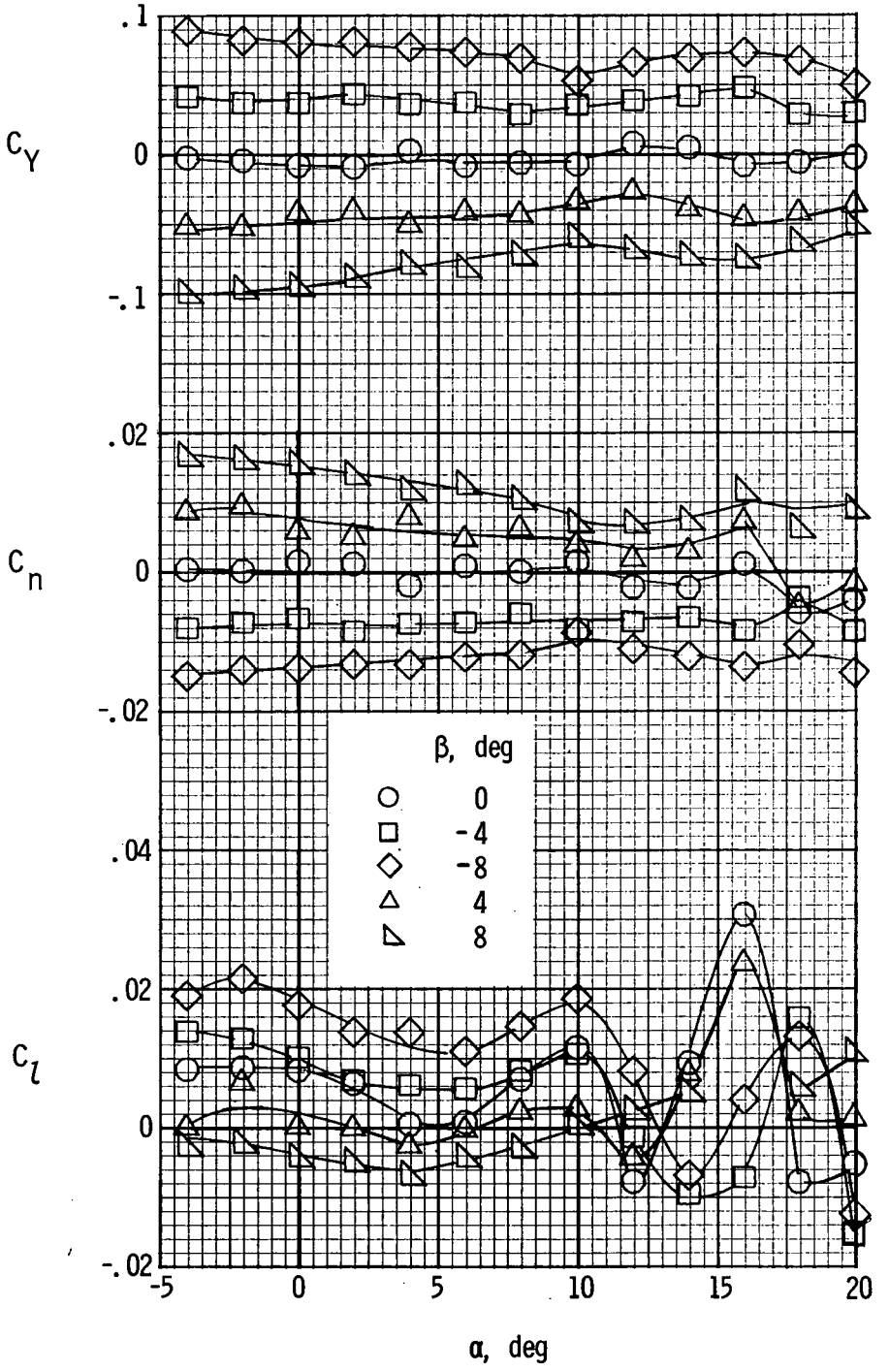

(b) $\delta_f = 27^o$.

Figure 40.- Concluded.

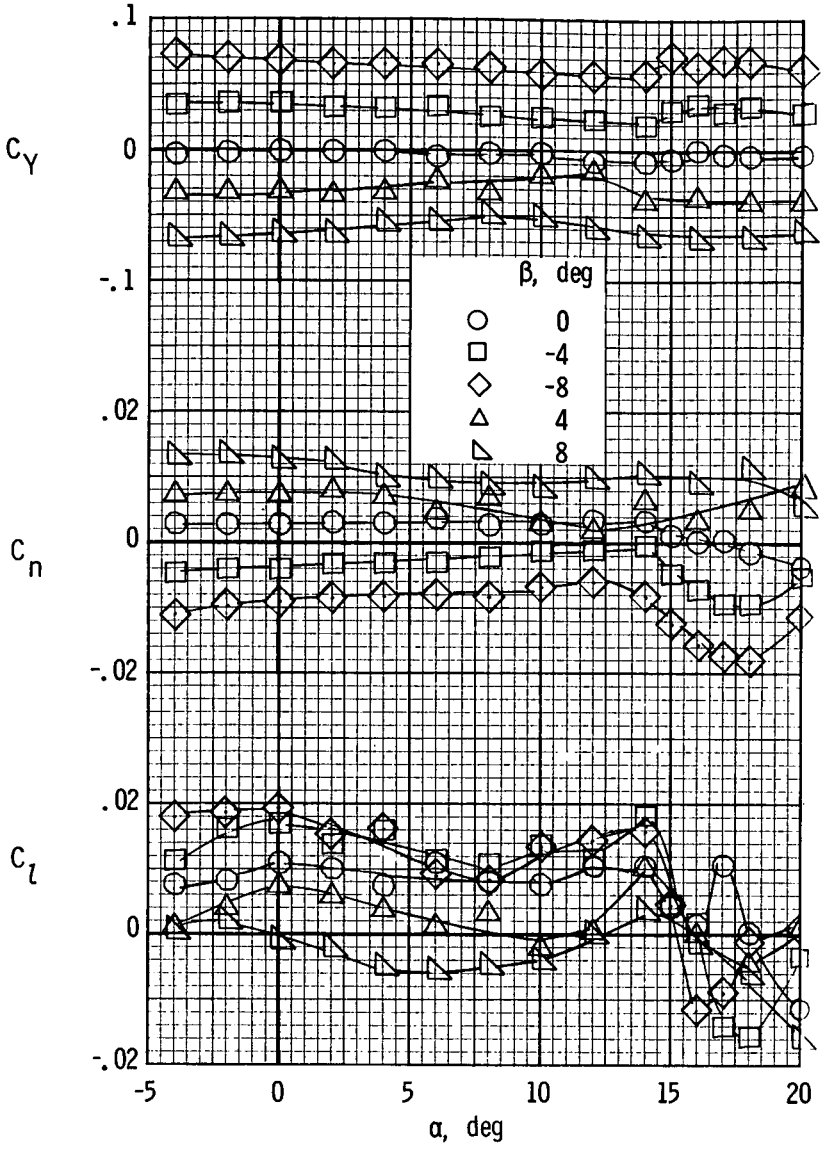

(a) $T_c' = 0$.

Figure 41.- Lateral aerodynamic characteristics of the model with nacelle A. $\delta_f = 0^o$.

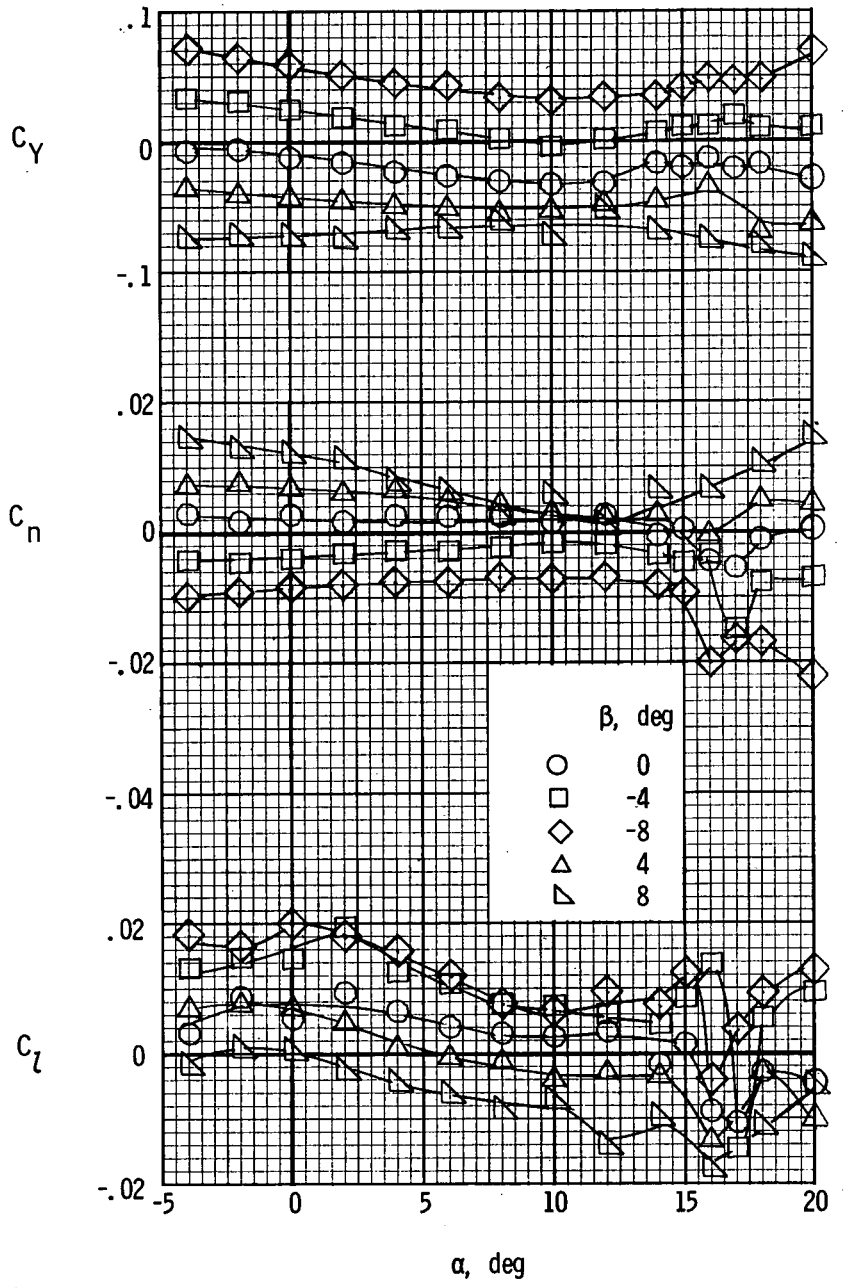

(b) $T_c' = 0.20$.

Figure 41.- Continued.

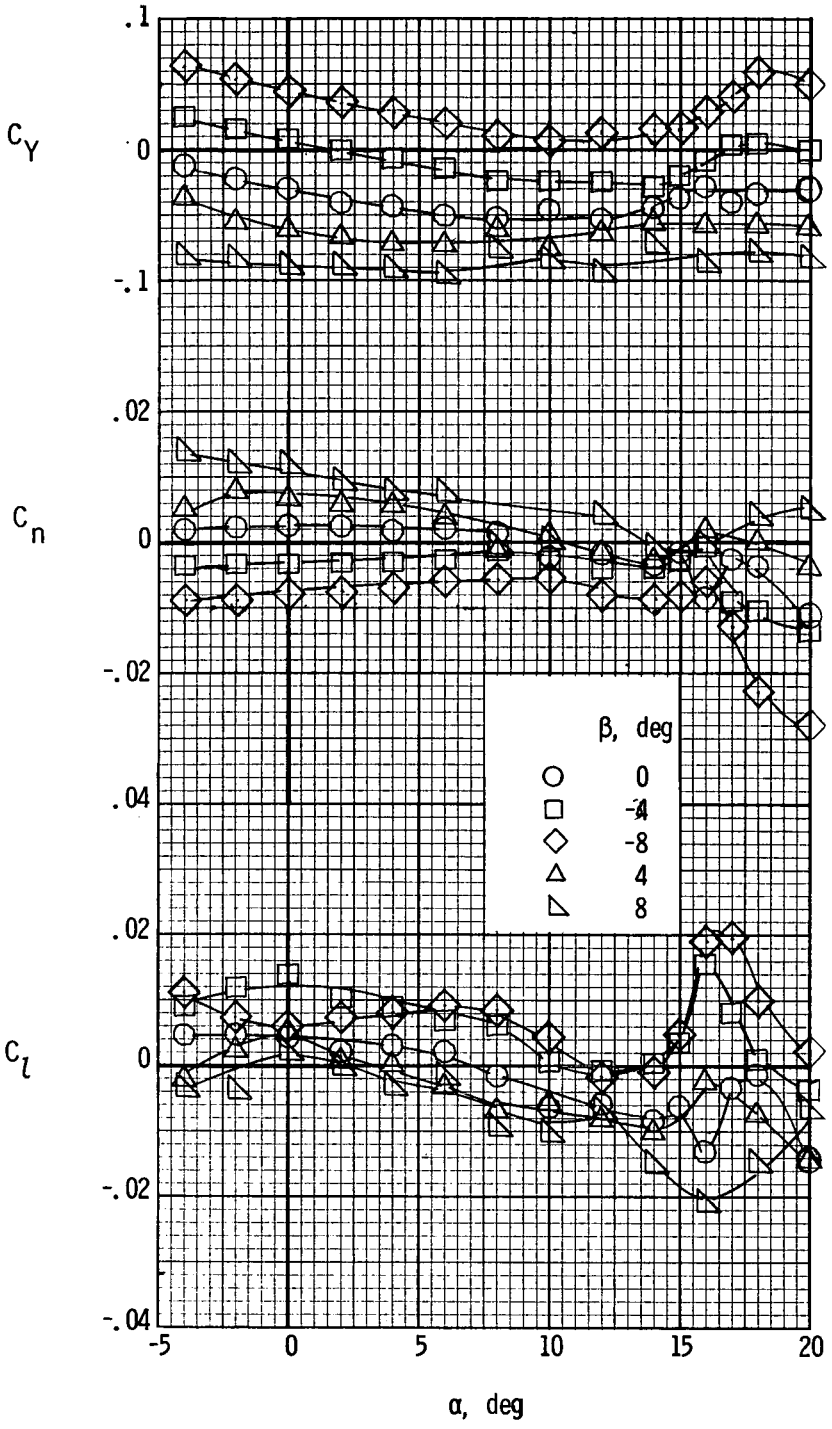

(c) $T_c' = 0.44$.

Figure 41.- Concluded.

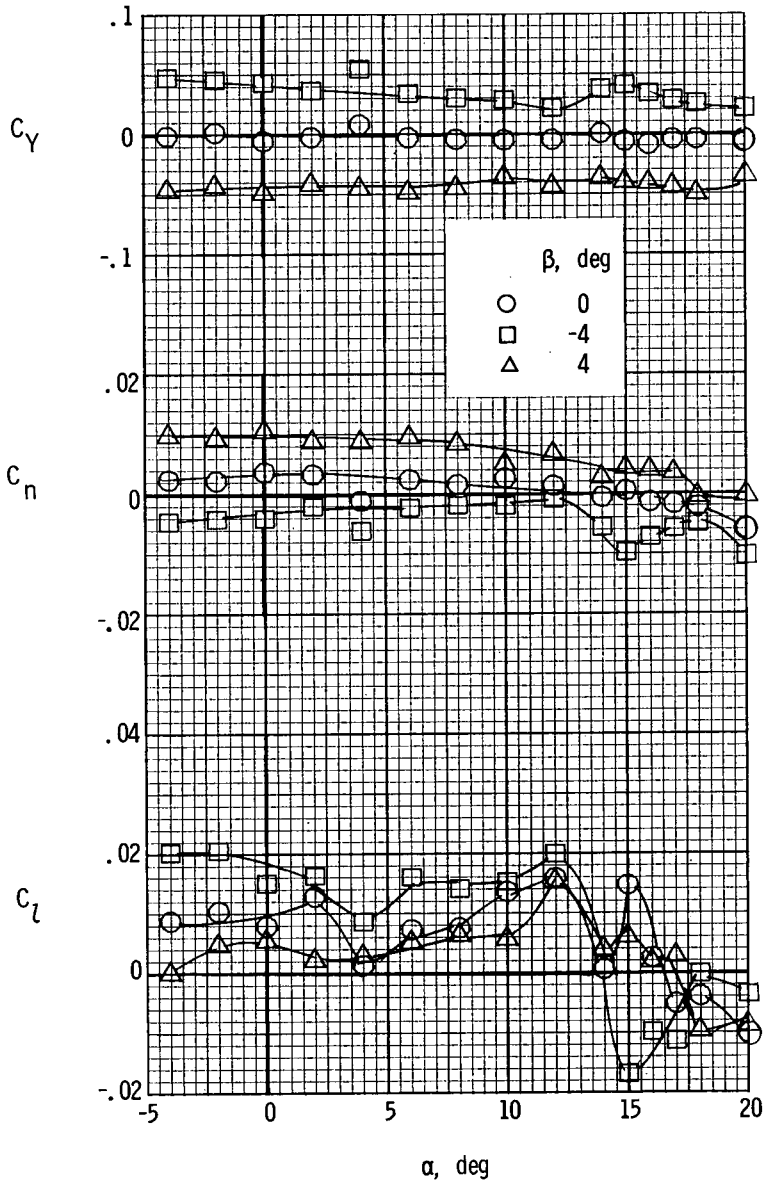

(a) $T_c' = 0$.

Figure 42.- Lateral aerodynamic characteristics of the model with nacelle A. $\delta_f = 27^o$.

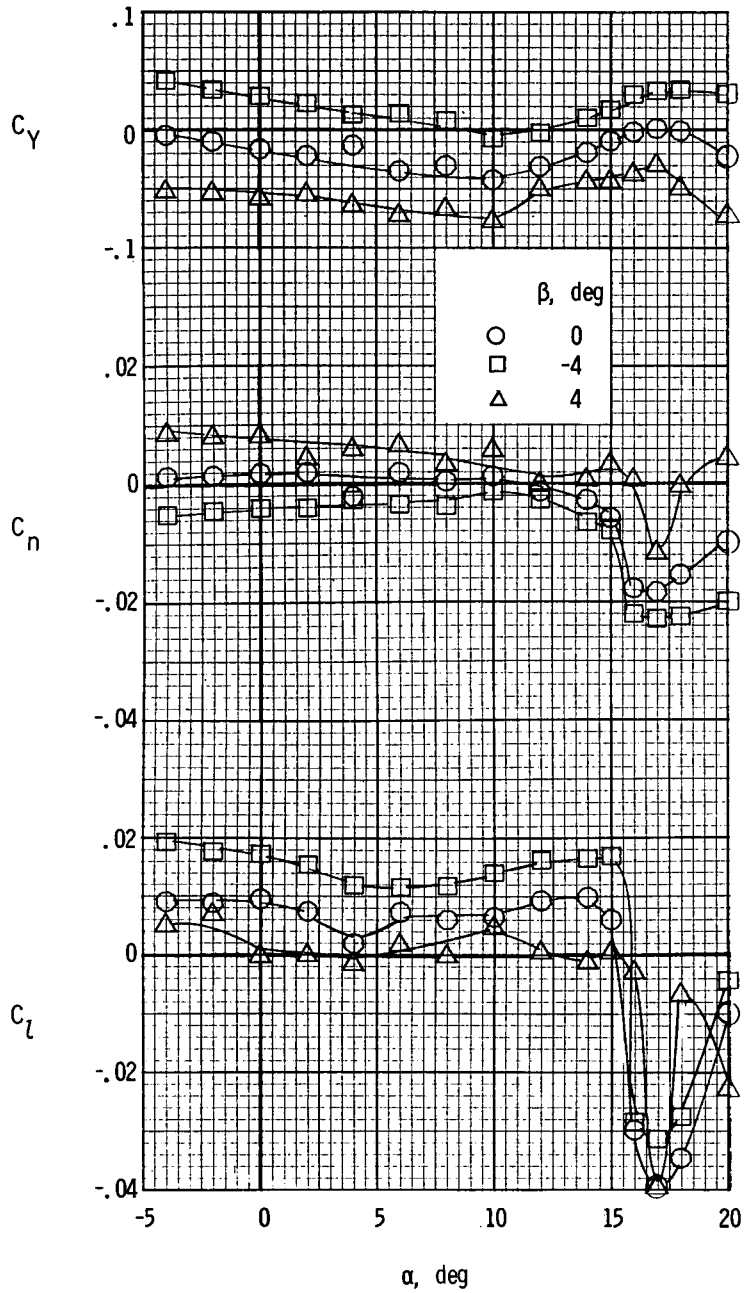

(b) $T_c' = 0.20$.

Figure 42.- Continued.

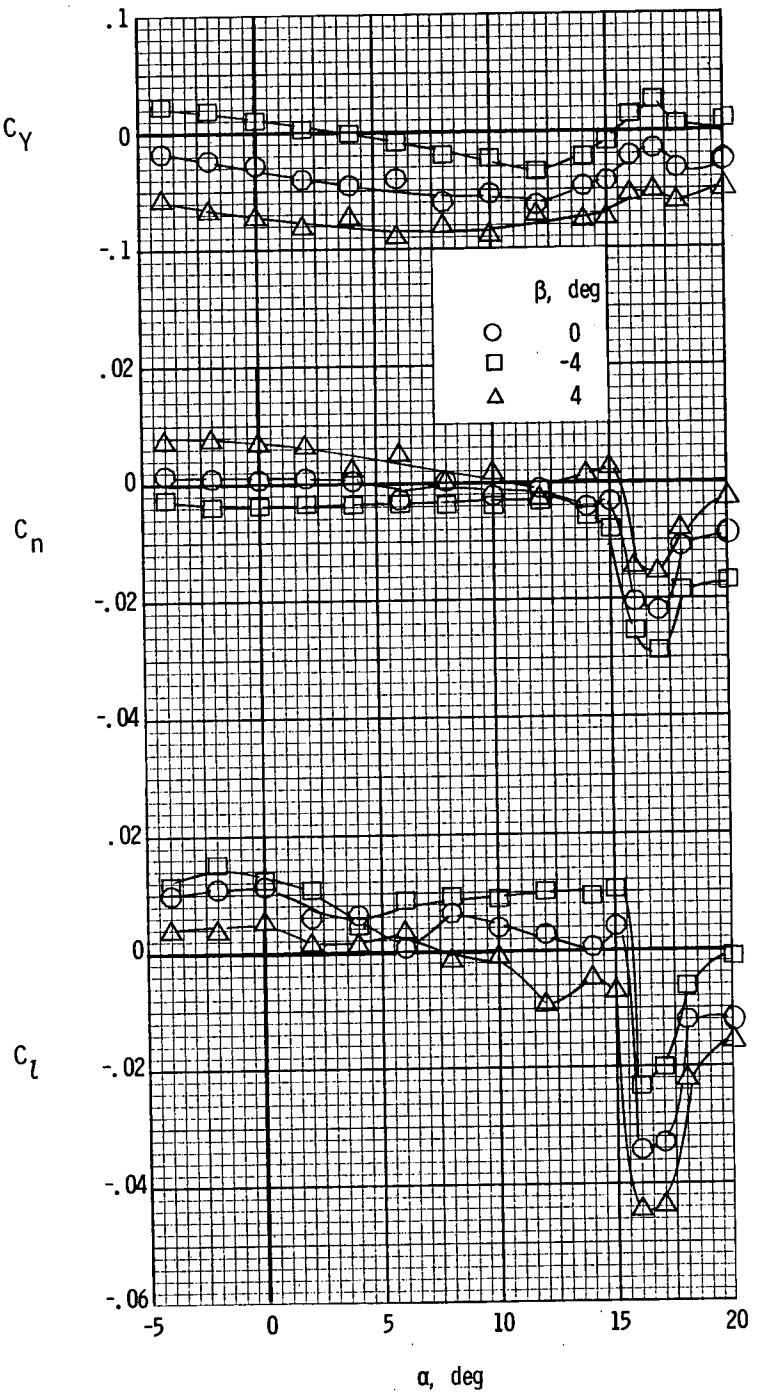

(c) $T_c' = 0.44$.

Figure 42.- Concluded.

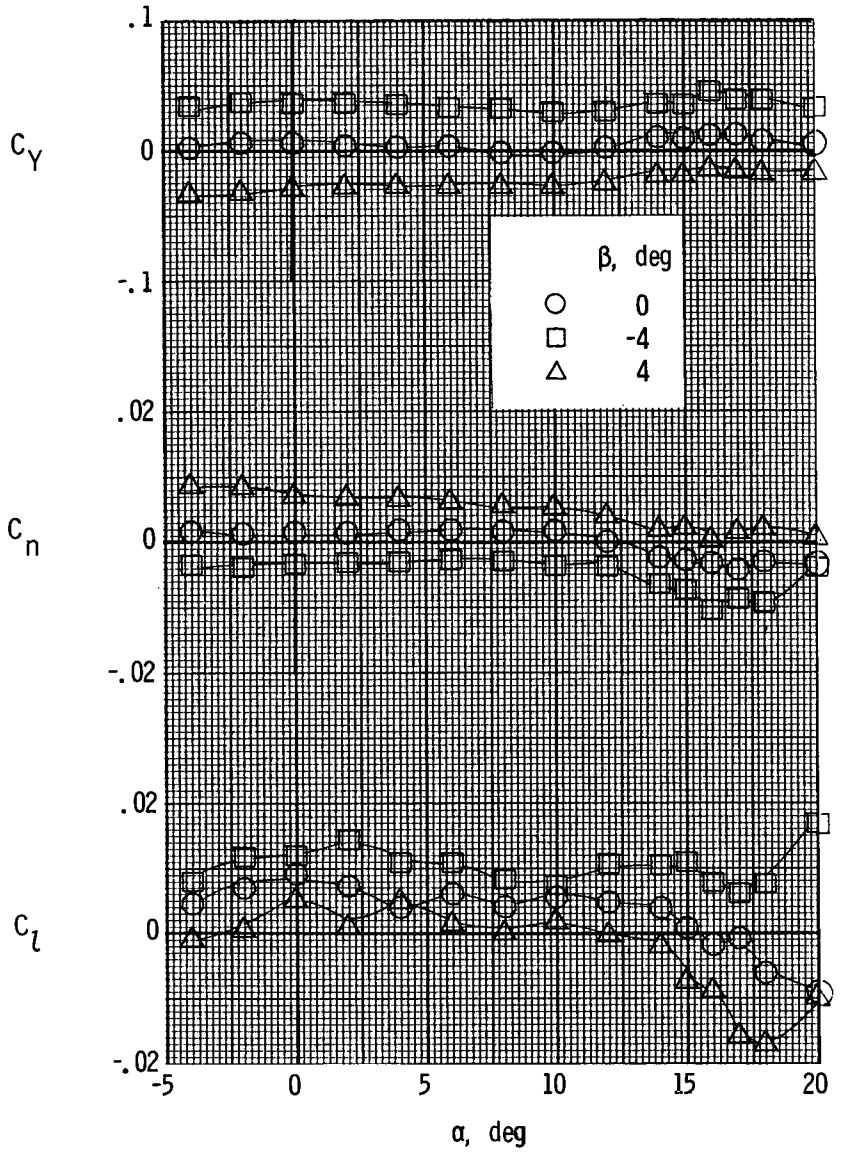

(a) $T_c' = 0.$

Figure 43.- Lateral aerodynamic characteristics of the model with nacelle B. $\delta_f = 0^o$.

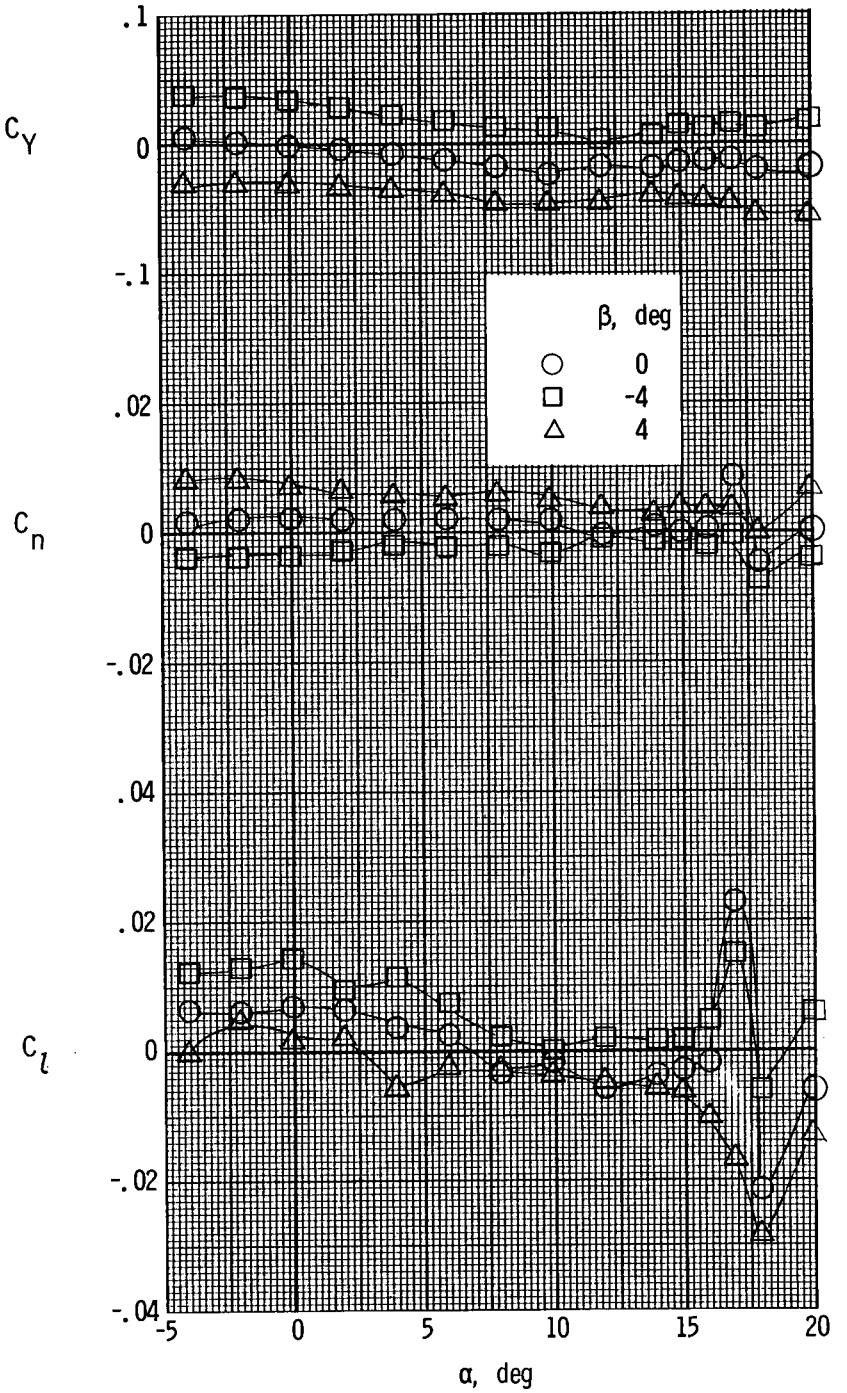

(b) $T_c' = 0.20$.

Figure 43.- Continued.

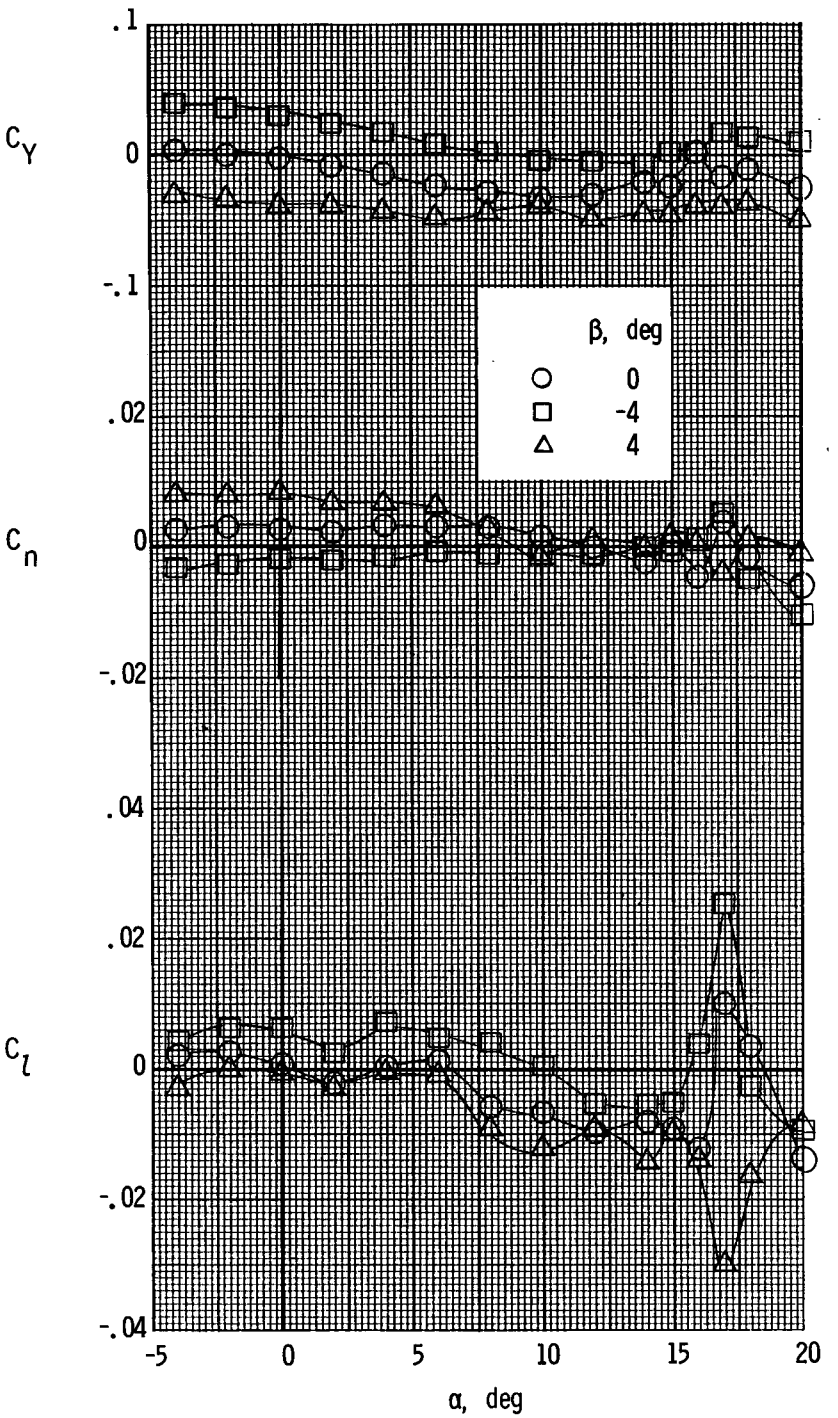

(c) $T_c' = 0.44$.

Figure 43.- Concluded.

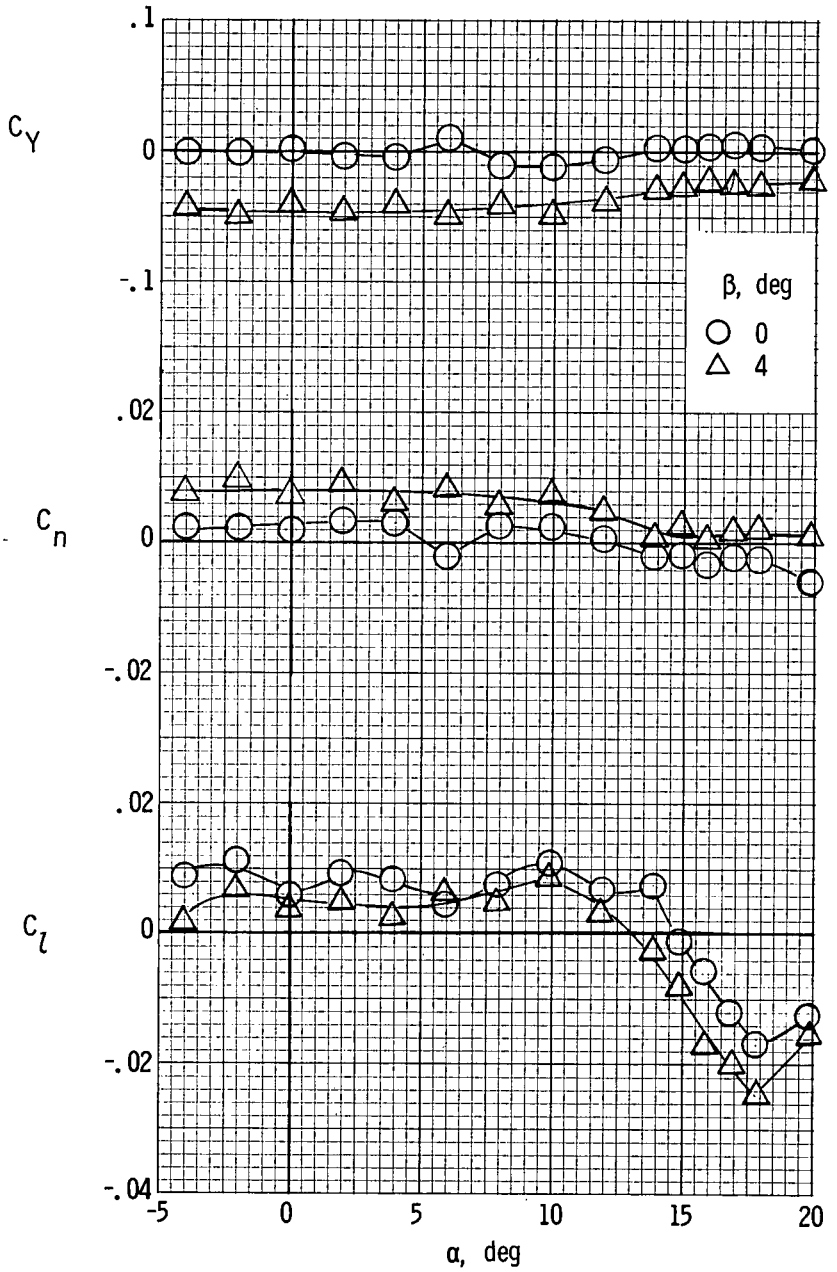

(a) $T_c' = 0$.

Figure 44.- Lateral aerodynamic characteristics of the model with nacelle B. $\delta_f = 27^o$.

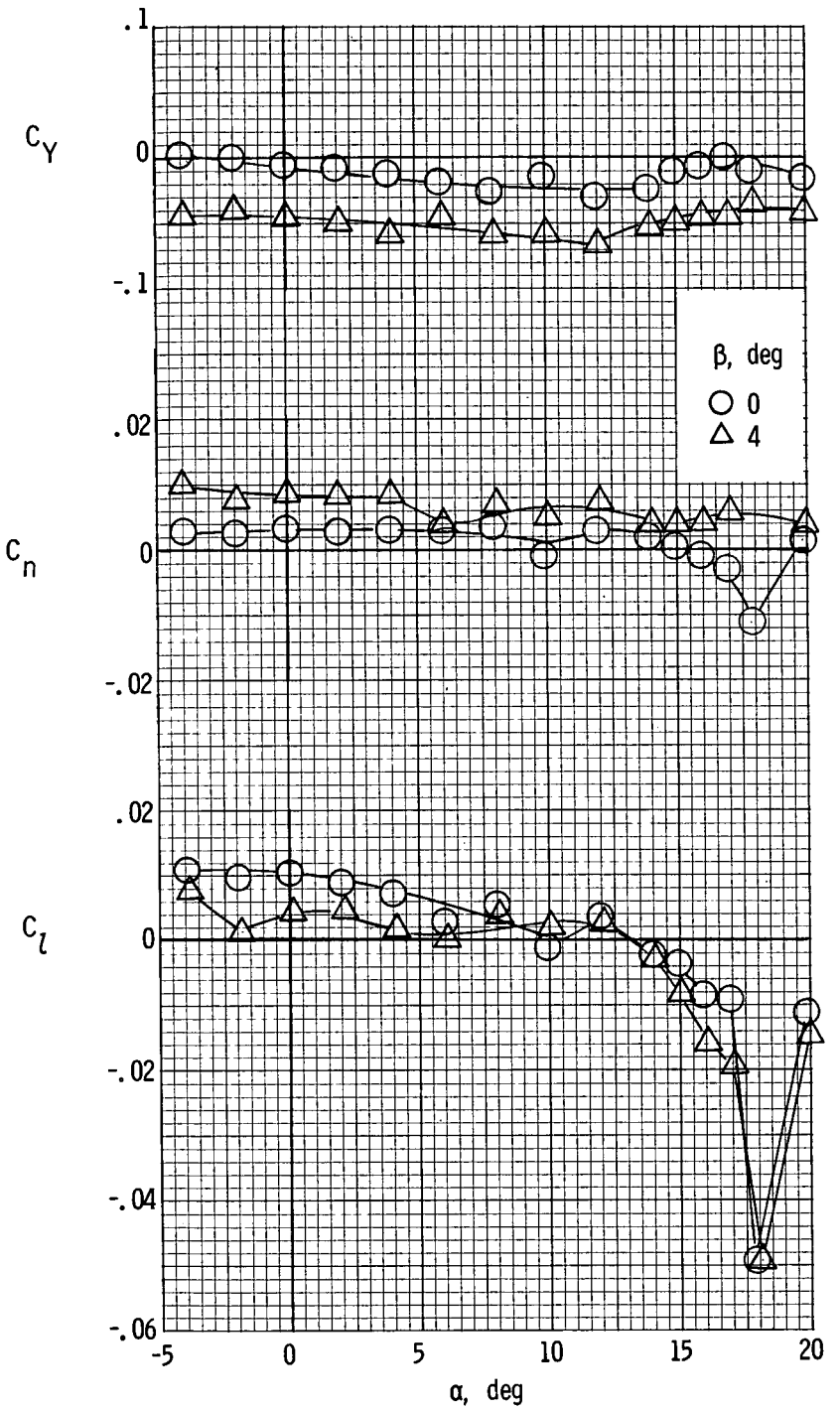

(b) $T_c' = 0.20$.

Figure 44.- Continued.

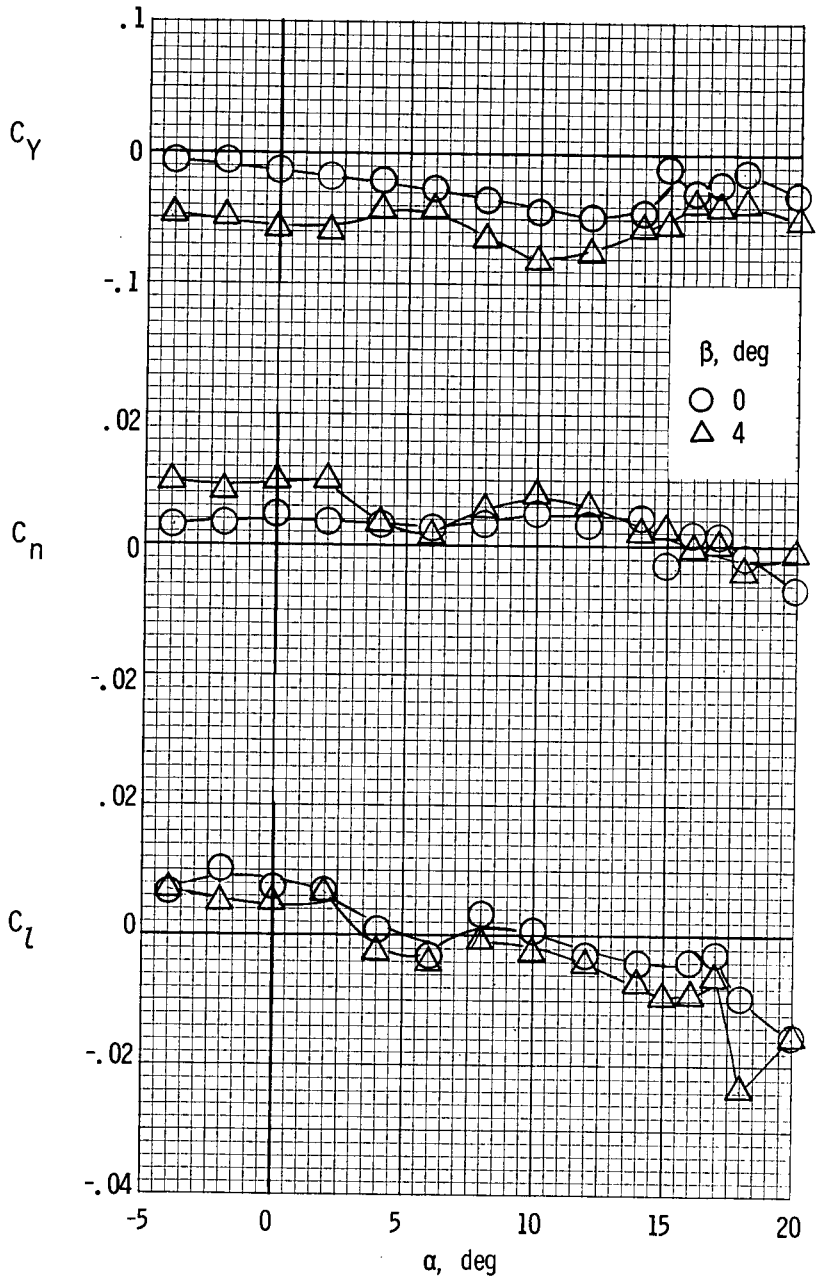

(c) $T_c' = 0.44$.

Figure 44.- Concluded.

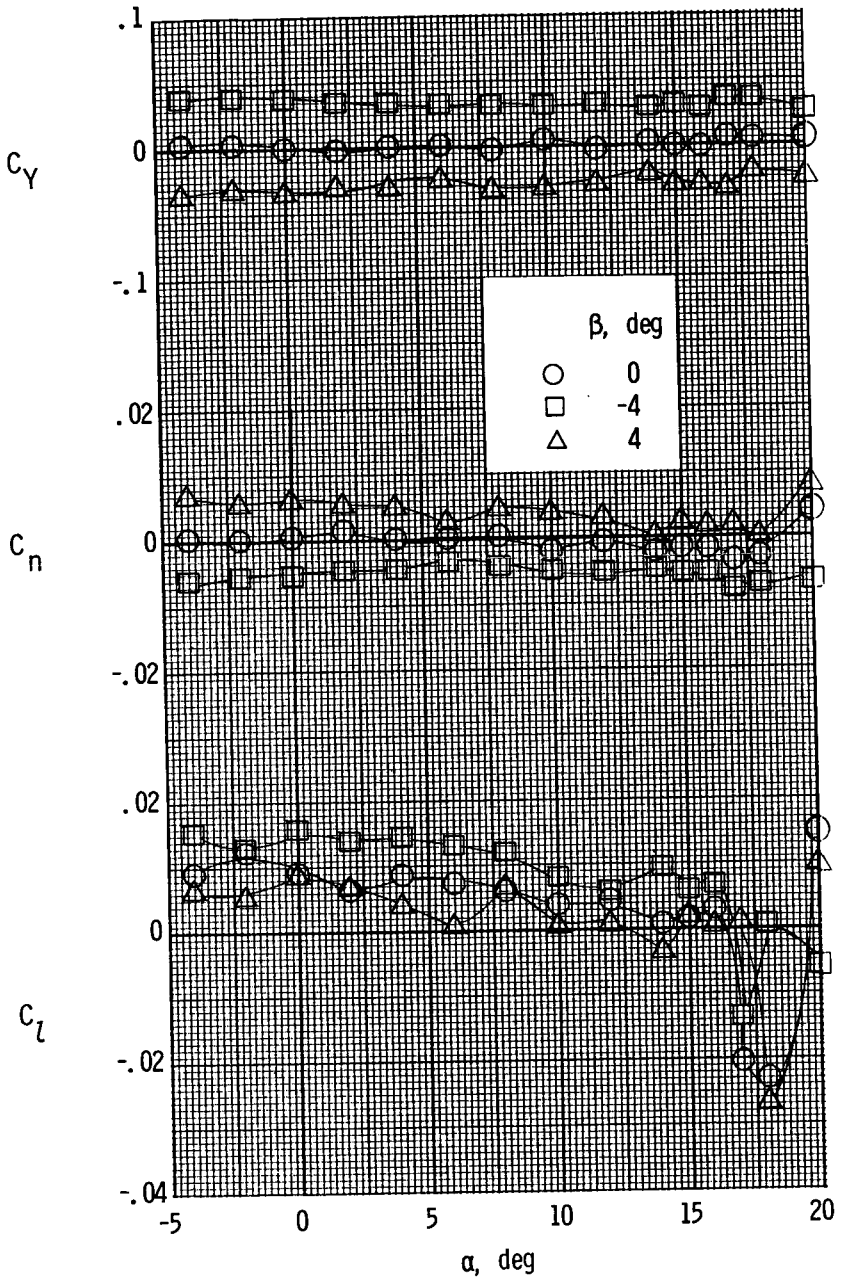

(a) $T_c' = 0$.

Figure 45.- Lateral aerodynamic characteristics of the model with nacelle C. $\delta_f = 0^o$.

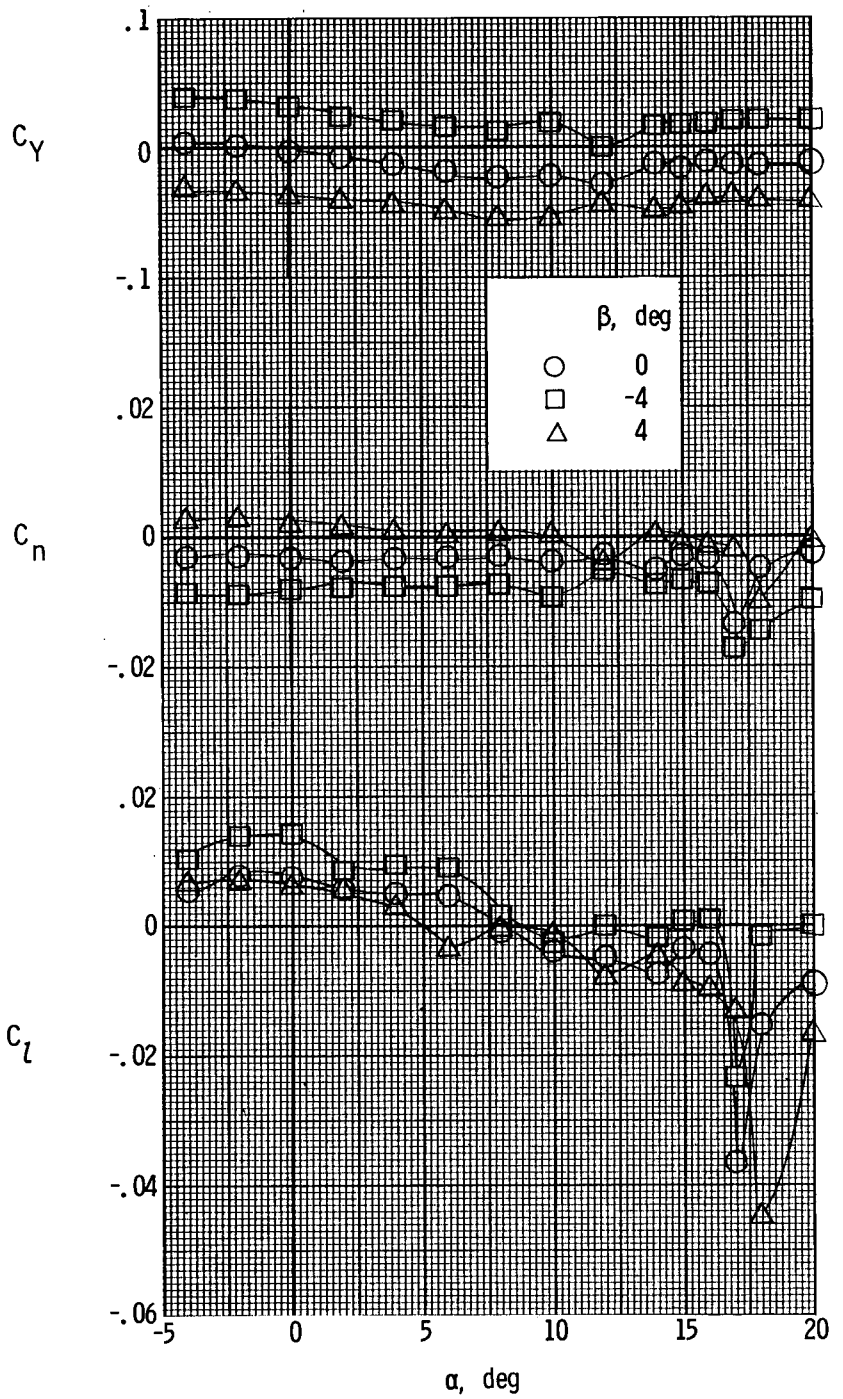

(b) $T_c' = 0.20$.

Figure 45.- Continued.

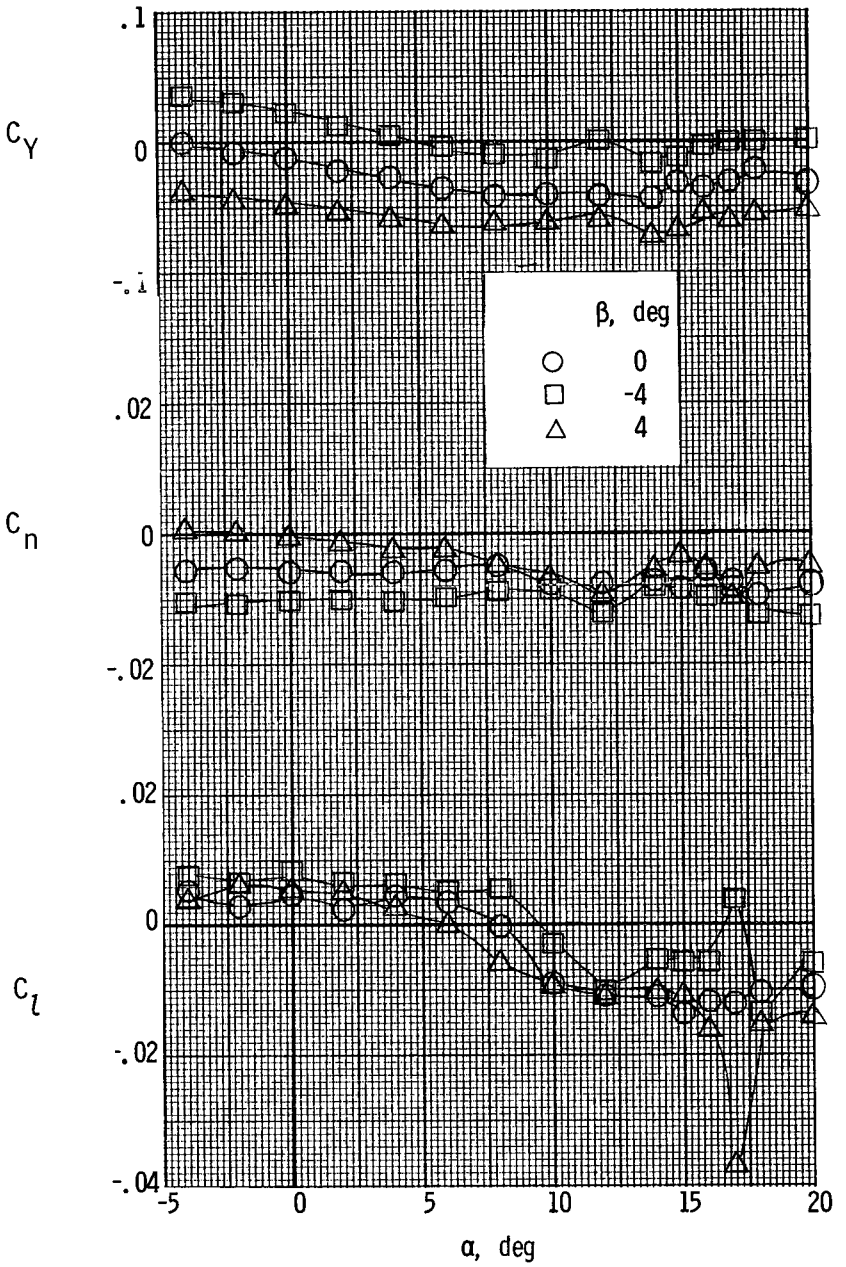

(c) $T_c' = 0.44$.

Figure 45.- Concluded.

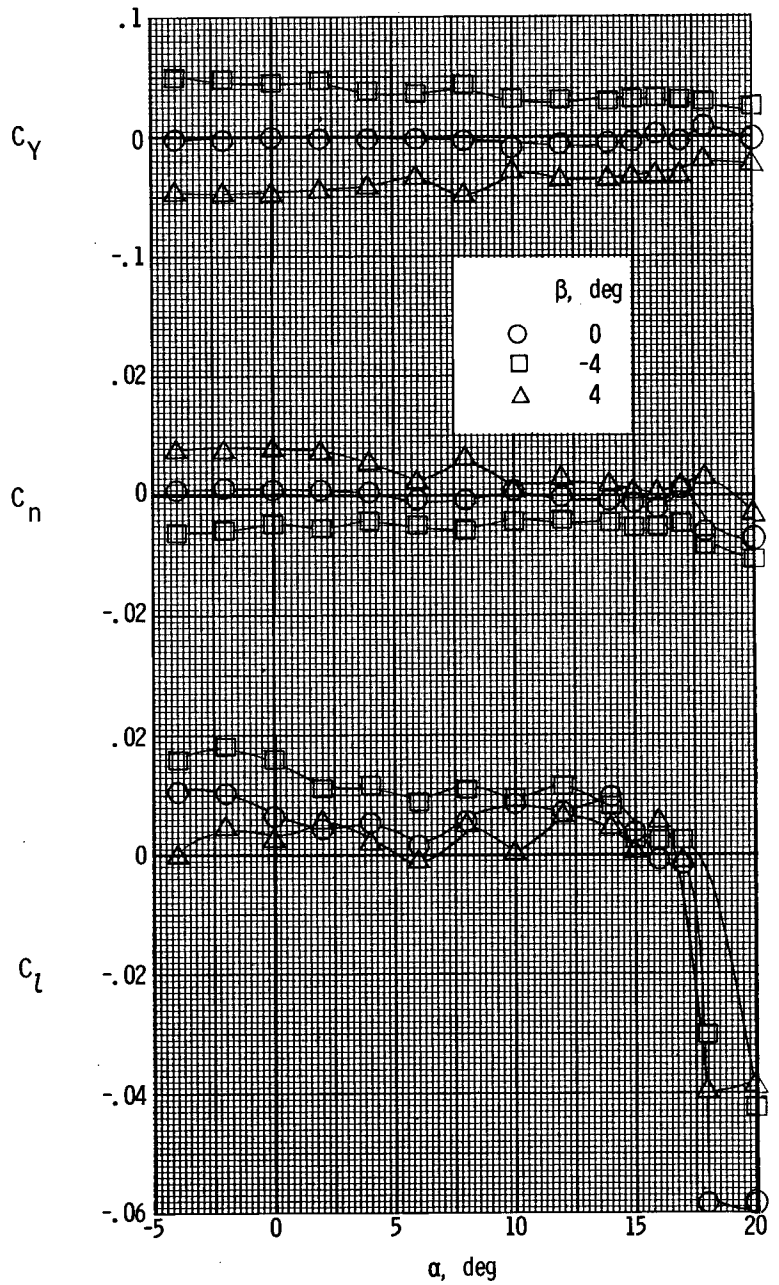

(a) $T_c' = 0$.

Figure 46.- Lateral aerodynamic characteristics of the model with nacelle C. $\delta_f = 27^o$.

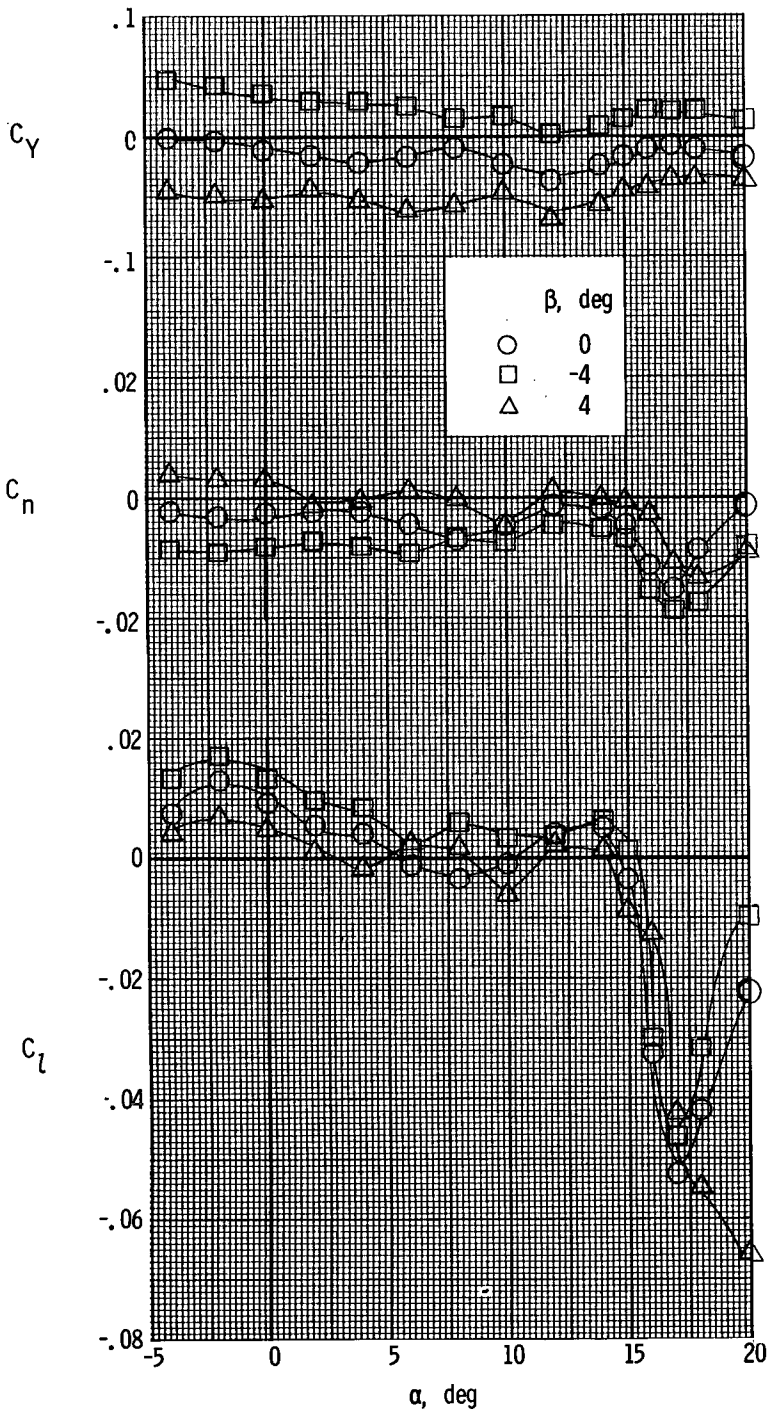

(b) $T_c' = 0.20$.

Figure 46.- Continued.

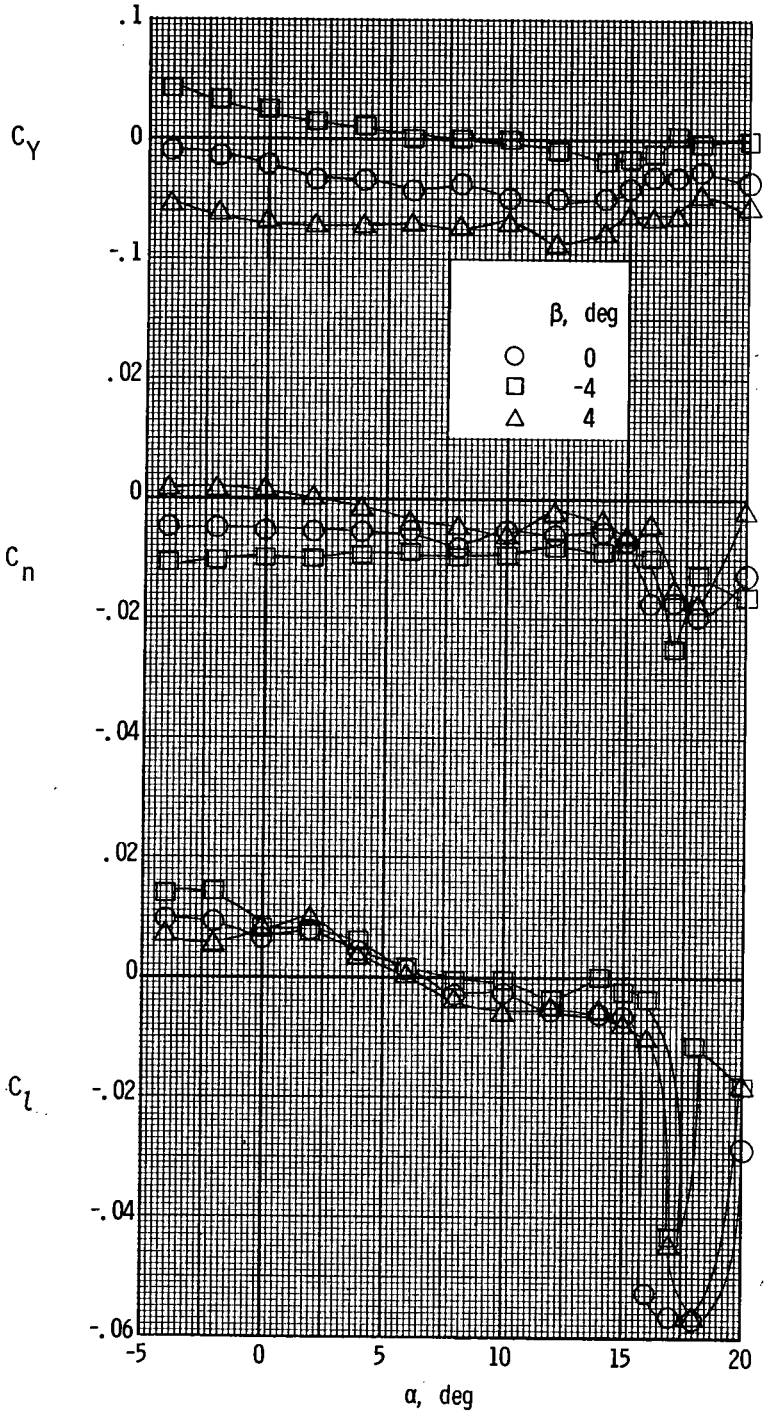

(c) $T_c' = 0.44$.

Figure 46.- Concluded.

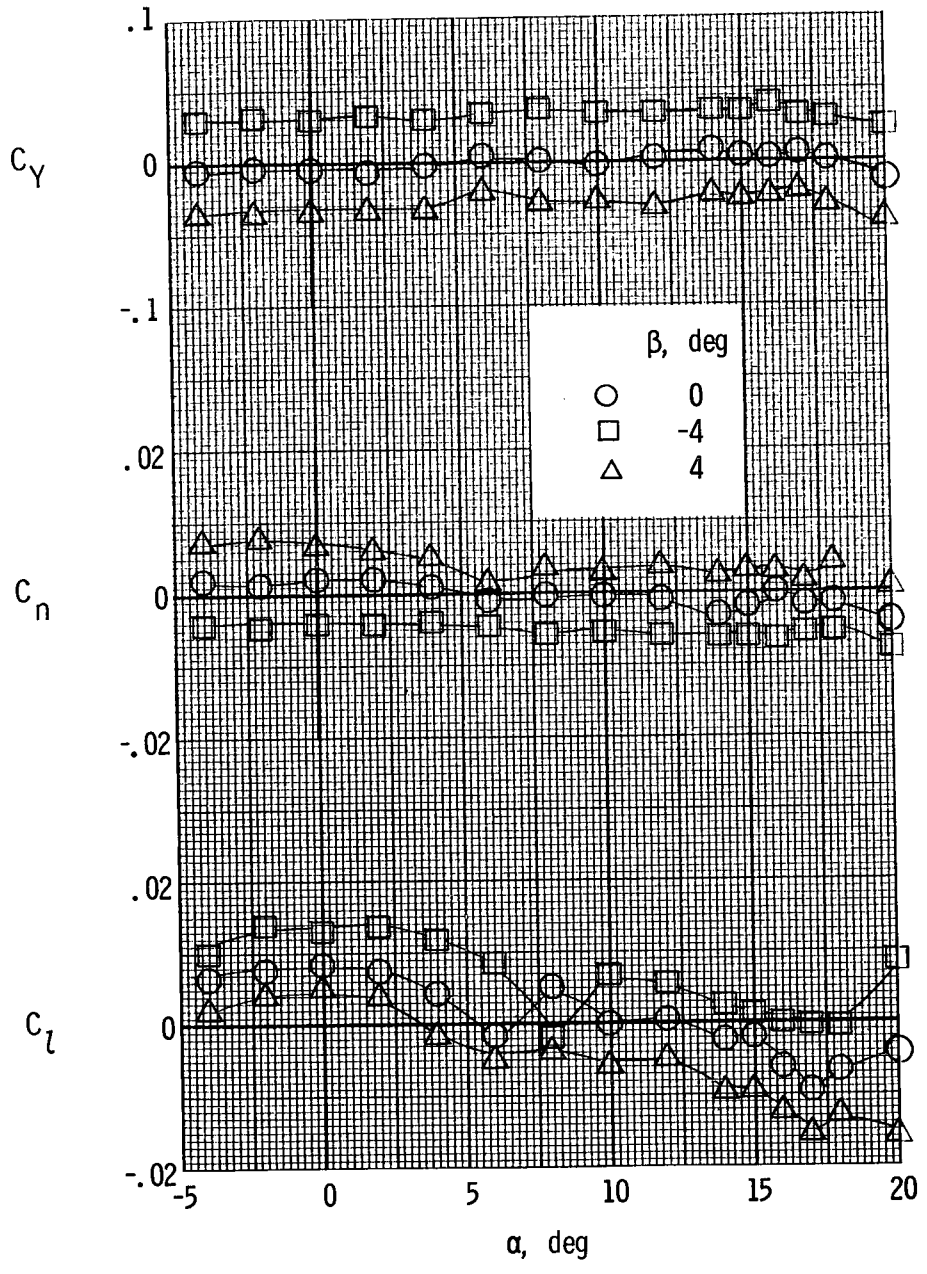

(a) $T_c' = 0$.

Figure 47.- Lateral aerodynamic characteristics of the model with nacelle D. $\delta_f = 0^o$.

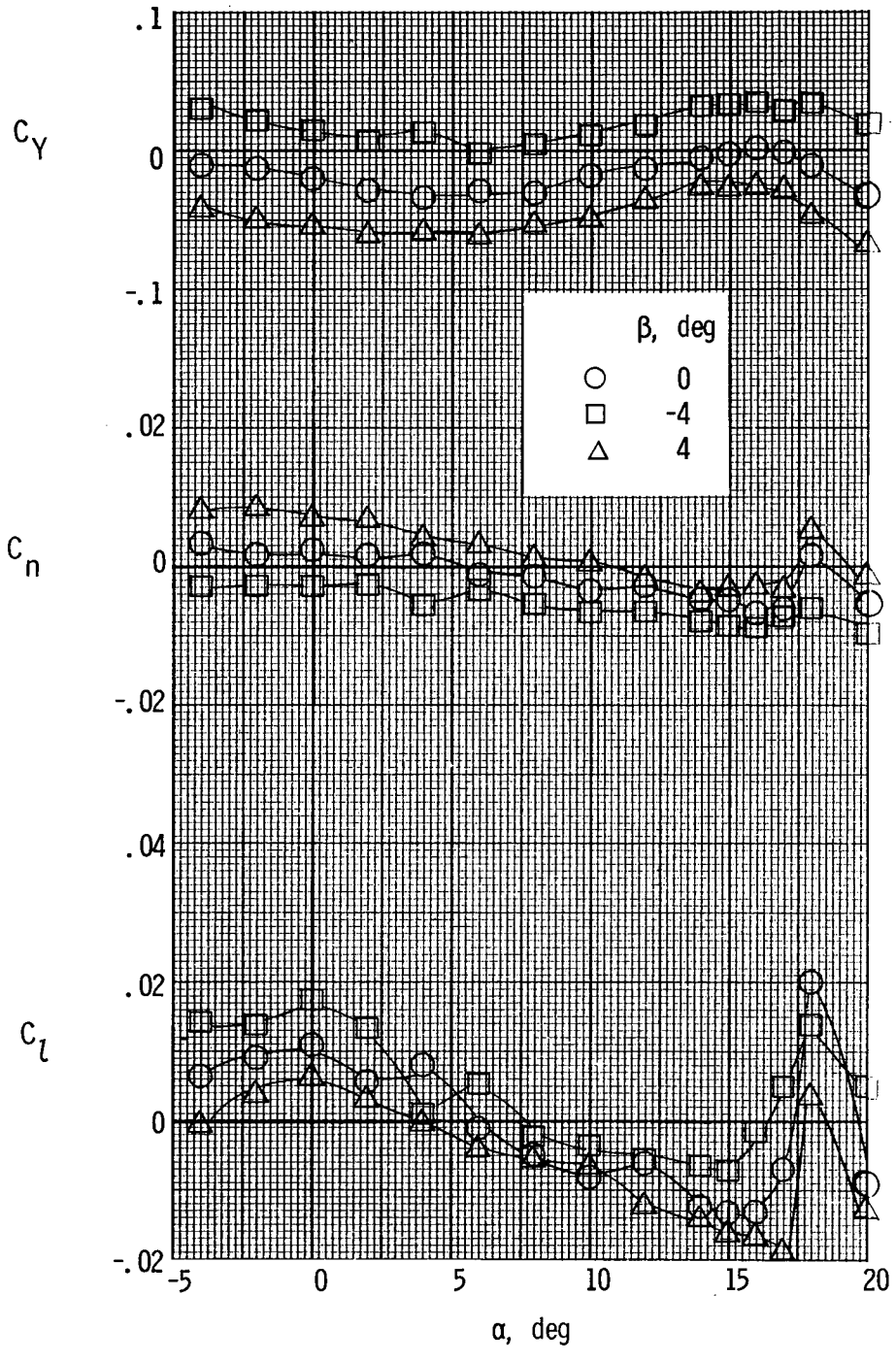

(b) $T_c' = 0.20$.

Figure 47.- Continued.

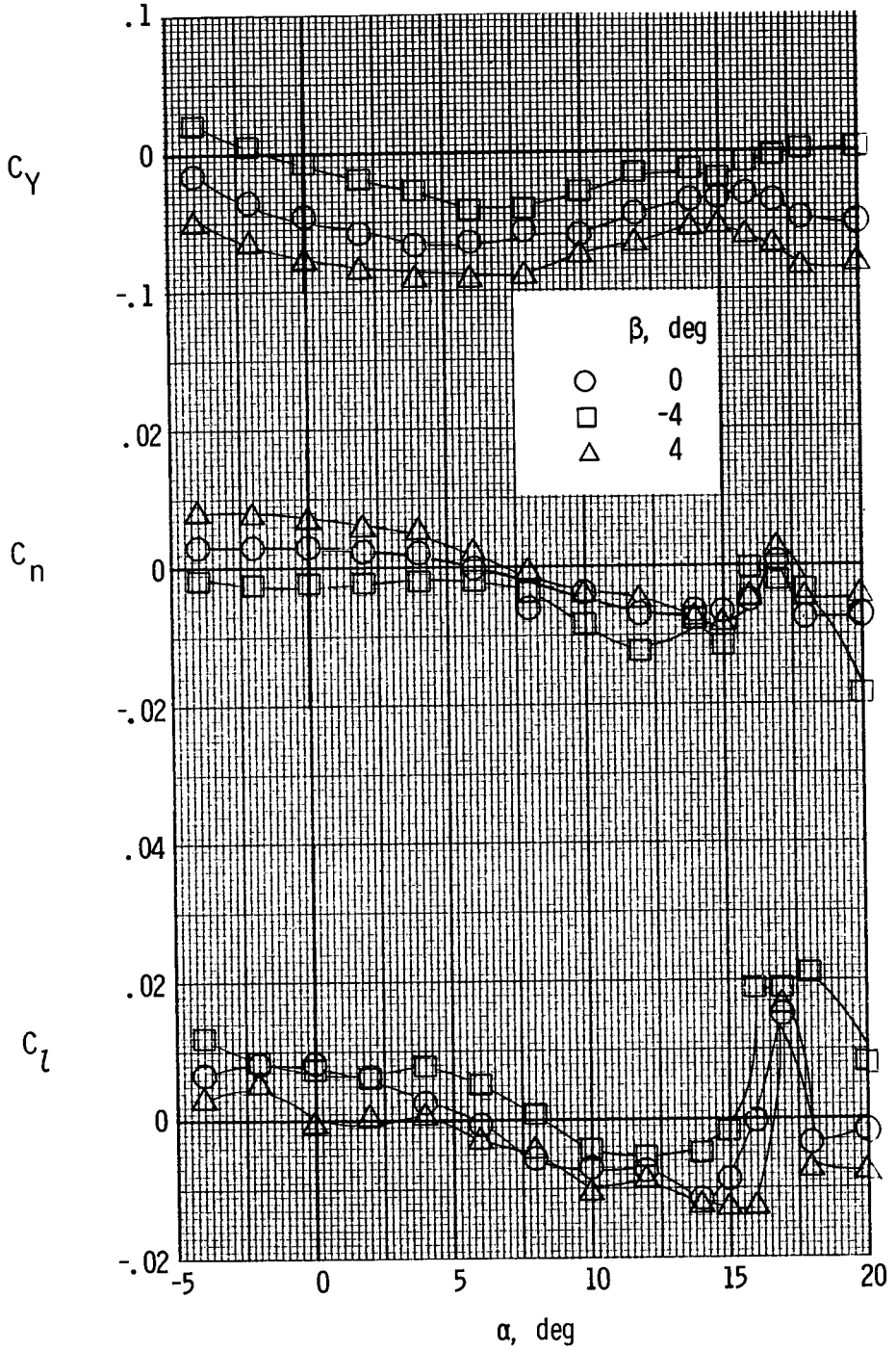

(c) $T_c' = 0.44$.

Figure 47.- Concluded.

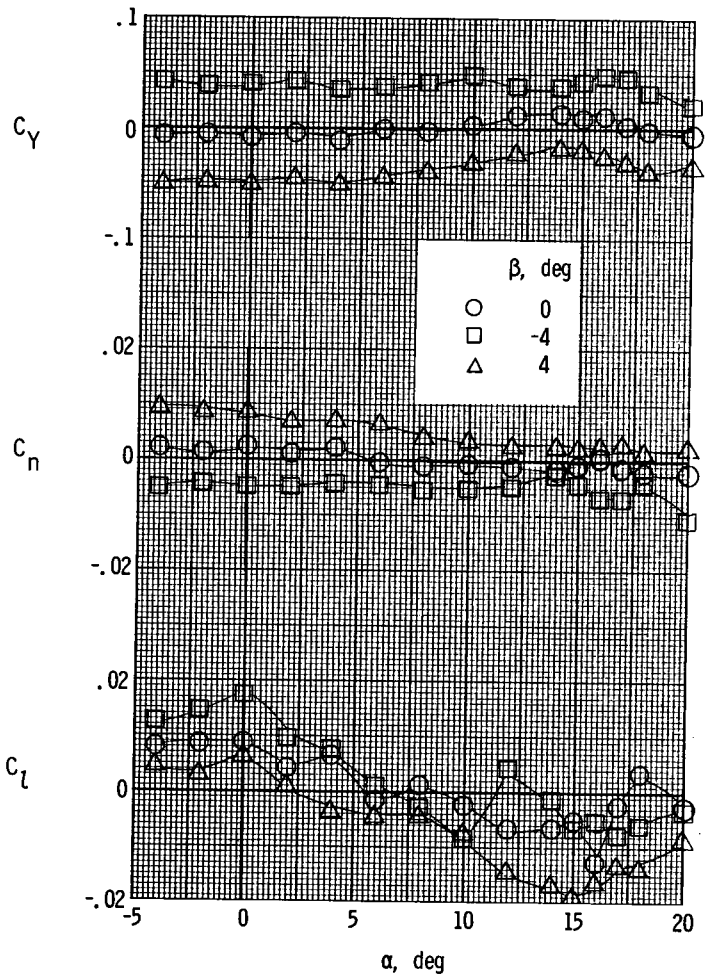

(a) $T_c' = 0$.

Figure 48.- Lateral aerodynamic characteristics of the model with nacelle D. $\delta_f = 27^o$.

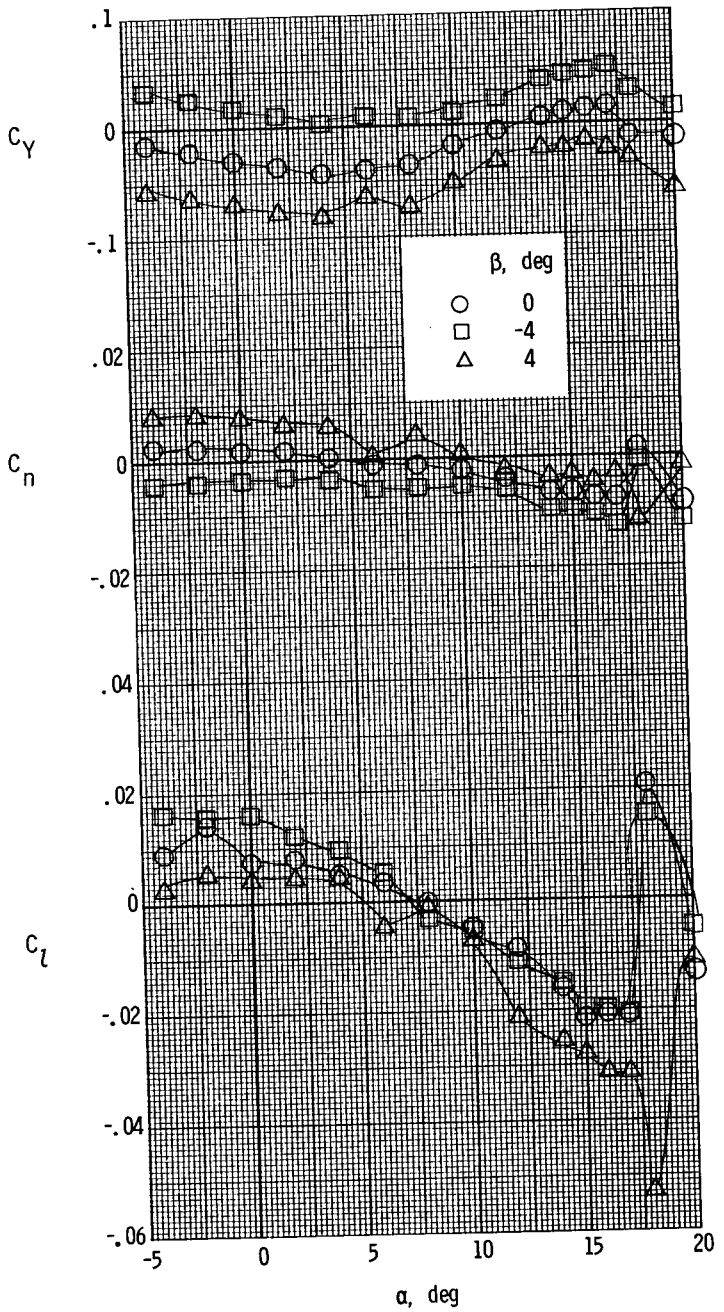

(b) $T_c' = 0.20$.

Figure 48.- Continued.

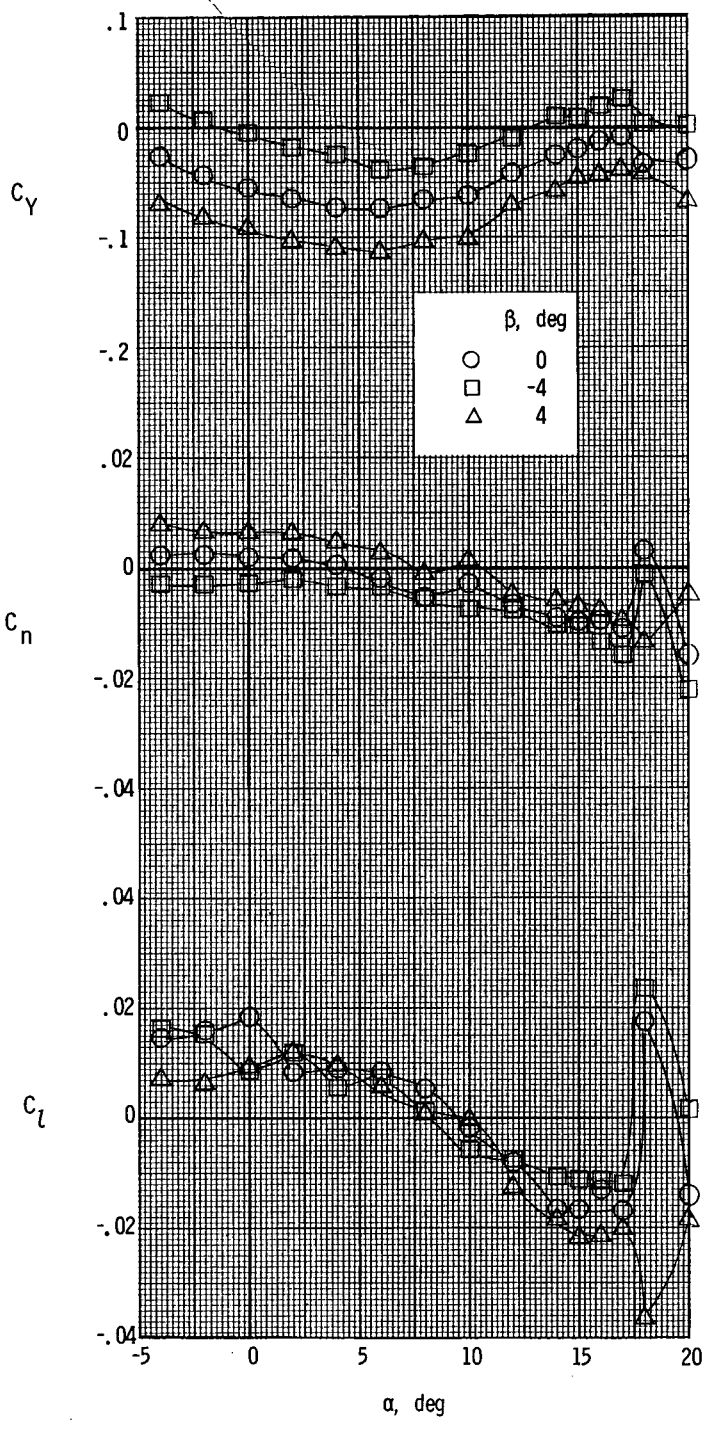

(c) $T_C' = 0.44$.

Figure 48.- Concluded.

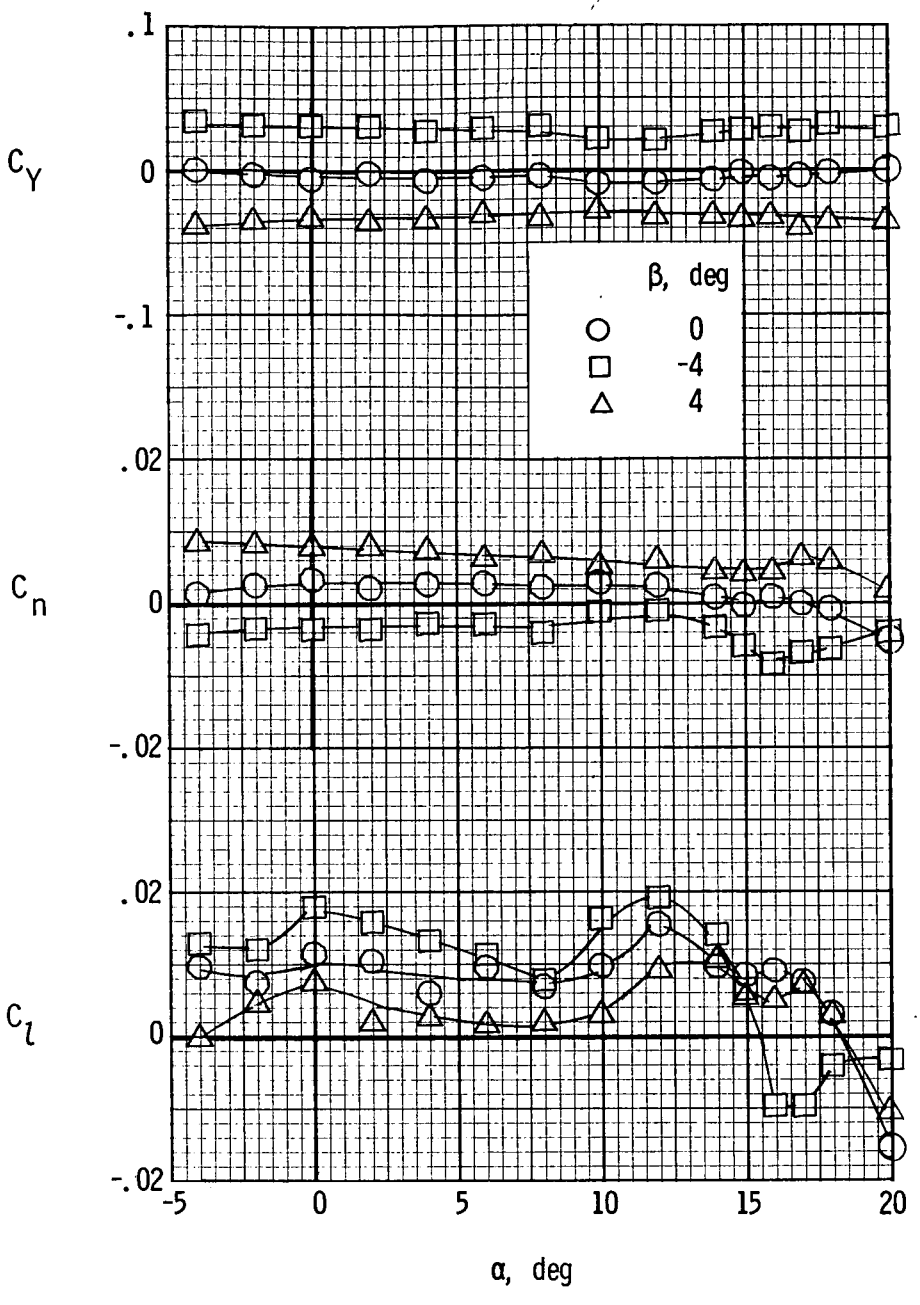

(a) $T_c' = 0$.

Figure 49.- Lateral aerodynamic characteristics of the model with down-at-the-center propeller rotation. $\delta_f = 0^o$; nacelle A.

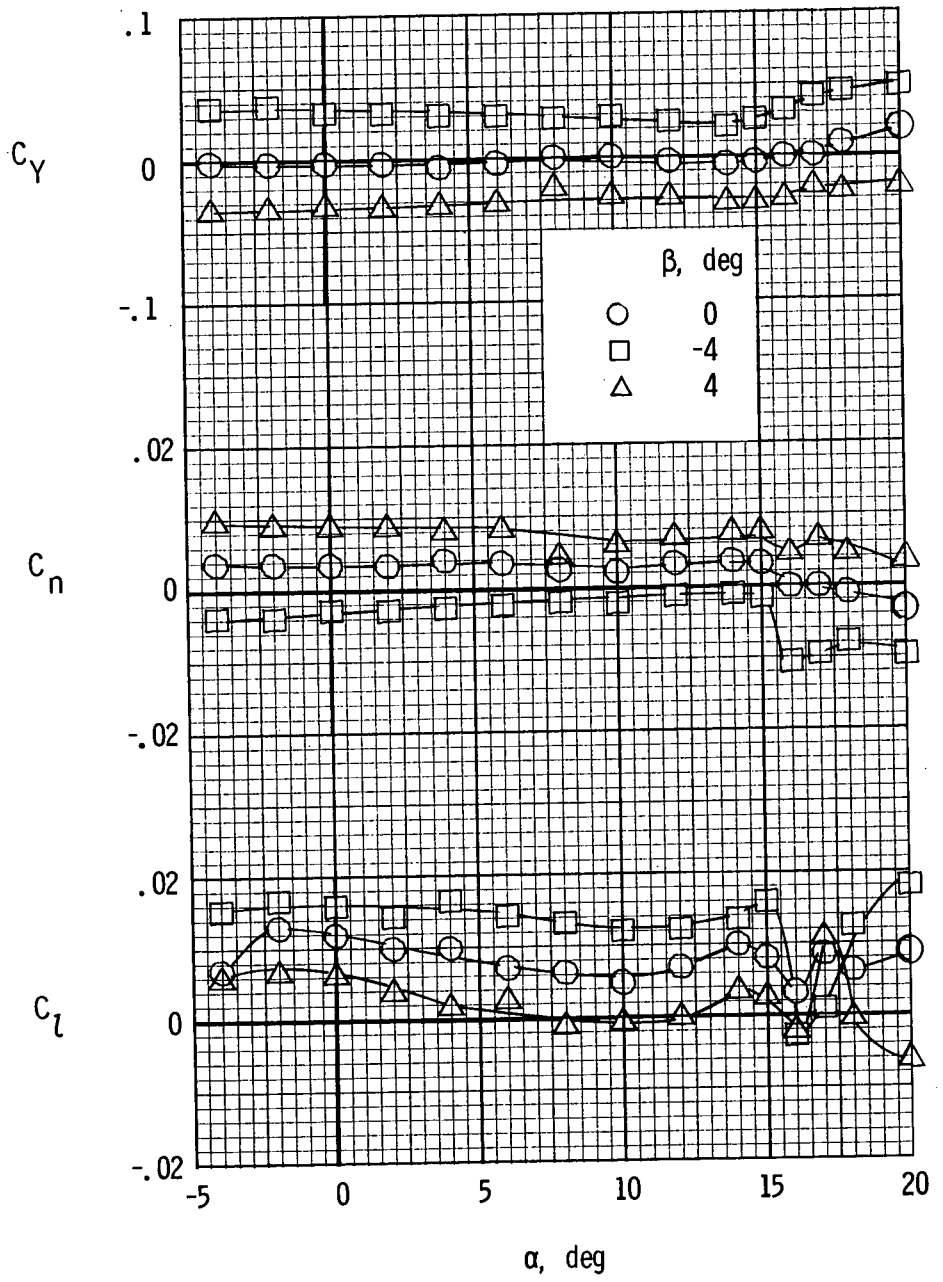

(b) $T_c' = 0.20$.

Figure 49.- Continued.

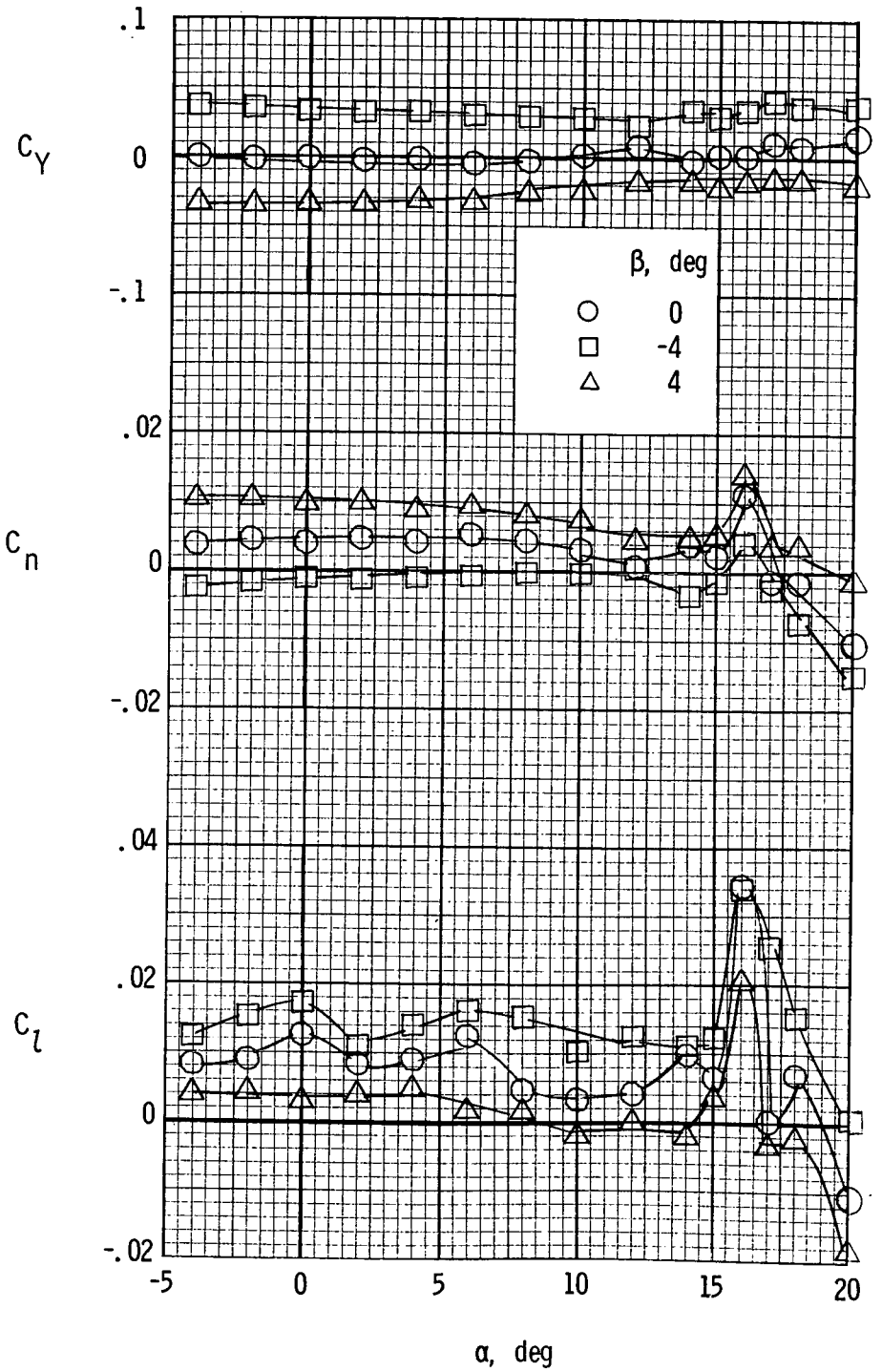

(c) $T_c' = 0.44$.

Figure 49.- Concluded.

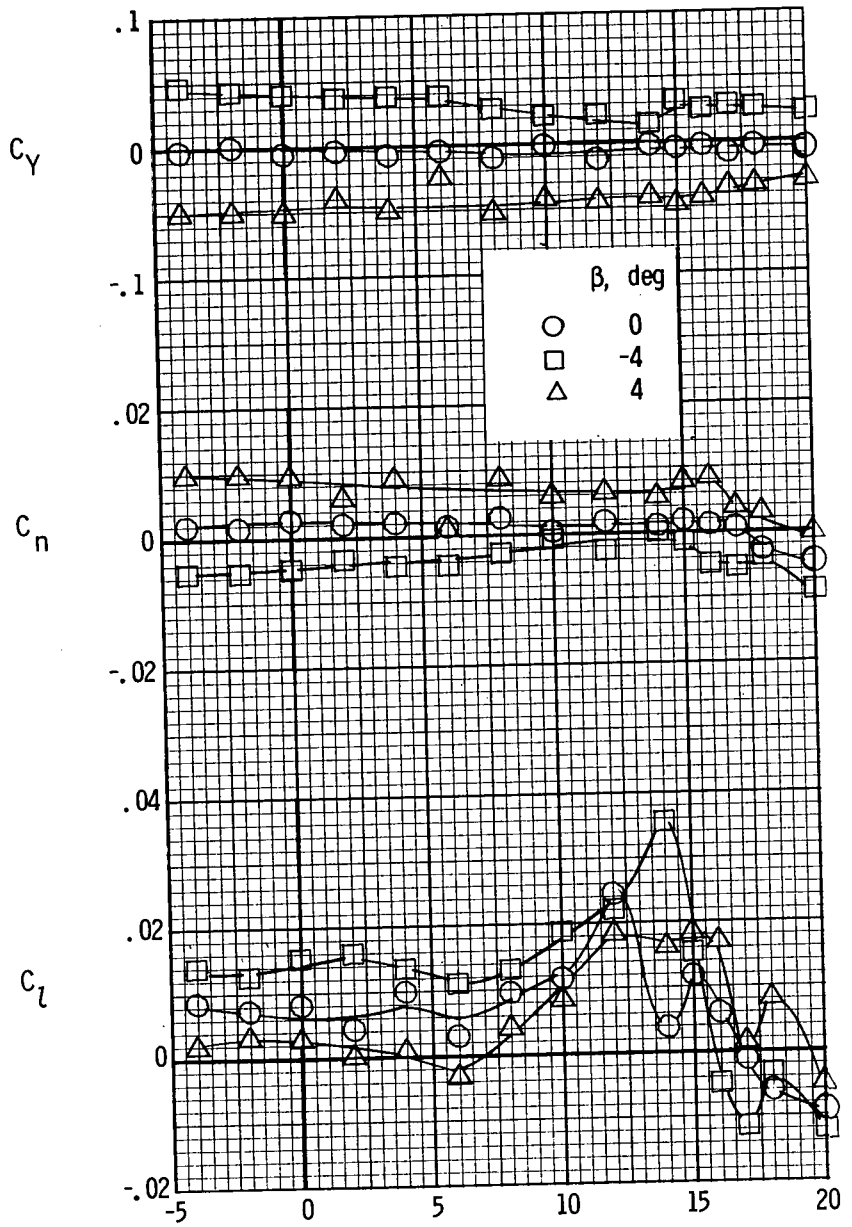

(a) $T_c' = 0$.

Figure 50.- Lateral aerodynamic characteristics of the model with down-at-the-center propeller rotation. $\delta_f = 27^o$; nacelle A.

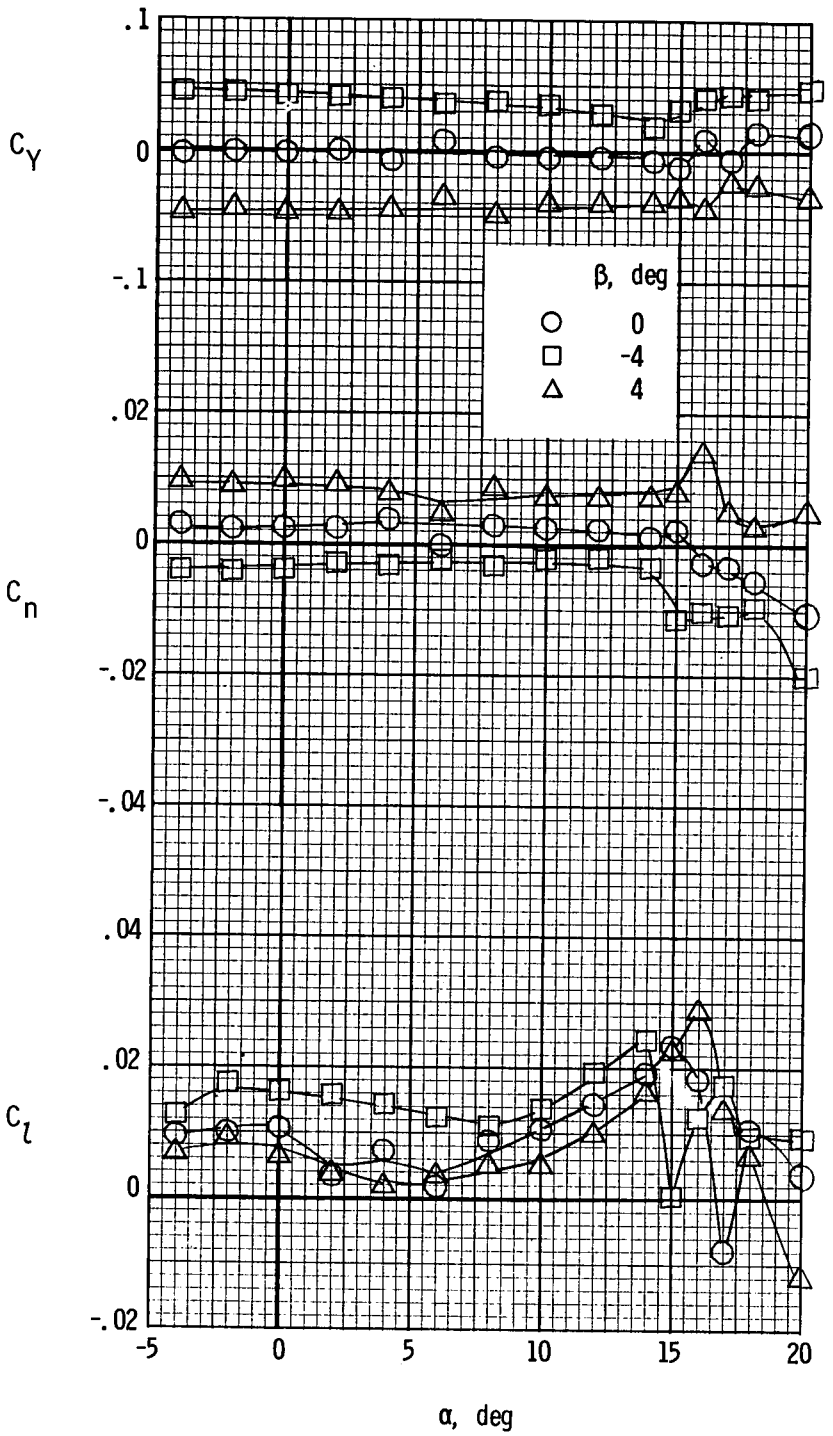

(b) $T_c' = 0.20$.

Figure 50.- Continued.

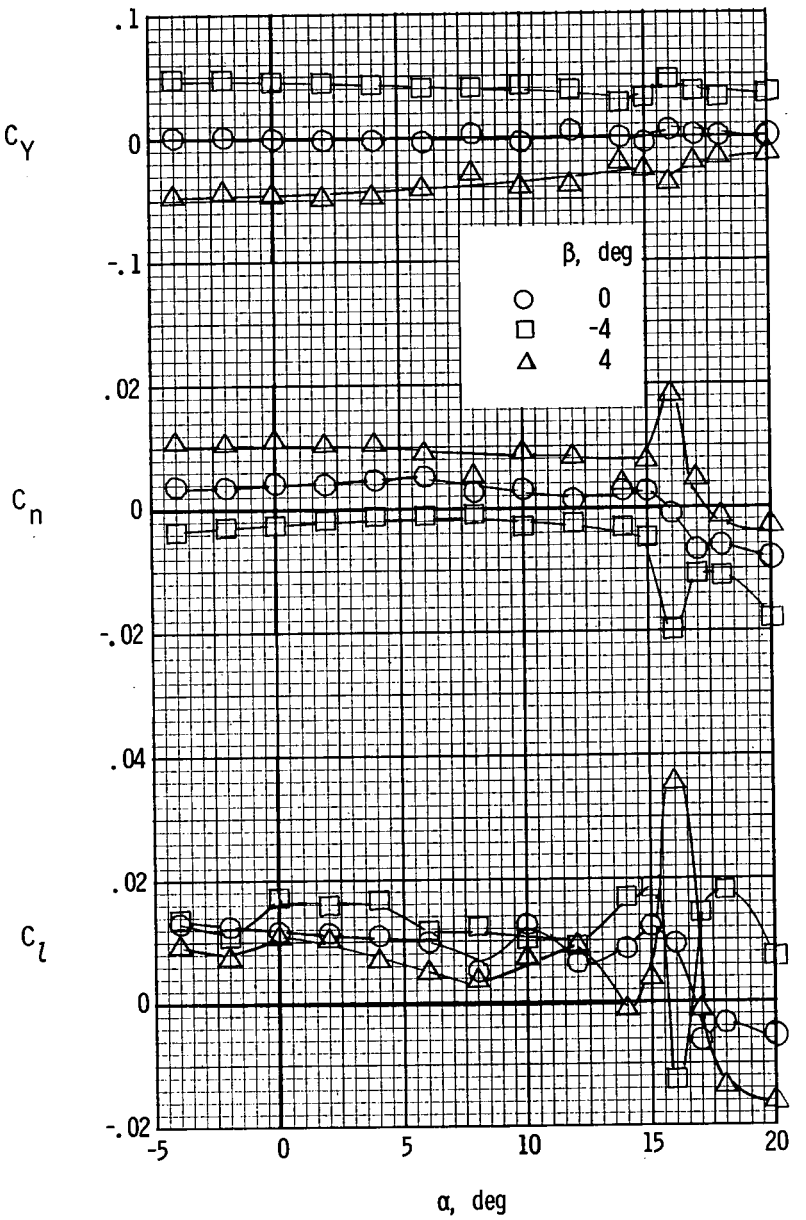

(c) $T_c' = 0.44$.

Figure 50.- Concluded.

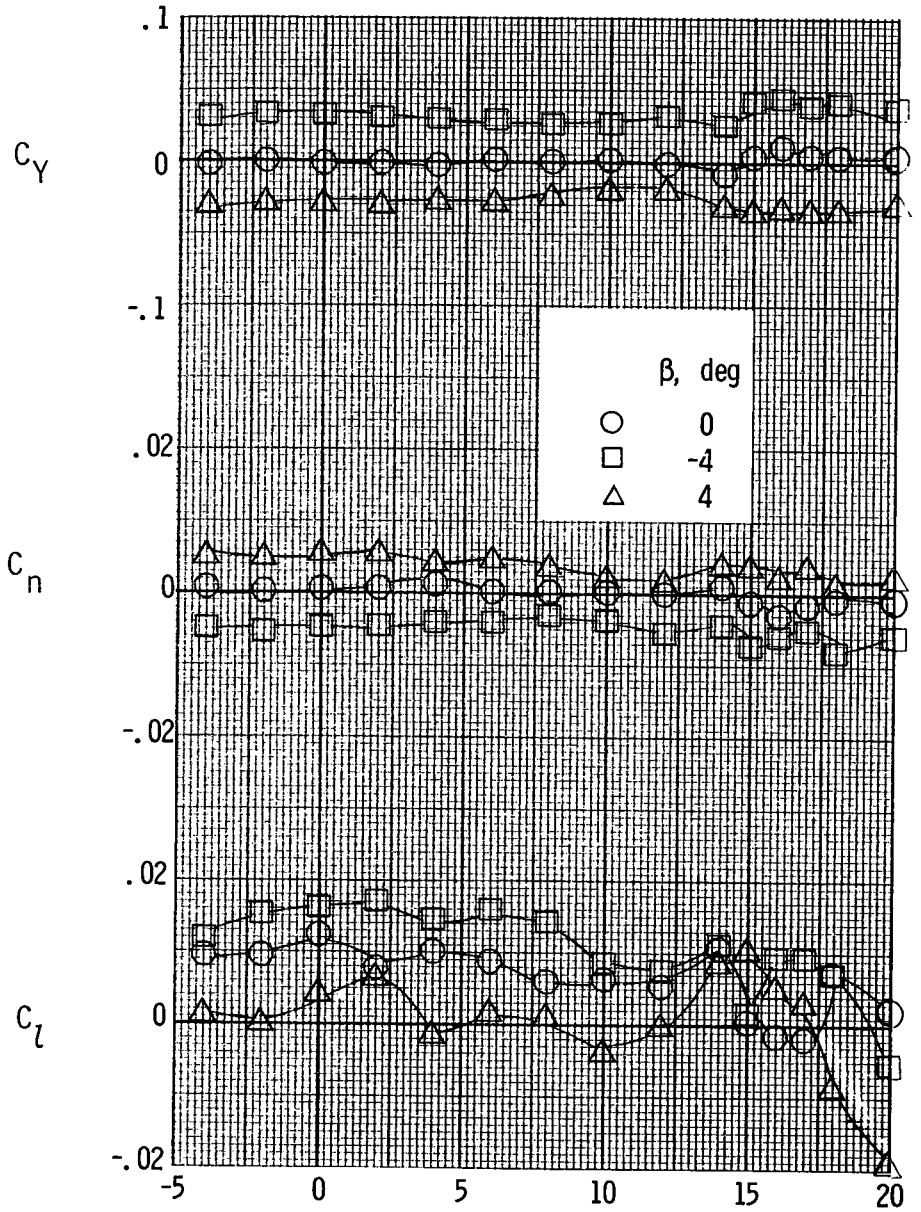

(a) $T_c' = 0$.

Figure 51.- Lateral aerodynamic characteristics of the model with up-at-the-center propeller rotation. $\delta_f = 0^o$; nacelle A.

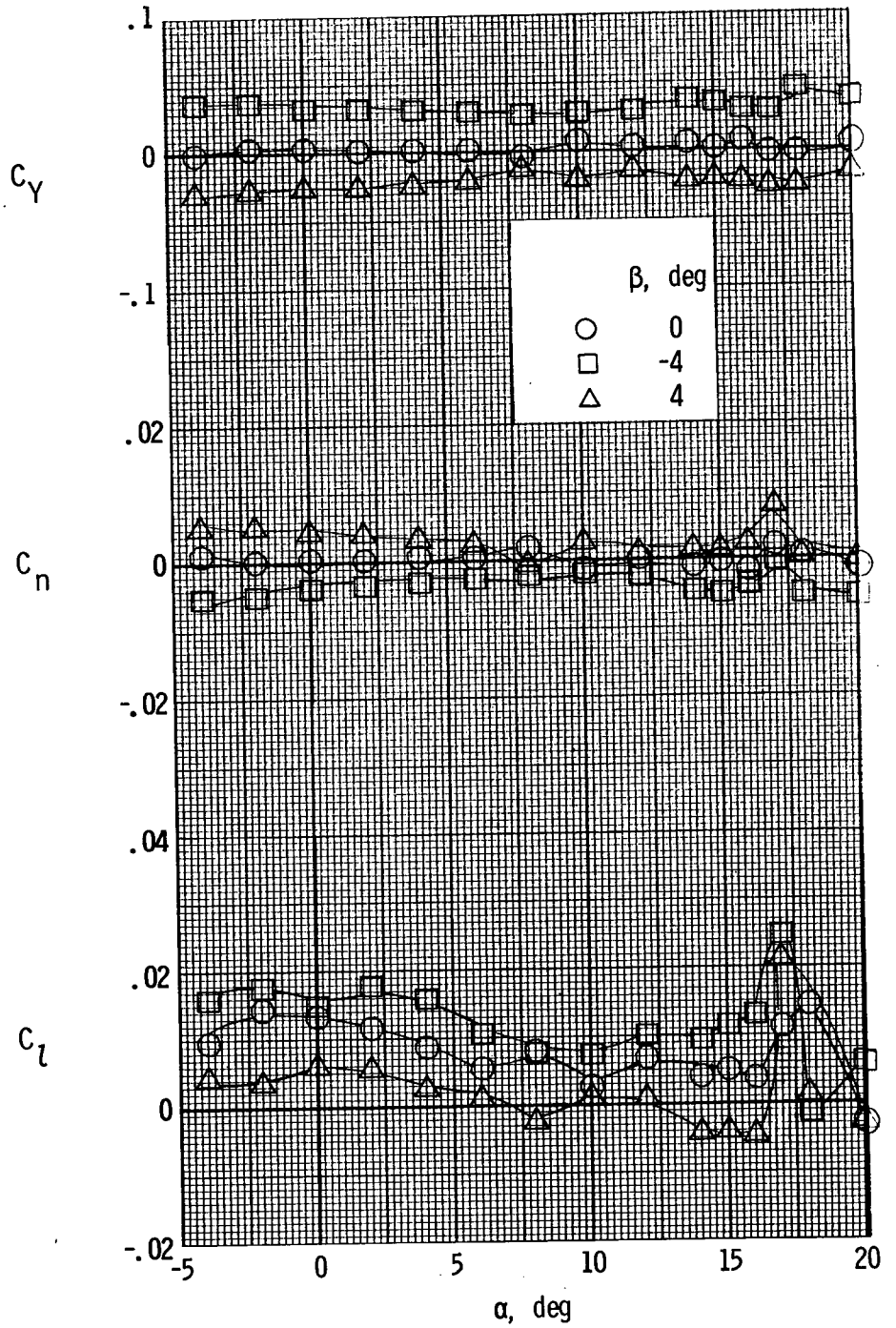

(b) $T_c' = 0.20$.

Figure 51.- Continued.

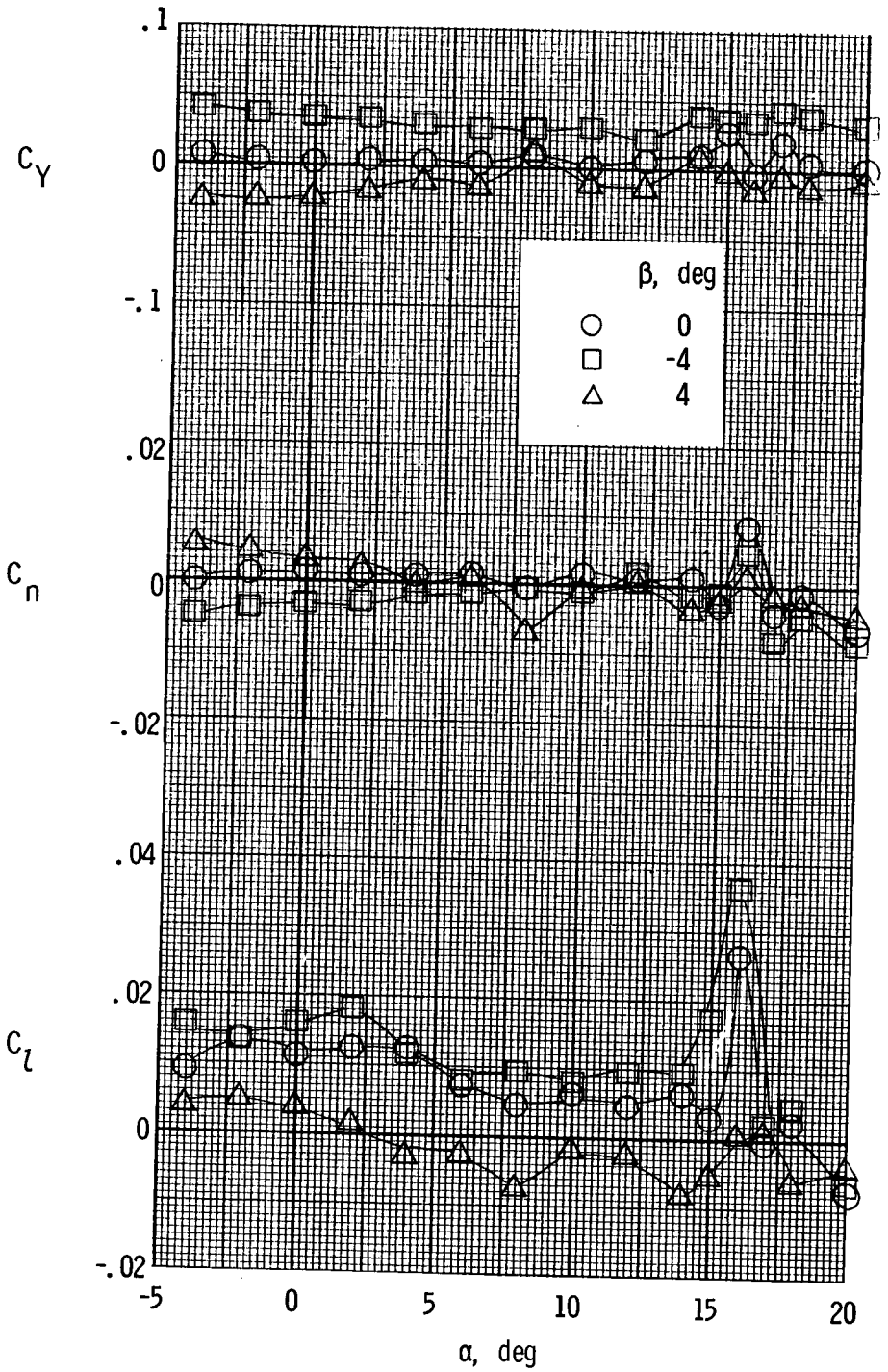

(c) $T_c' = 0.44$.

Figure 51.- Concluded.

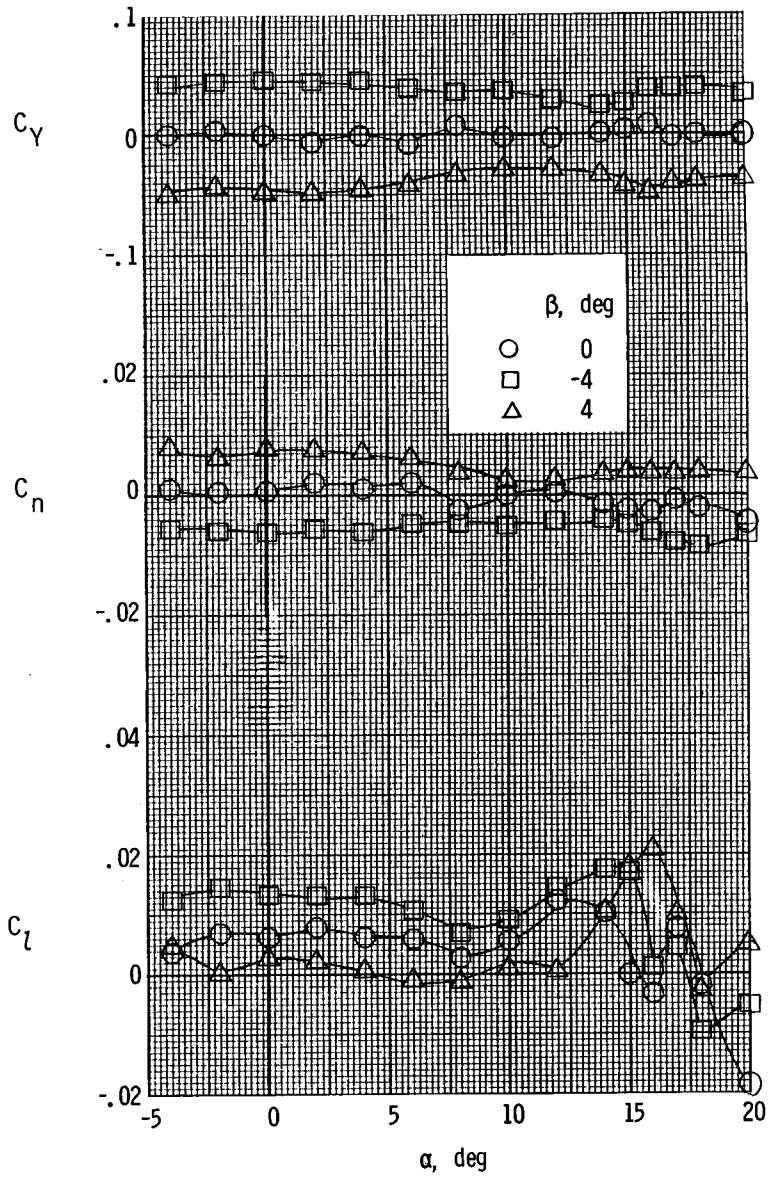

(a) $T_c' = 0$.

Figure 52.- Lateral aerodynamic characteristics of the model with up-at-the-center propeller rotation. $\delta_f = 27^o$; nacelle A.

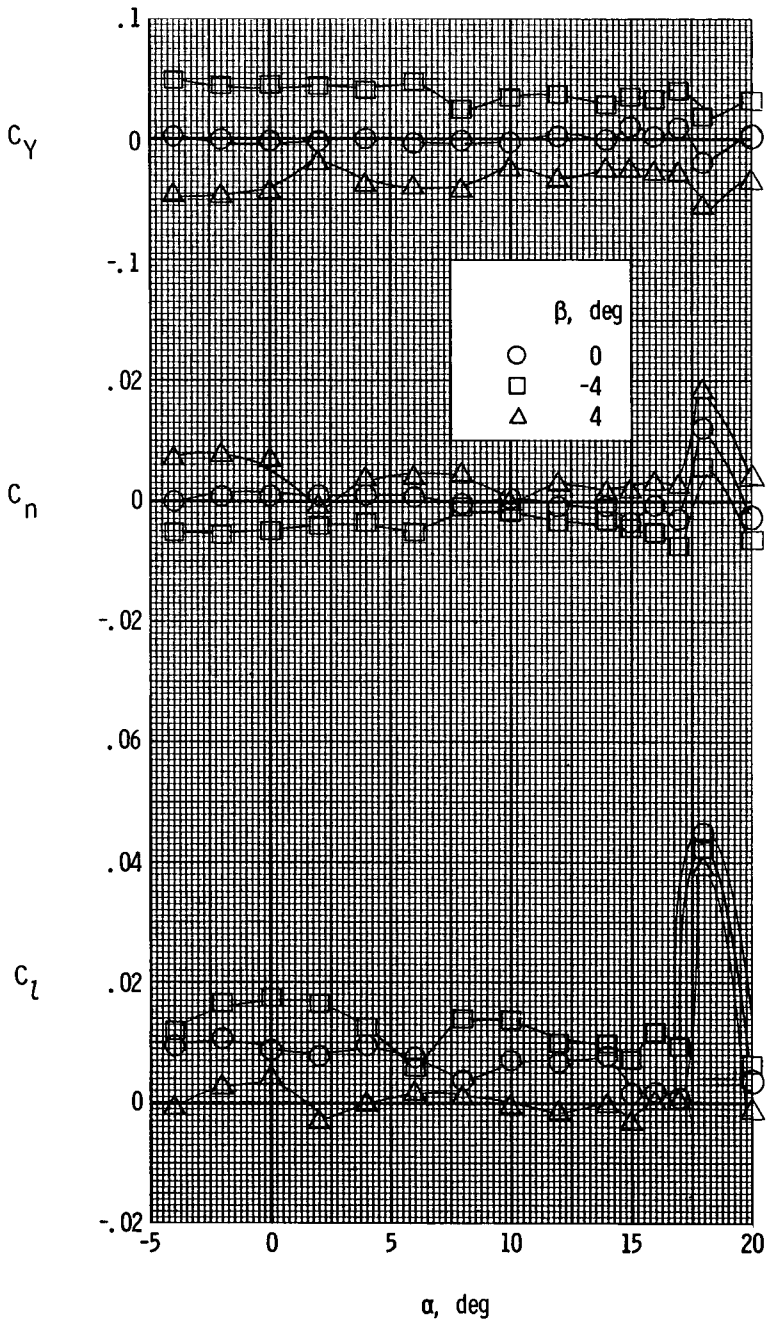

(b) $T_c' = 0.20$.

Figure 52.- Continued.

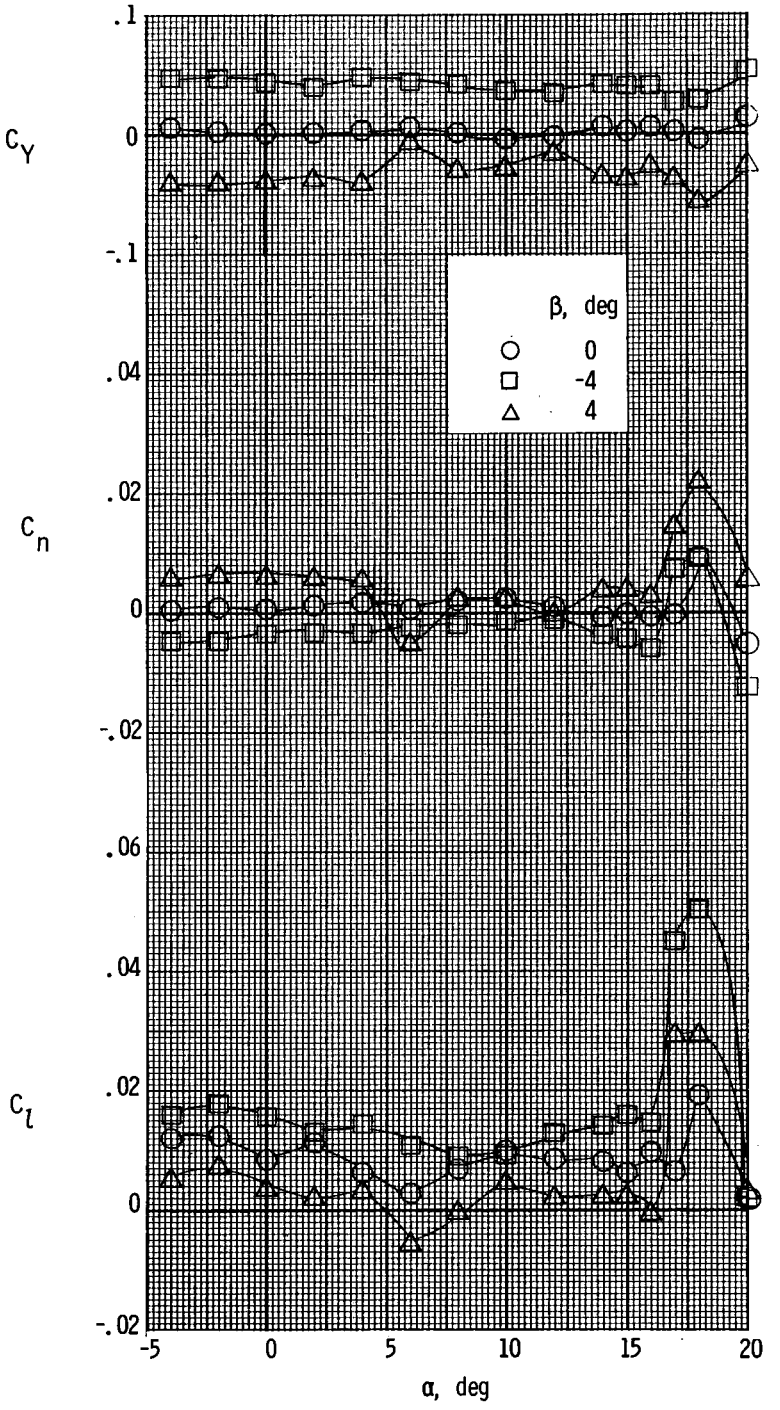

(c) $T_c' = 0.44$.

Figure 52.- Concluded.

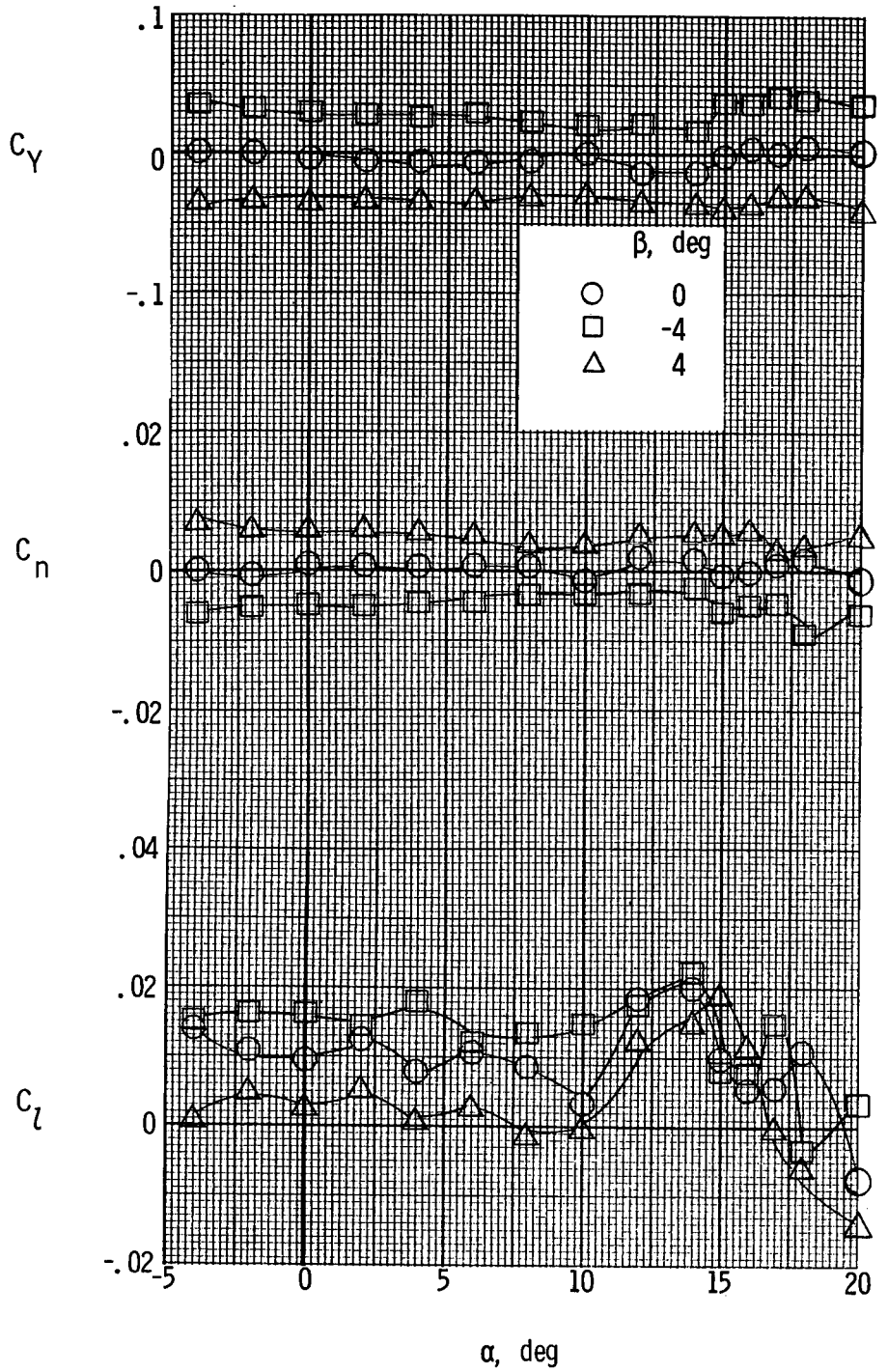

(a) $T_c' = 0$.

Figure 53.- Lateral aerodynamic characteristics of model with counterclockwise propeller rotation. $\delta_f = 0^o$; nacelle A.

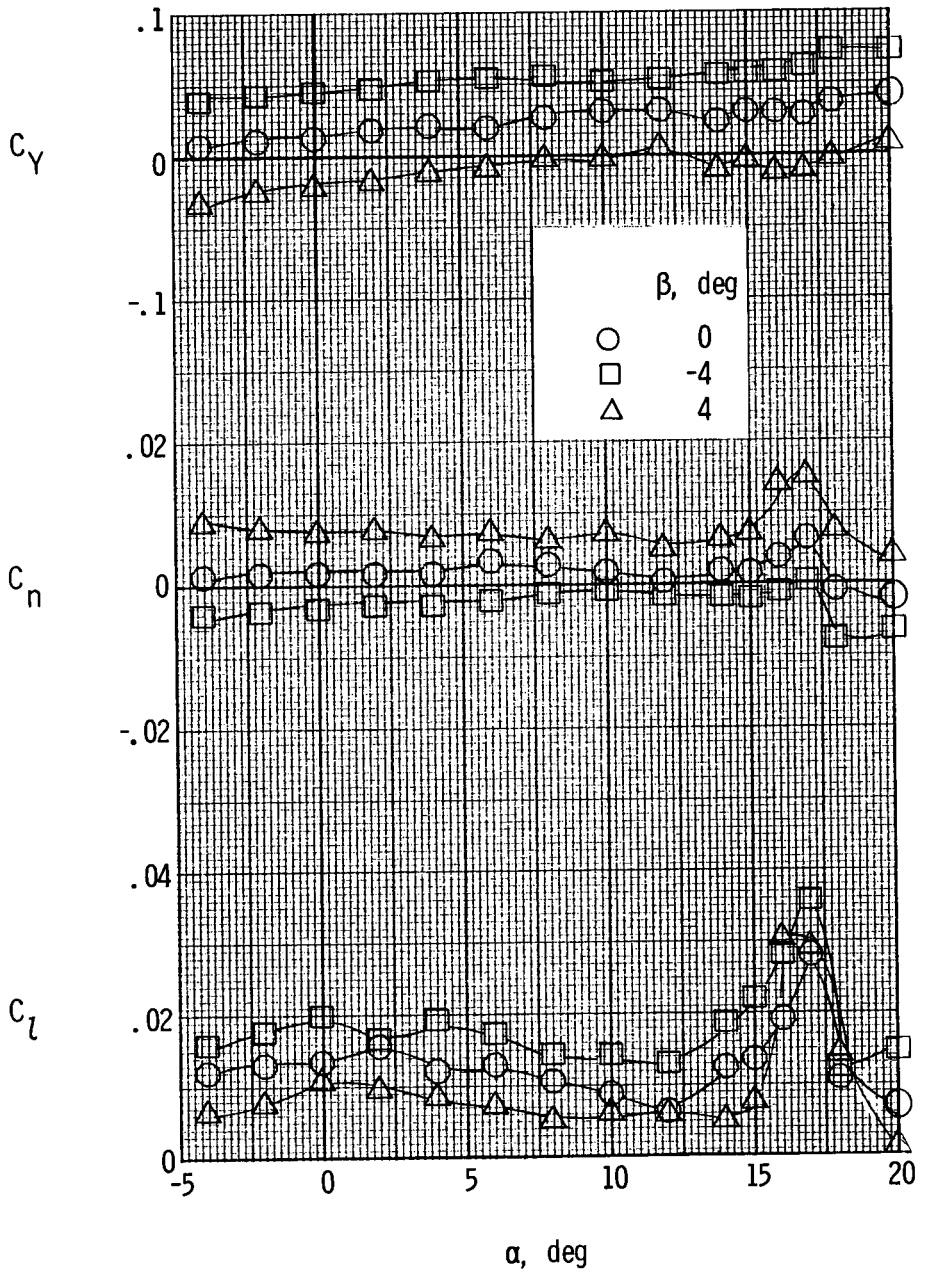

(b) $T_c' = 0.20$.

Figure 53.- Continued.

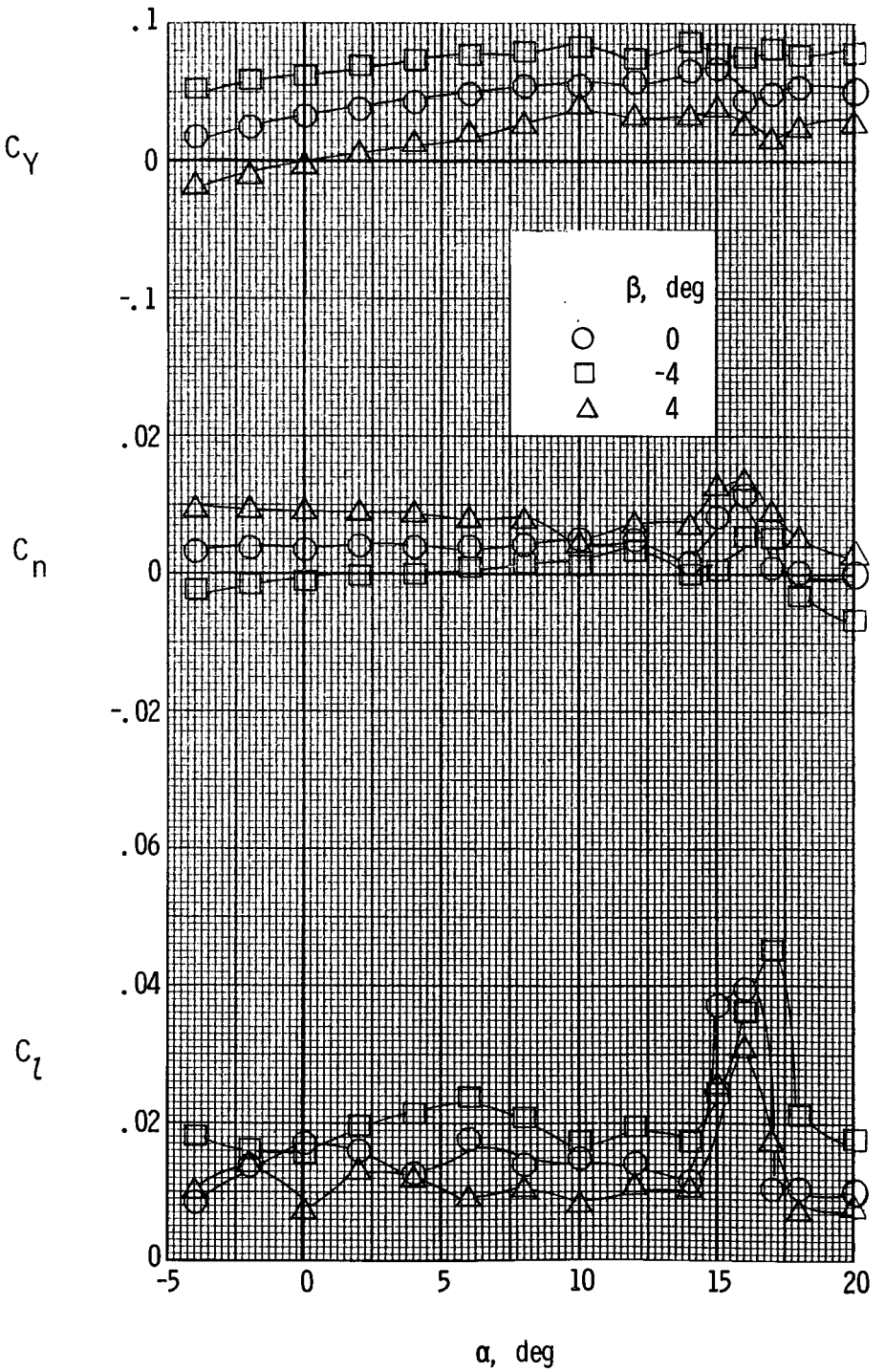

(c) $T_c' = 0.44$.

Figure 53.- Concluded.

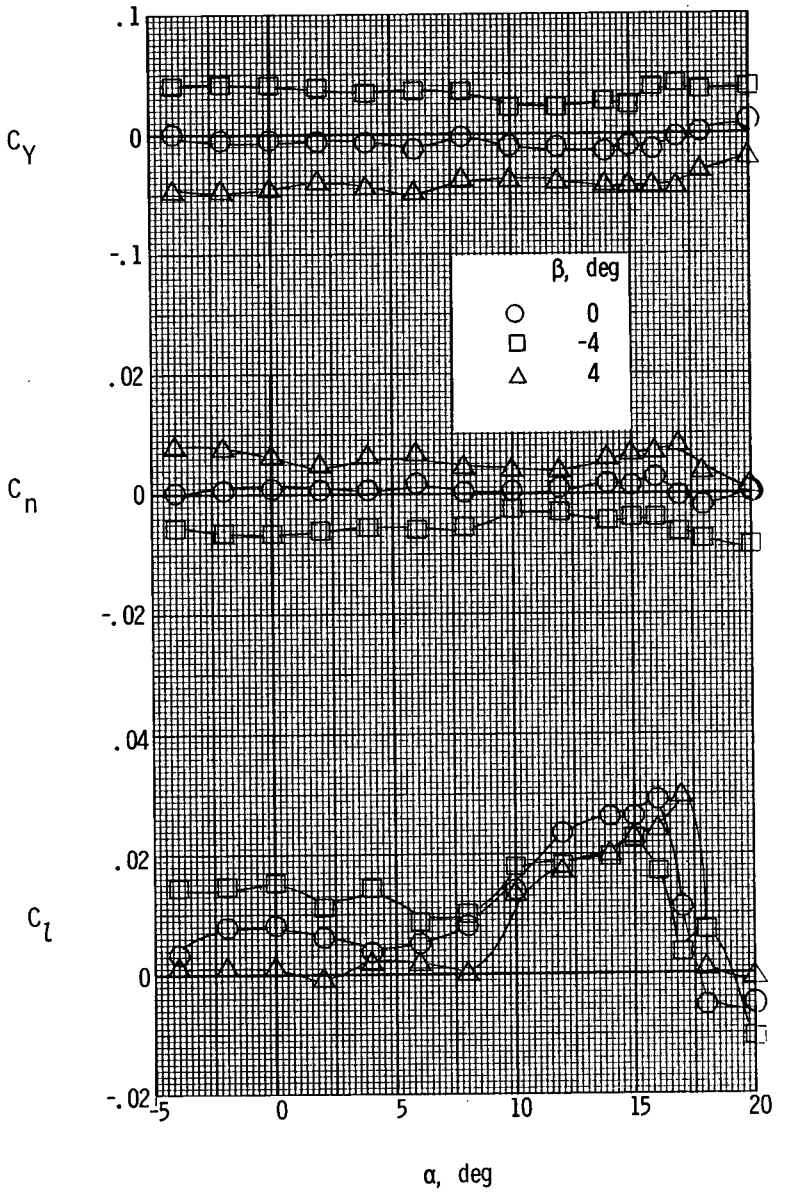

(a) $T_c' = 0$.

Figure 54.- Lateral aerodynamic characteristics of the model with counterclockwise propeller rotation. $\delta_f = 27^o$; nacelle A.

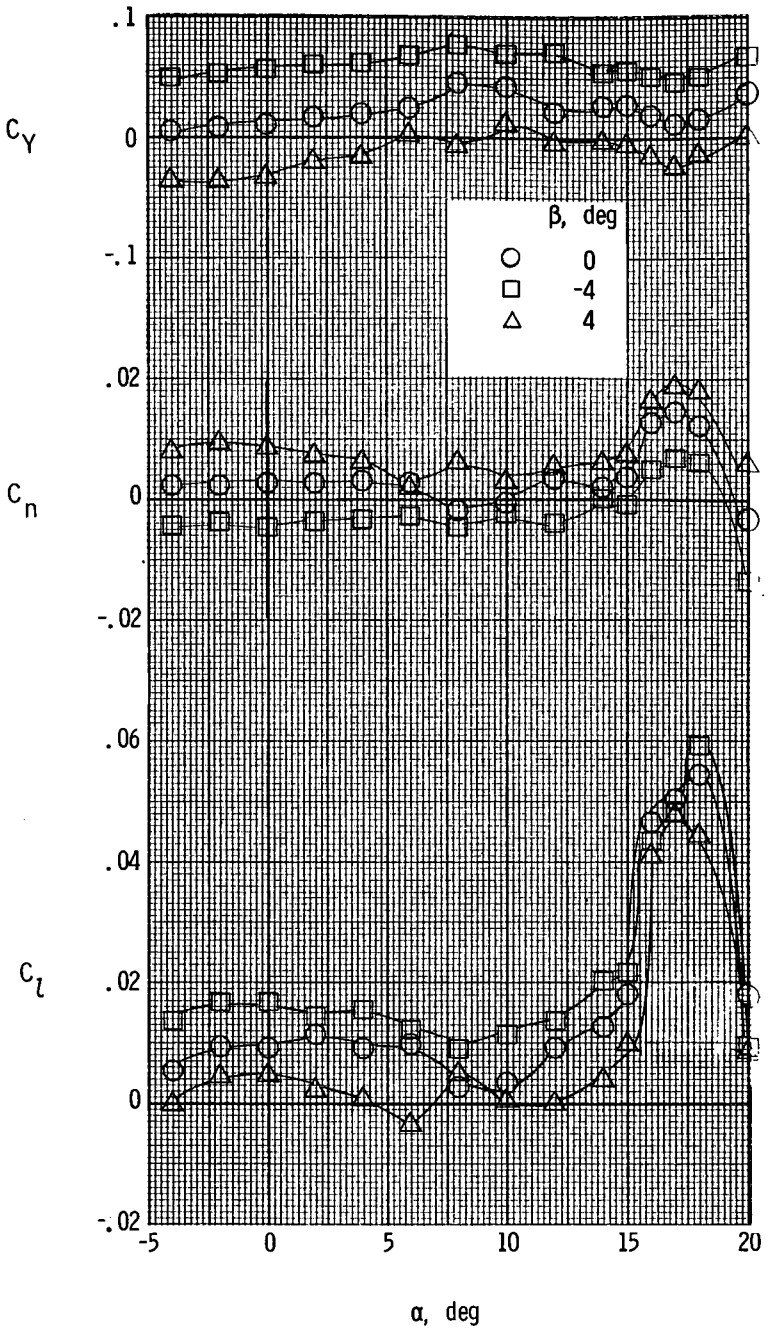

(b) $T_c' = 0.20$.

Figure 54.- Continued.

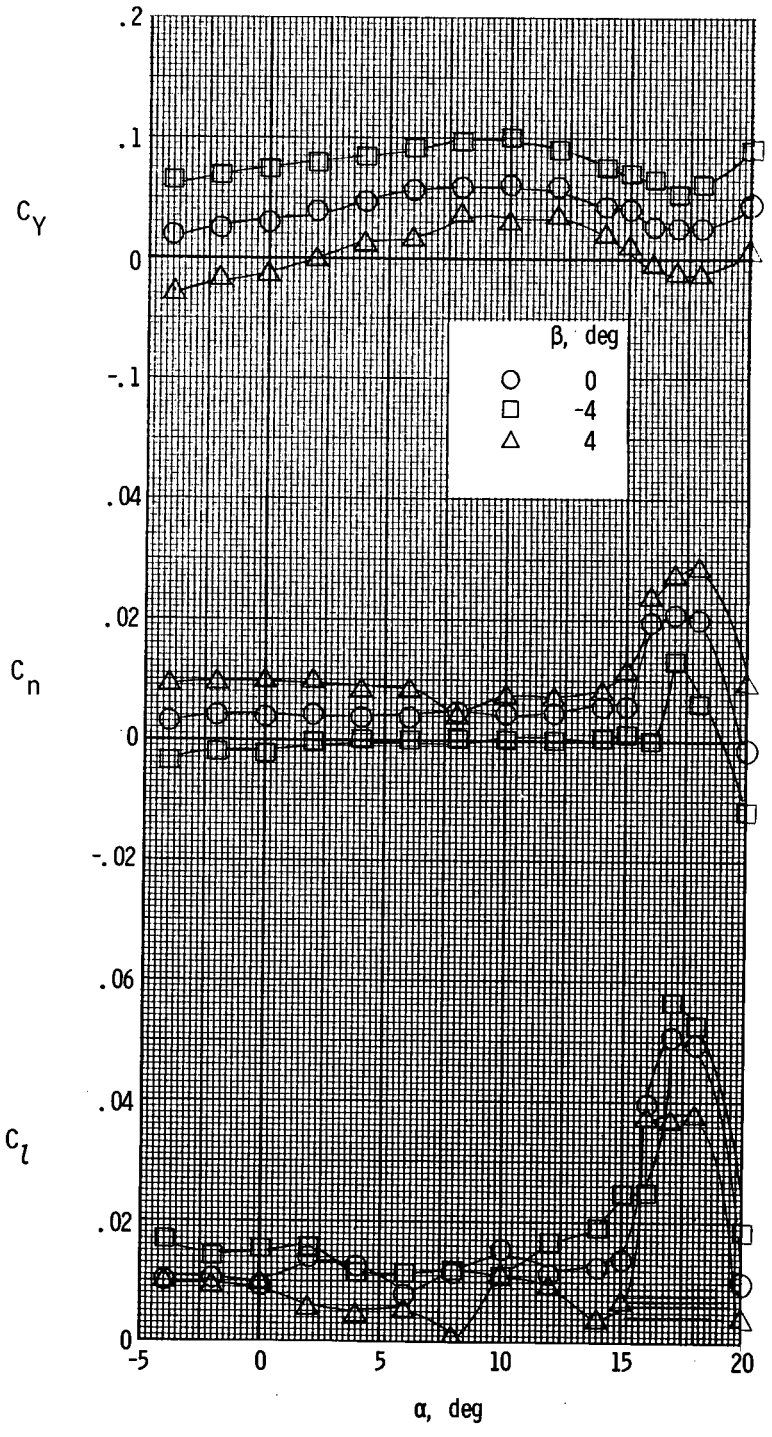

(c) $T_c' = 0.44$.

Figure 54.- Concluded.

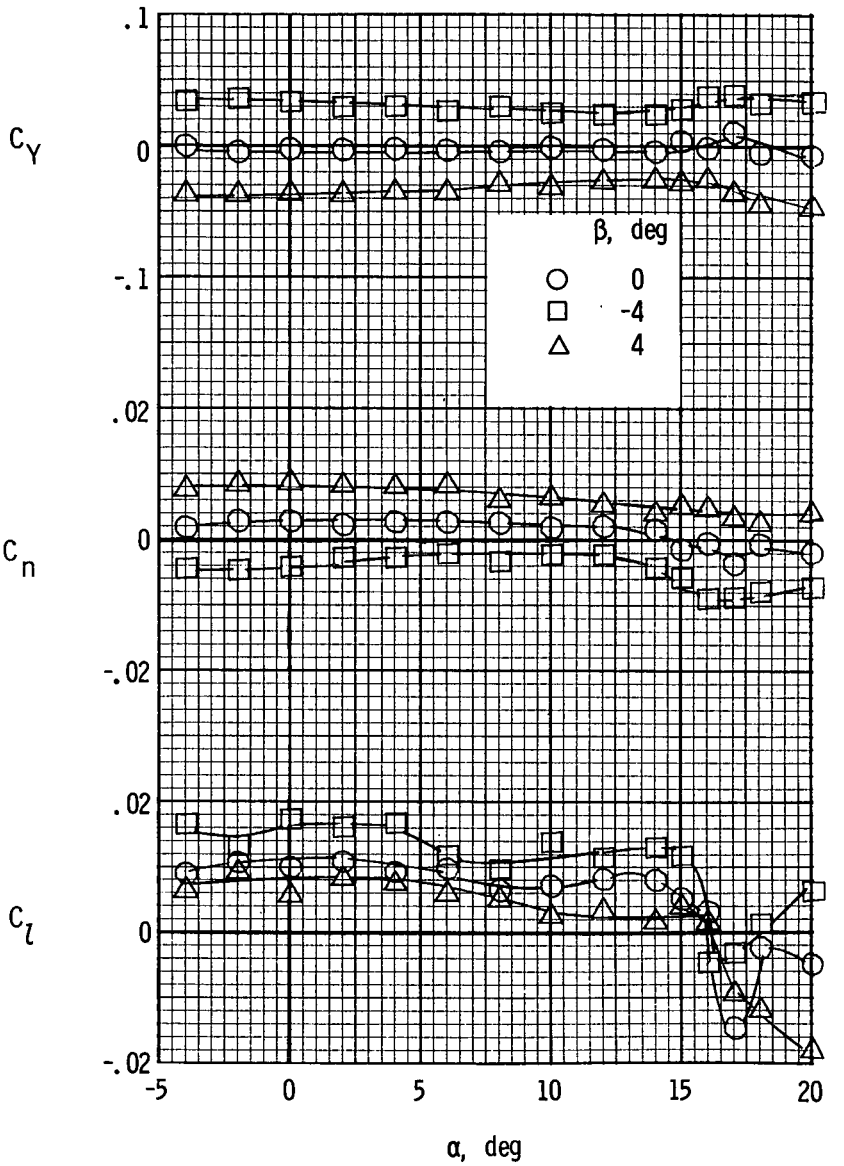

(a) $T_c' = 0$.

Figure 55.- Lateral aerodynamic characteristics of the model with the modified airfoil section. $\delta_f = 0^o$; nacelle A.

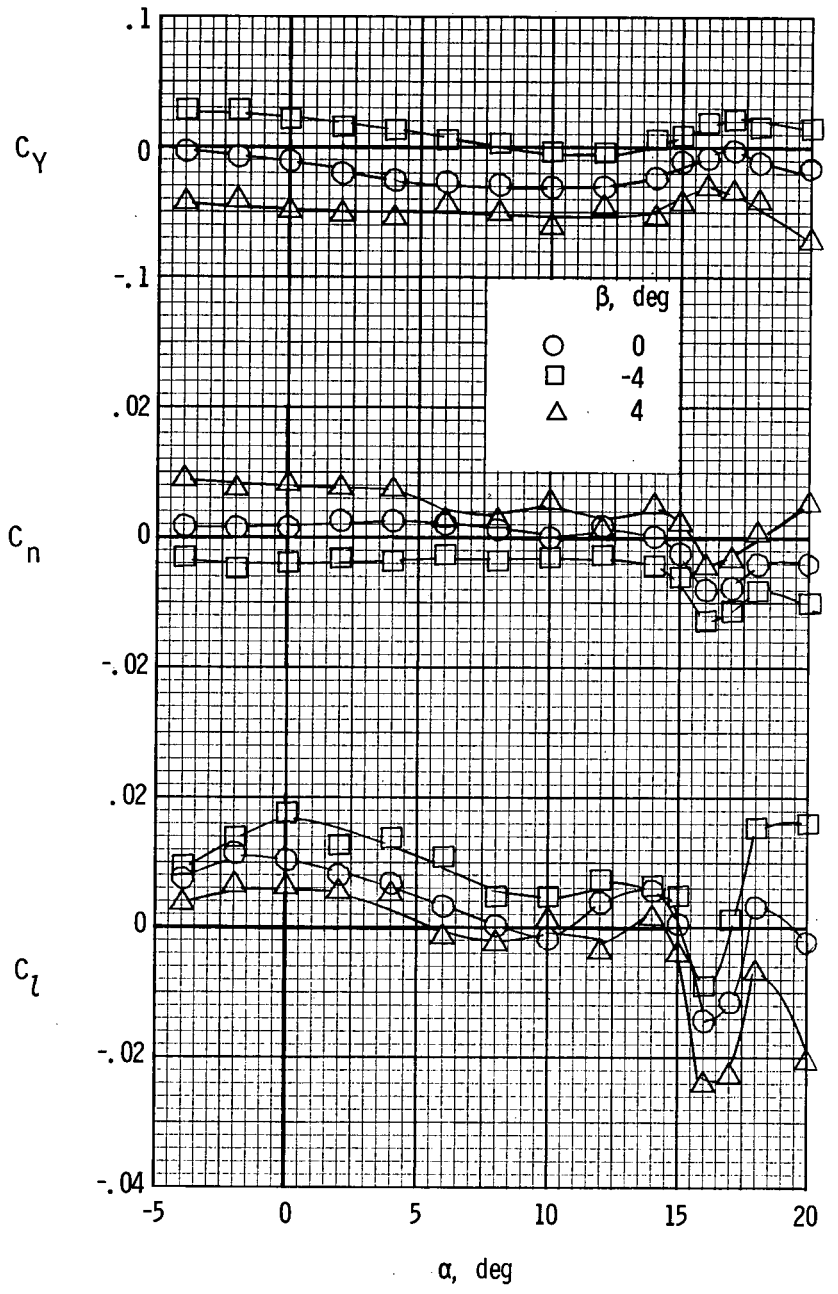

(b) $T_c' = 0.20$.

Figure 55.- Continued.

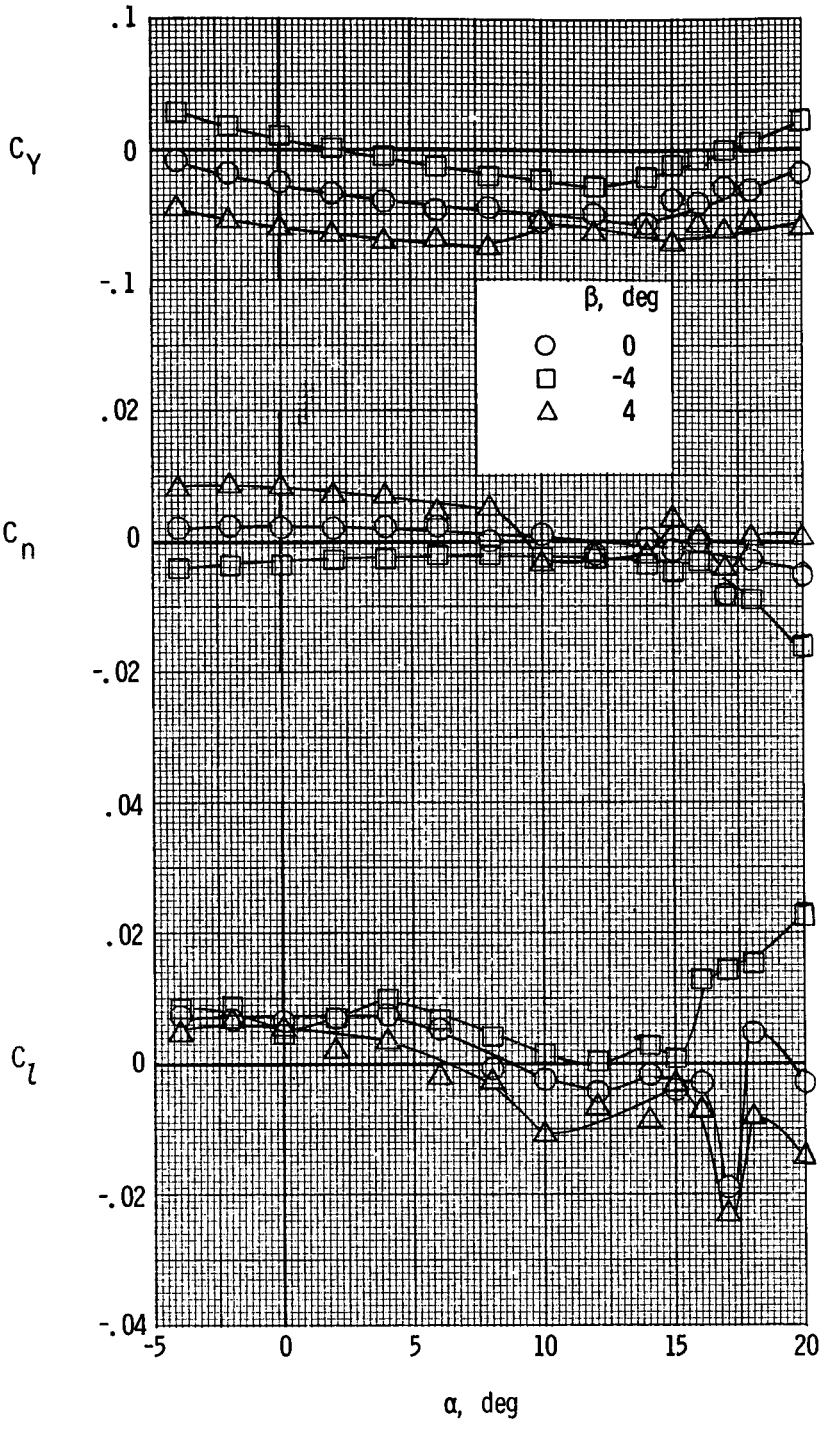

(c) $T_c' = 0.44$.

Figure 55.- Concluded.

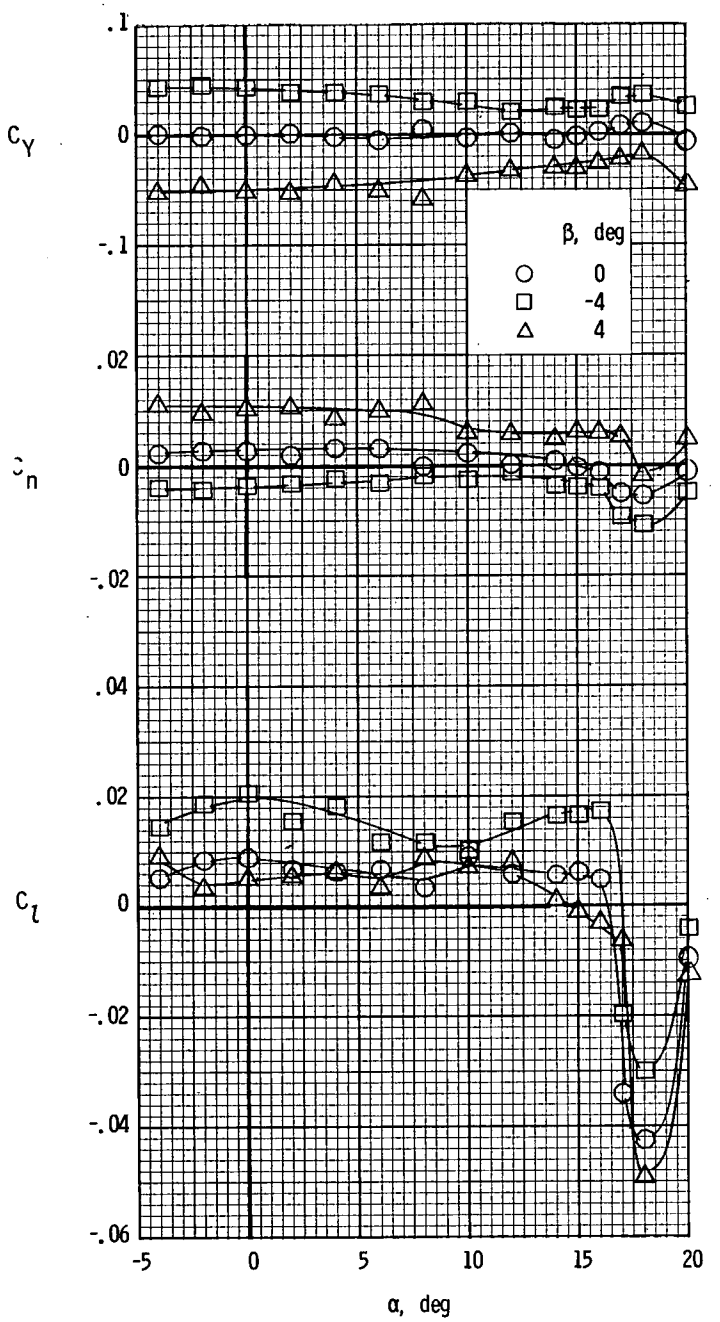

(a) $T'_c = 0$.

Figure 56.- Lateral aerodynamic characteristics of the model with the modified airfoil section. $\delta_f = 27^o$; nacelle A.

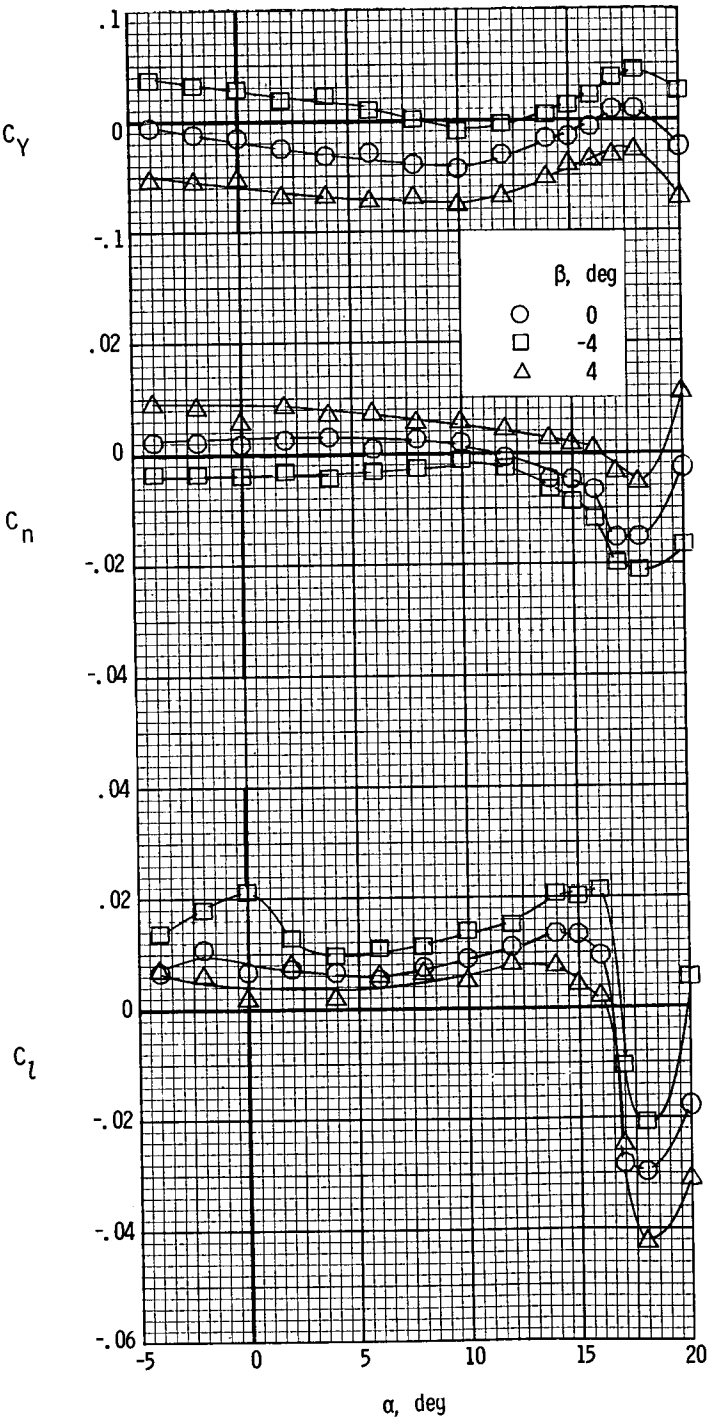

(b) $T_c' = 0.20$.

Figure 56.- Continued.

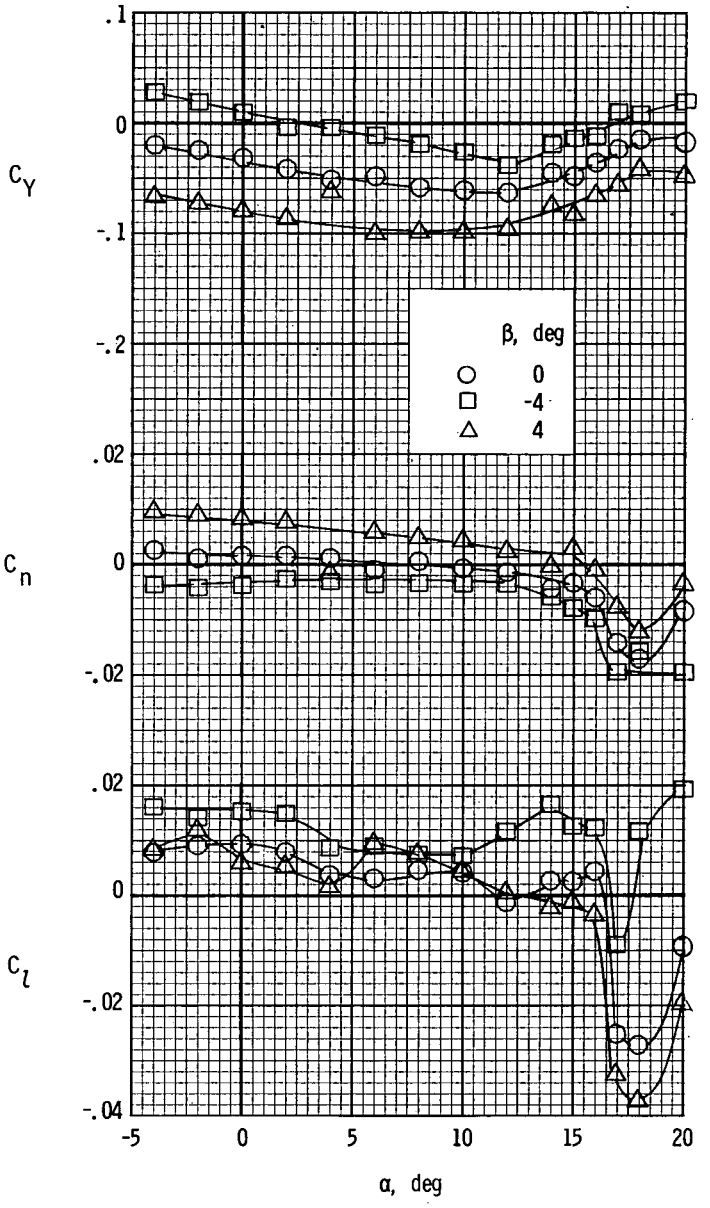

(c) $T_c' = 0.44$.

Figure 56.- Concluded.

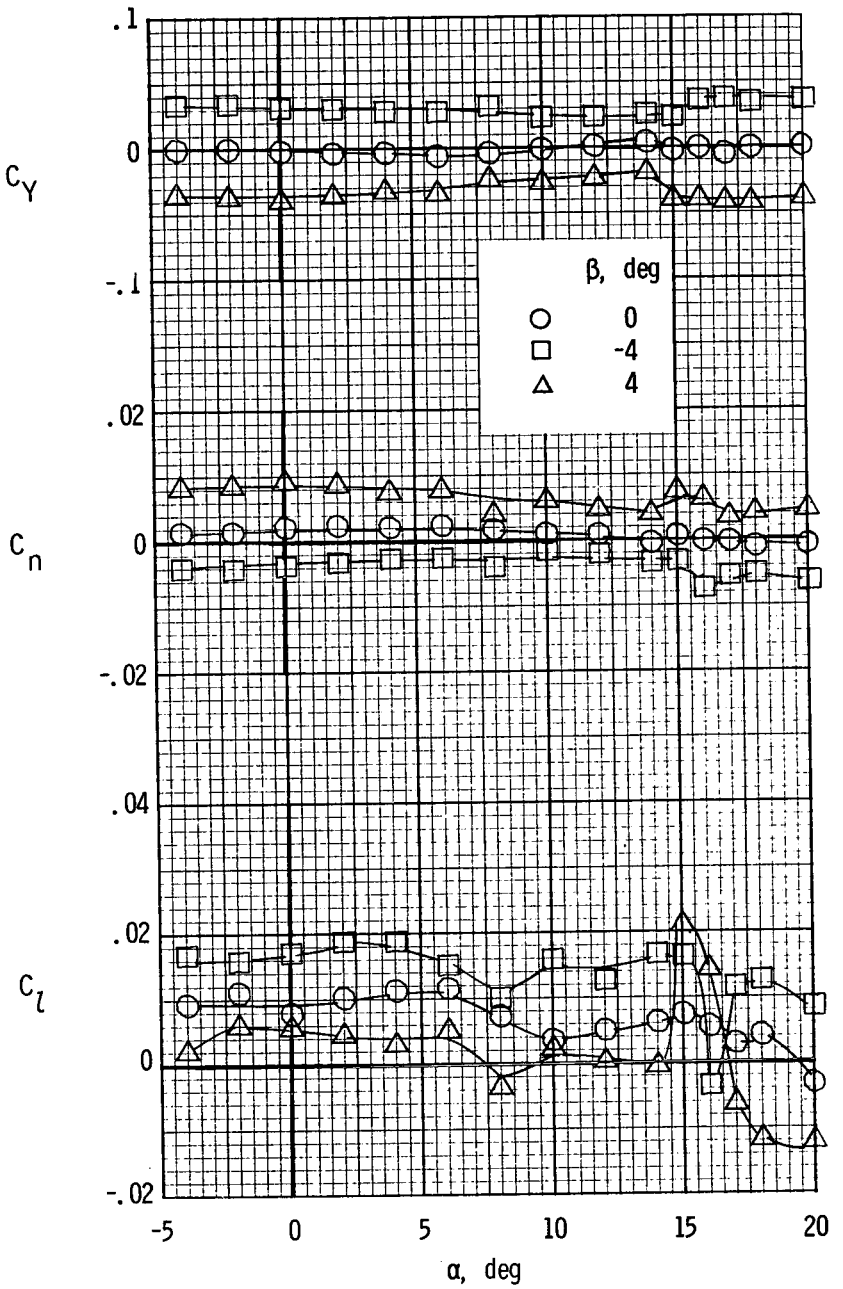

(a) $T_c' = 0$.

Figure 57.- Lateral aerodynamic characteristics of the model with the modified airfoil section and down-at-the-center propeller rotation. $\delta_f = 0^o$; nacelle A.

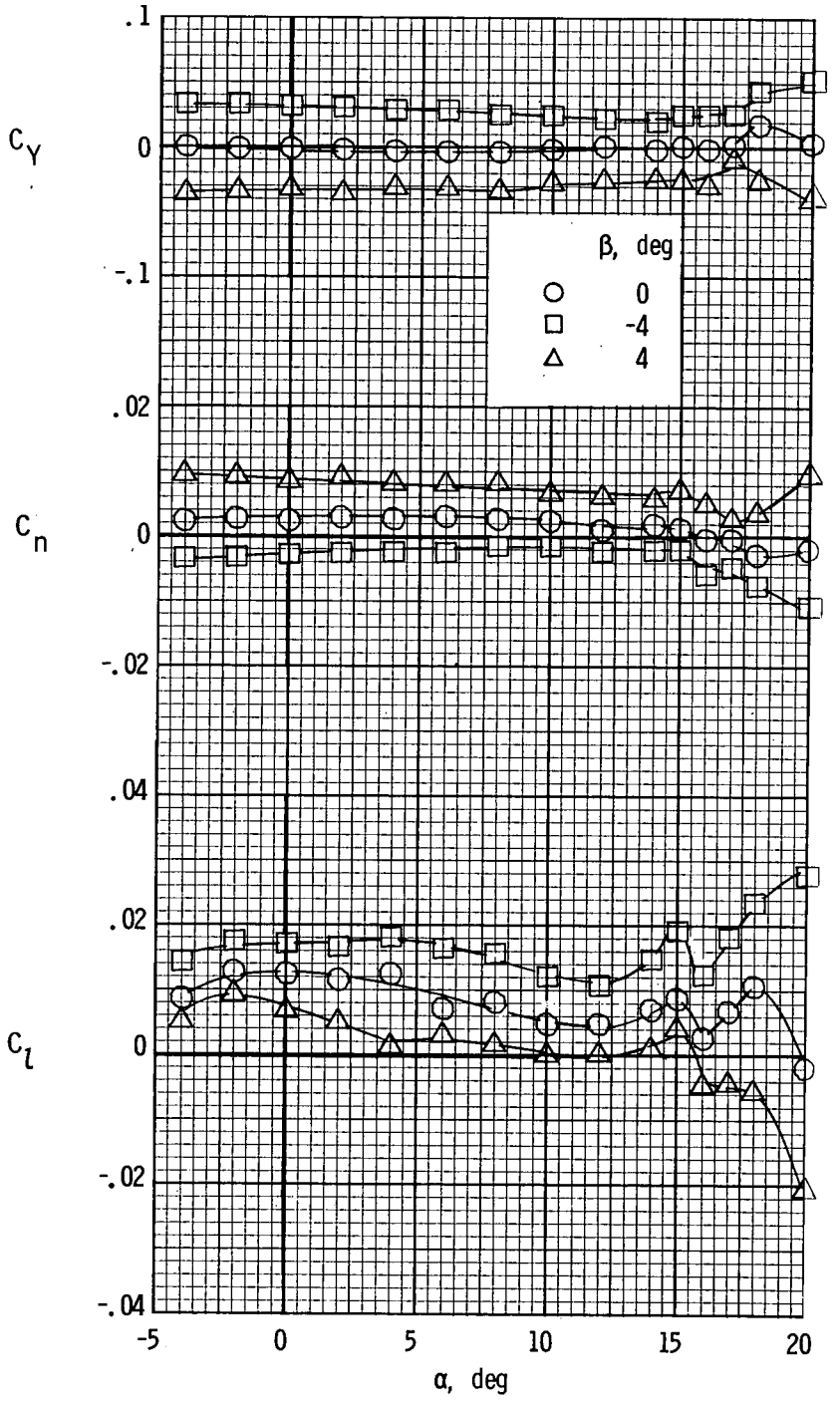

(b) $T_c' = 0.20$.

Figure 57.- Continued.

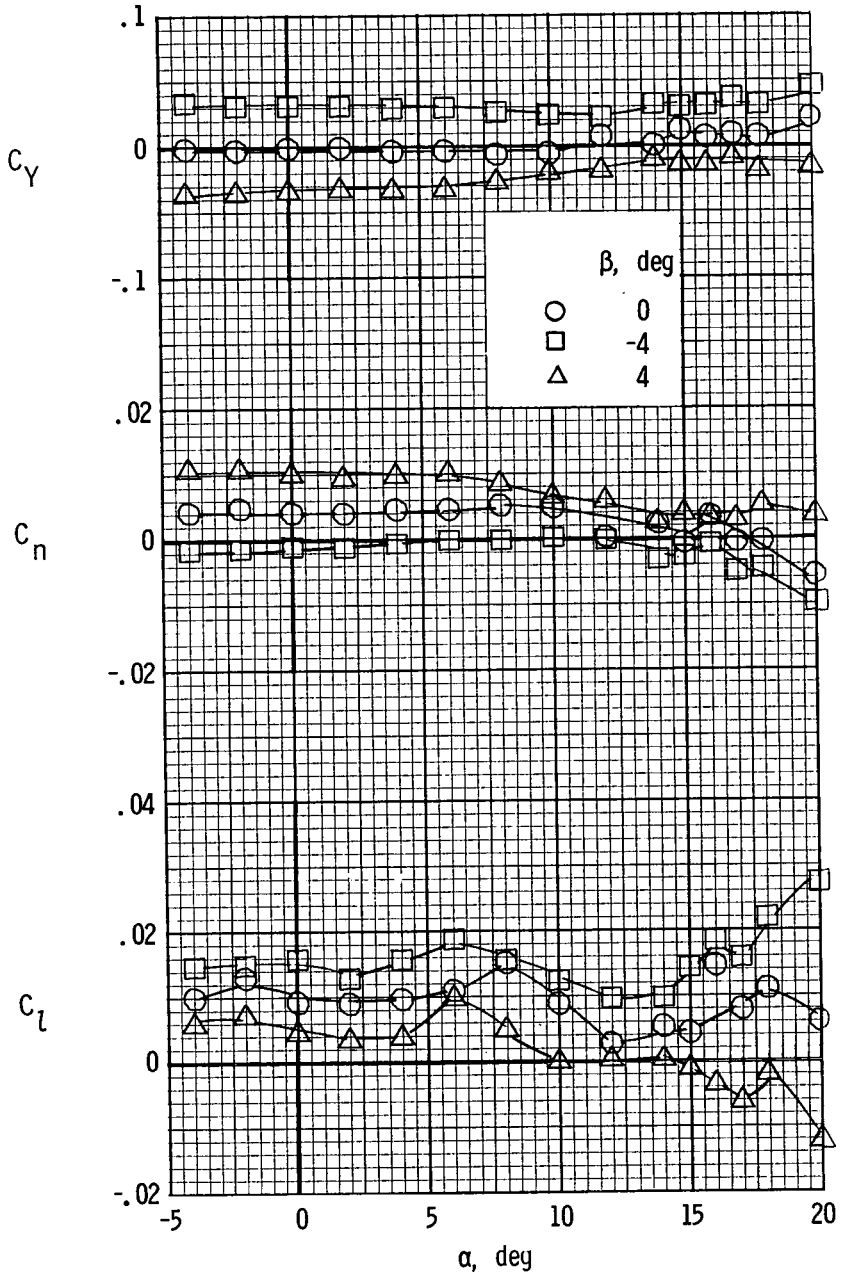

(c) $T_c' = 0.44$.

Figure 57.- Concluded.

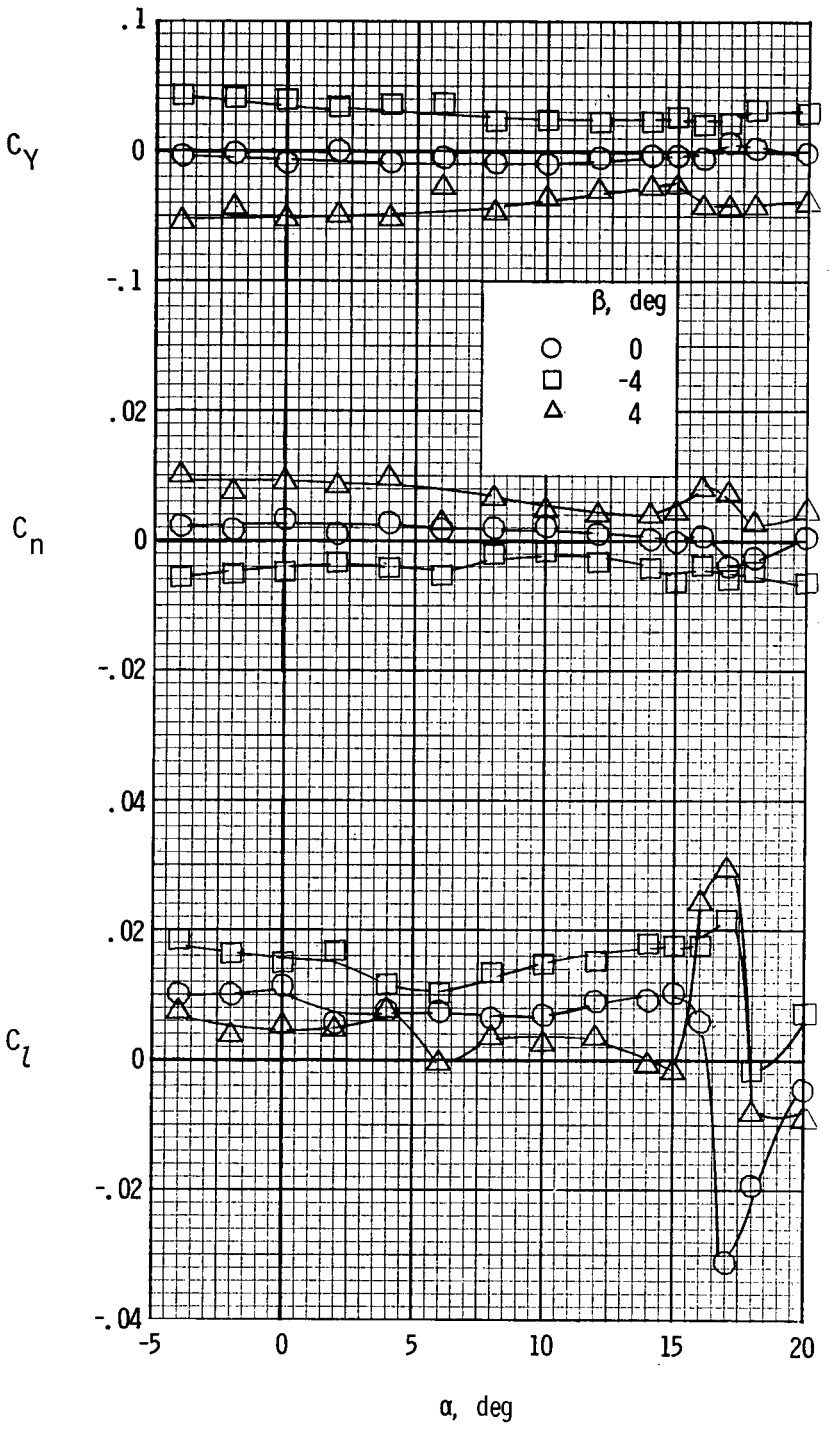

(a) $T_c' = 0$.

Figure 58.- Lateral aerodynamic characteristics of the model with the modified airfoil section and down-at-the-center propeller rotation. $\delta_f = 27^o$; nacelle A.

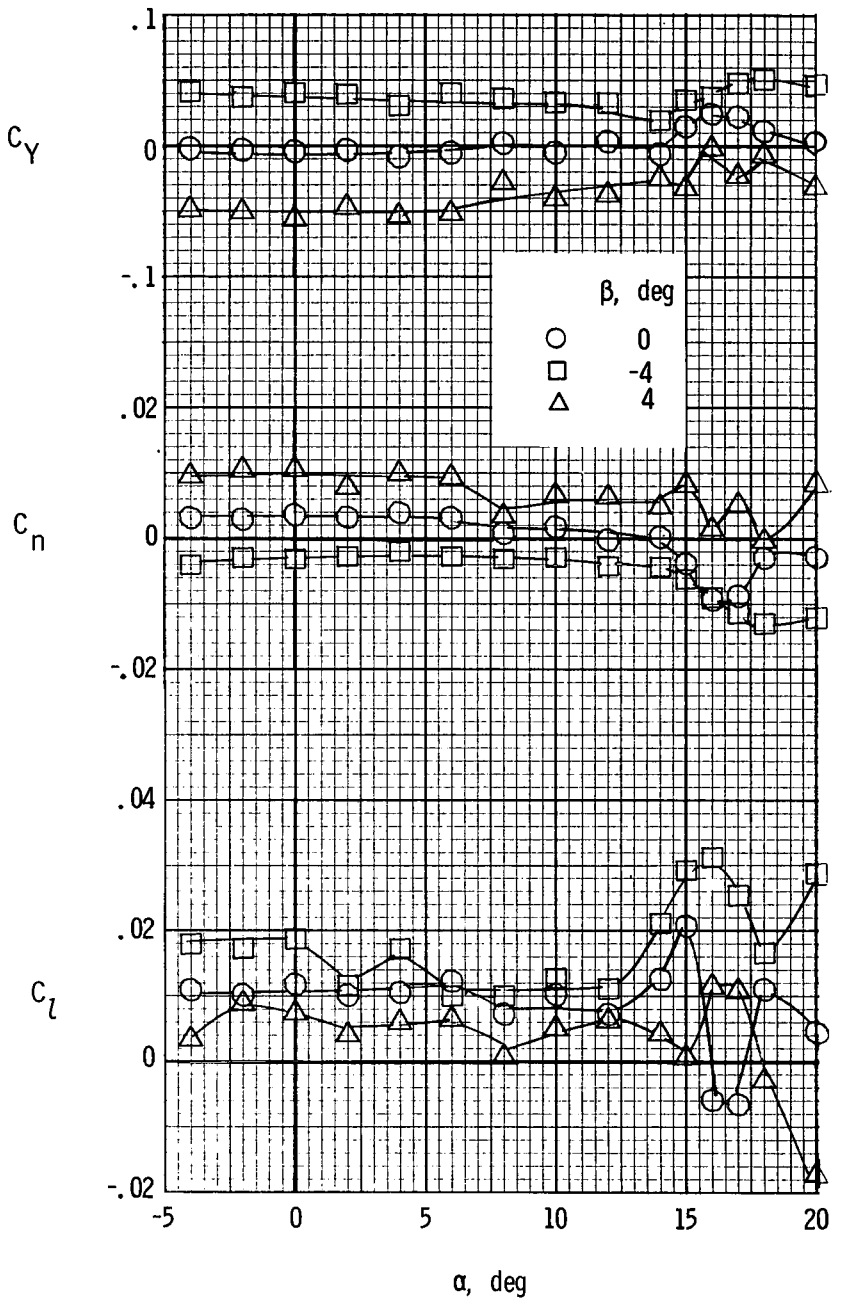

(b) $T_c' = 0.20$.

Figure 58.- Continued.

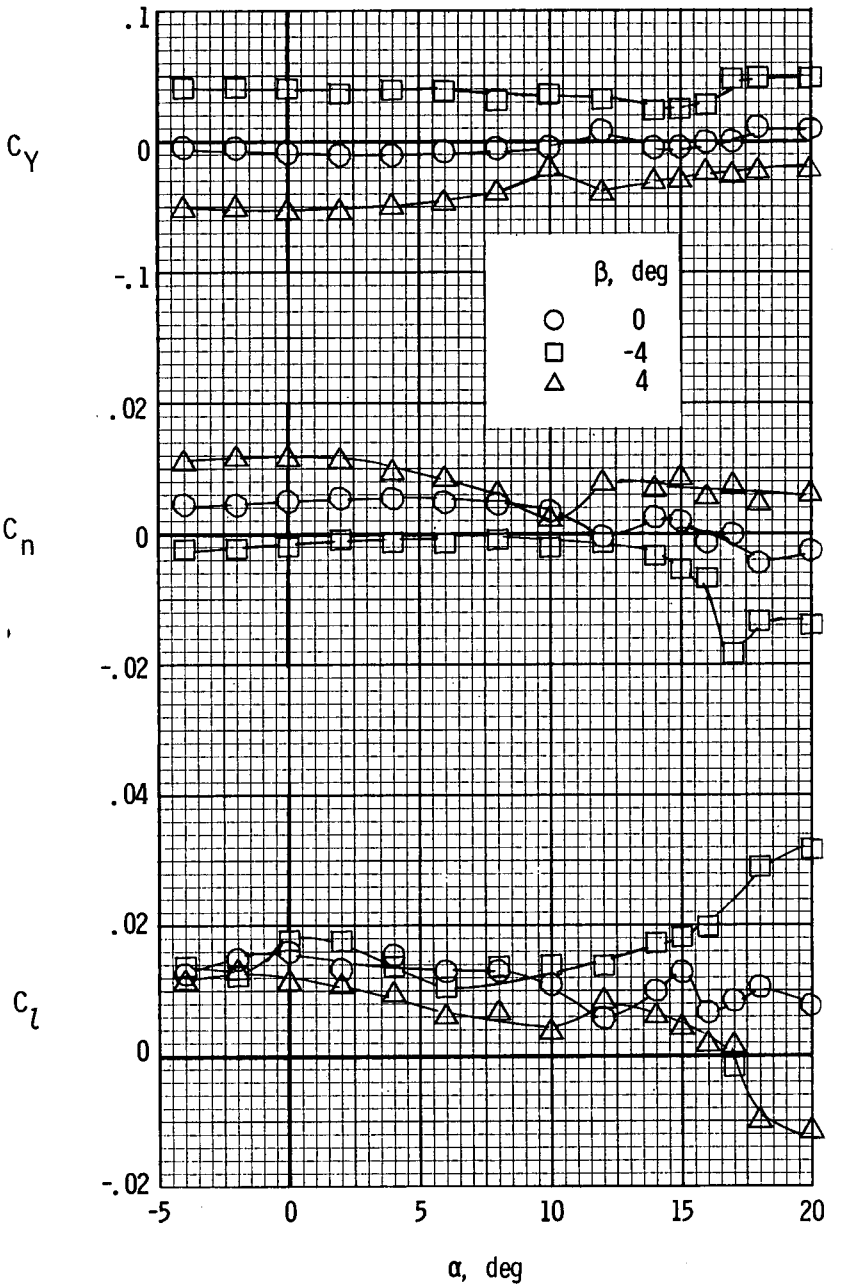

(c) $T_c' = 0.44$.

Figure 58.- Concluded.

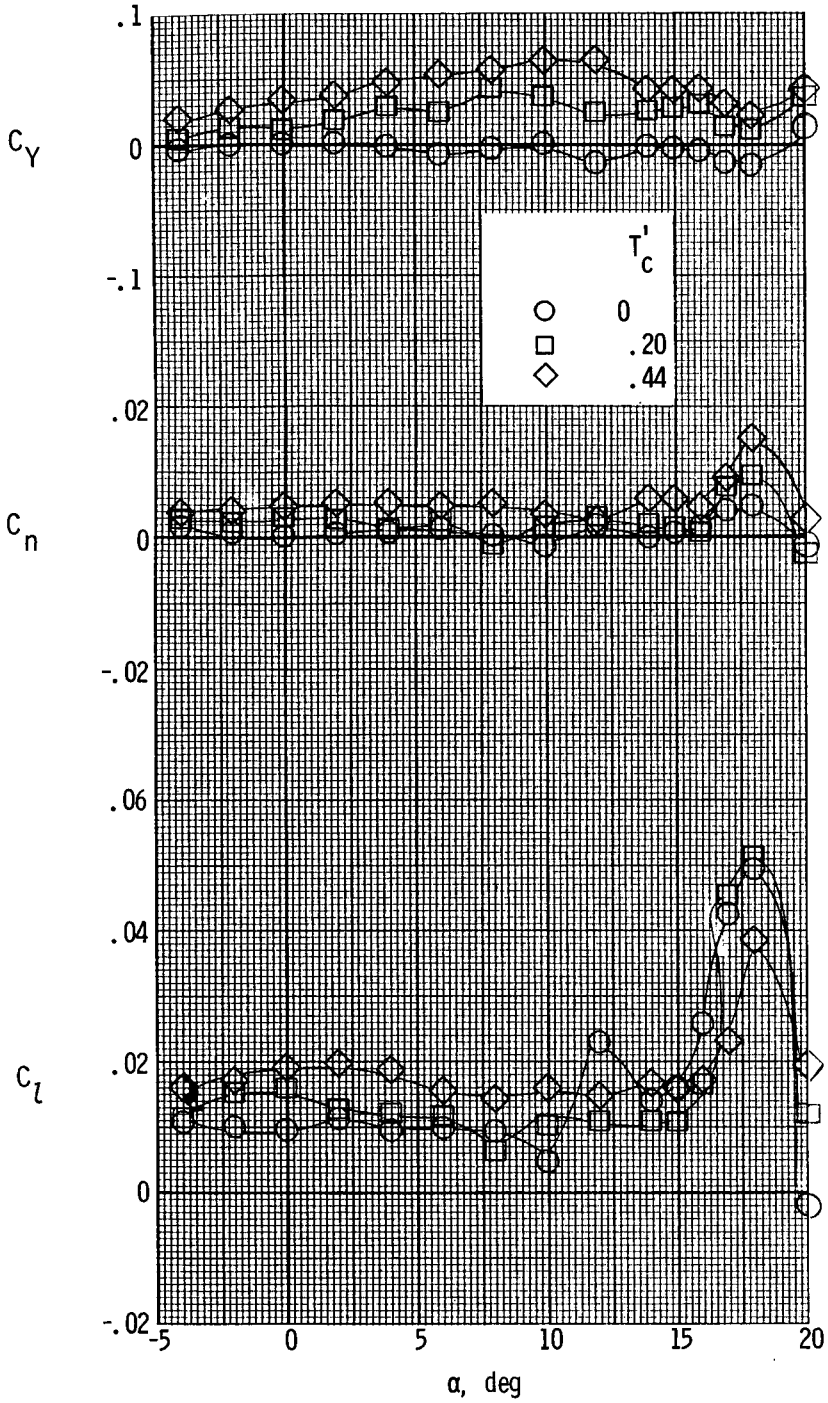

Figure 59.- Lateral aerodynamic characteristics of the model with the modified airfoil section and counterclockwise propeller rotation. $\delta_f = 27^o$; nacelle A.

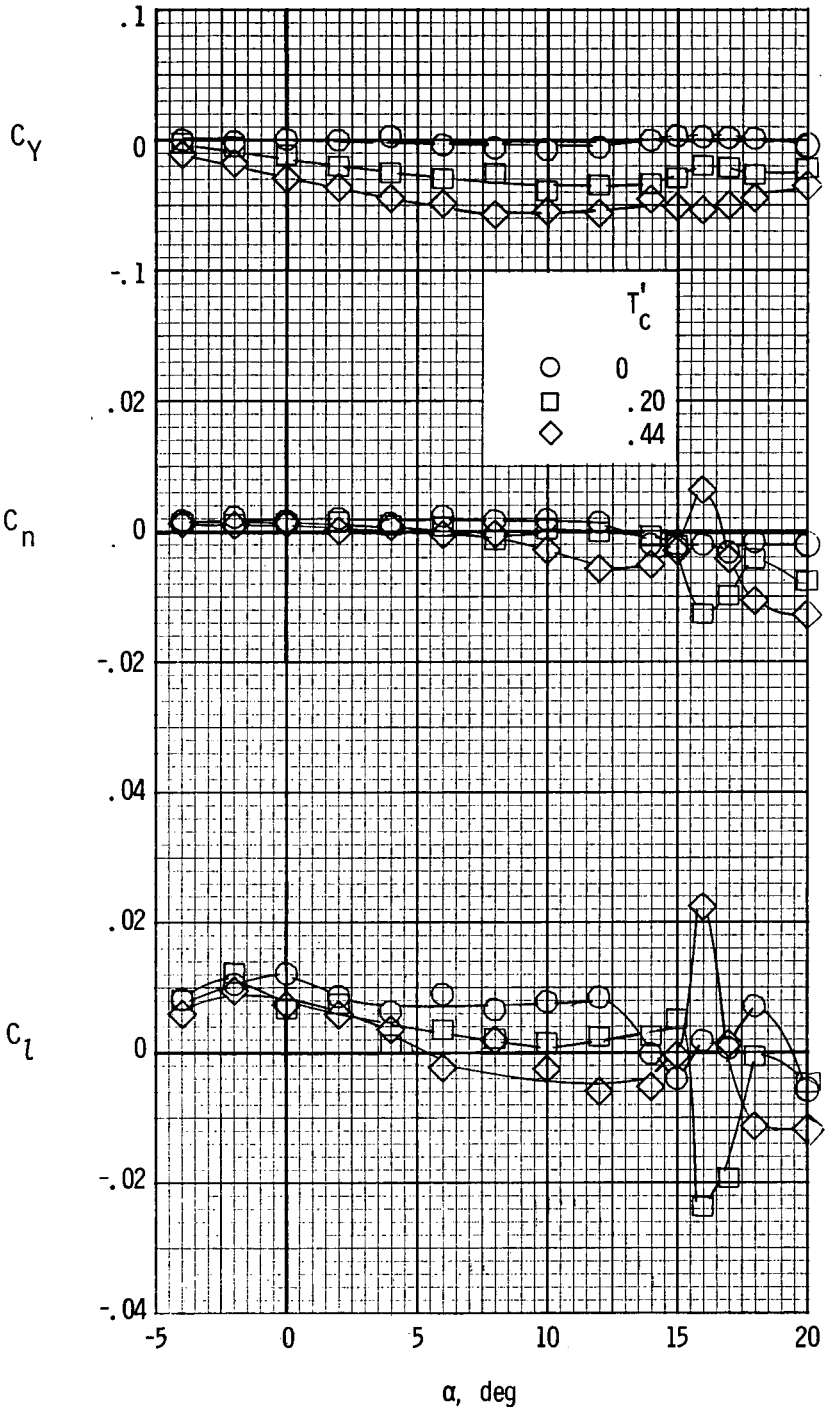

Figure 60.- Lateral aerodynamic characteristics of the model with the modified cowl. $\delta_f = 0^o$.

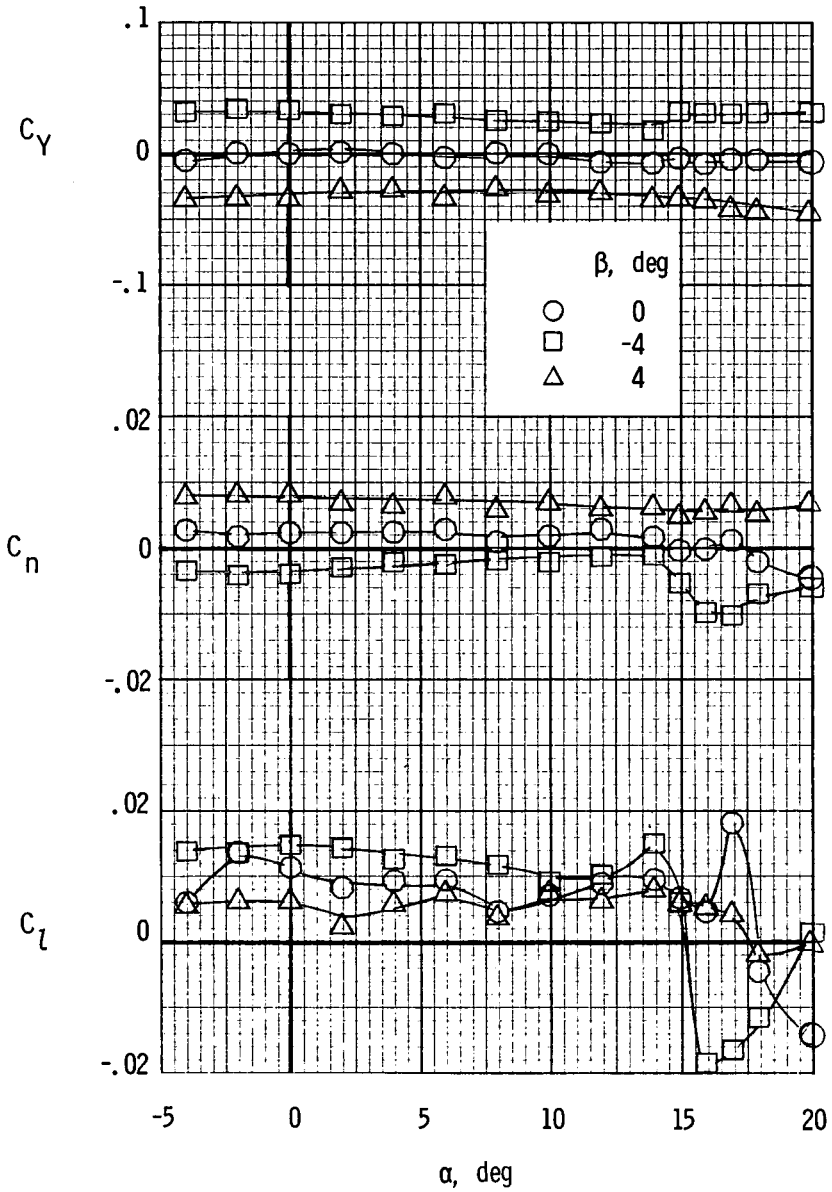

(a) $T_c' = 0.$

Figure 61.- Lateral aerodynamic characteristics of the model with the modified afterbody. $\delta_f = 0^o$.

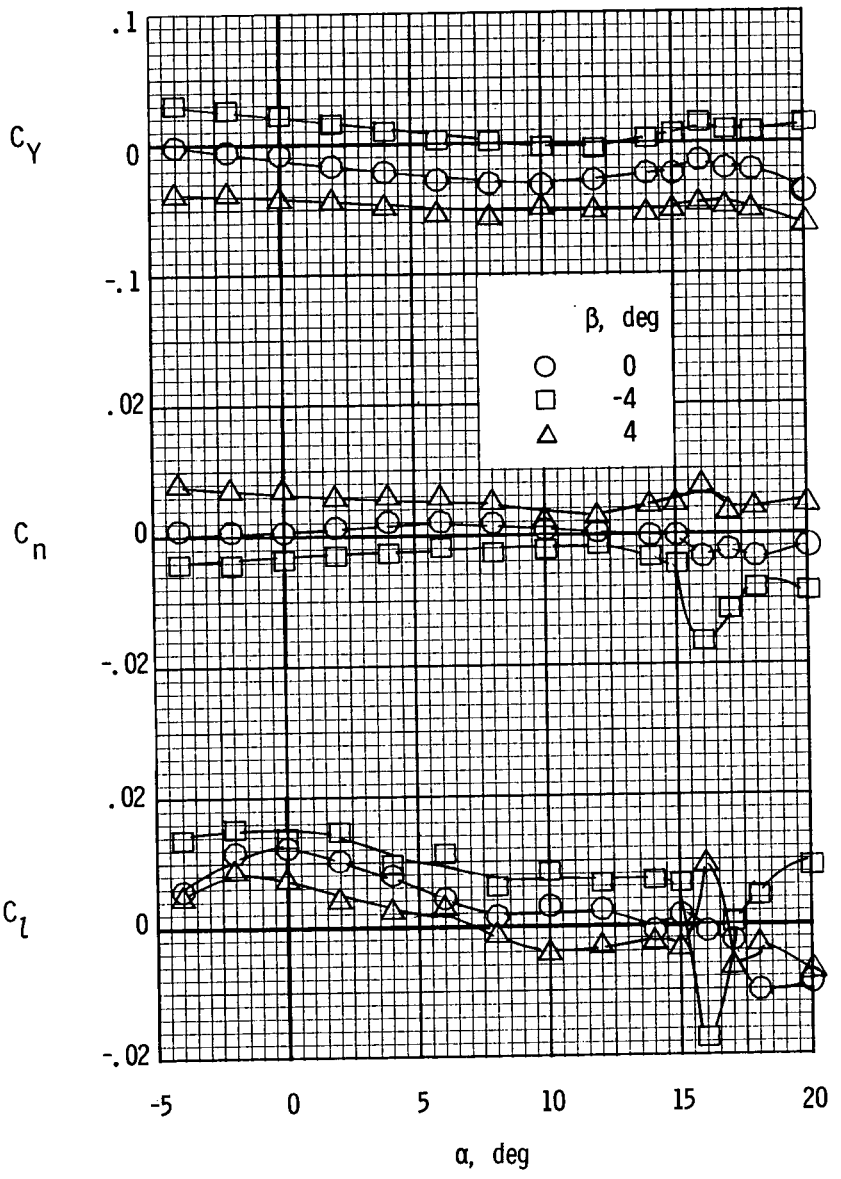

(b) $T_c' = 0.20$.

Figure 61.- Continued.

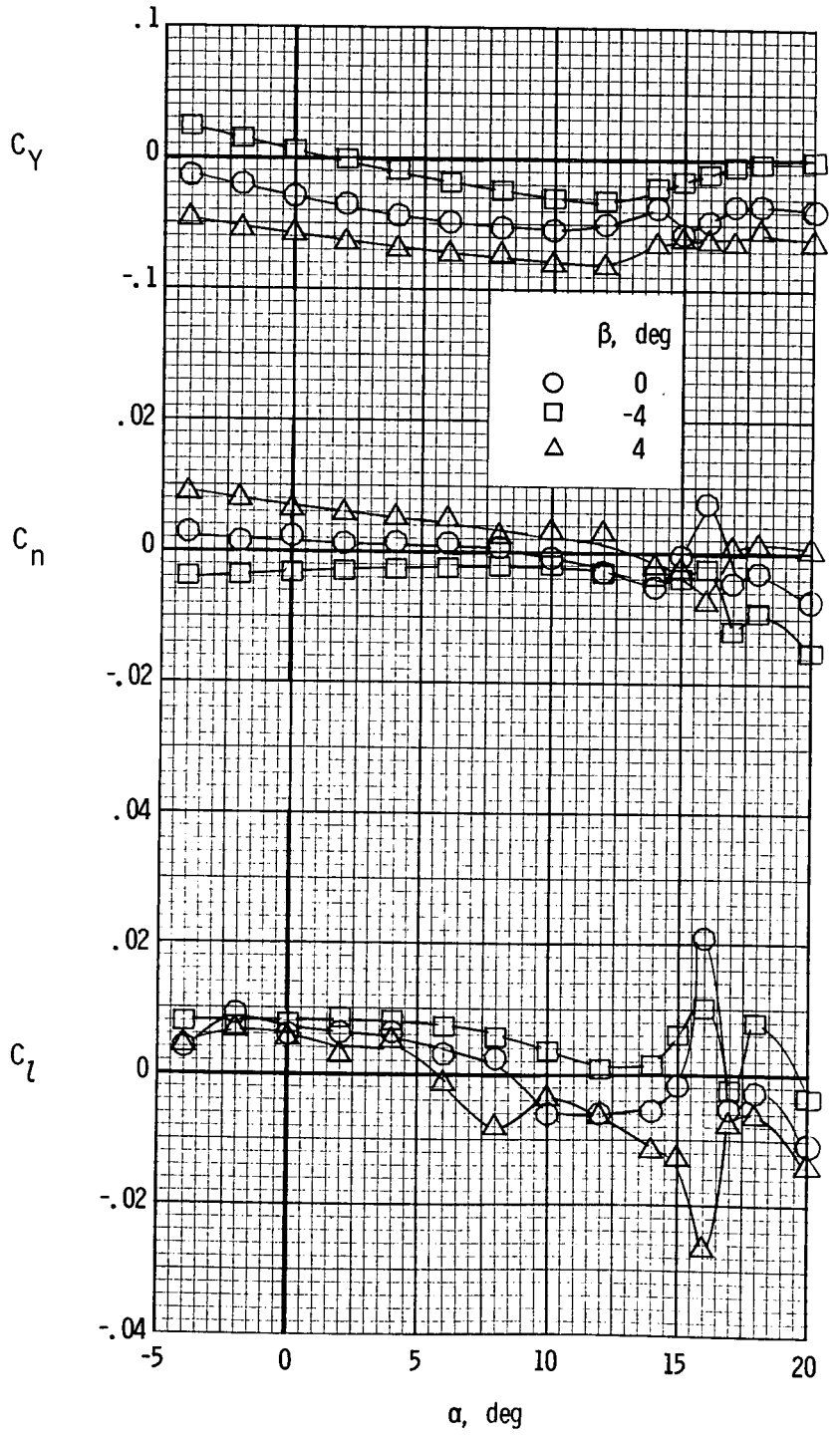

(c) $T_c' = 0.44$.

Figure 61.- Concluded.

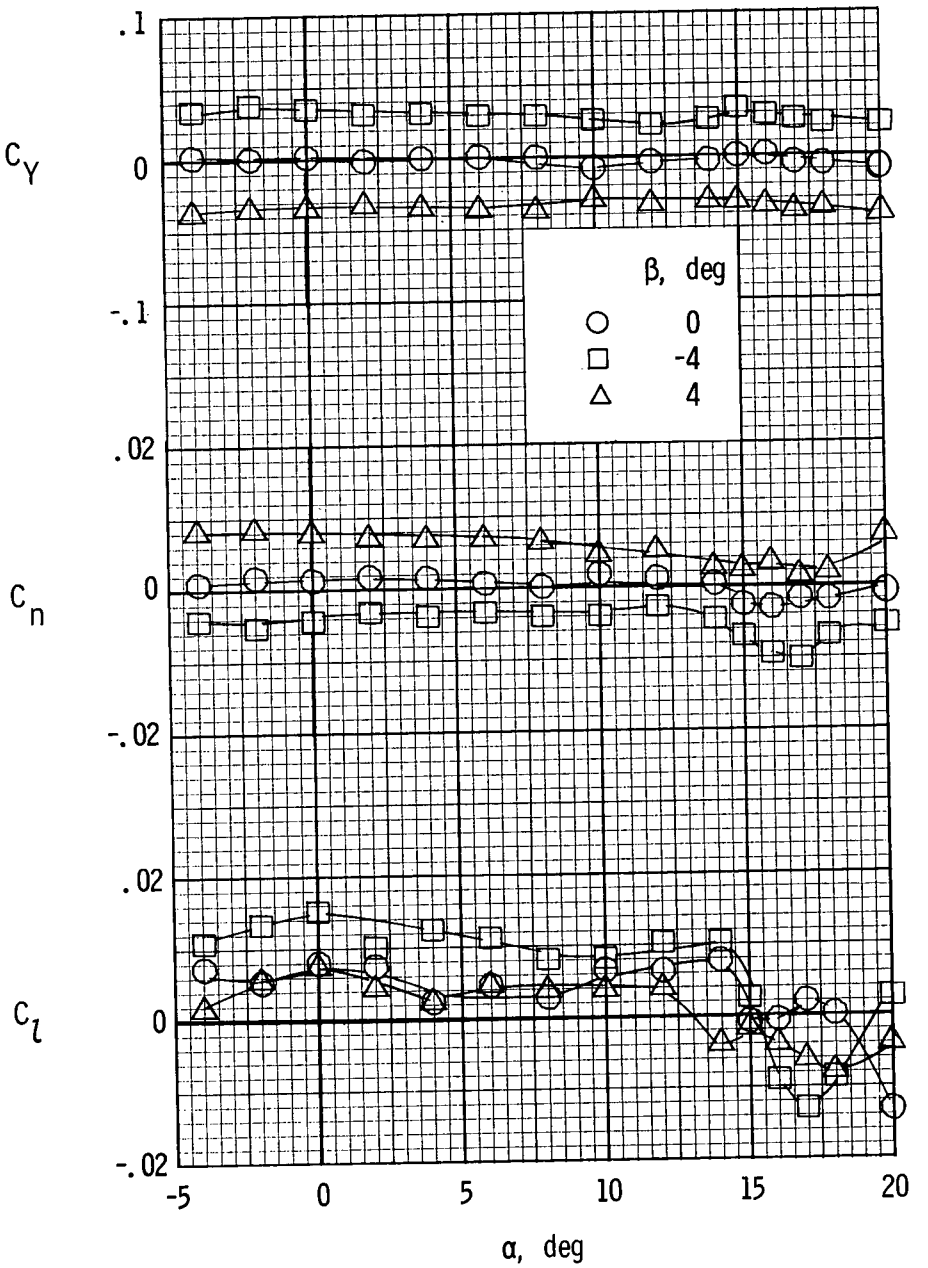

(a) $T_c' = 0$.

Figure 62.- Lateral aerodynamic characteristics of the model with the modified cowl and the modified afterbody. $\delta_f = 0^o$.

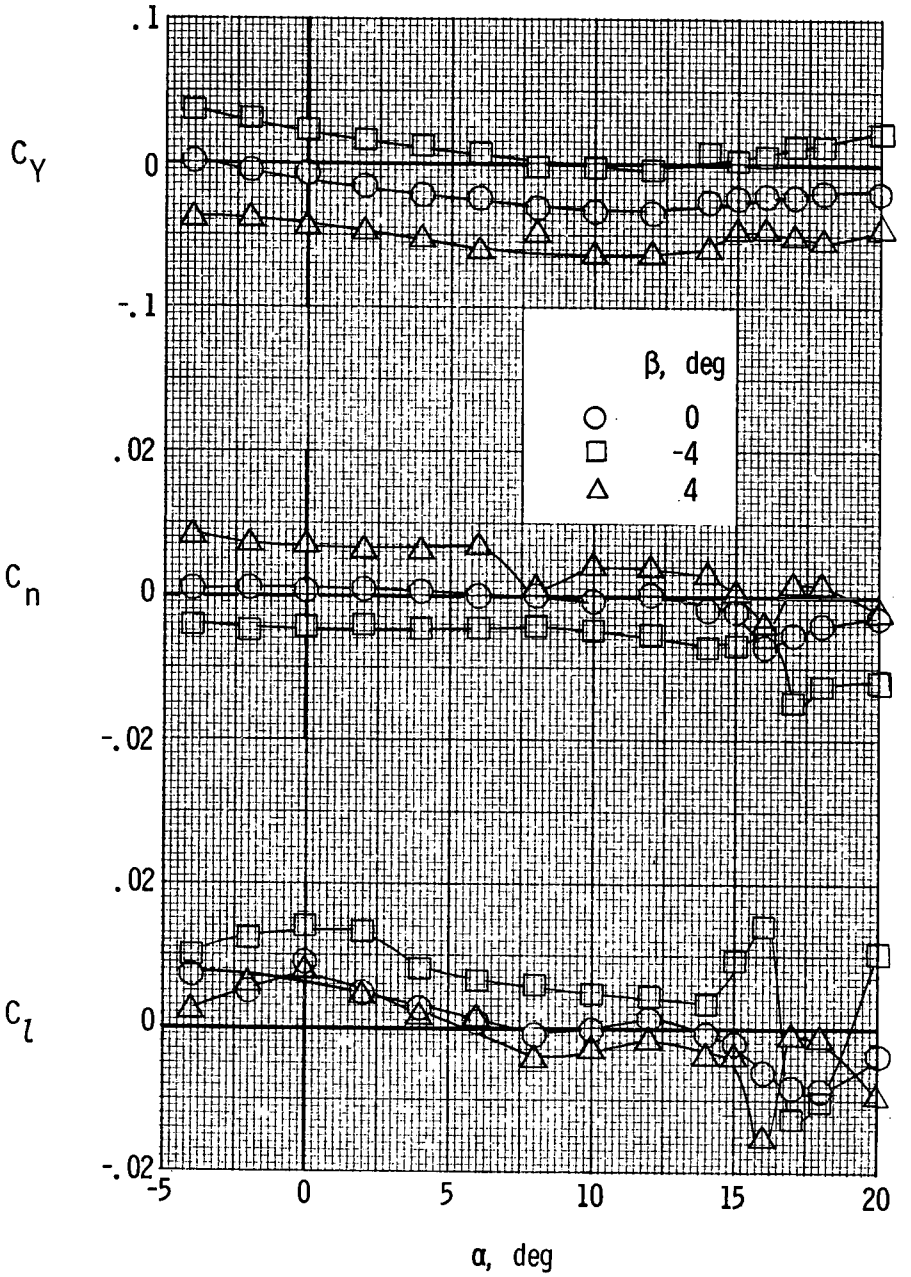

(b) $T_c' = 0.20$.

Figure 62.- Continued.

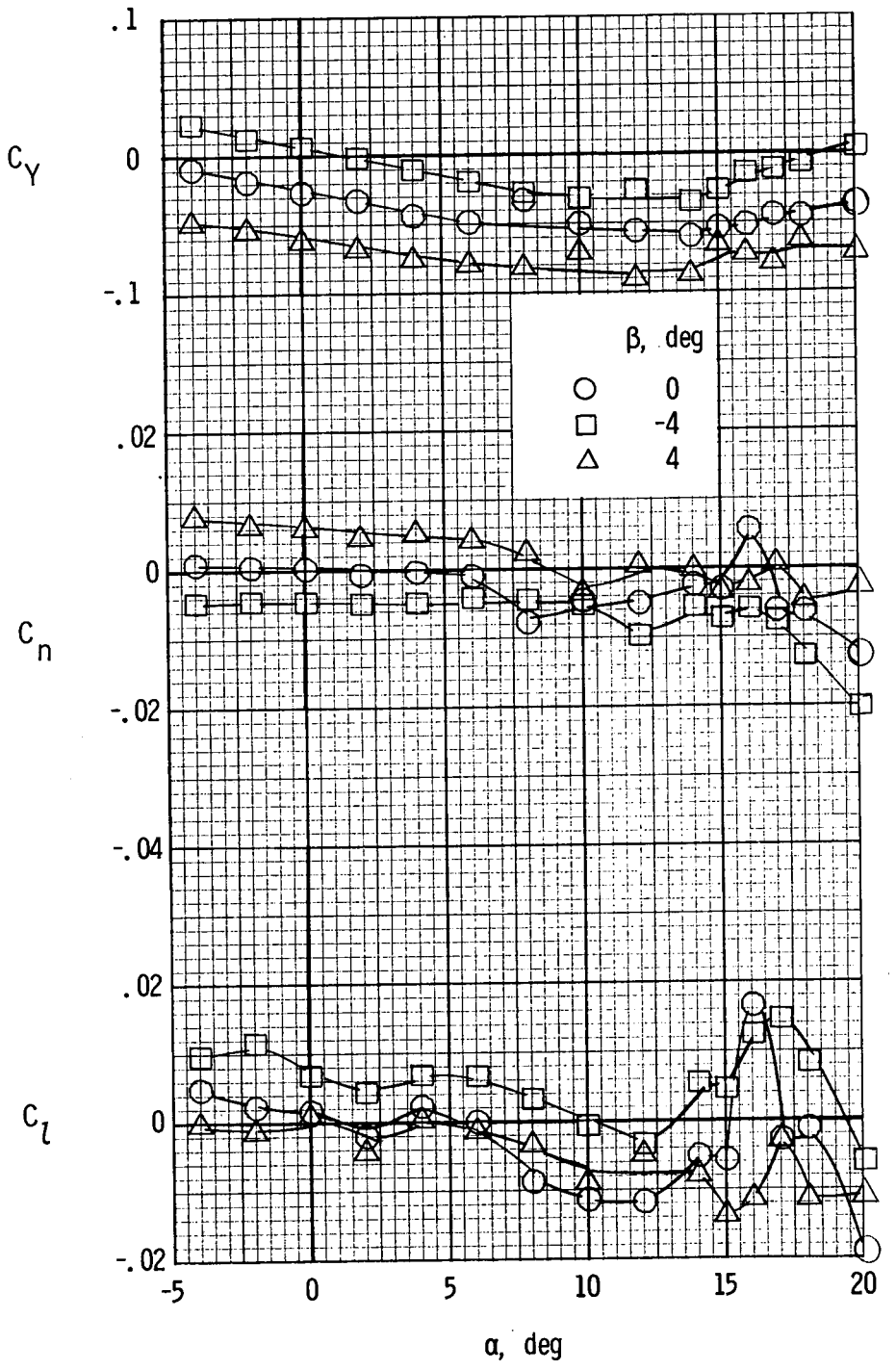

(c) $T_c' = 0.44$.

Figure 62.- Concluded.

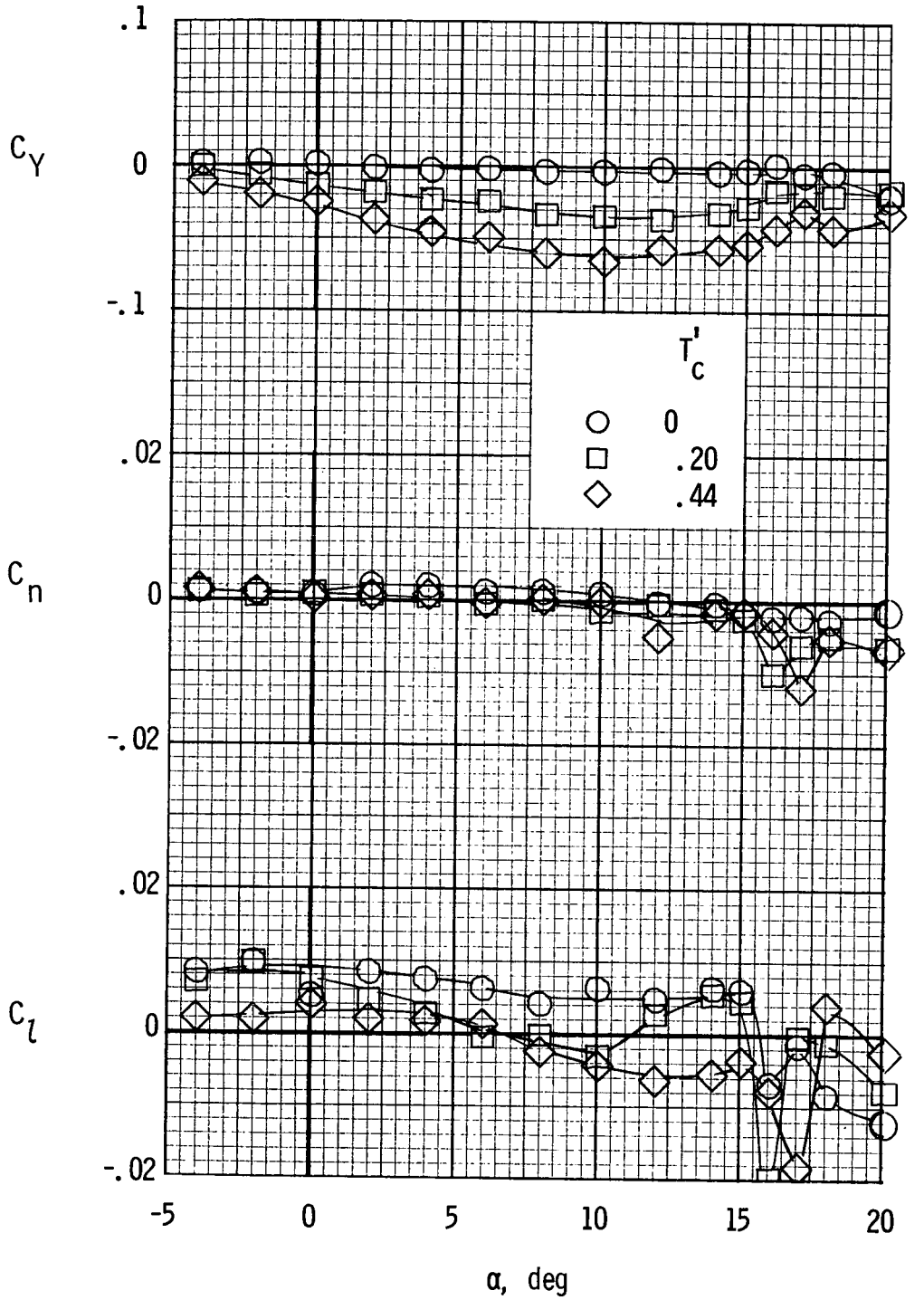

Figure 63.- Lateral aerodynamic characteristics of the model with the modified cowl and the modified airfoil. $\delta_f = 0^o$.

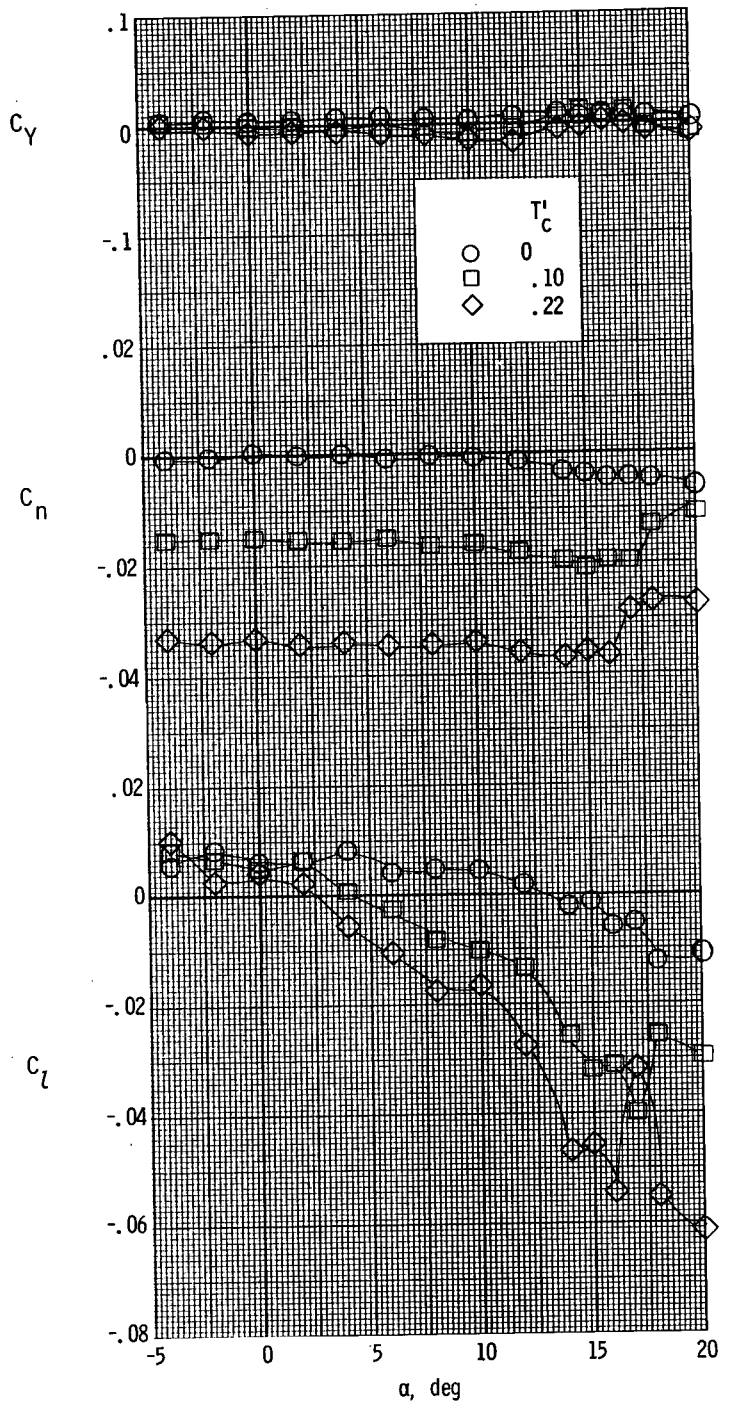

(a) Right propeller powered, left windmilling.

Figure 64.- Lateral aerodynamic characteristics of the model with asymmetric power. $\delta_f = 0^o$; nacelle A.

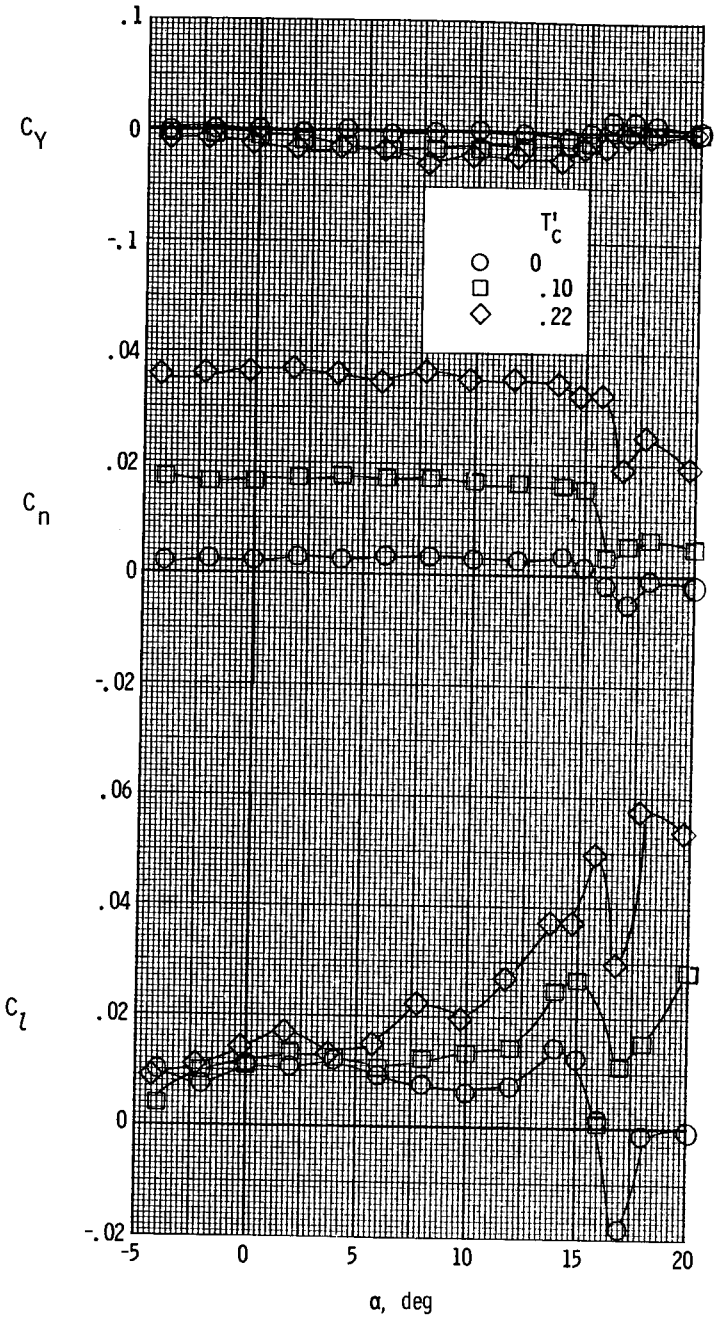

(b) Left propeller powered, right windmilling.

Figure 64.- Concluded.

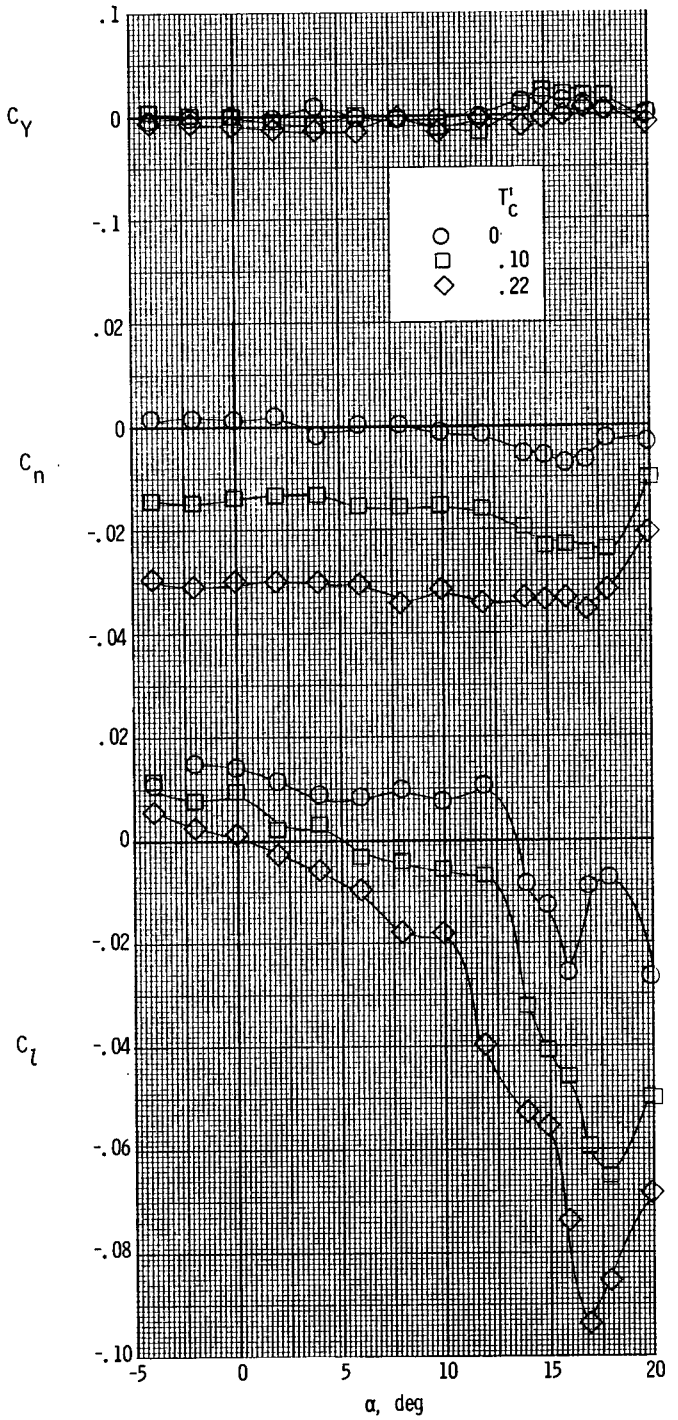

(a) Right propeller powered, left windmilling.

Figure 65.- Lateral aerodynamic characteristics of the model with asymmetric power. $\delta_f = 27^o$; nacelle A.

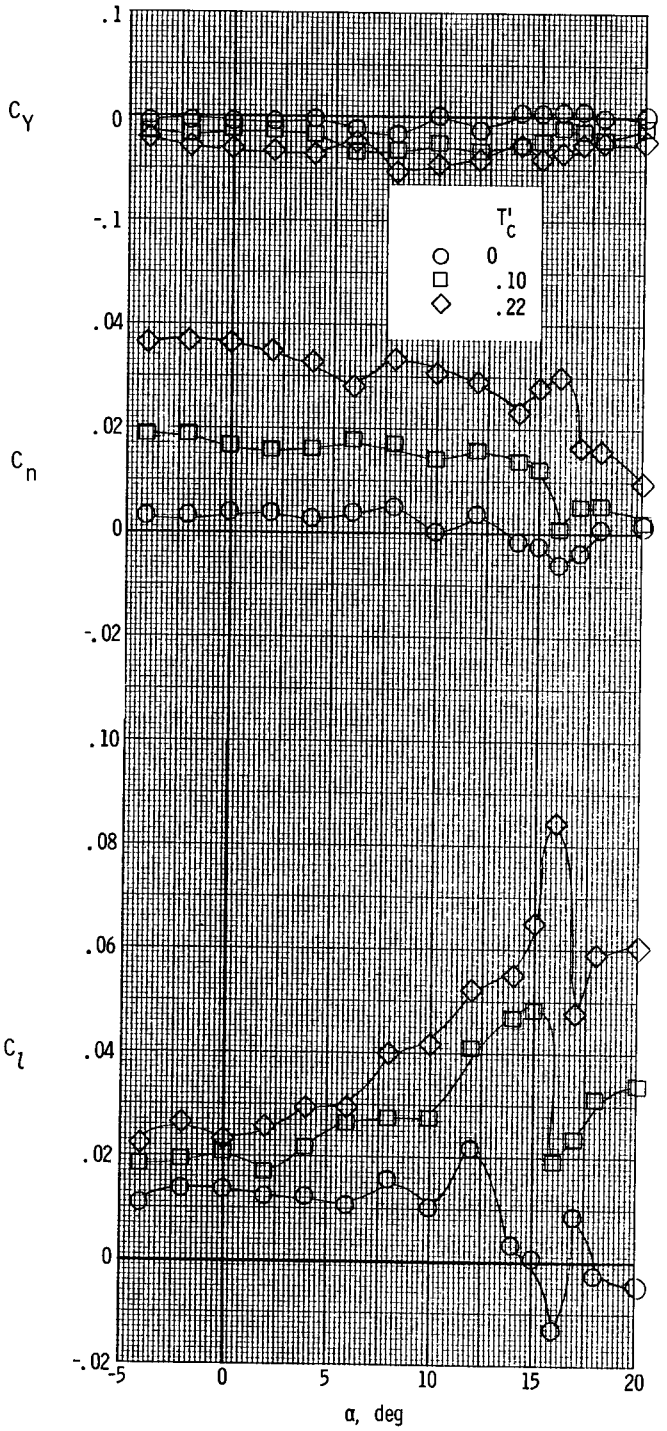

(b) Left propeller powered, right windmilling.

Figure 65.- Concluded.

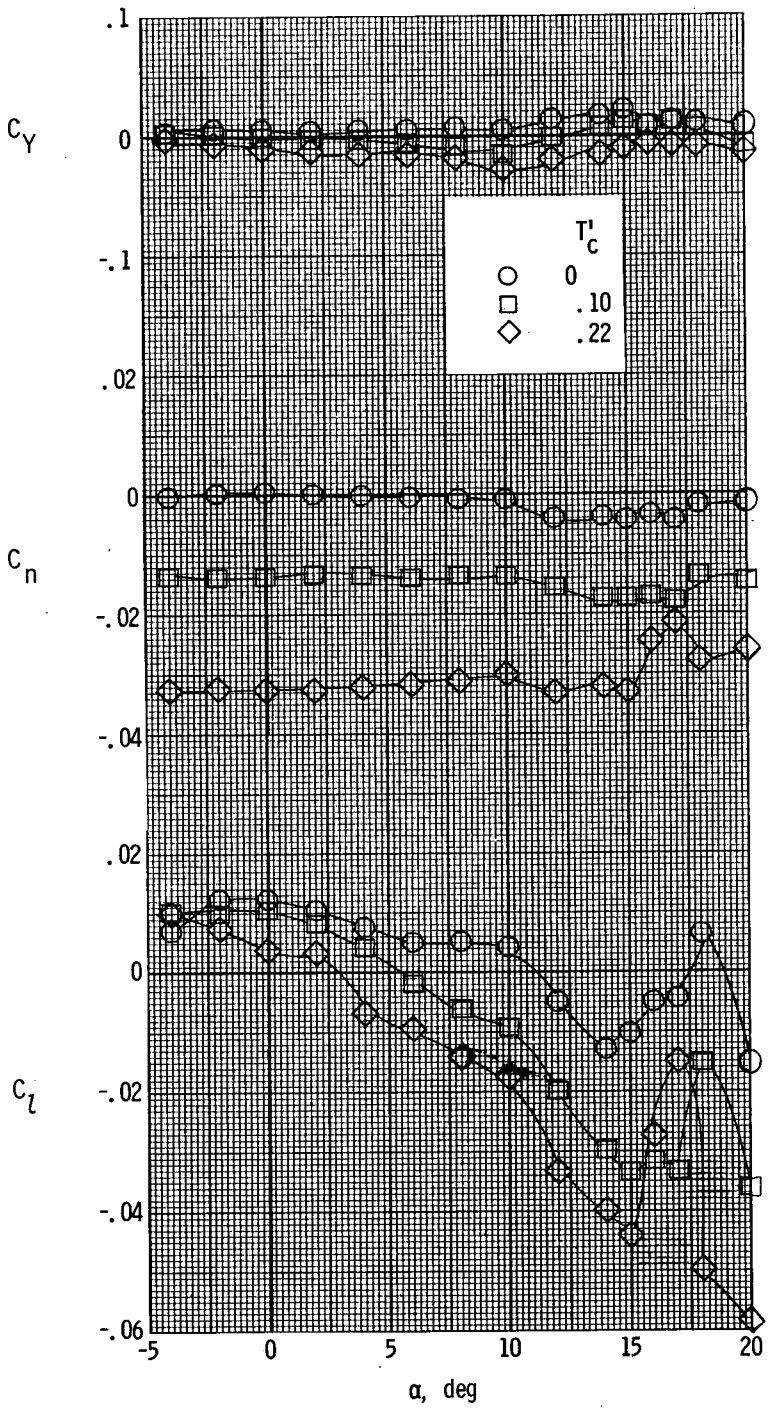

(a) Right propeller powered, left windmilling.

Figure 66.- Lateral aerodynamic characteristics of the model with asymmetric power and the vertical tail removed. $\delta_f = 0^o$; nacelle A.

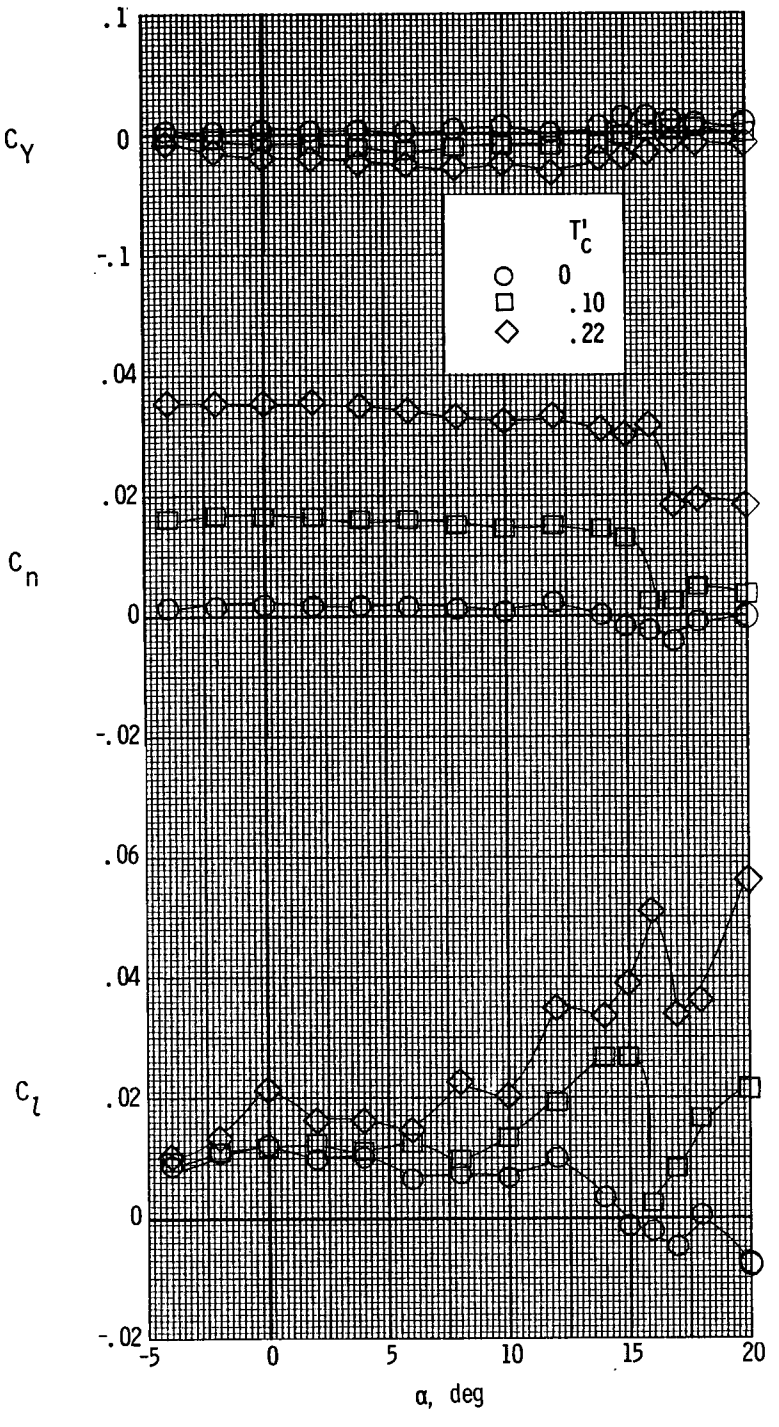

(b) Left propeller powered, right windmilling.

Figure 66.- Concluded.

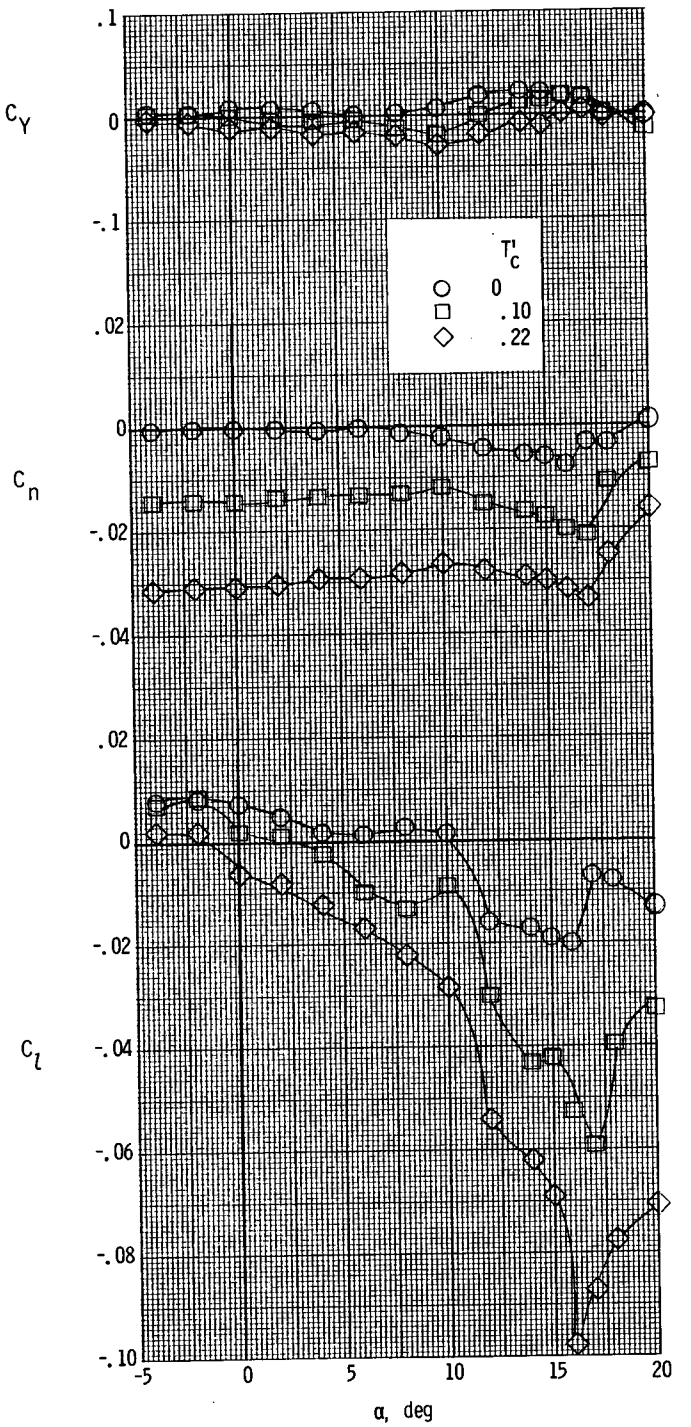

(a) Right propeller powered, left windmilling.

Figure 67.- Lateral aerodynamic characteristics of the model with asymmetric power and the vertical tail removed. $\delta_f = 27^o$; nacelle A.

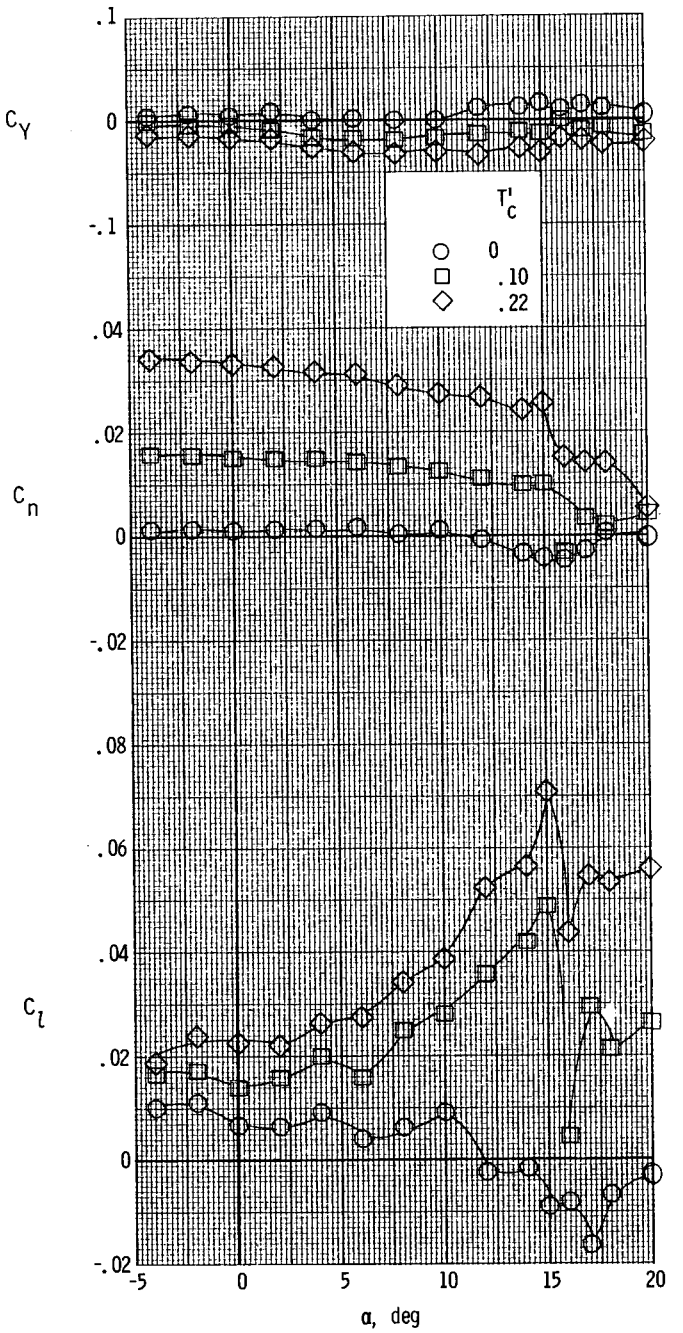

(b) Left propeller powered, right windmilling.

Figure 67.- Concluded.

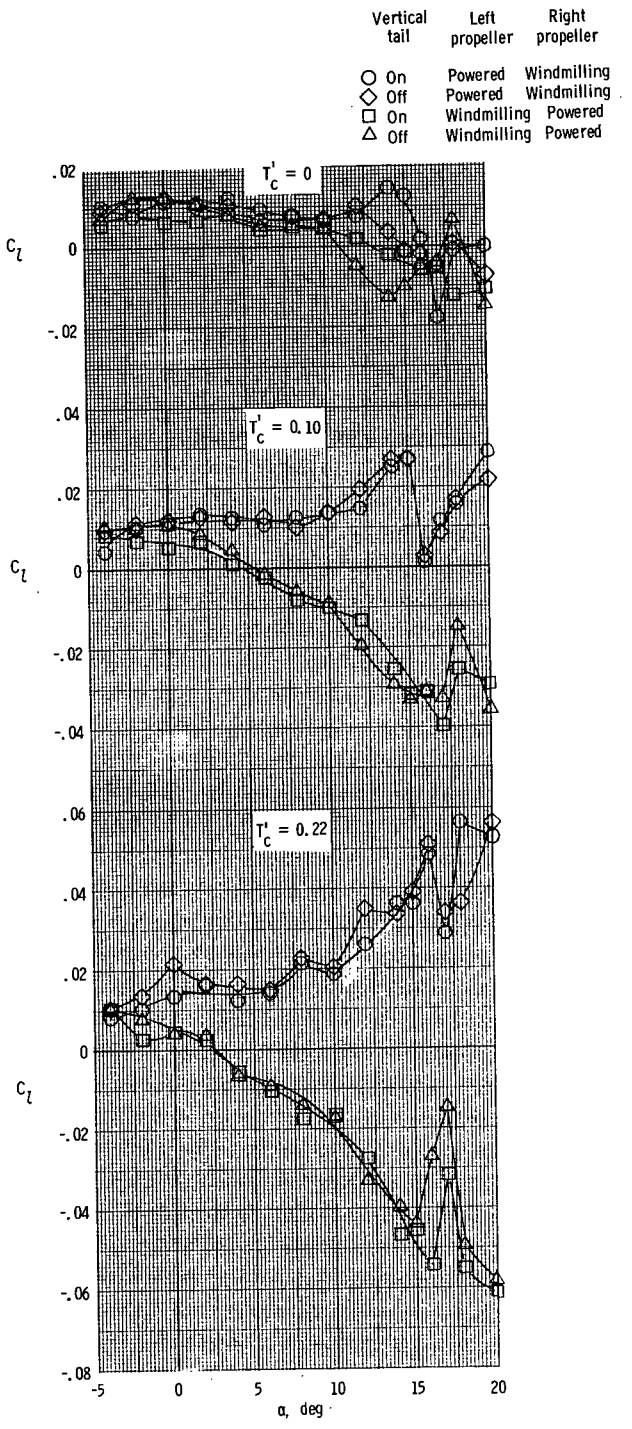

(a) $\delta_f = 0^o$.

Figure 68.- Comparison of the vertical-tail-removed configuration with the tail-on configuration with asymmetric power. Nacelle A.

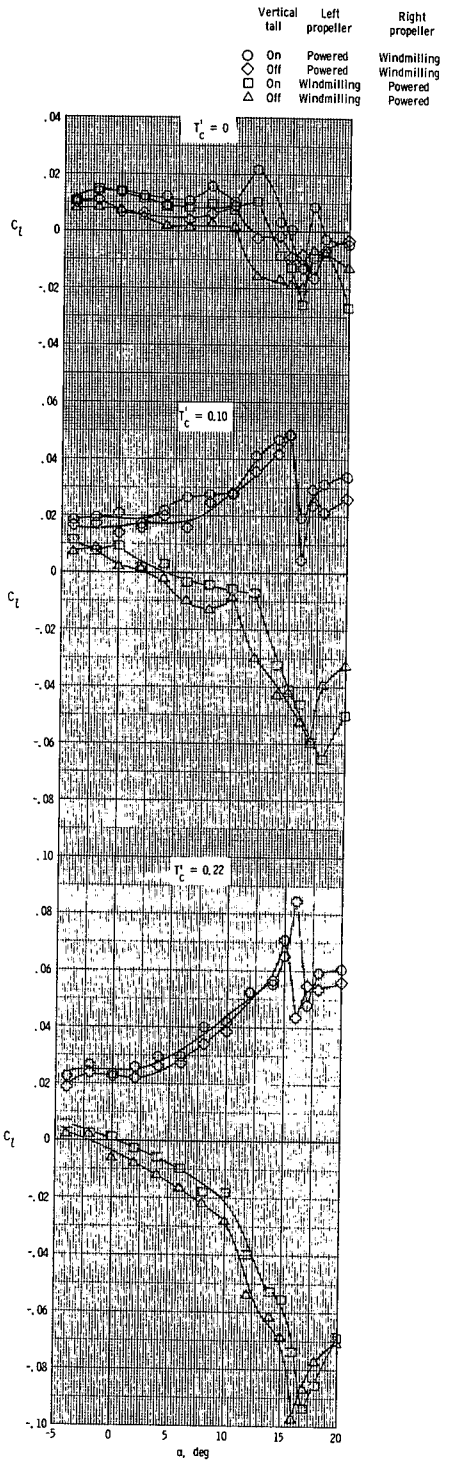

(b) $\delta_f = 27^o$.

Figure 68.- Concluded.

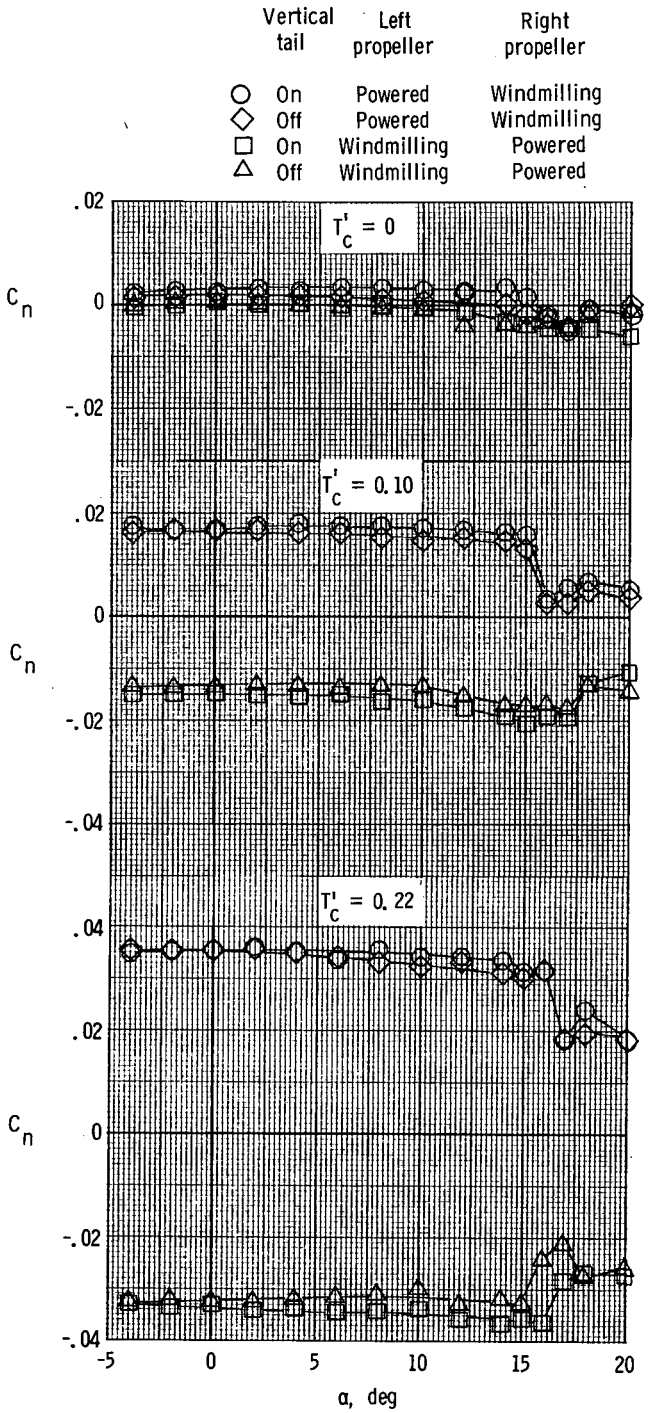

(a) $\delta_f = 0^o$.

Figure 69.- Comparison of the vertical-tail-removed configuration with the tail-on configuration with asymmetric power. $\beta = 0^o$; nacelle A.

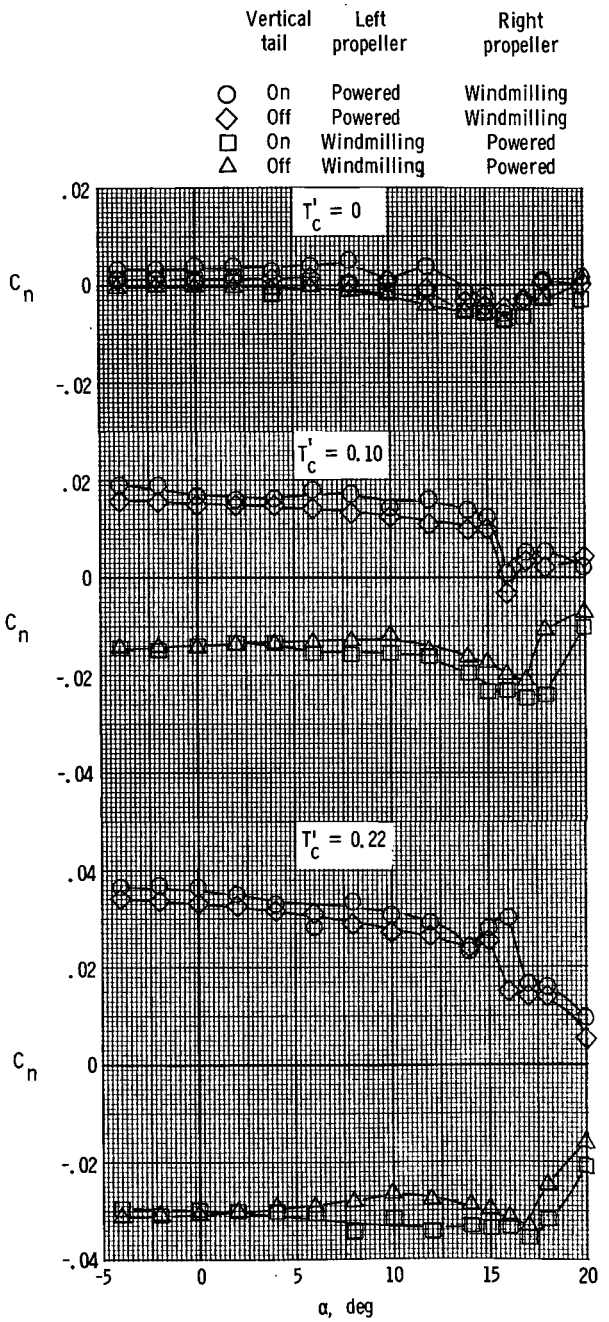

(b) $\delta_f = 27^o$.

Figure 69.- Concluded.

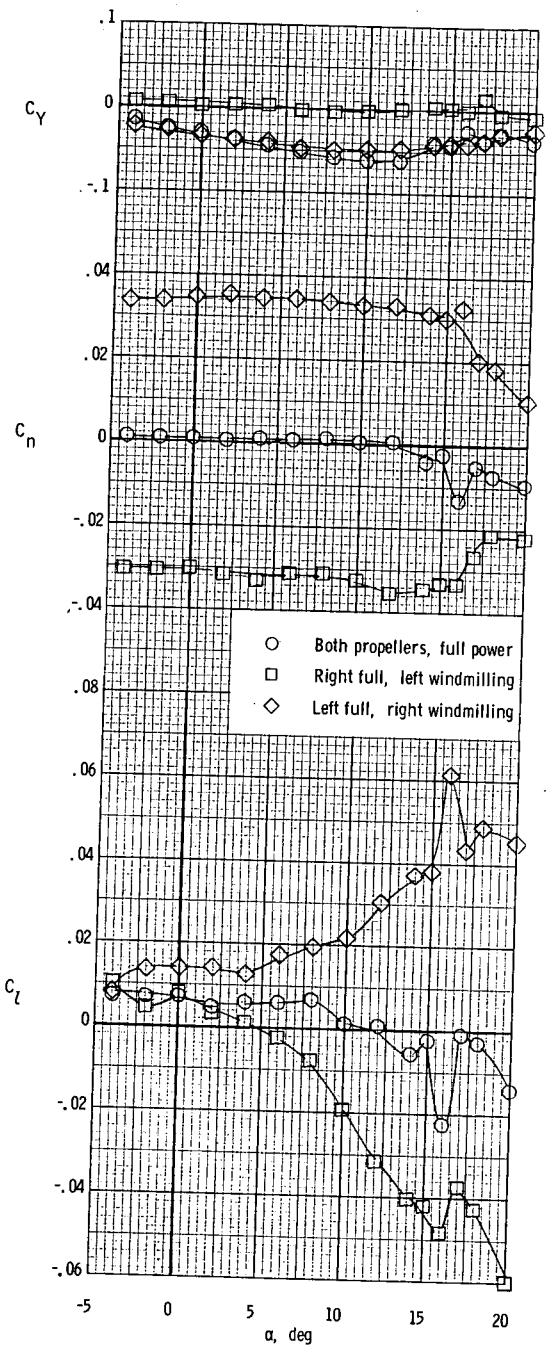

(a) $\phi = 3^{o}$.

Figure 70.- Lateral aerodynamic characteristics of the model with asymmetric power and toed-out thrust axes. $\delta_f = 0^{o}$; nacelle A.

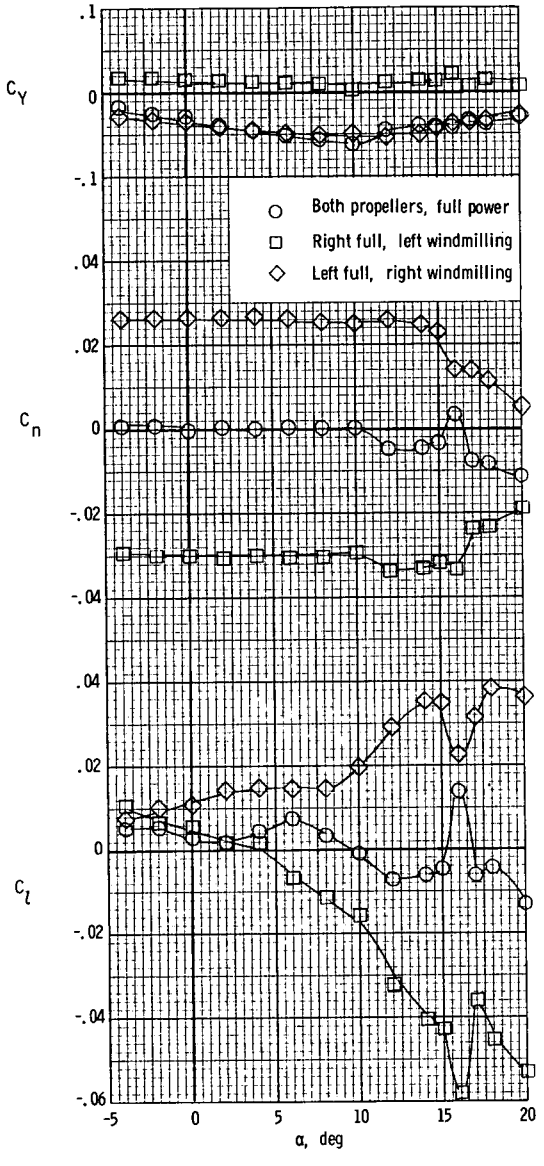

(b) $\phi = 6^{o}$.

Figure 70.- Concluded.

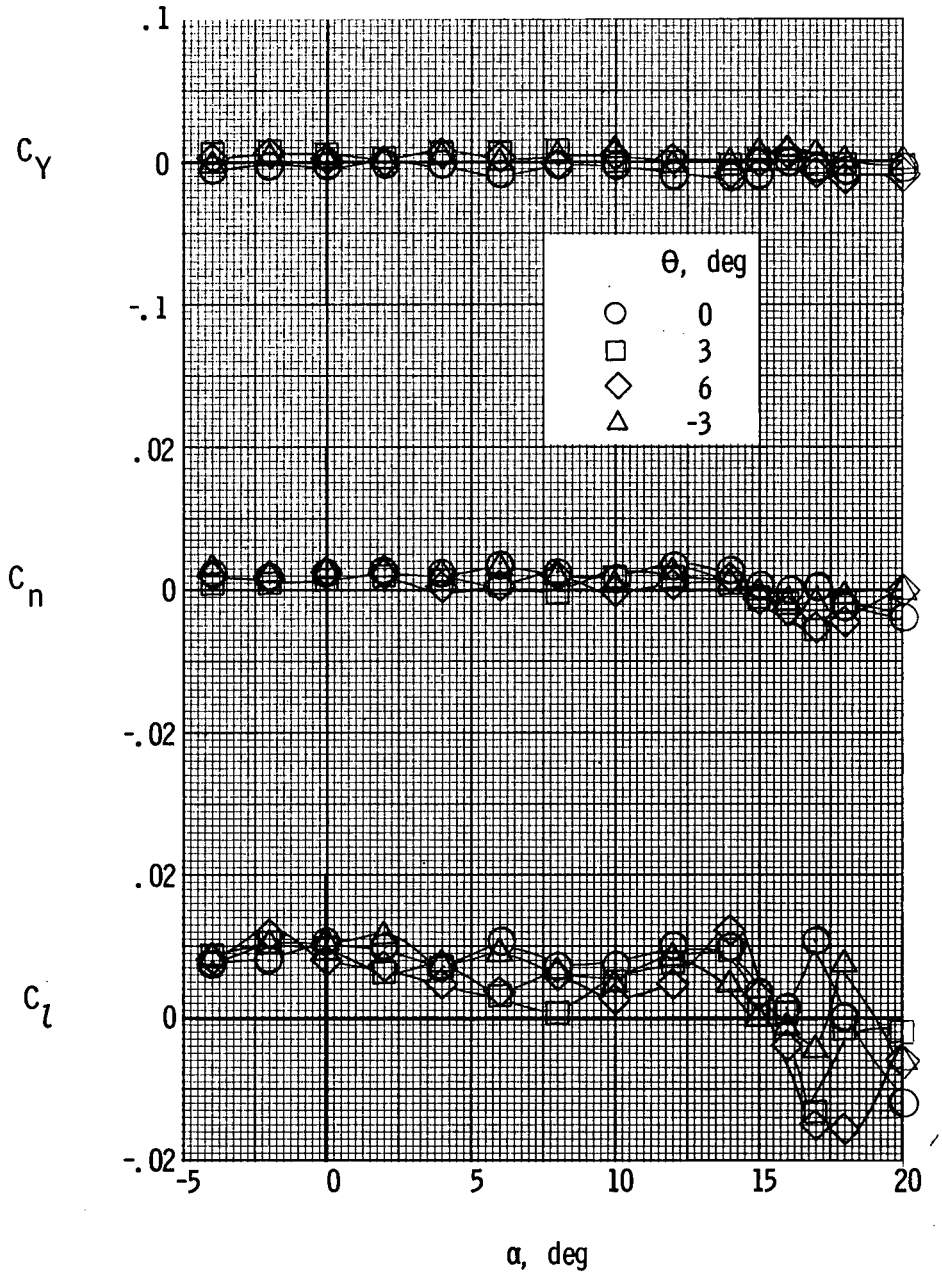

(a) $T_c' = 0$.

Figure 71.- Lateral aerodynamic characteristics of the model with the thrust axes pitched. $\delta_f = 0^o$; nacelle A.

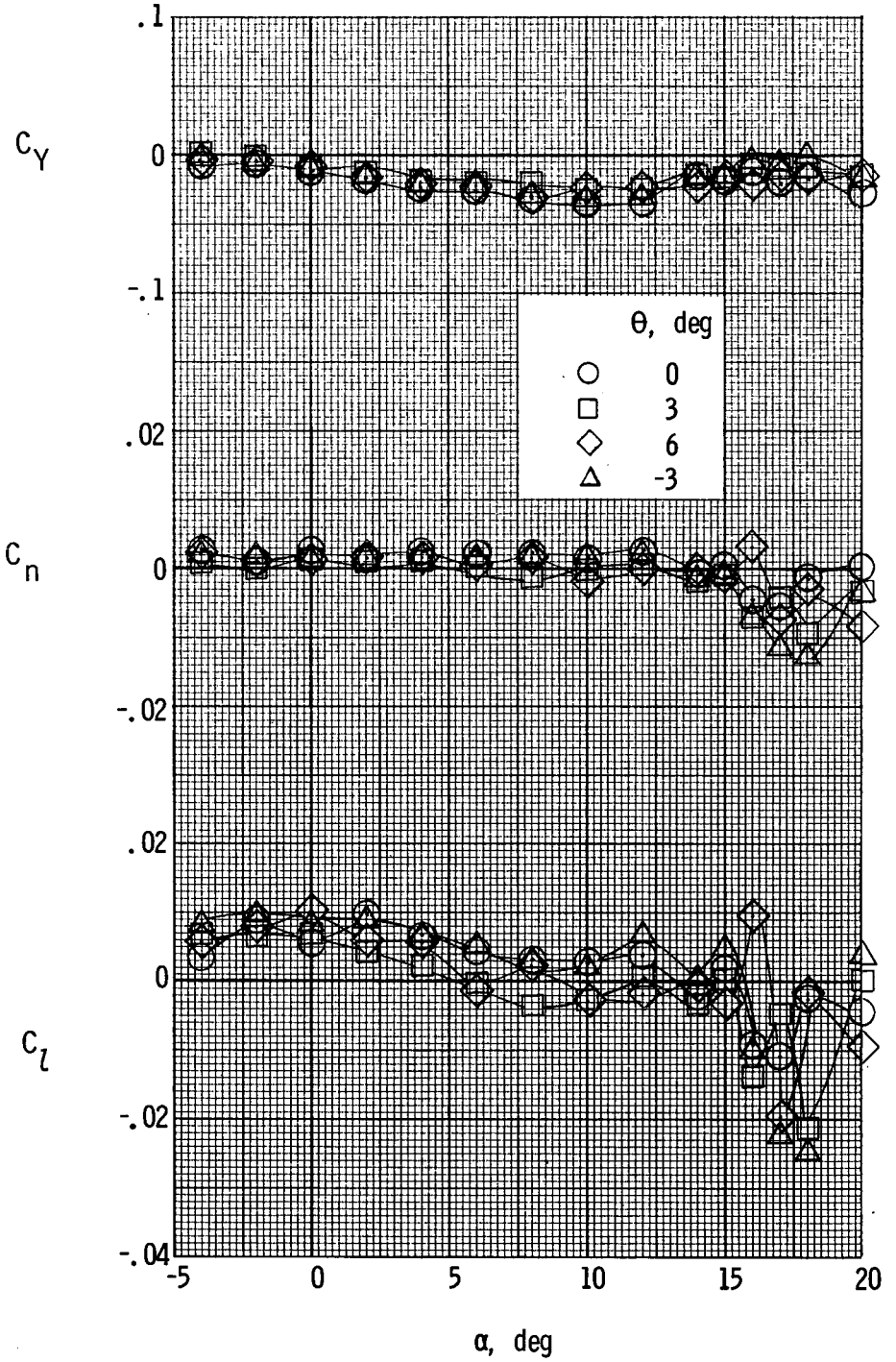

(b) $T_c' = 0.20$.

Figure 71.- Continued.

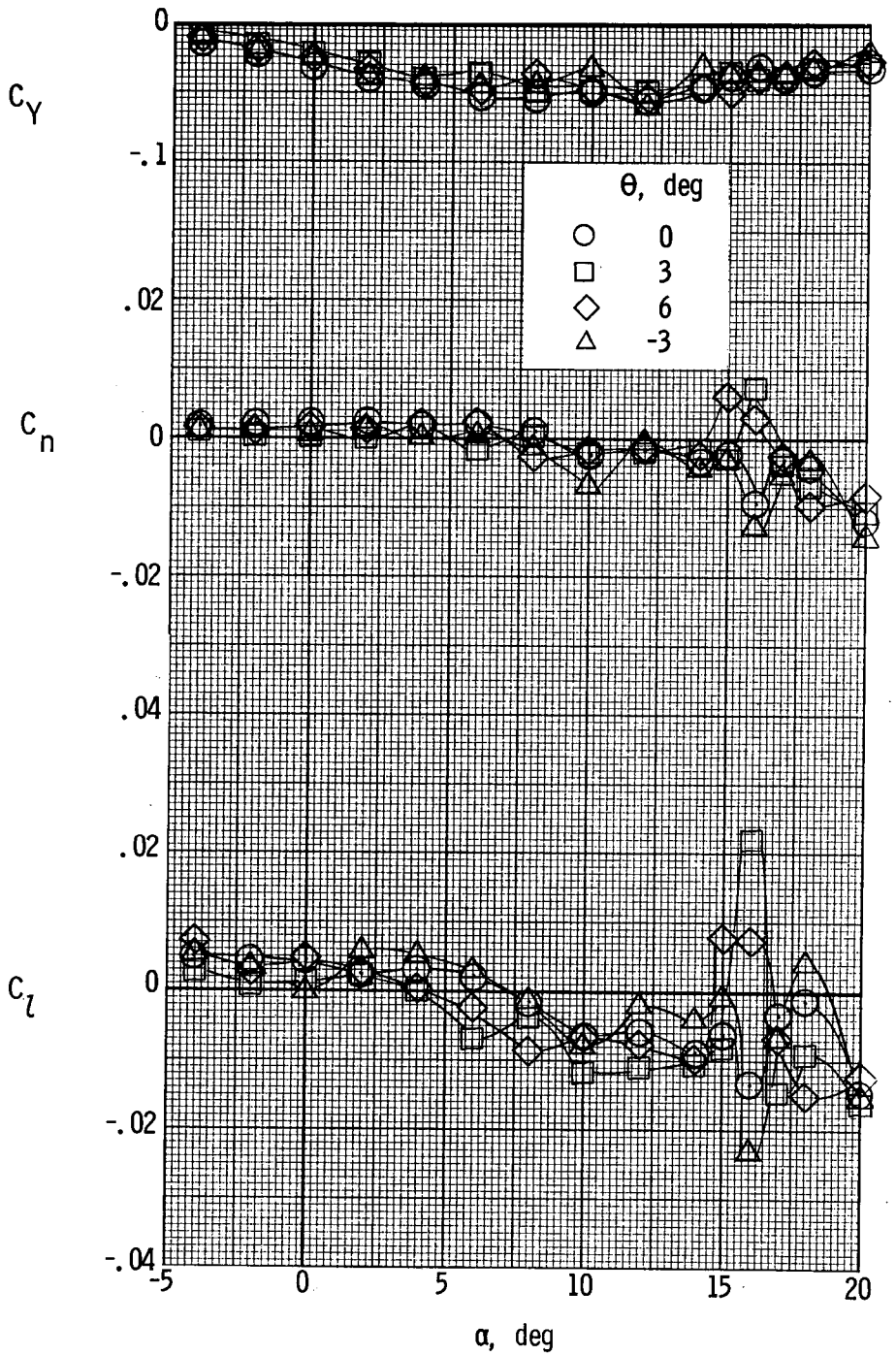

(c) $T_c' = 0.44$.

Figure 71.- Concluded.

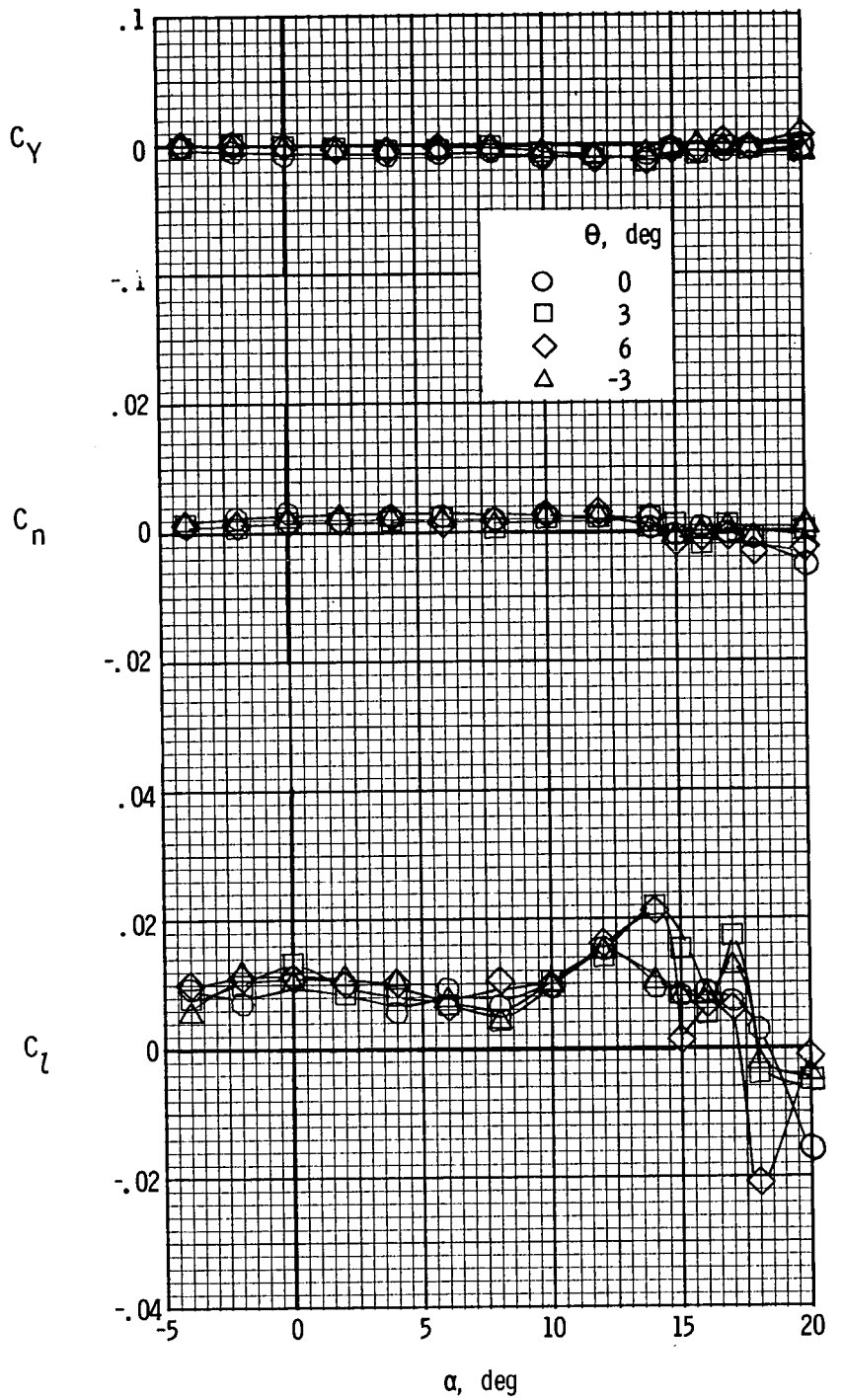

(a) $T_c' = 0$.

Figure 72.- Lateral aerodynamic characteristics of the model with the thrust axes pitched and with down-at-the-center propeller rotation. $\delta_f = 0^o$; nacelle A.

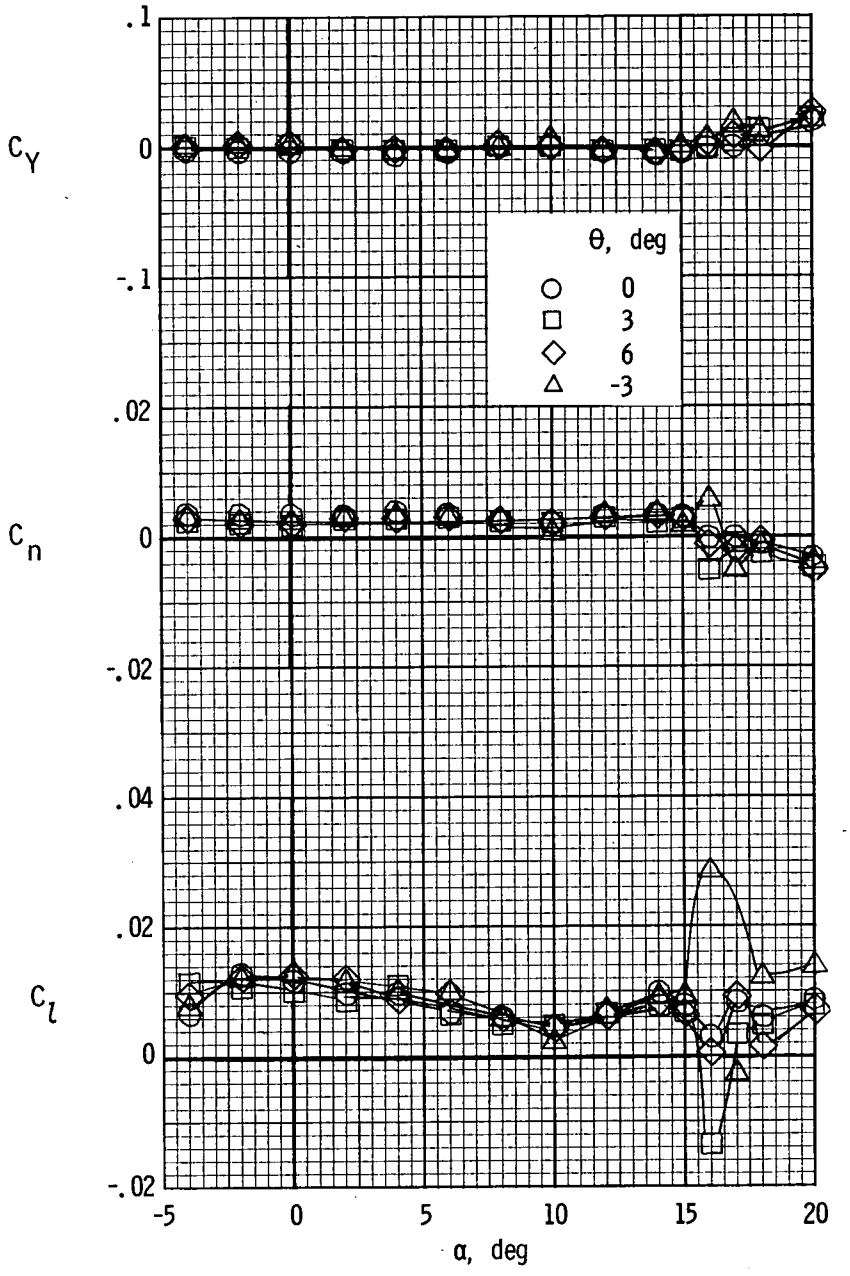

(b) $T_c' = 0.20$.

Figure 72.- Continued.

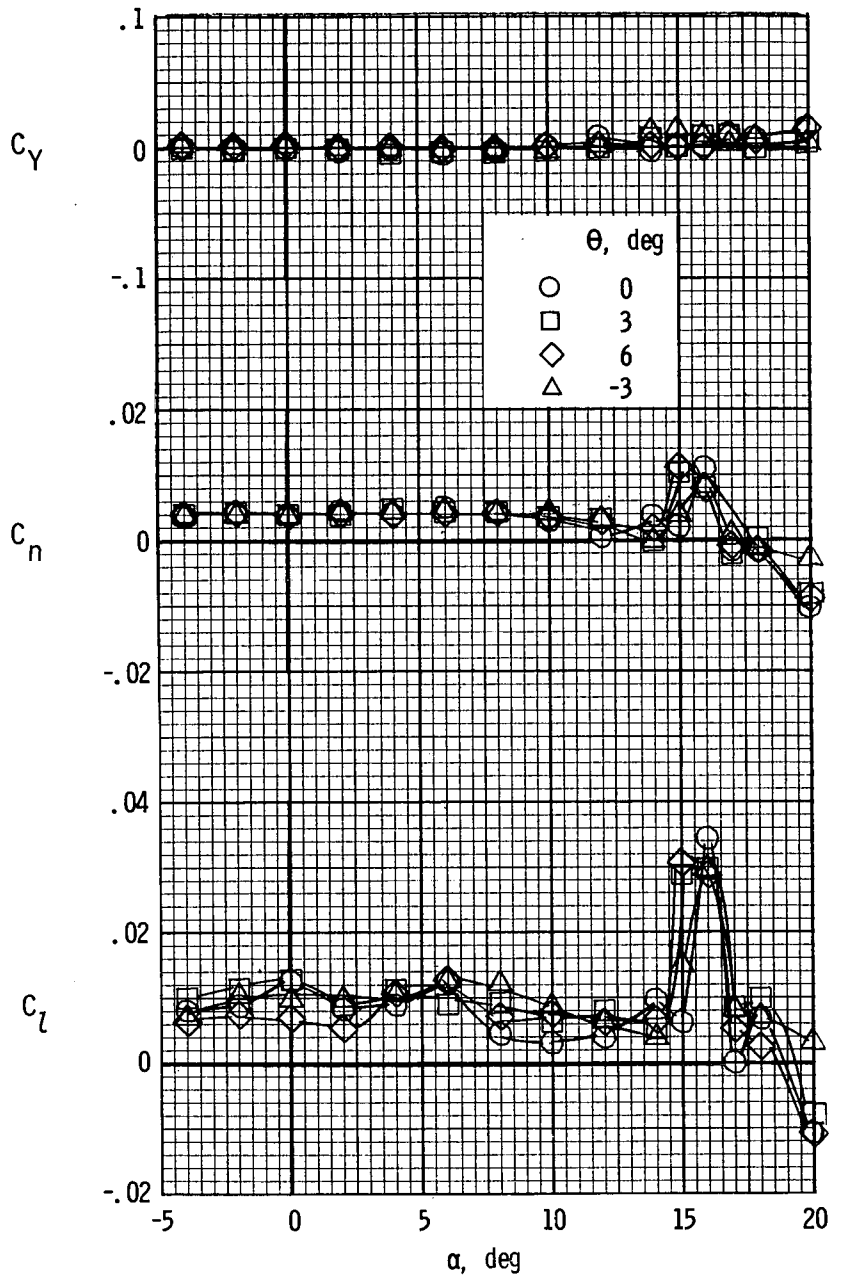

(c) $T_c' = 0.44$.

Figure 72.- Concluded.

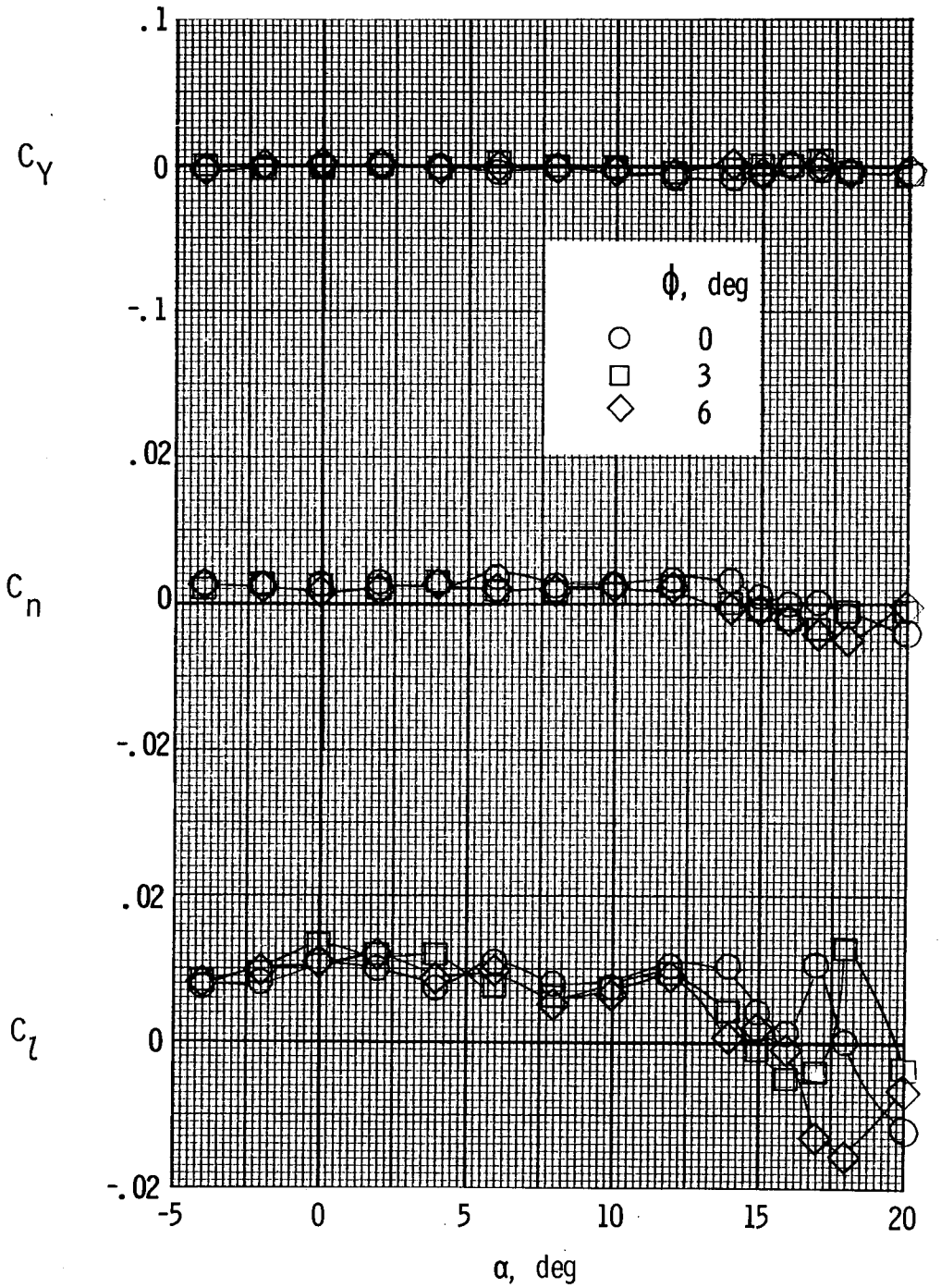

(a) $T_c' = 0$.

Figure 73.- Lateral aerodynamic characteristics of the model with the thrust axes toed out. $\delta_f = 0^o$; nacelle A.

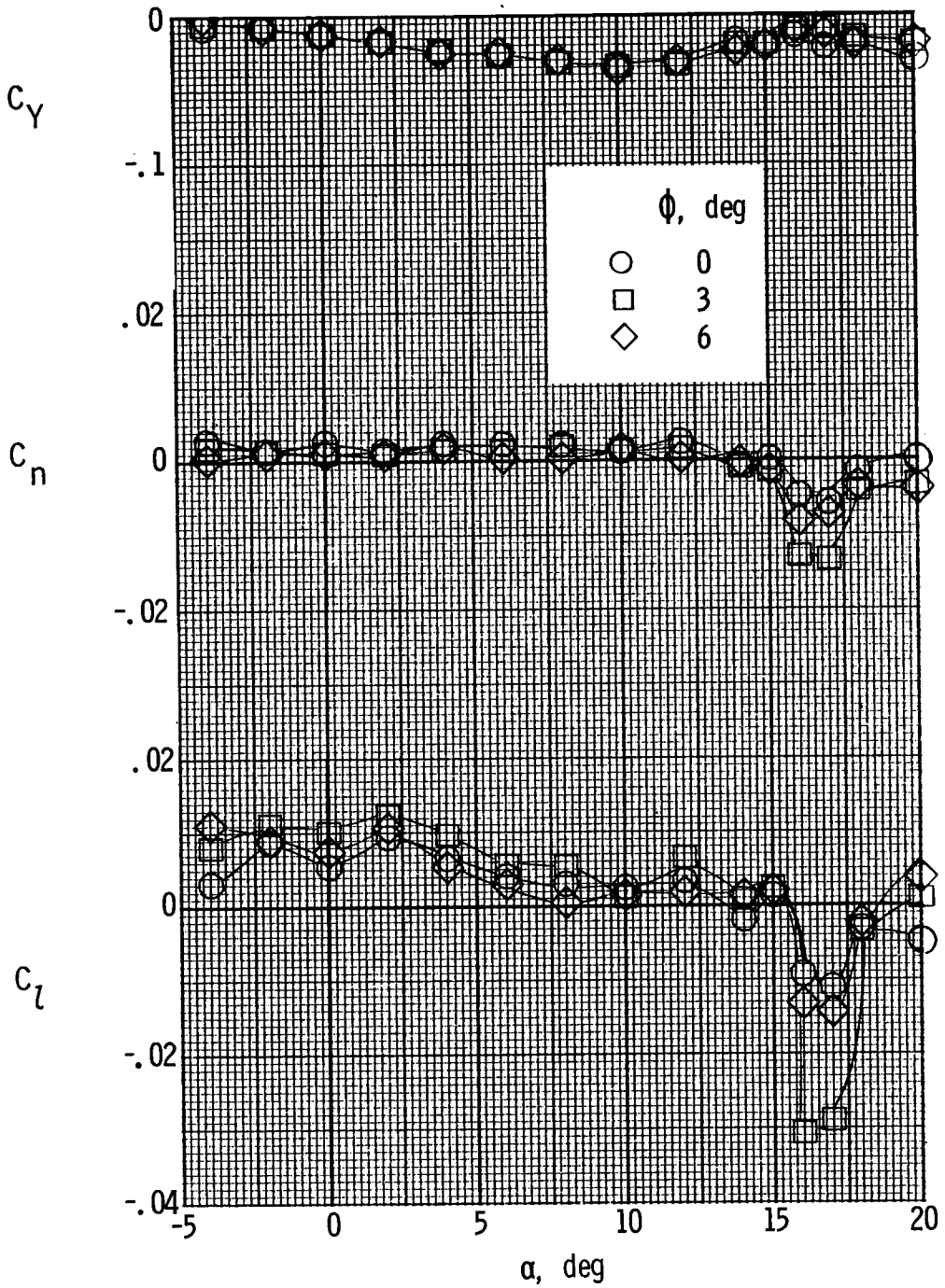

(b) $T_c' = 0.20$.

Figure 73.- Continued.

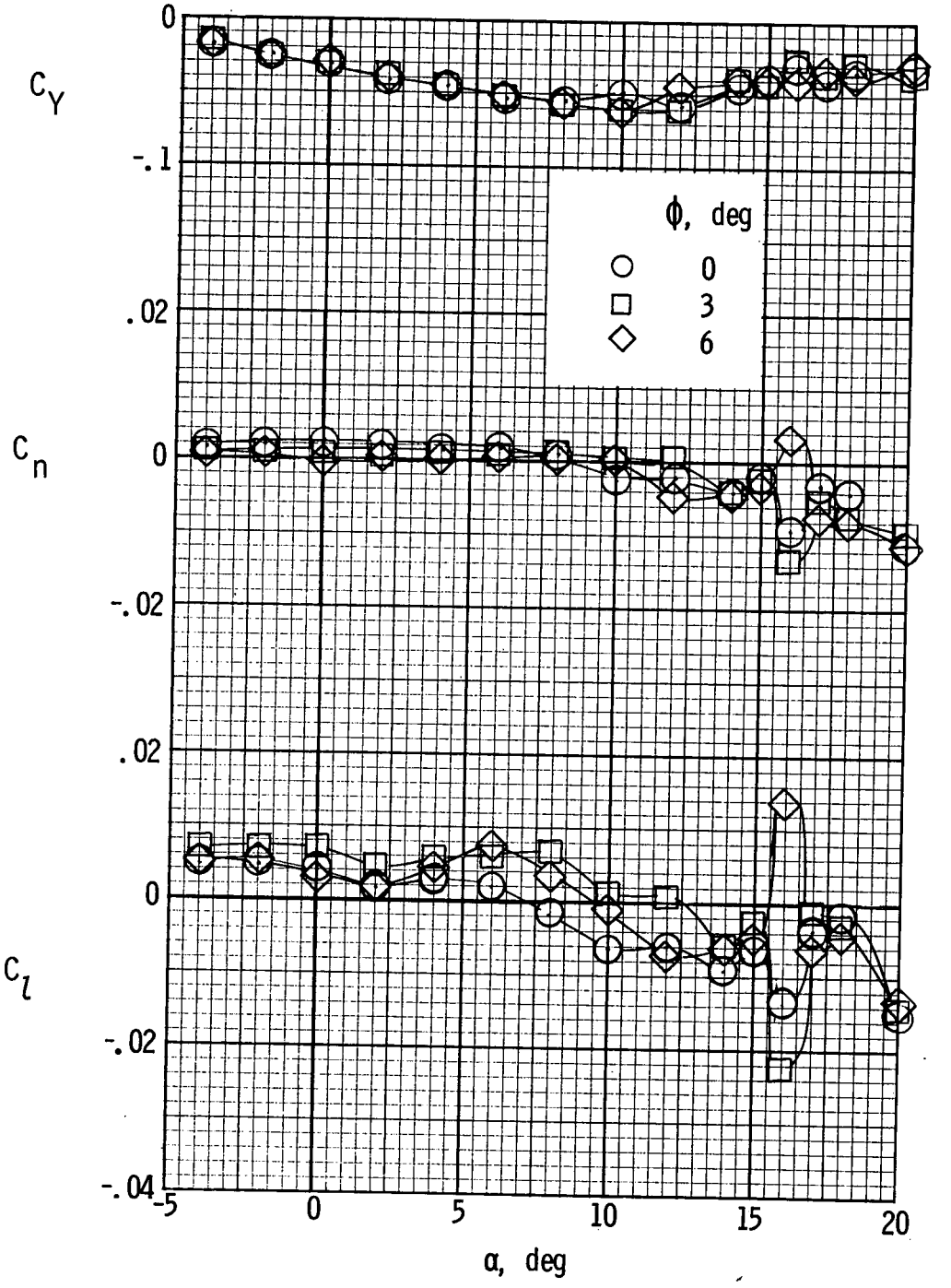

(c) $T_c' = 0.44$.

Figure 73.- Concluded.

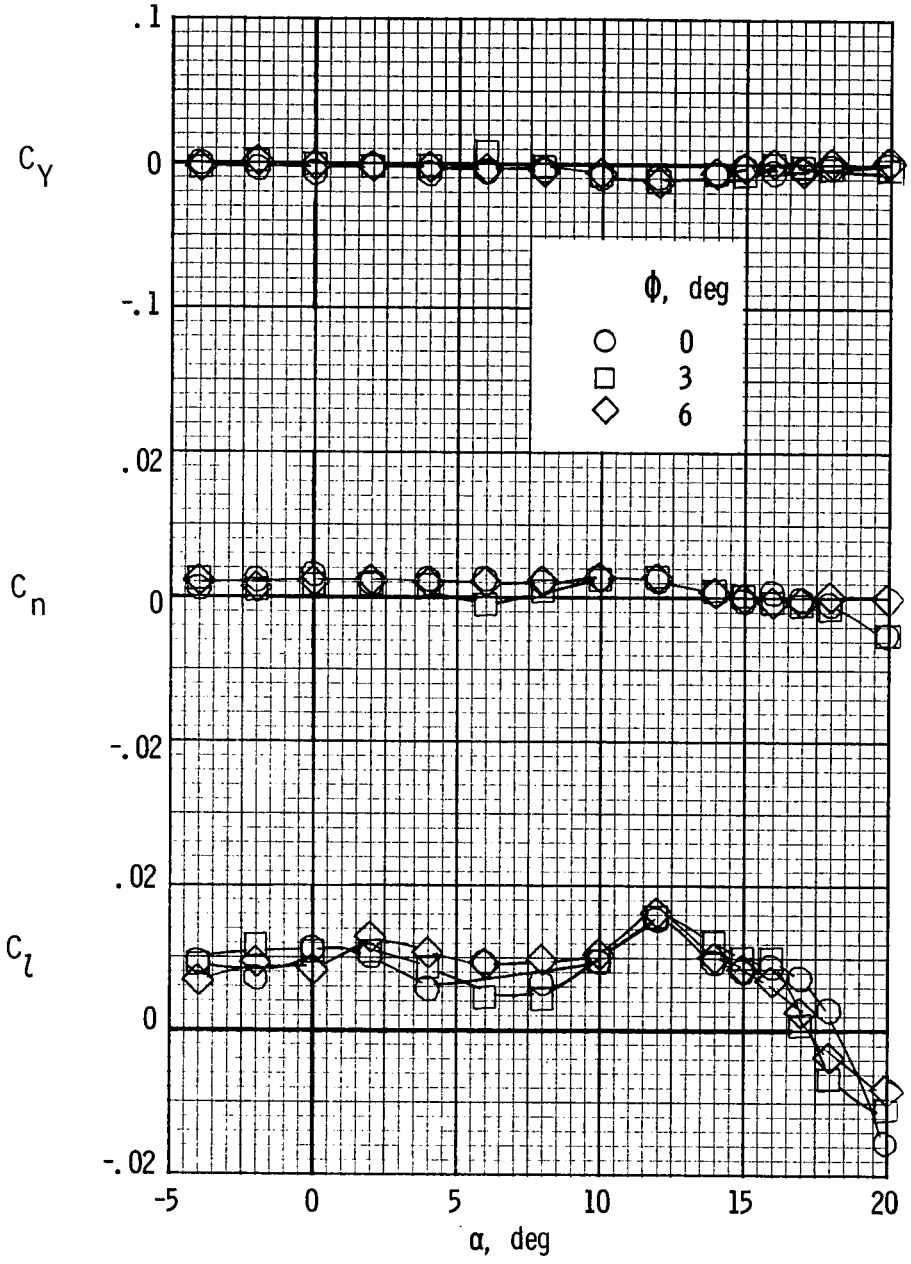

(a) $T_c' = 0$.

Figure 74.- Lateral aerodynamic characteristics of the model with the thrust axes toed out and with down-at-the-center propeller rotation. $\delta_f = 0^o$; nacelle A.

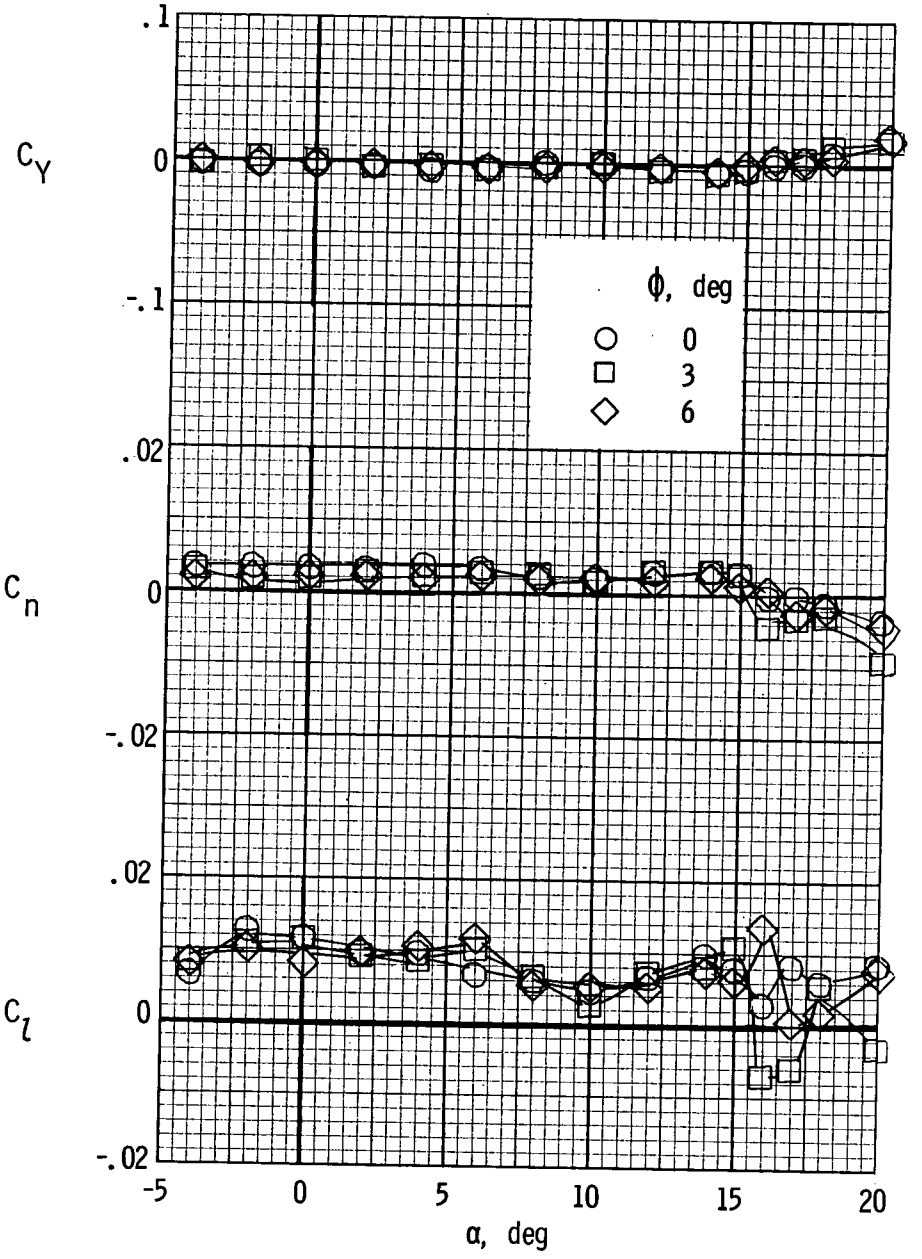

(b) $T_c' = 0.20$.

Figure 74.- Continued.

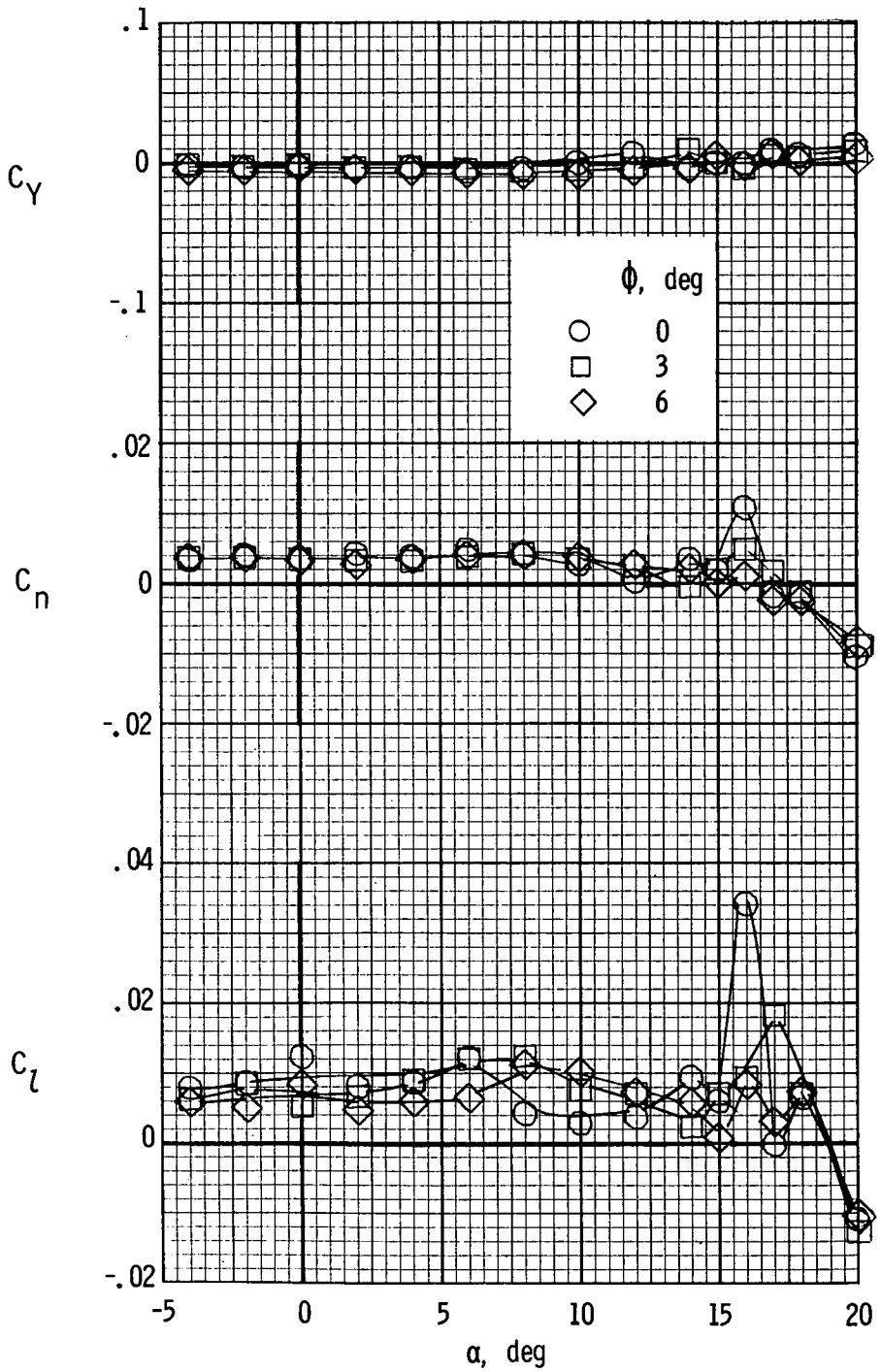

(c) $T_c' = 0.44$.

Figure 74.- Concluded.

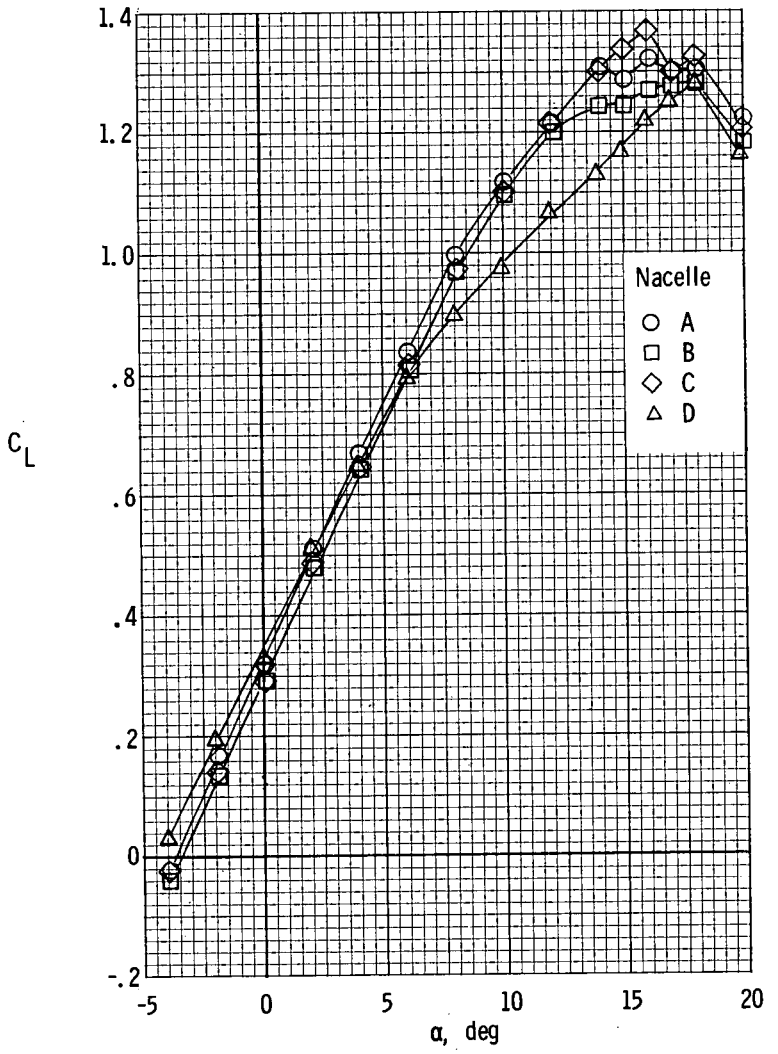

(a) $T_c' = 0$.

Figure 75.- Comparison of lift coefficients of the various nacelle configurations. $\delta_f = 0^o$.

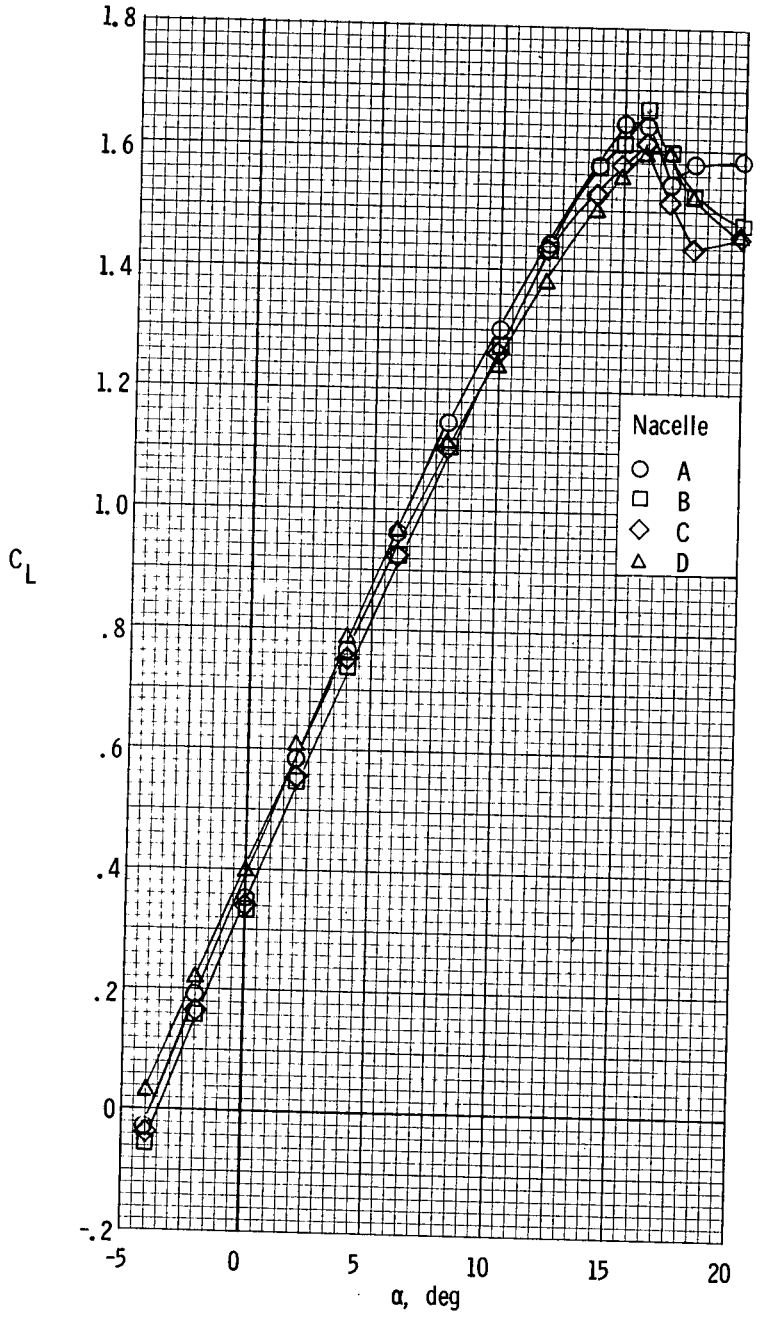

(b) $T_C' = 0.20$.

Figure 75.- Continued.

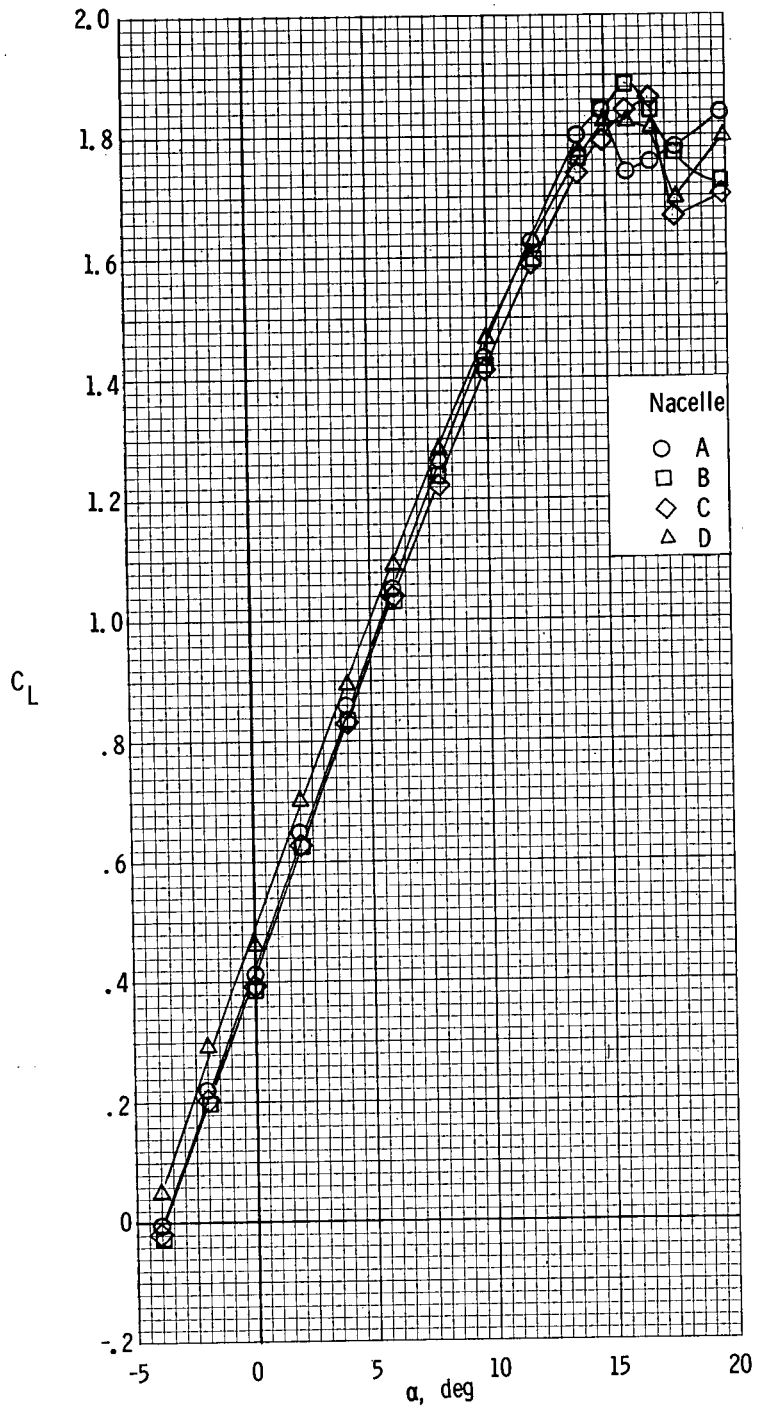

(c) $T_C' = 0.44$.

Figure 75.- Concluded.

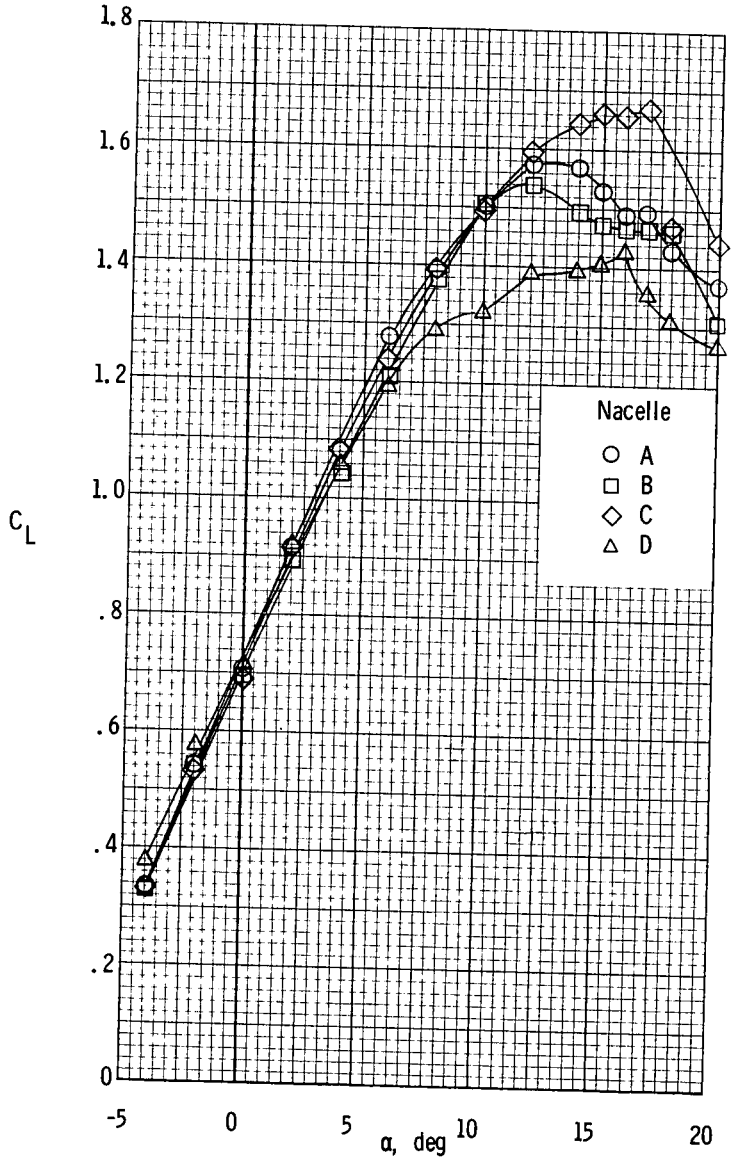

(a) $T_C' = 0$.

Figure 76.- Comparison of lift coefficients of the various nacelle configurations. $\delta_f = 27^o$.

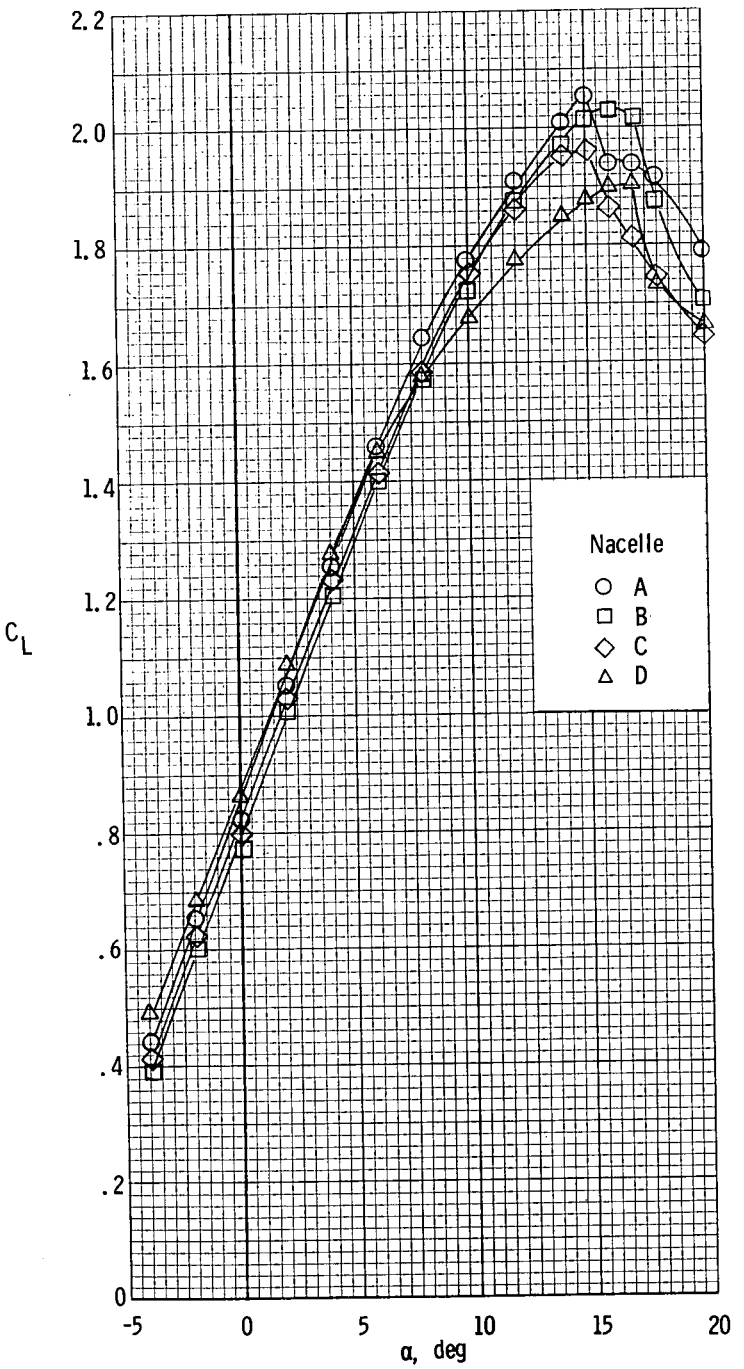

(b) $T_C' = 0.20$.

Figure 76.- Continued.

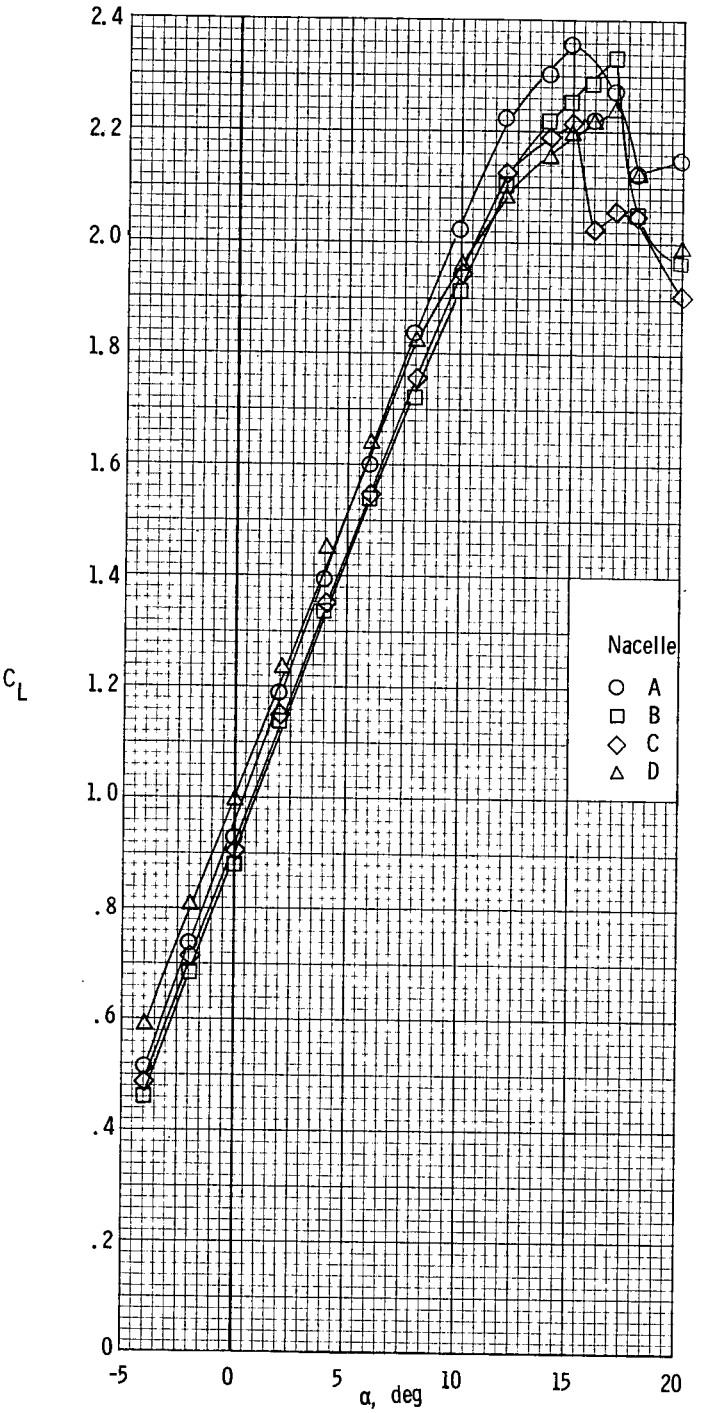

(c) $T_C' = 0.44$.

Figure 76.- Concluded.

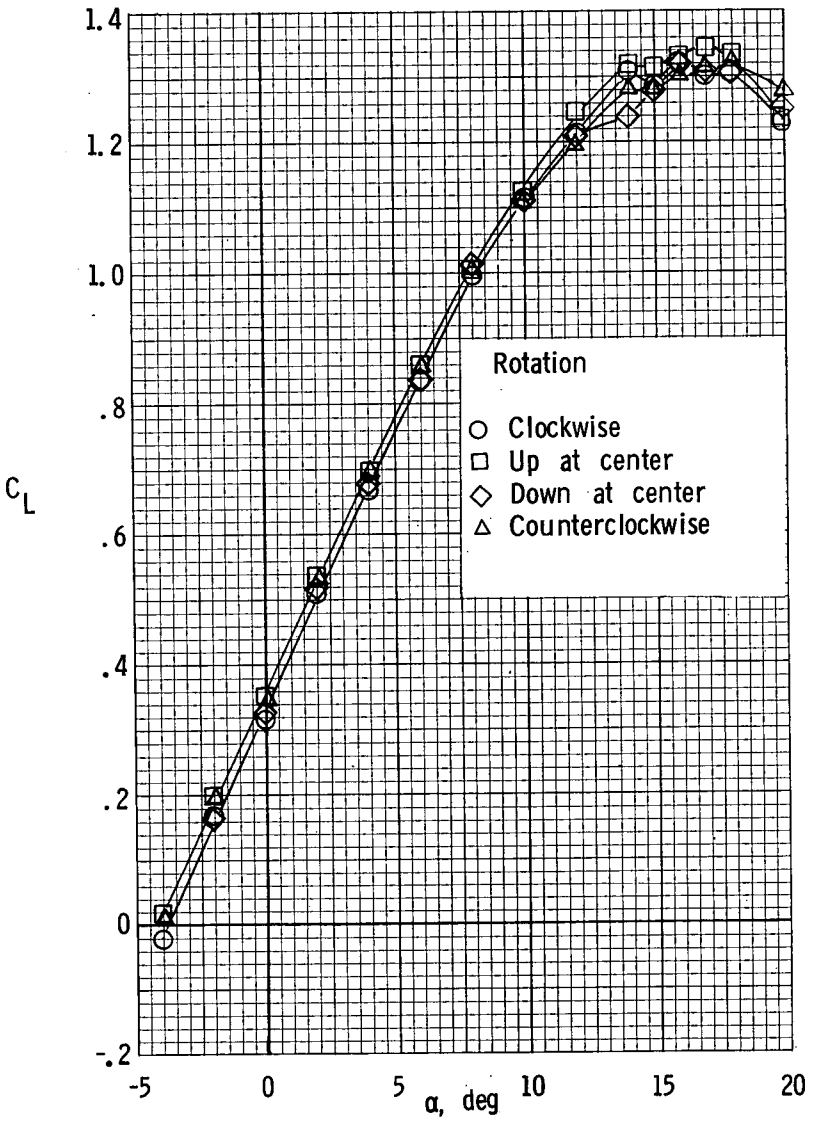

(a) $T_c' = 0.$

Figure 77.- Comparison of lift coefficients of the various modes of propeller rotation. $\delta_f = 0^o$; nacelle A.

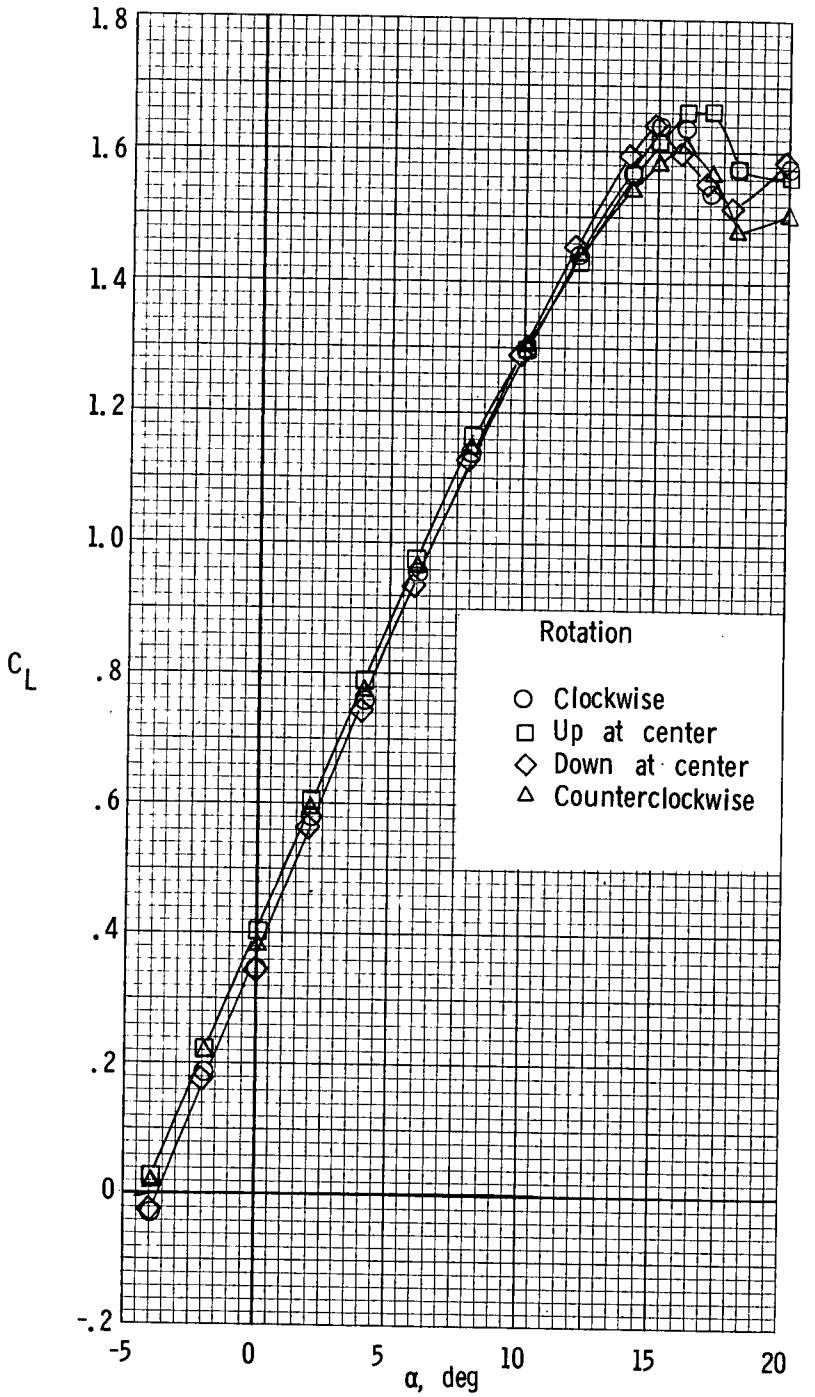

(b) $T_c' = 0.20$.

Figure 77.- Continued.

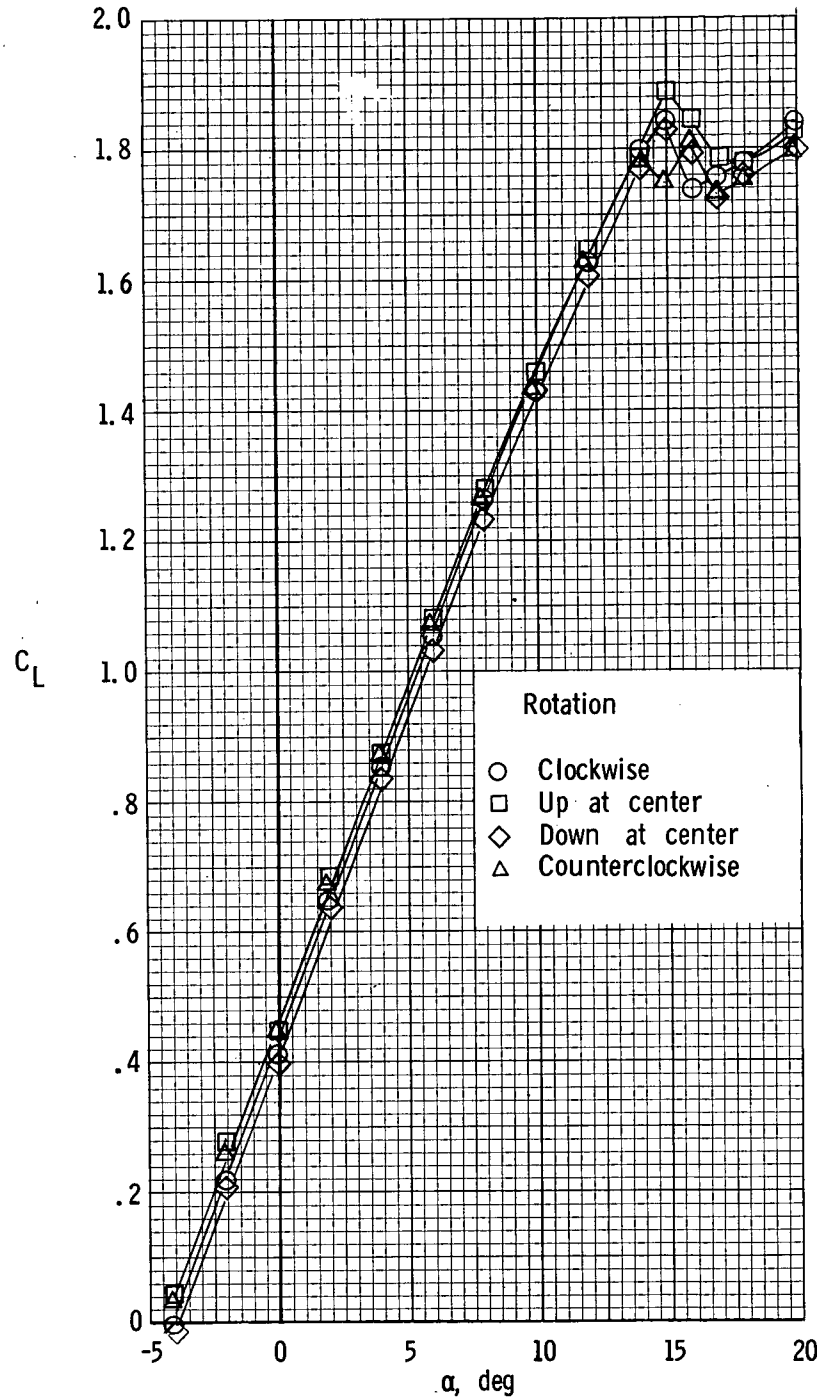

(c) $T_c' = 0.44$.

Figure 77.- Concluded.

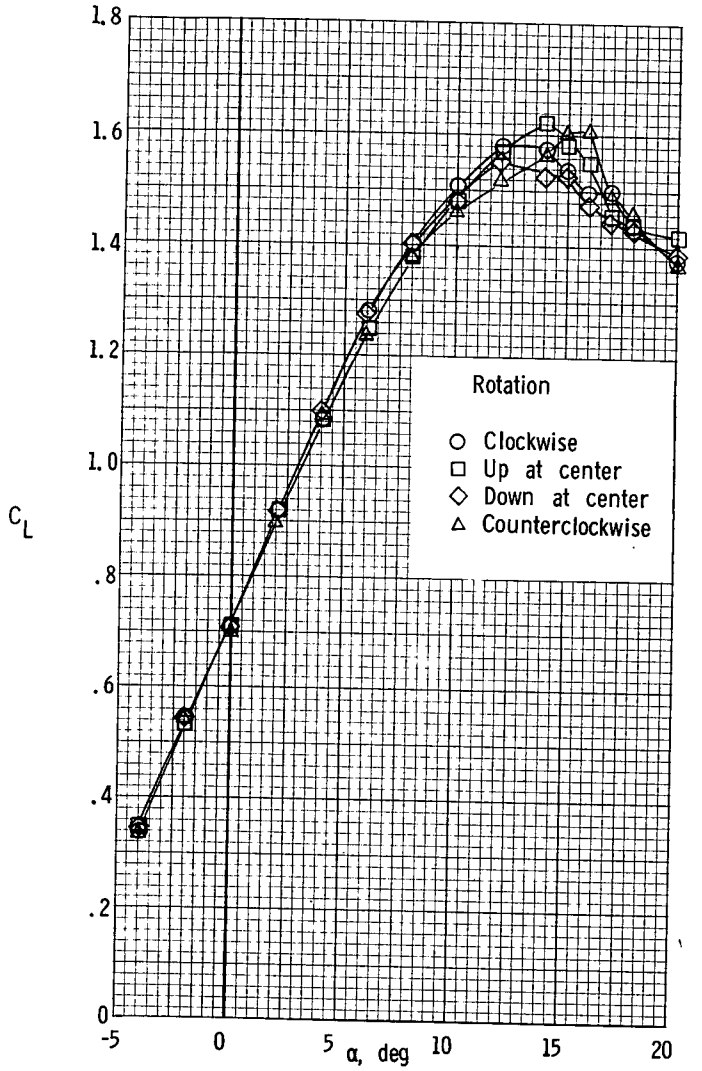

(a) $T_C' = 0$.

Figure 78.- Comparison of lift coefficients of the various modes of propeller rotation. $\delta_f = 27^o$; nacelle A.

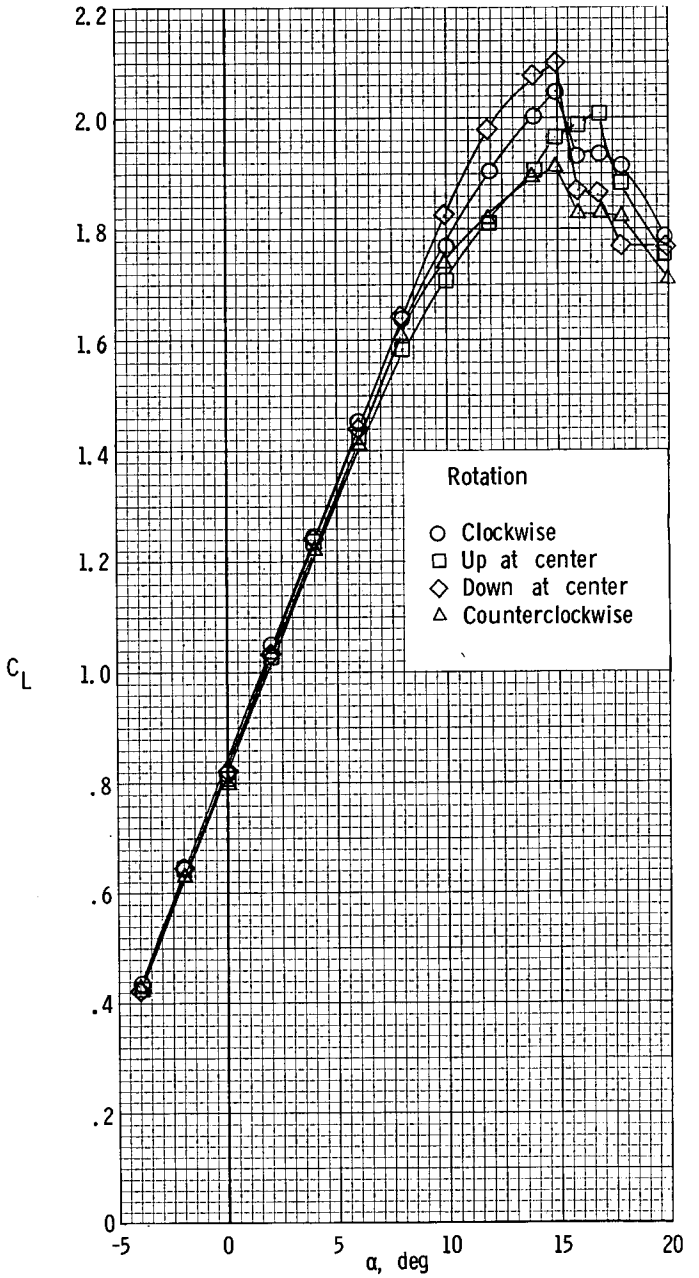

(b) $T_c' = 0.20$.

Figure 78.- Continued.

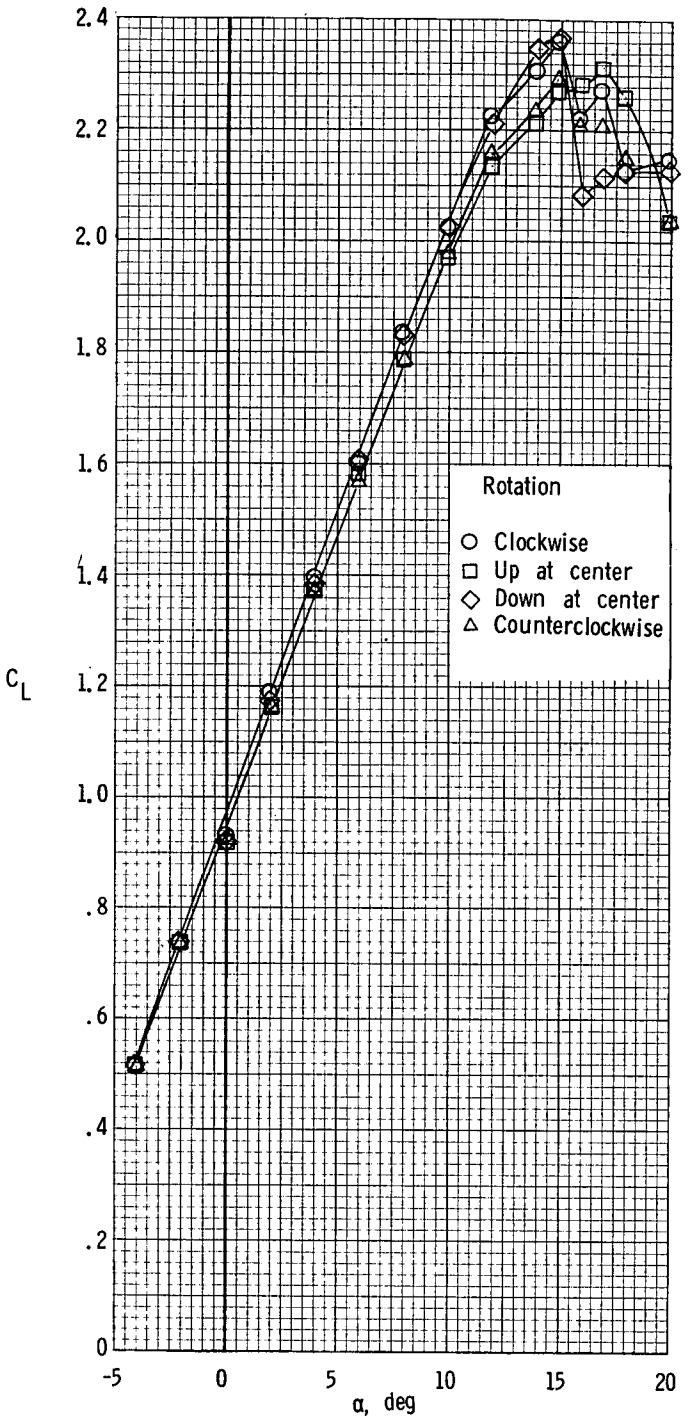

(c) $T_C' = 0.44$.

Figure 78.- Concluded.

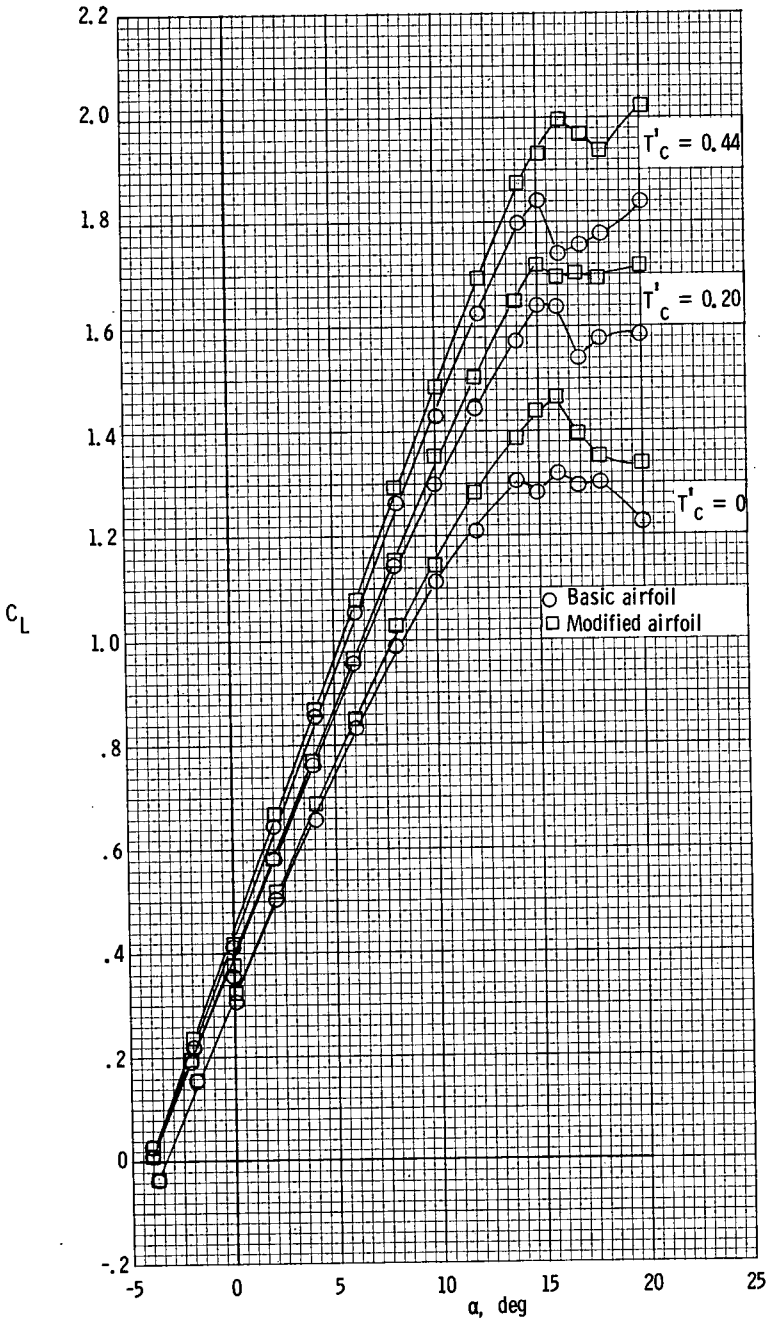

(a) $\delta_f = 0^o$.

Figure 79.- Comparison of lift coefficients of the basic and modified airfoil section configuration. Nacelle A.

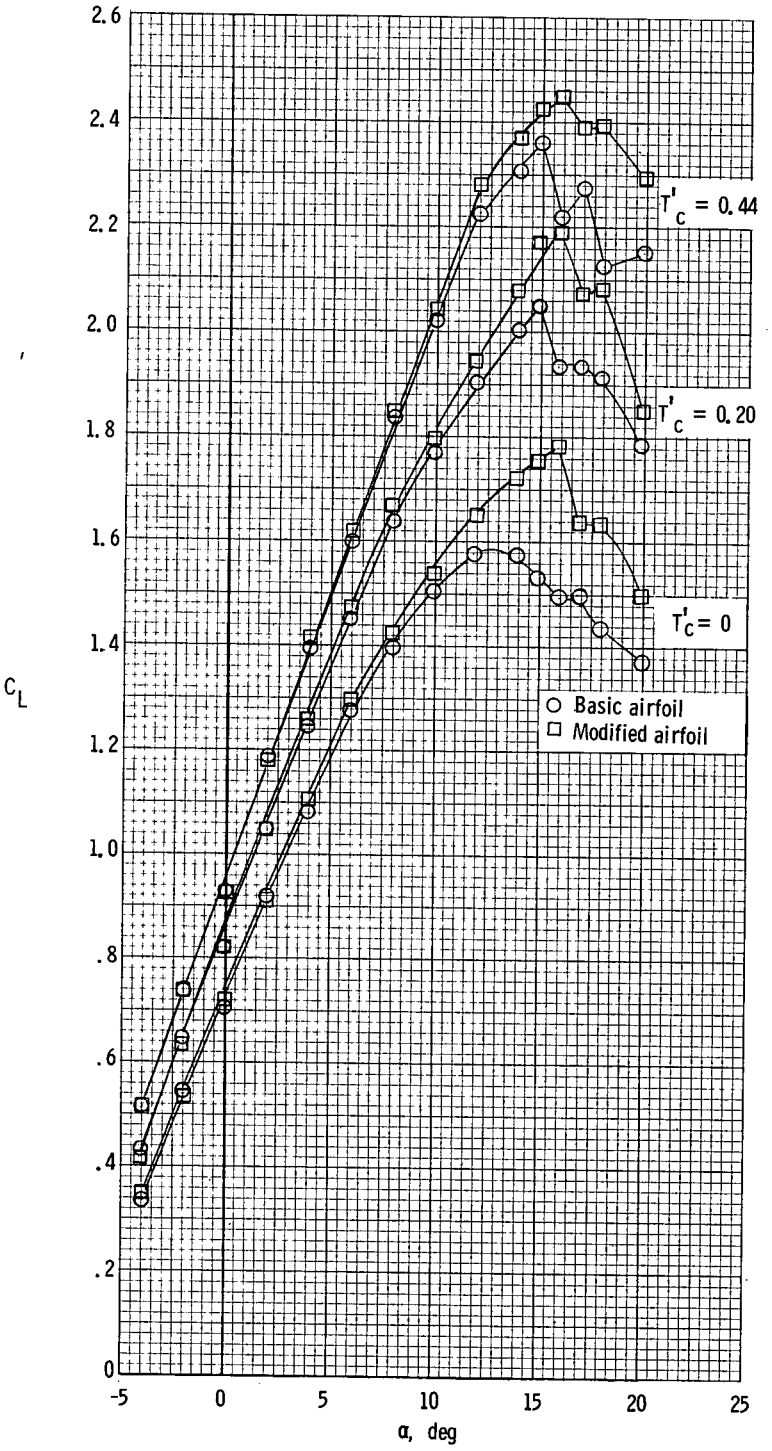

(b) $\delta_f = 27^o$.

Figure 79.- Concluded.

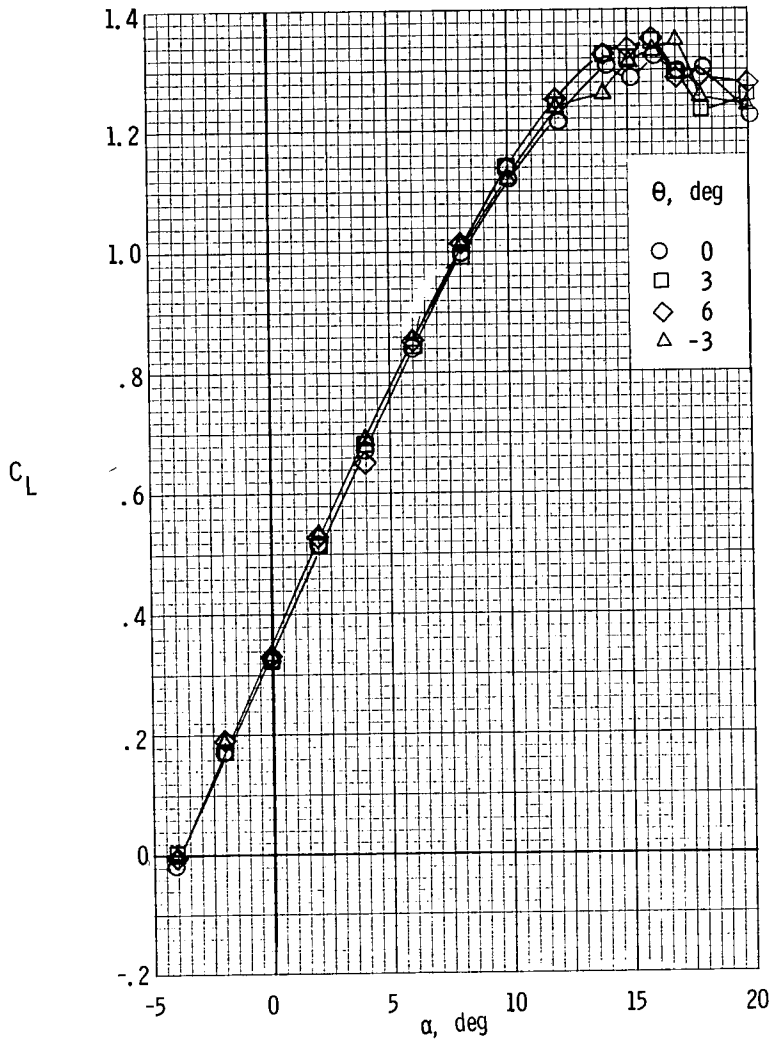

(a) $T_c' = 0$.

Figure 80.- Comparison of lift coefficients with thrust axes pitched. $\delta_f = 0^o$; nacelle A.

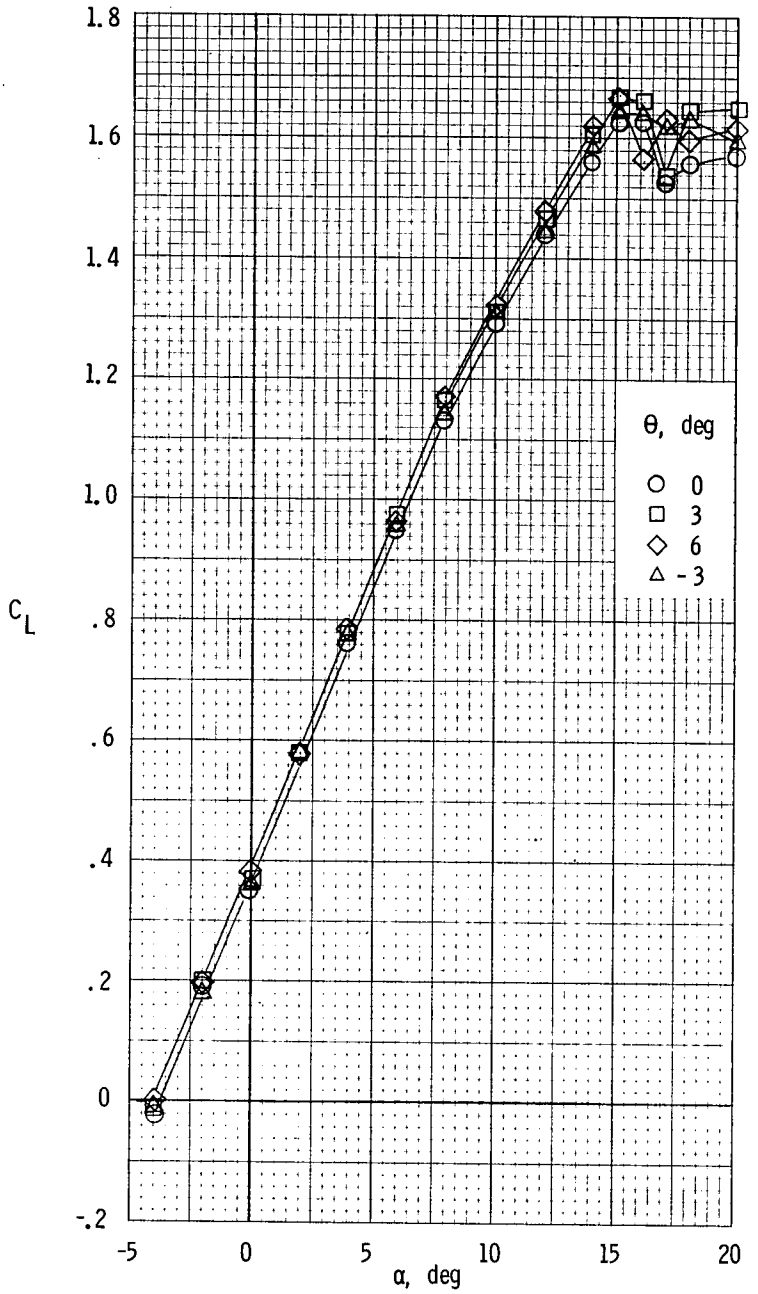

(b) $T_C' = 0.20$.

Figure 80.- Continued.

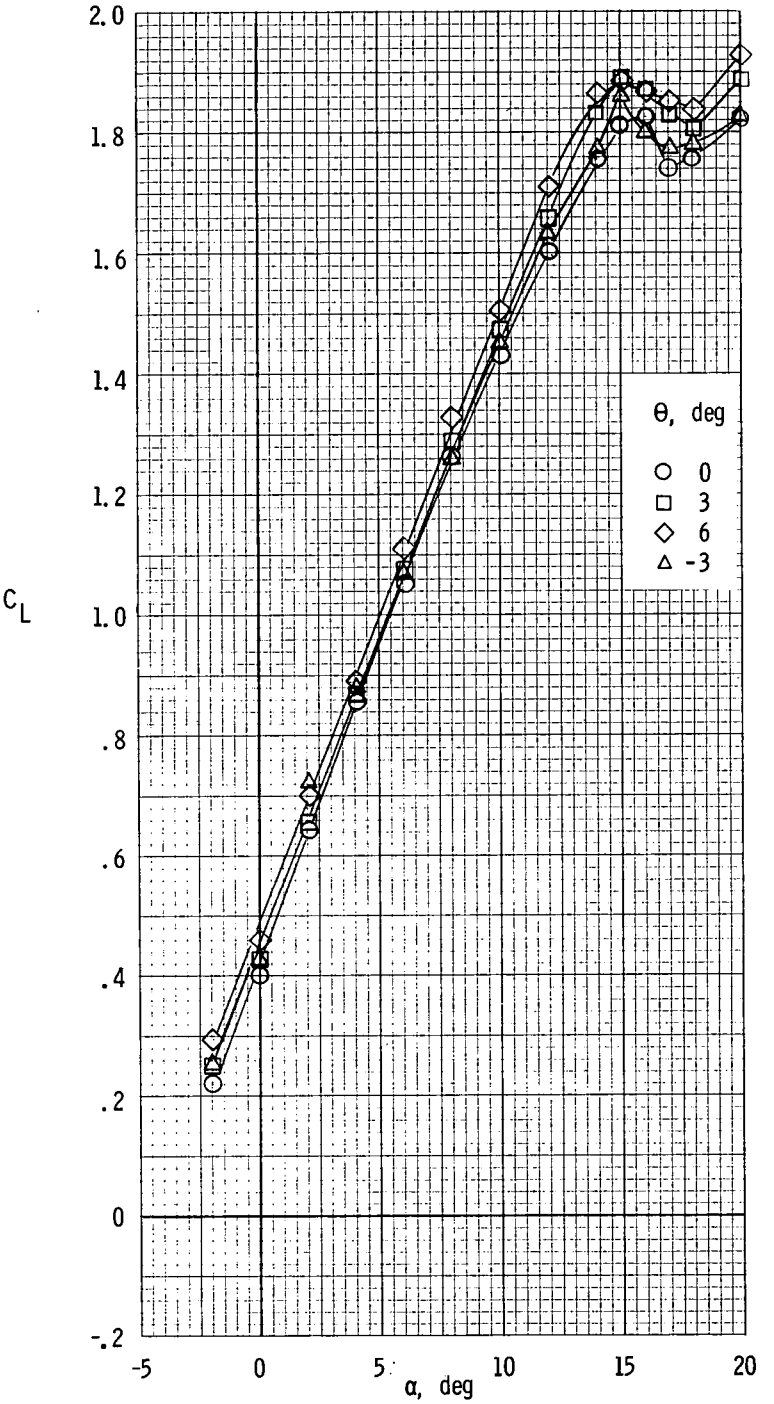

(c) $T_c' = 0.44$.

Figure 80.- Concluded.

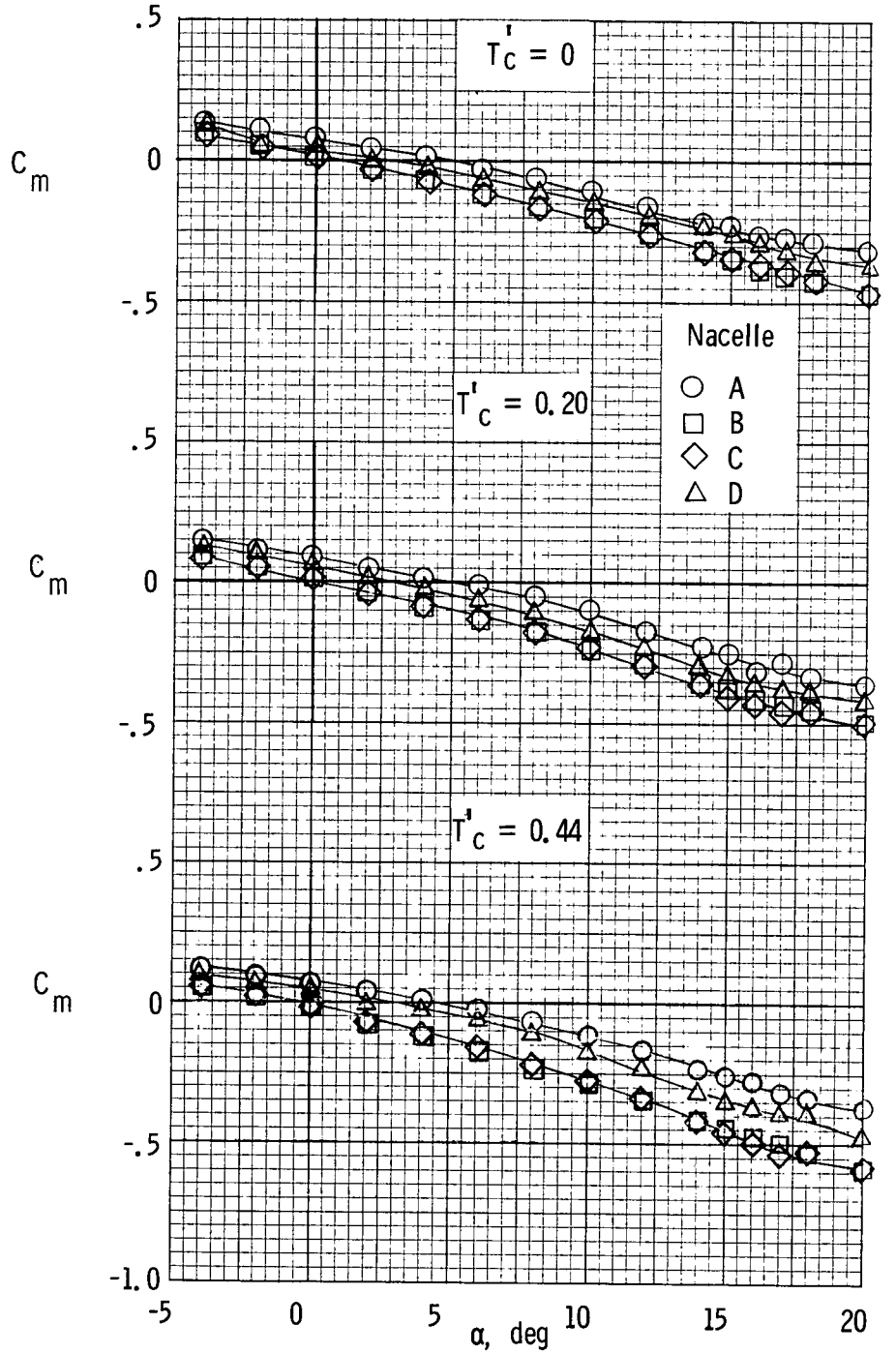

(a) $\delta_f = 0^o$.

Figure 81.- Variation of pitching-moment coefficient with angle of attack for several thrust coefficients and nacelle configurations. $i_t = 0^o$.

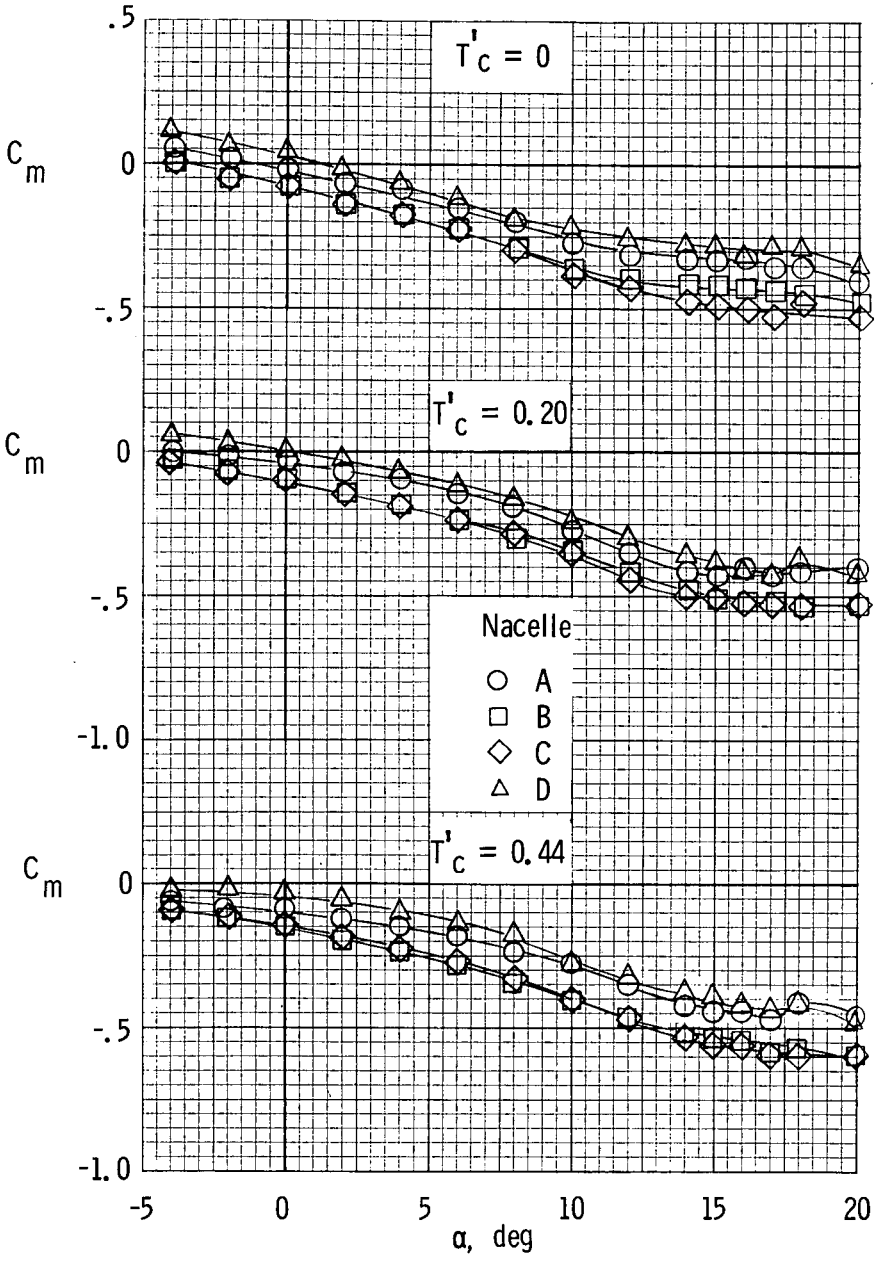

(b) $\delta_f = 27^o$.

Figure 81.- Concluded.

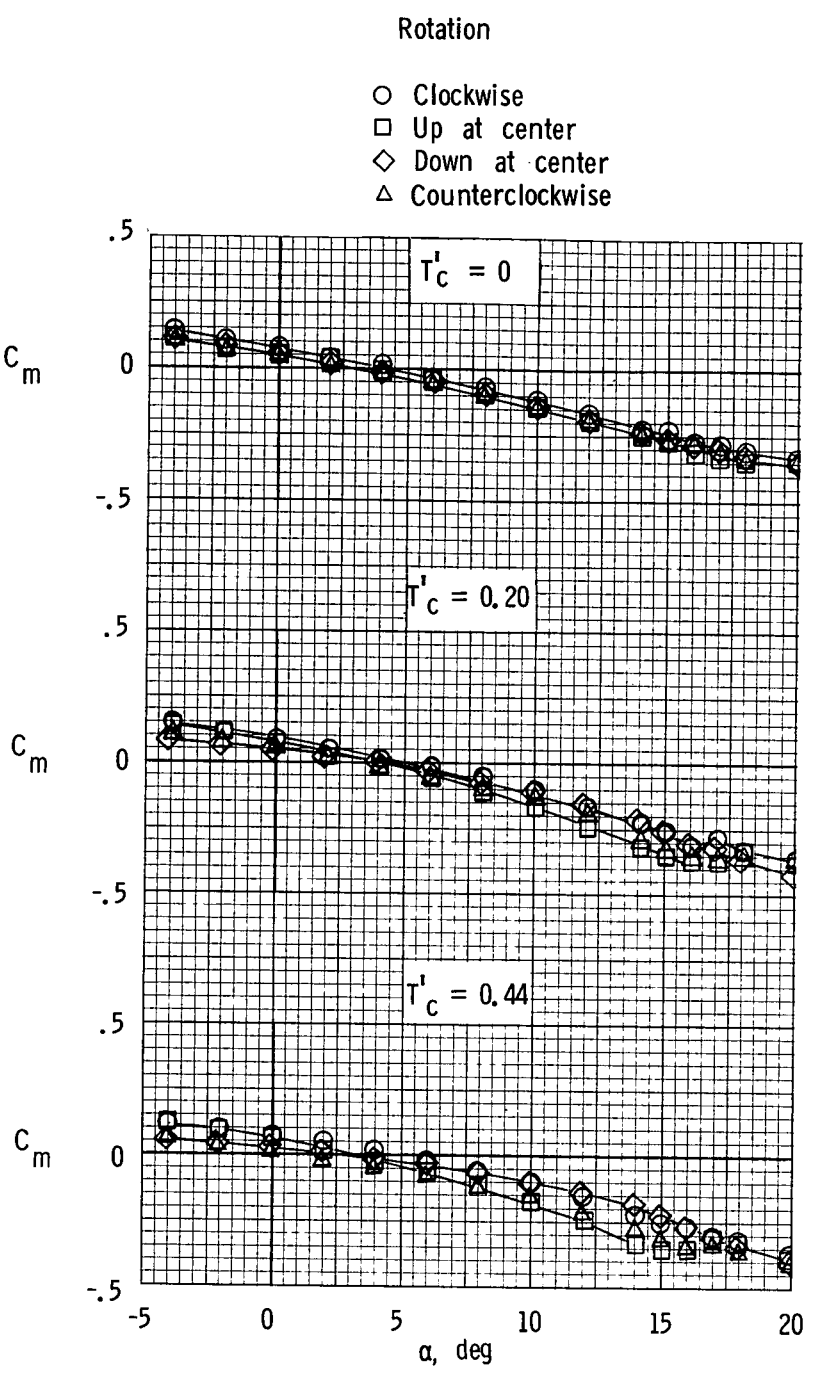

(a) $\delta_f = 0^o$.

Figure 82.- Variation of pitching-moment coefficient with angle of attack for various modes of propeller rotation. $i_t = 0^o$.

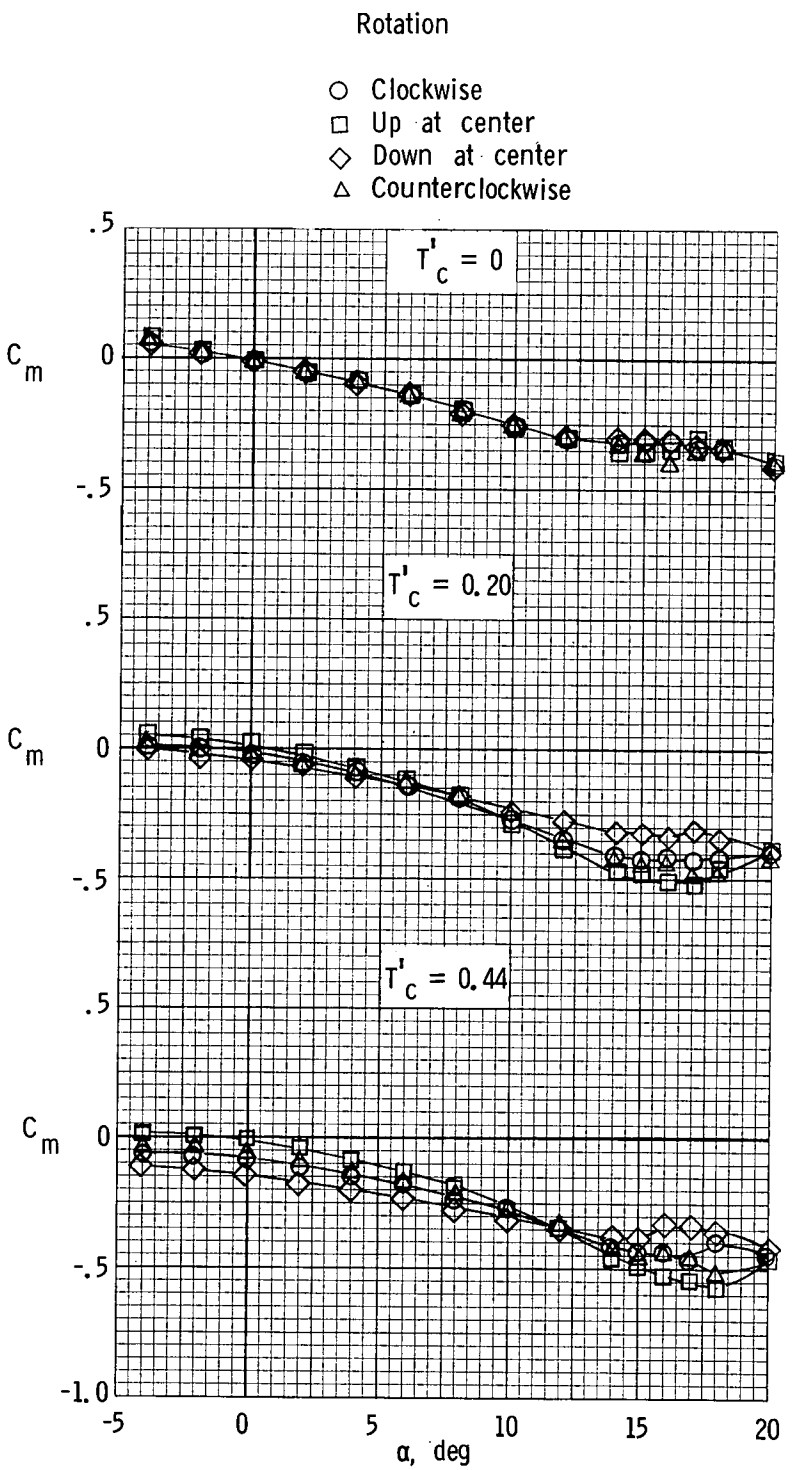

(b) $\delta_f = 27^o$.

Figure 82.- Concluded.

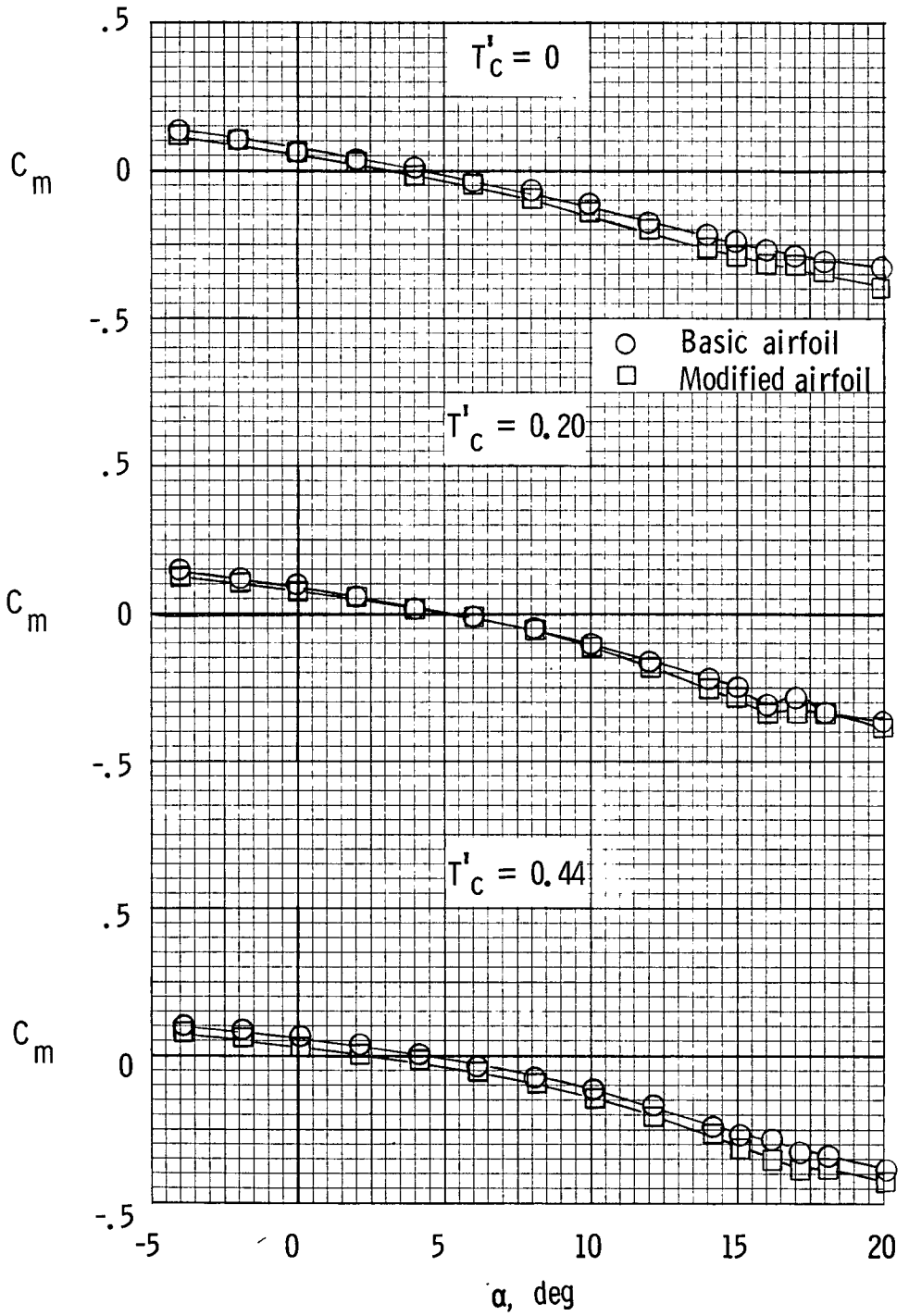

(a) $\delta_f = 0^o$.

Figure 83.- Variation of pitching-moment coefficient with angle of attack for basic and modified airfoil section configurations. $i_t = 0^o$.

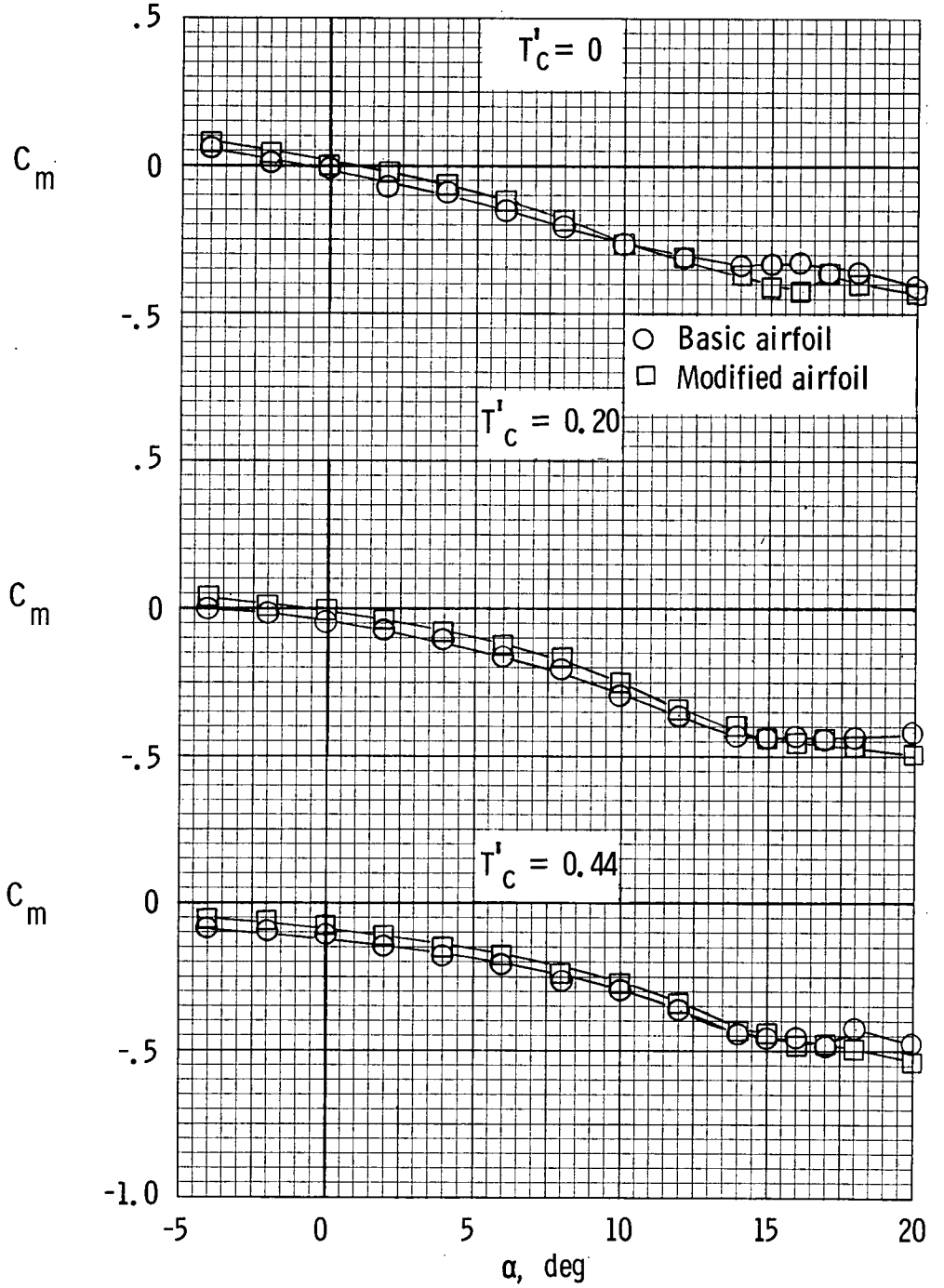

(b) $\delta_f = 27^o$.

Figure 83.- Concluded.

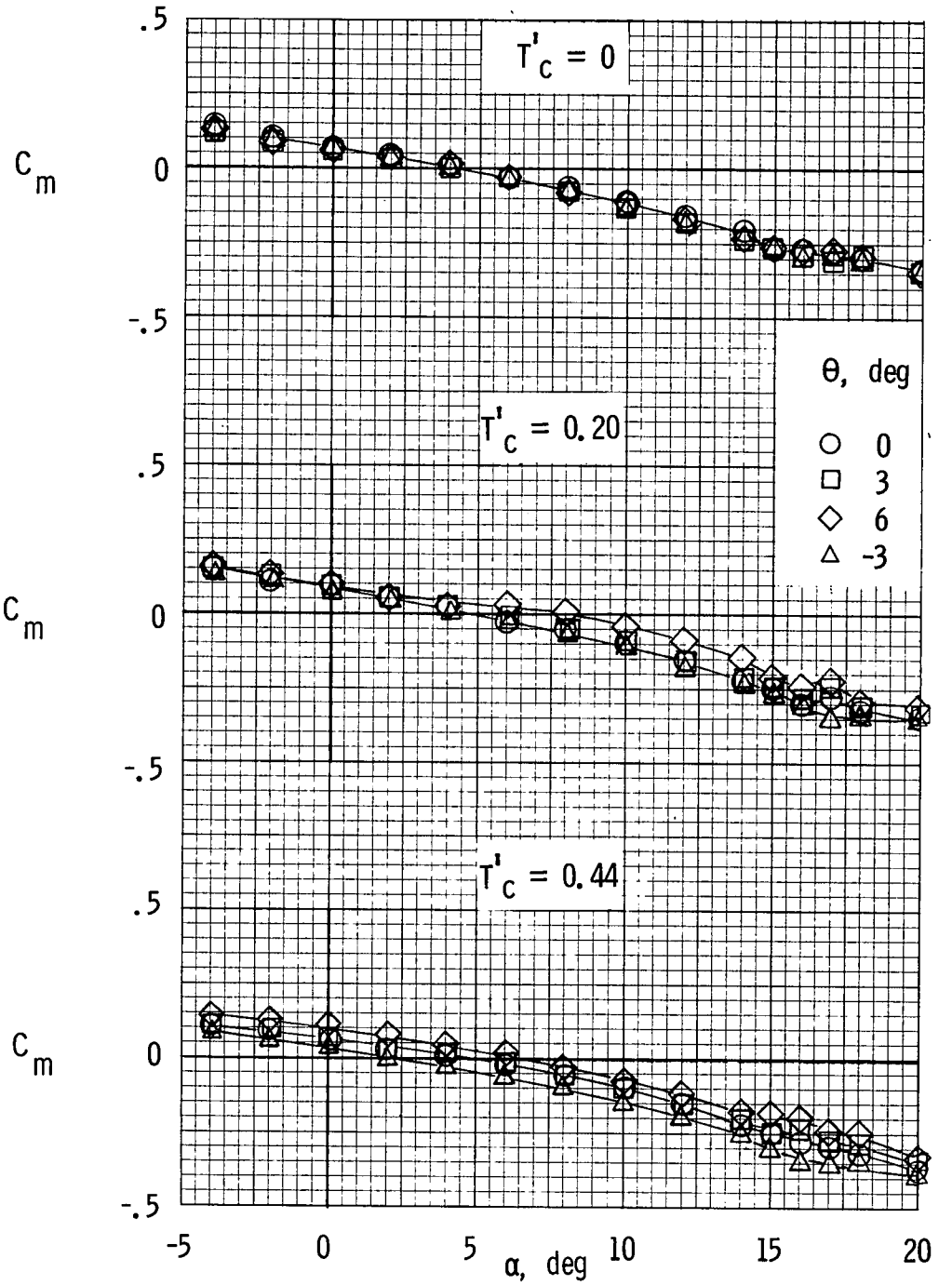

Figure 84.- Comparison of pitching-moment coefficients with the thrust axis pitched. $\delta_f = 0^o$.

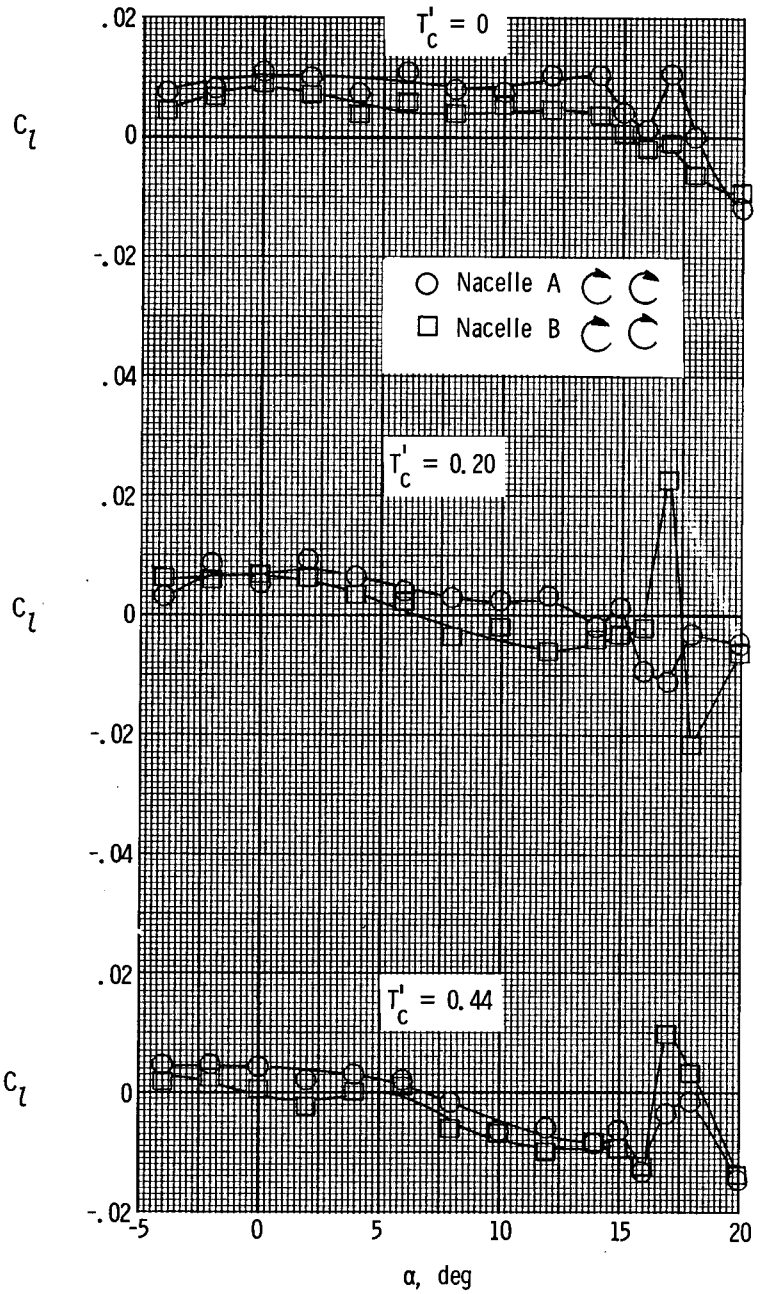

(a) $\delta_f = 0^o$.

Figure 85.- Comparison of rolling-moment coefficients of nacelle B with the basic nacelle configuration. $\beta = 0^o$.

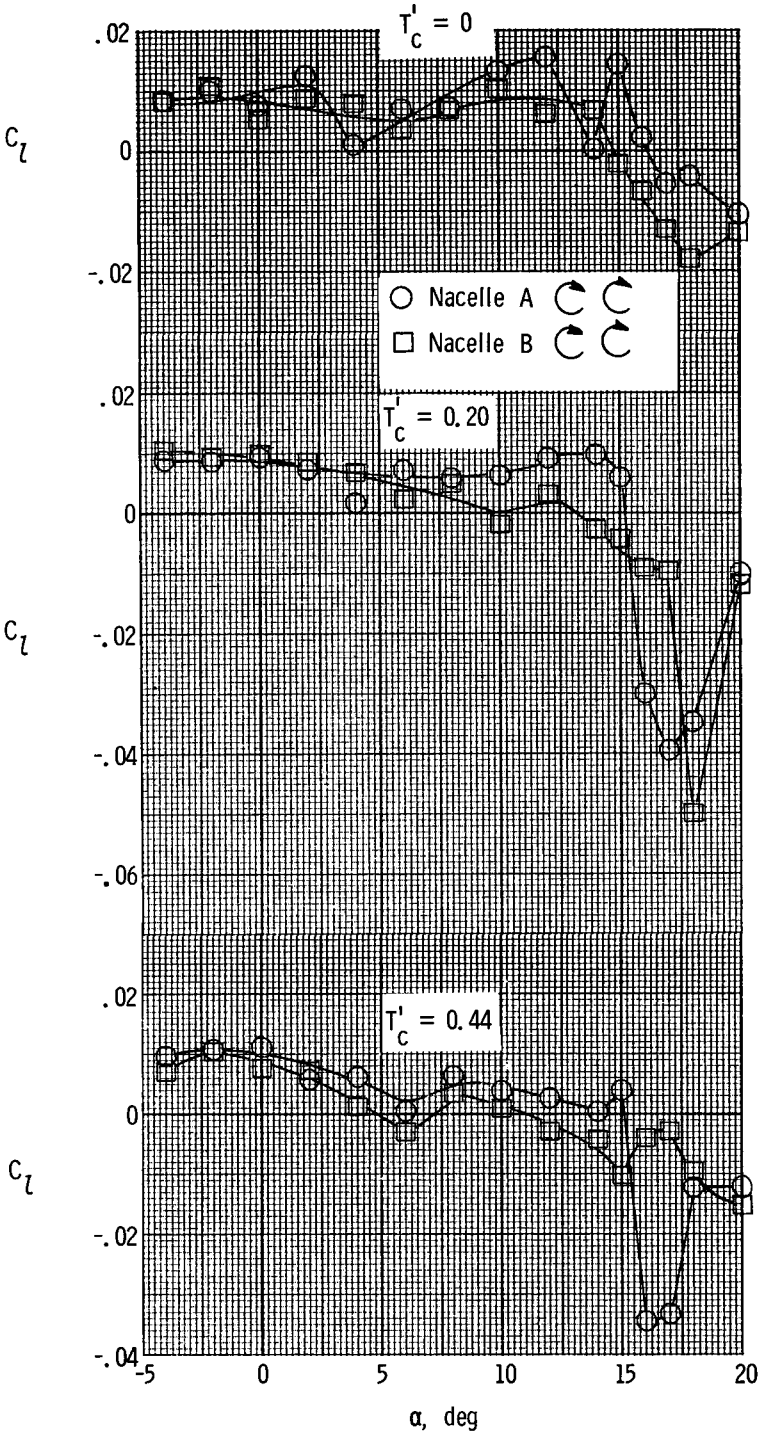

(b) $\delta_f = 27^o$.

Figure 85.- Concluded.

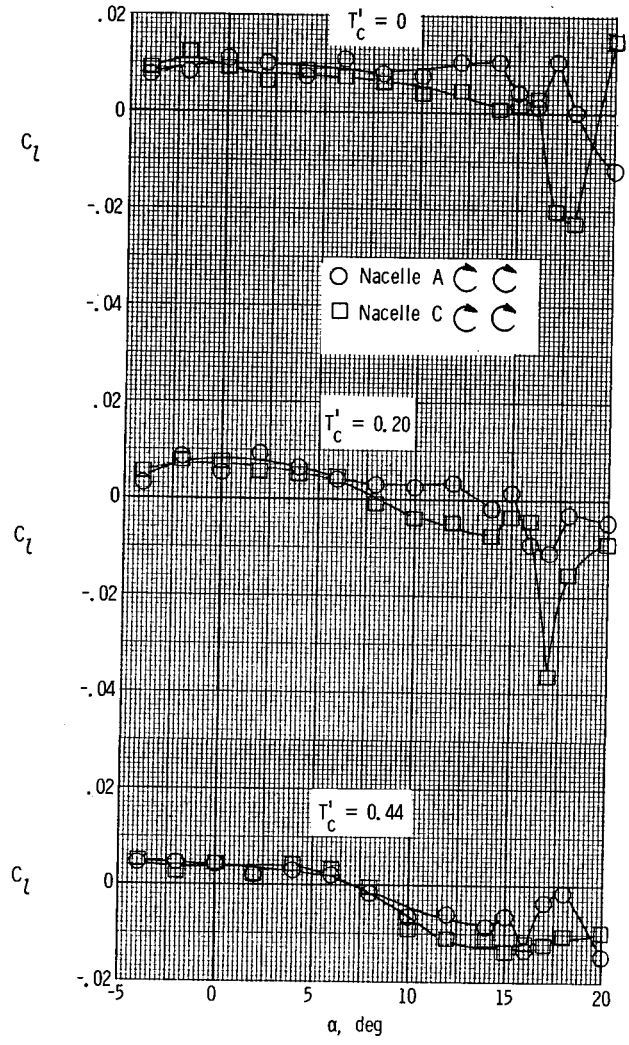

(a) $\delta_f = 0^o$.

Figure 86.- Comparison of rolling-moment coefficients of nacelle C with the basic nacelle configuration. $\beta = 0^o$.

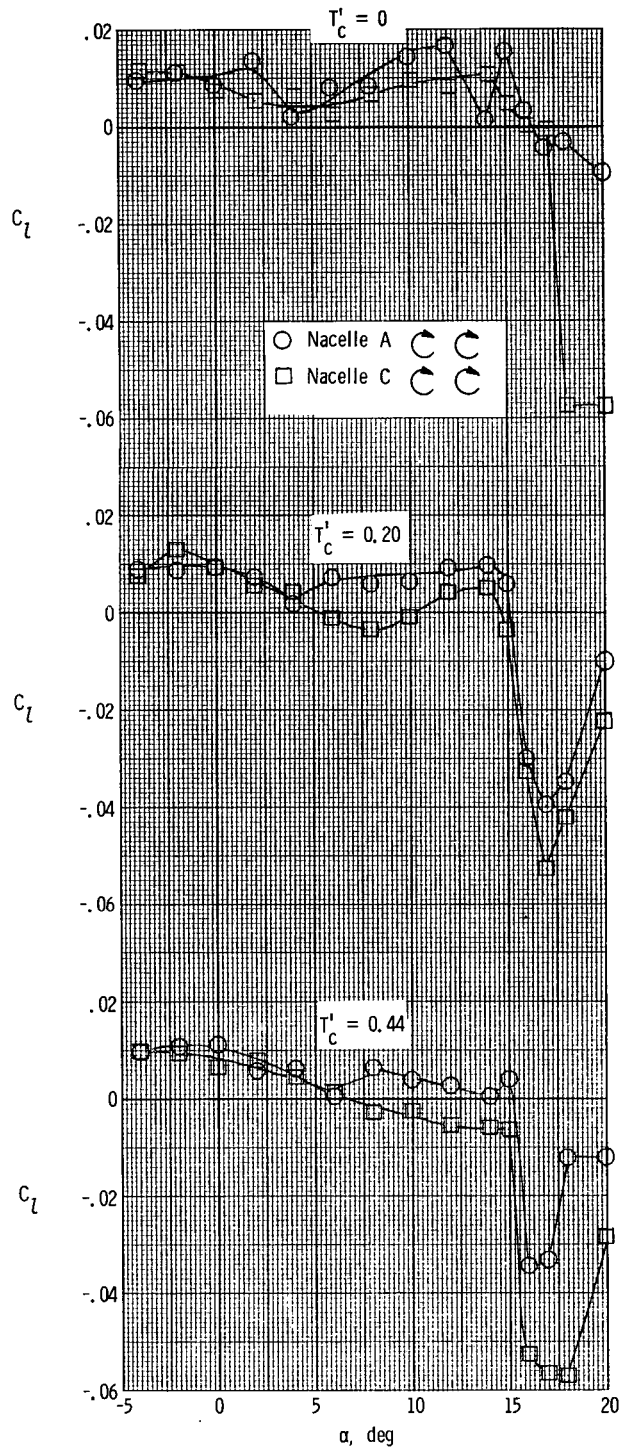

(b) $\delta_f = 27^o$.

Figure 86.- Concluded.

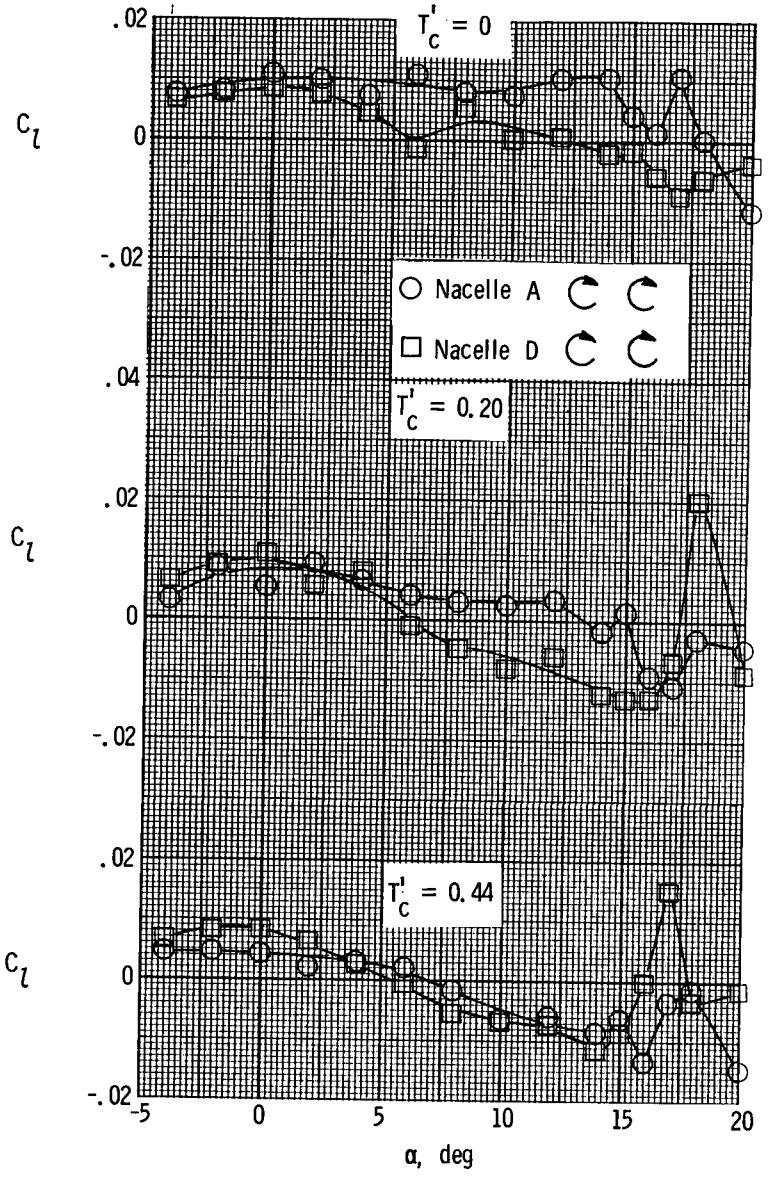

(a) $\delta_f = 0^o$.

Figure 87.- Comparison of rolling-moment coefficients of nacelle D with the basic nacelle configuration. $\beta = 0^o$.

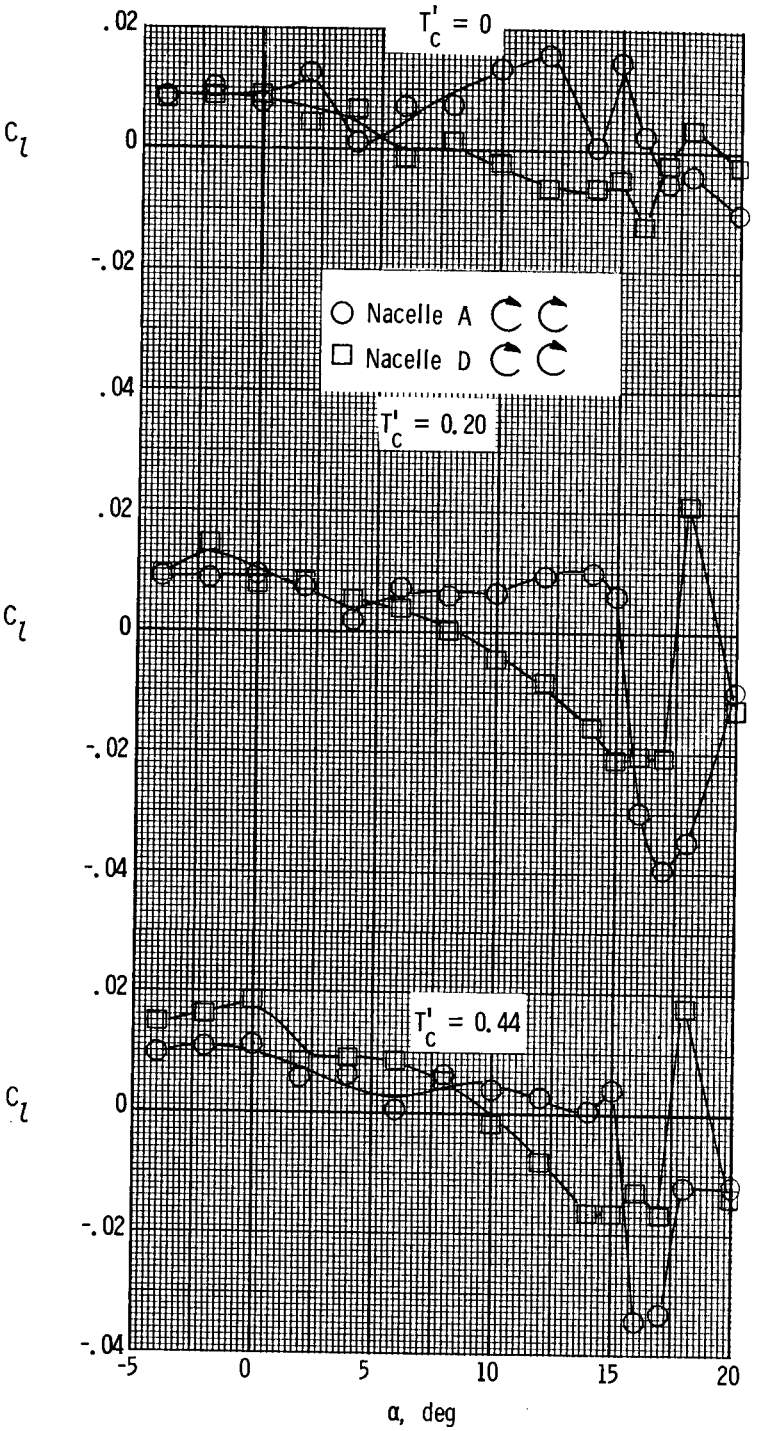

(b) $\delta_f = 27^o$.

Figure 87.- Concluded.

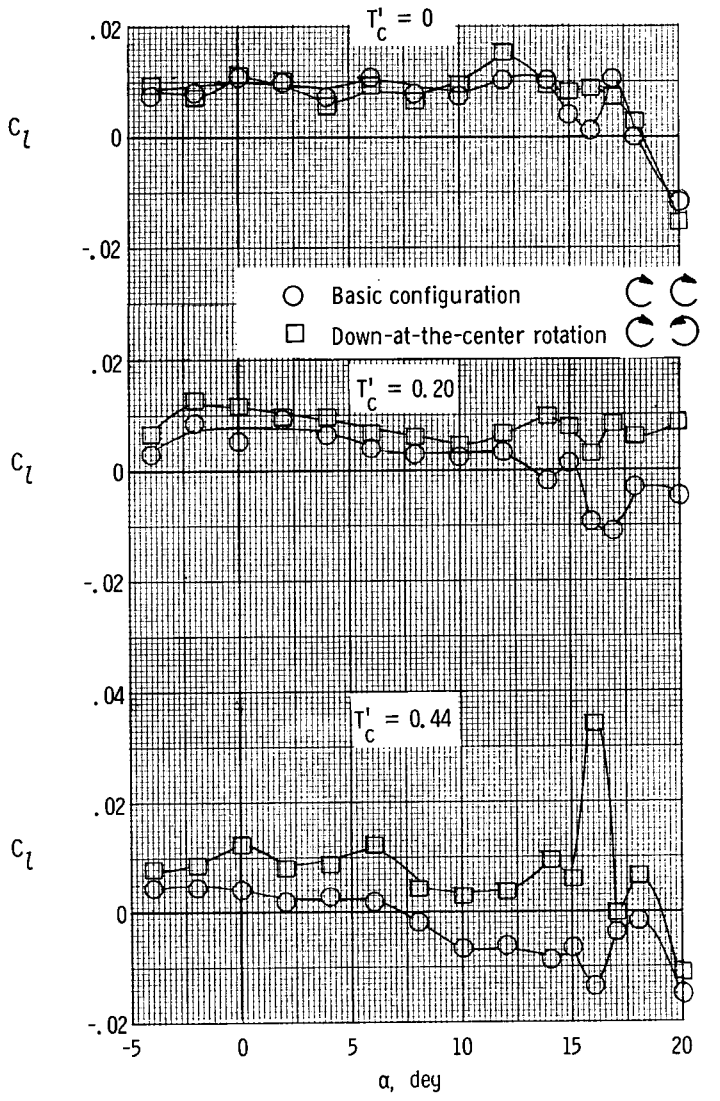

(a) $\delta_f = 0^o$.

Figure 88.- Comparison of rolling-moment coefficients of down-at-the-center propeller rotation with the basic configuration. $\beta = 0^o$; nacelle A.

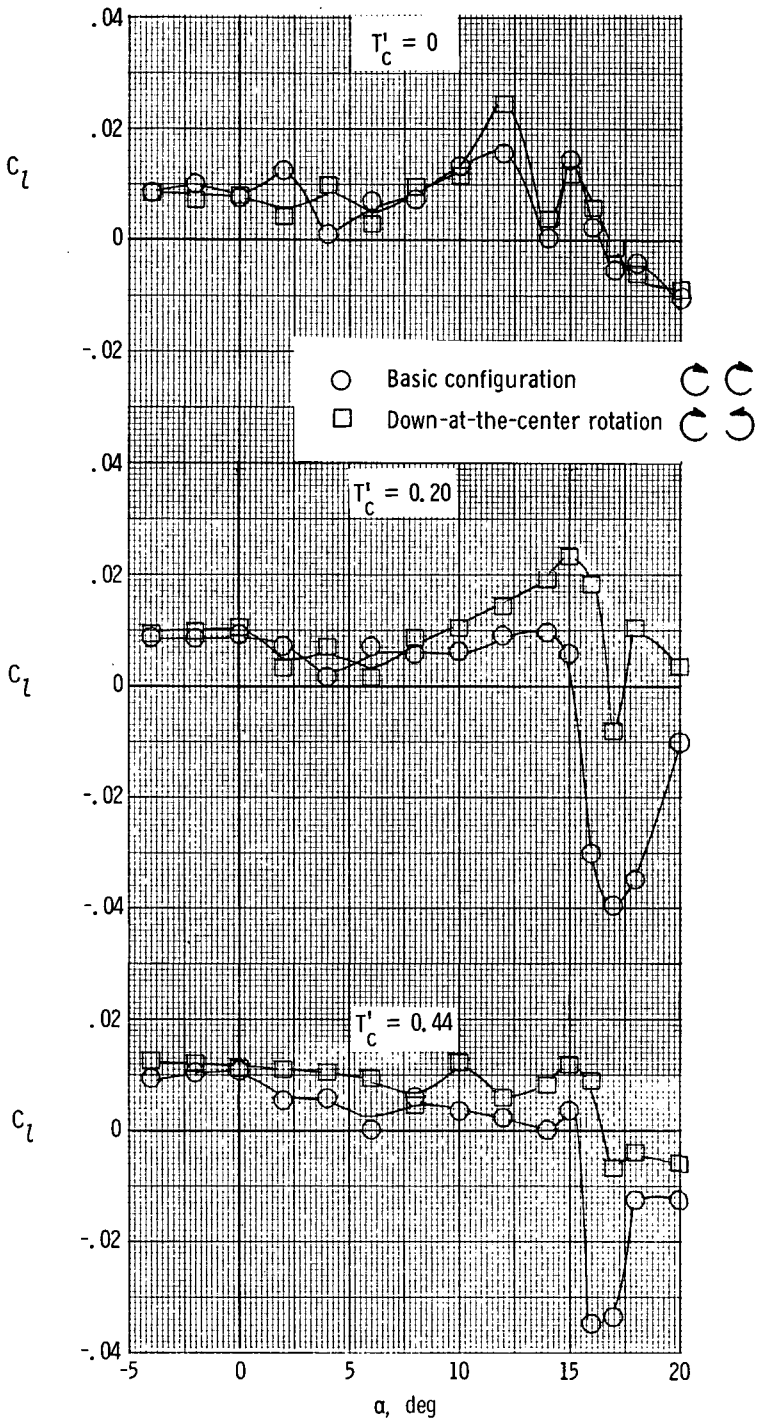

(b) $\delta_f = 27^o$.

Figure 88.- Concluded.

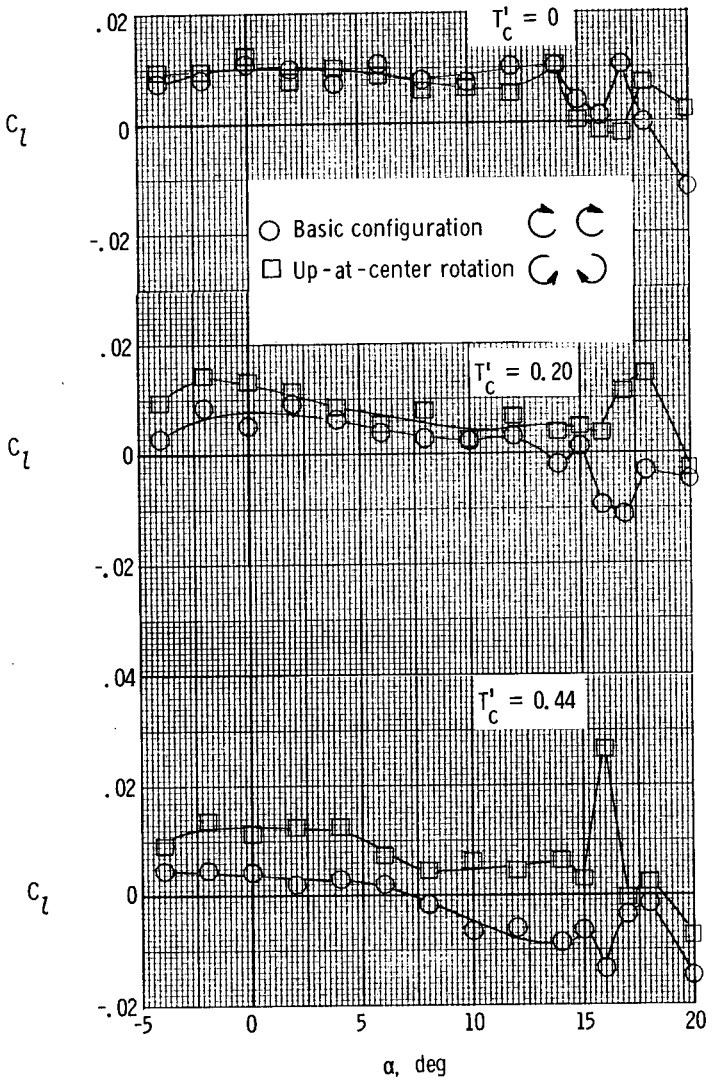

(a) $\delta_f = 0^o$.

Figure 89.- Comparison of rolling-moment coefficients of up-at-the-center propeller rotation with the basic configuration. $\beta = 0^o$; nacelle A.

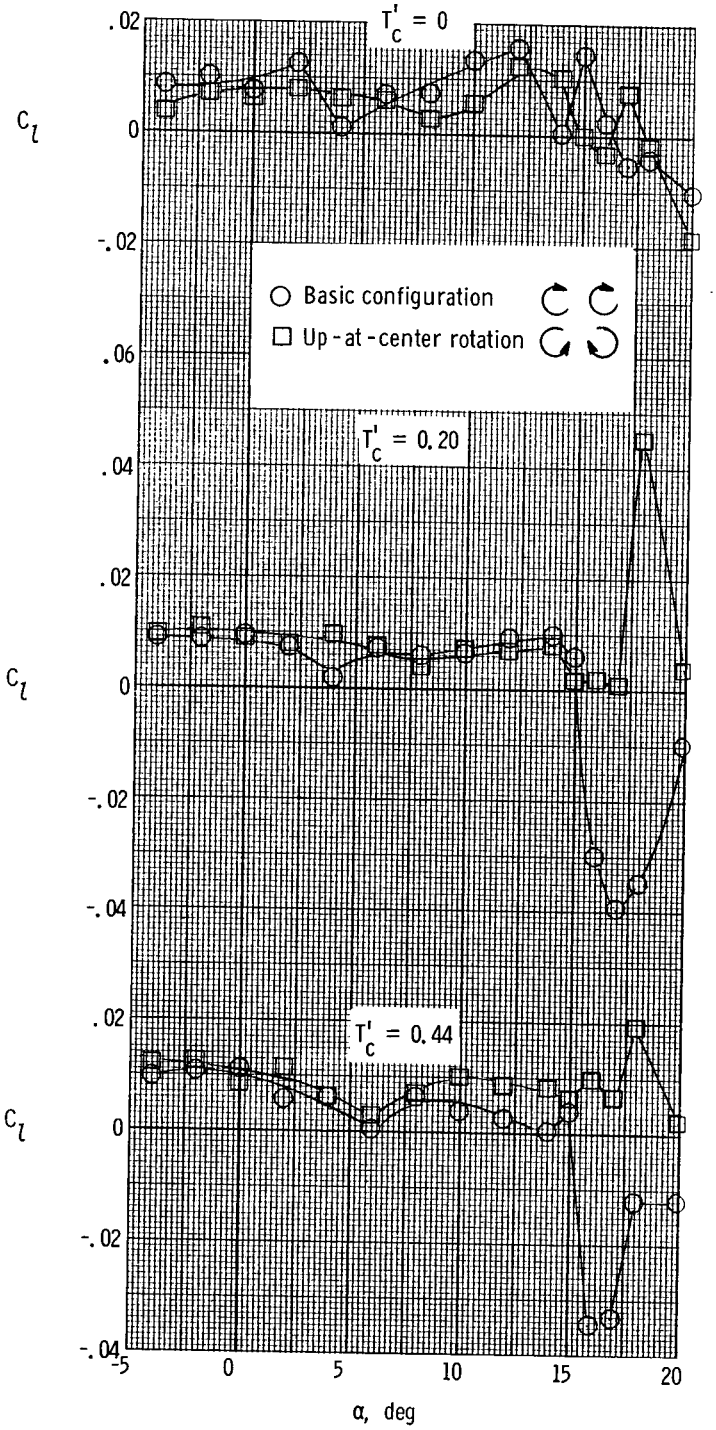

(b) $\delta_f = 27^o$.

Figure 89.- Concluded.

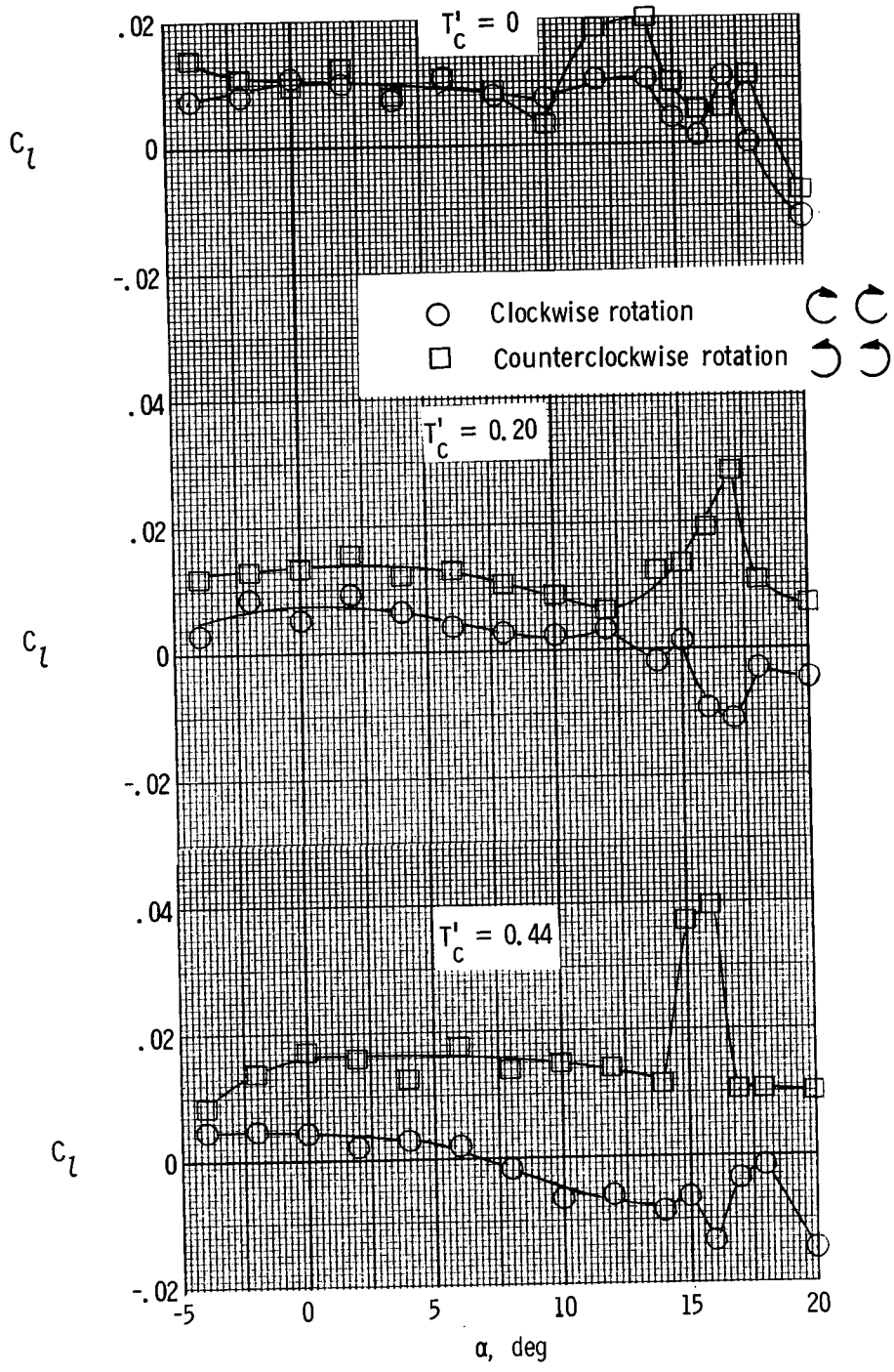

(a) $\delta_f = 0^o$.

Figure 90.- Comparison of rolling-moment coefficients of counterclockwise propeller rotation with clockwise rotation. $\beta = 0^o$; nacelle A.

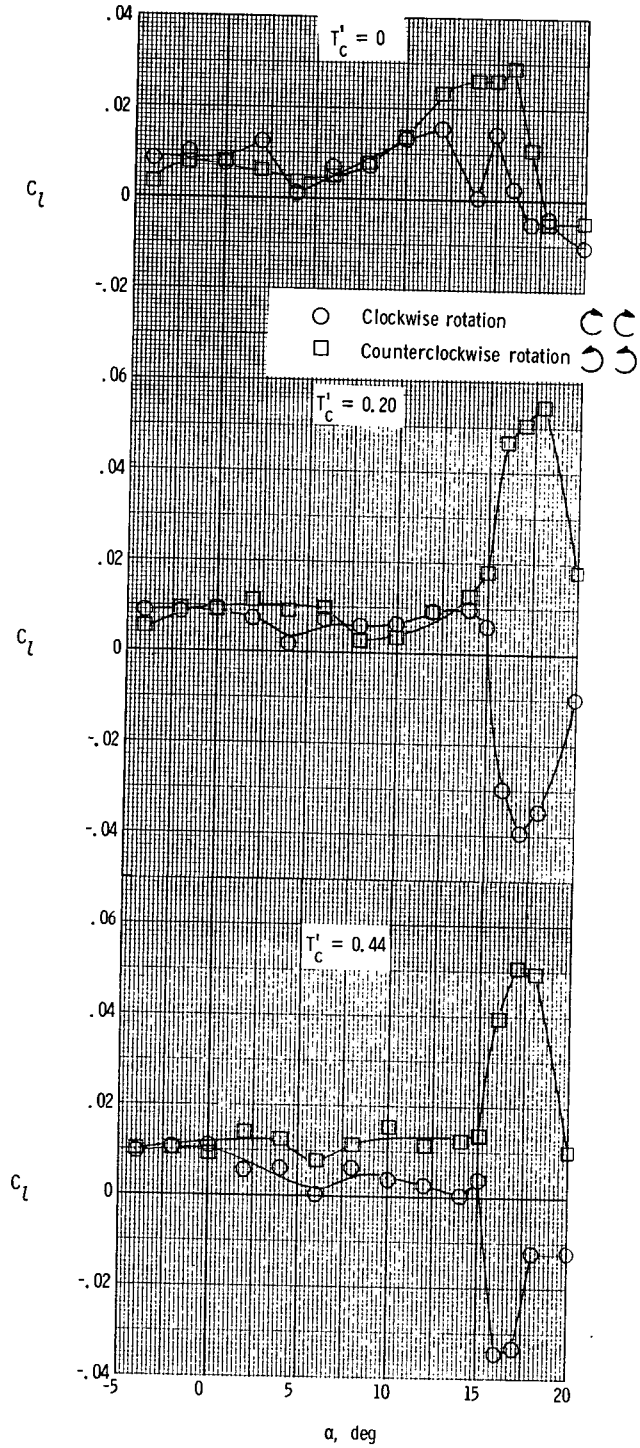

(b) $\delta_f = 27^o$.

Figure 90.- Concluded.

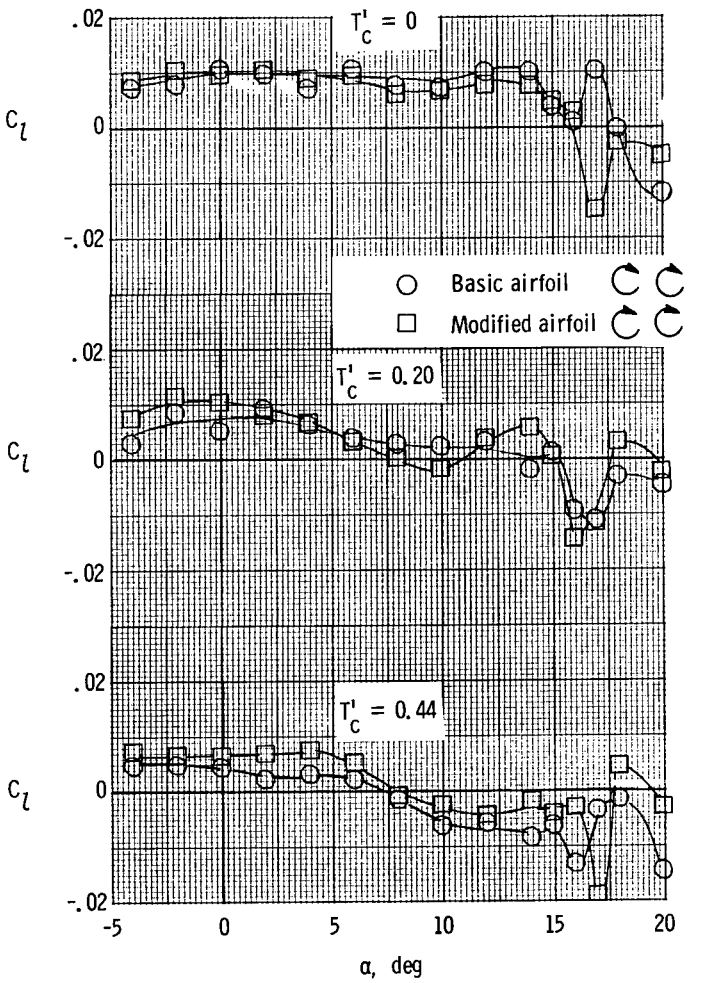

(a) $\delta_f = 0^o$.

Figure 91.- Comparison of rolling-moment coefficients of the modified airfoil-section configuration with the basic airfoil-section configuration. $\beta = 0^o$; nacelle A.

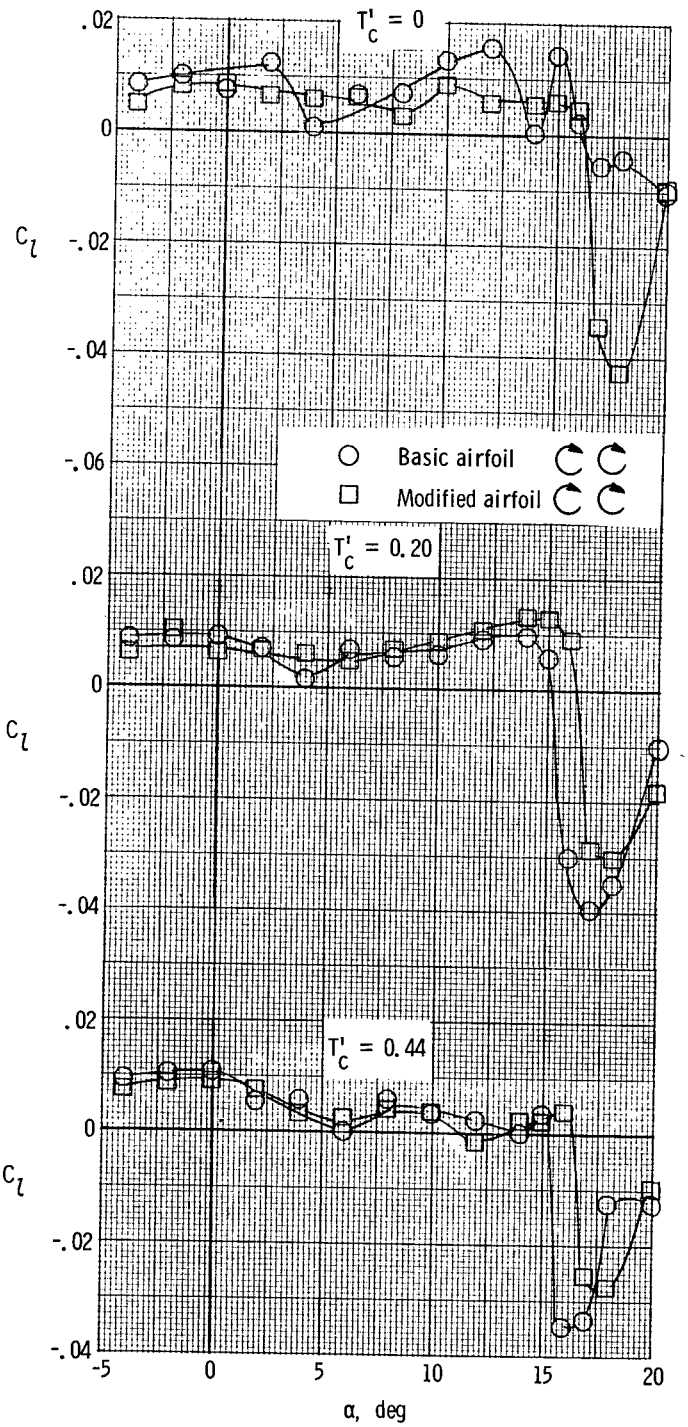

(b) $\delta_f = 27^o$.

Figure 91.- Concluded.

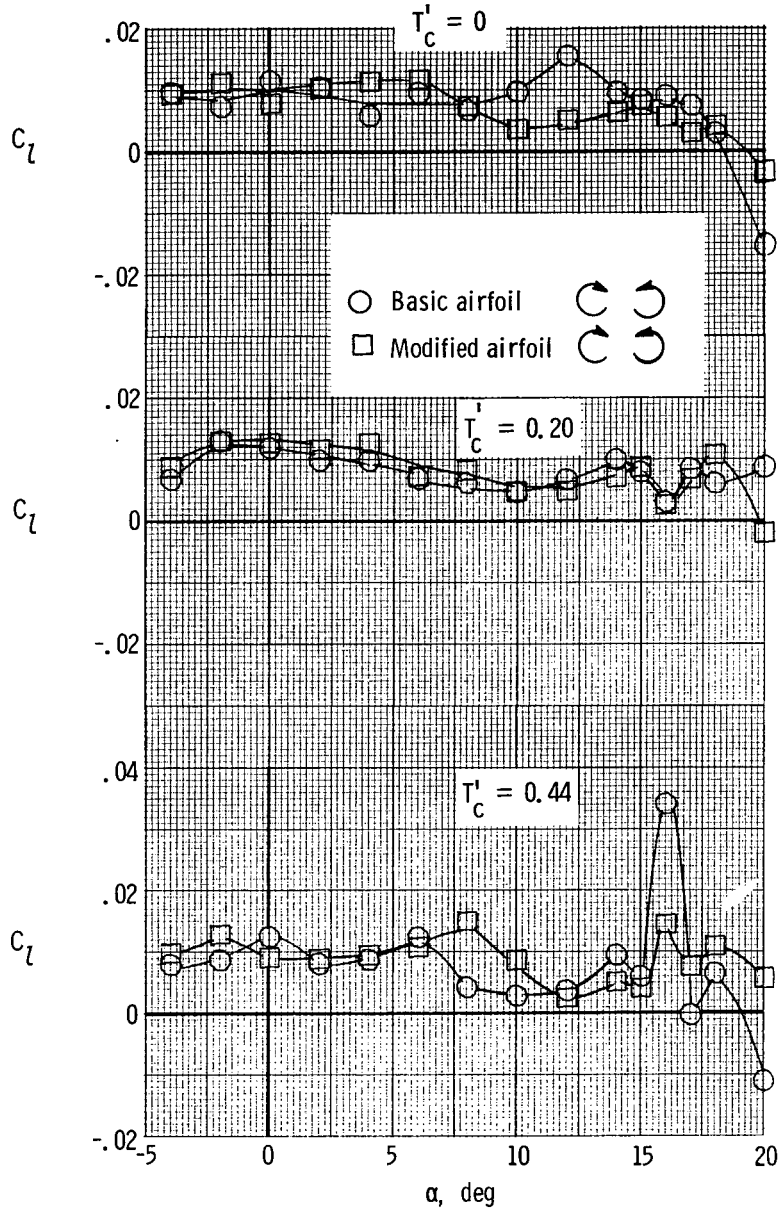

(a) $\delta_f = 0^o$.

Figure 92.- Comparison of rolling-moment coefficients of the modified and the basic airfoil sections both with down-at-the-center propeller rotation. $\beta = 0^o$; nacelle A.

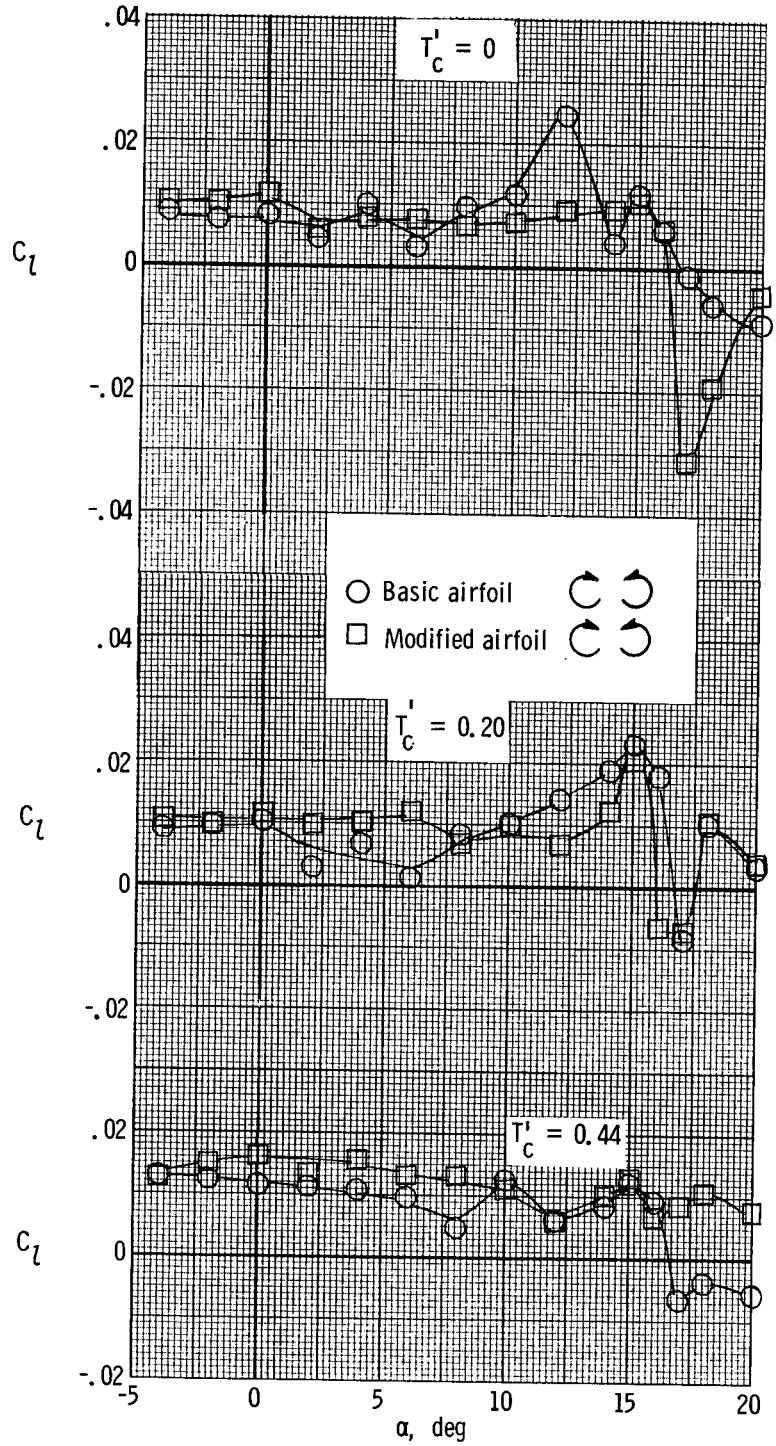

(b) $\delta_f = 27^o$.

Figure 92.- Concluded.

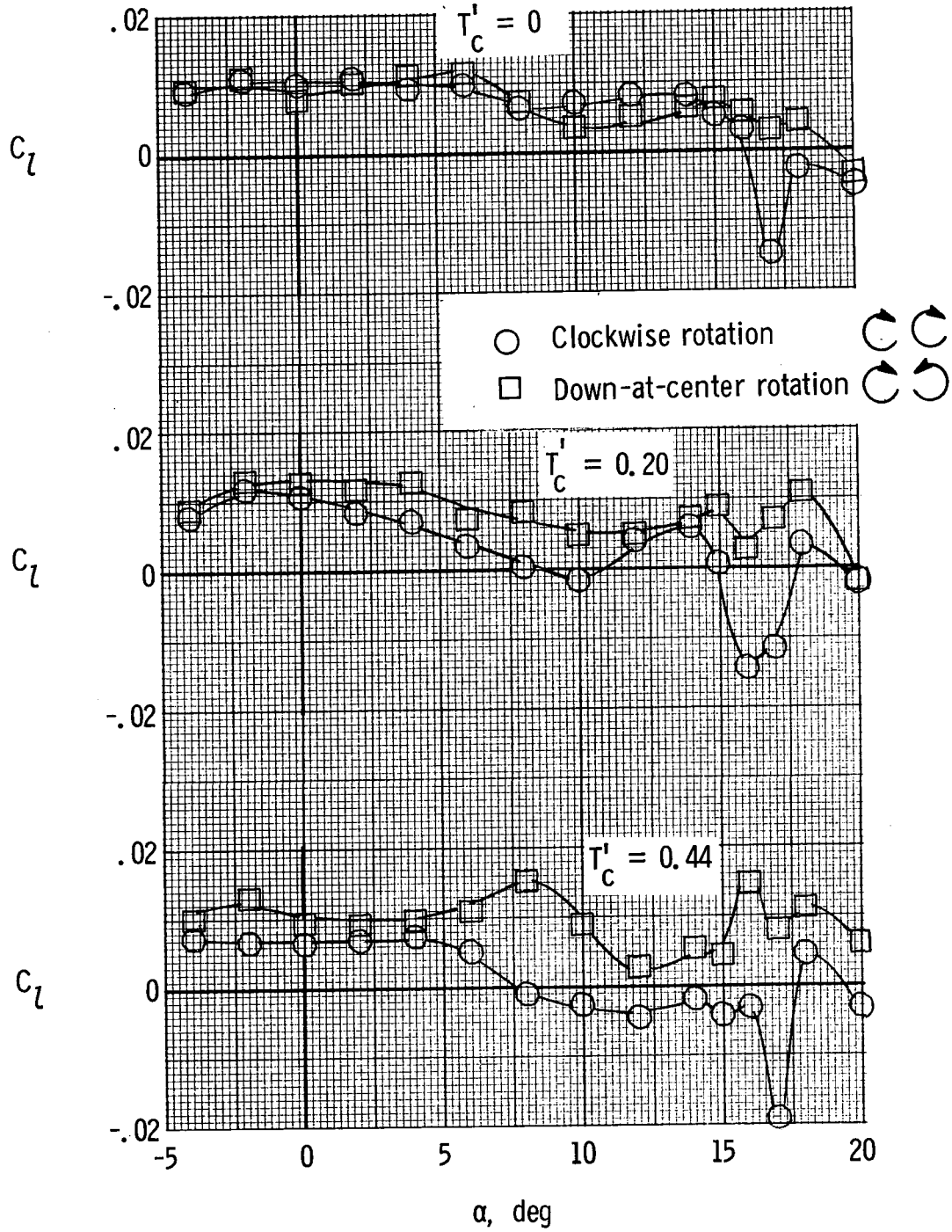

(a) $\delta_f = 0^o$.

Figure 93.- Comparison of rolling-moment coefficients of down-at-the-center propeller rotation with clockwise rotation for the modified airfoil-section configuration. $\beta = 0^o$; nacelle A.

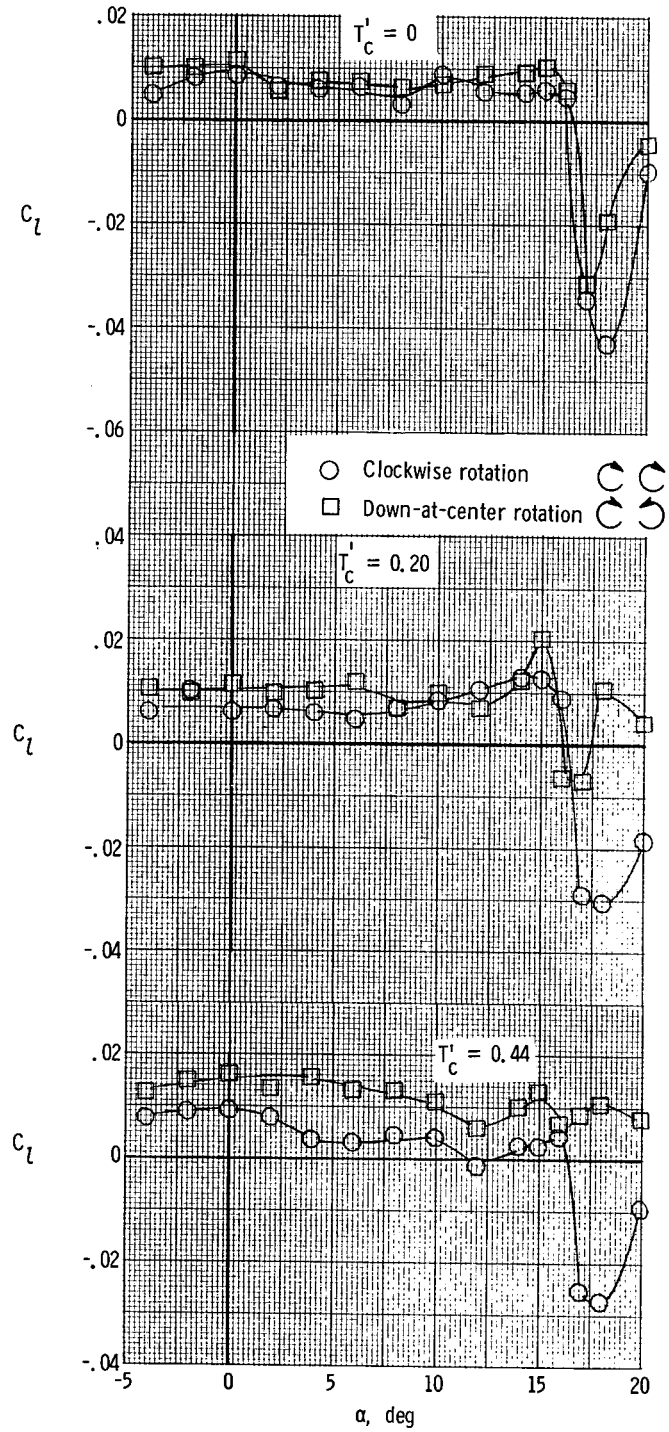

(b) $\delta_f = 27^o$.

Figure 93.- Concluded.

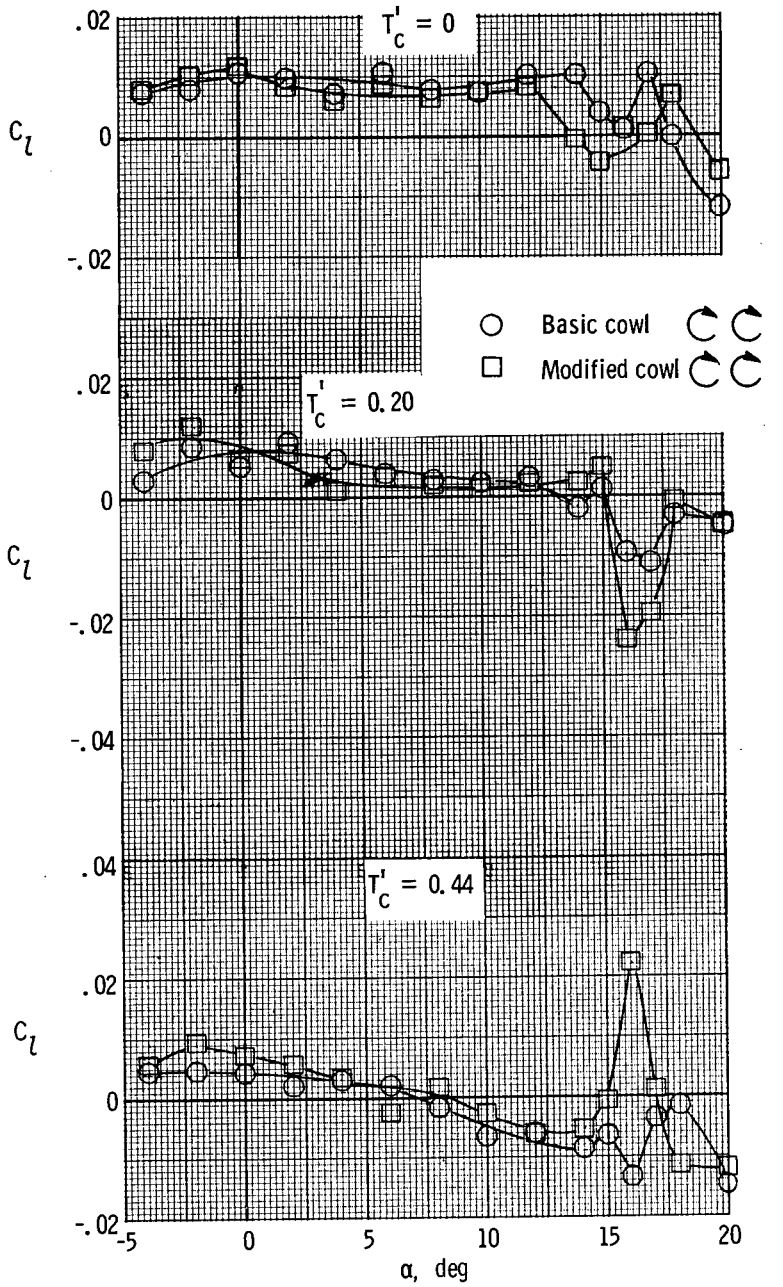

Figure 94.- Comparison of rolling-moment coefficients of the modified cowl with the basic cowl configuration. $\beta = 0^o$; $\delta_f = 0^o$.

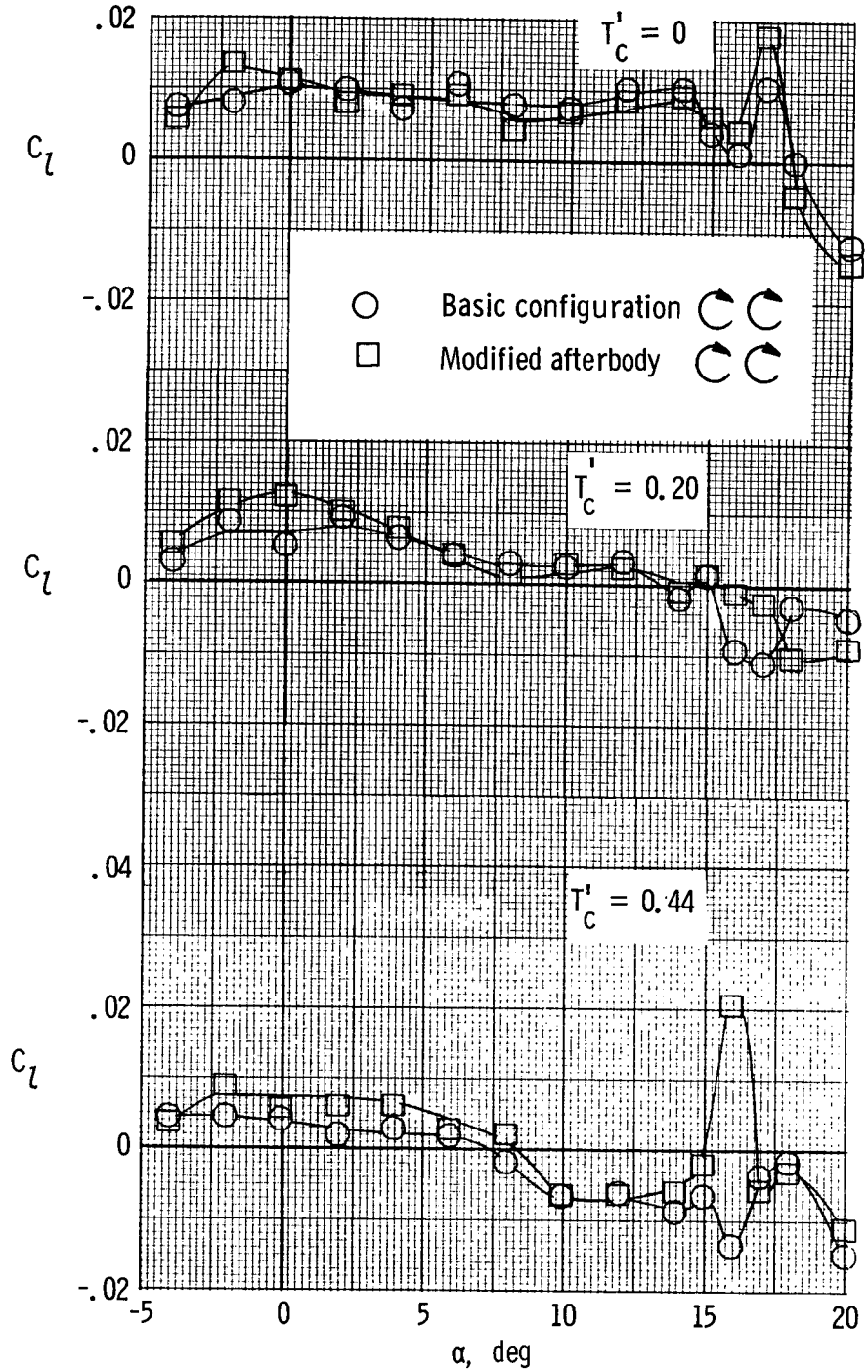

Figure 95.- Comparison of rolling-moment coefficients of the modified afterbody with the basic afterbody configuration. $\beta = 0^o$; $\delta_f = 0^o$.

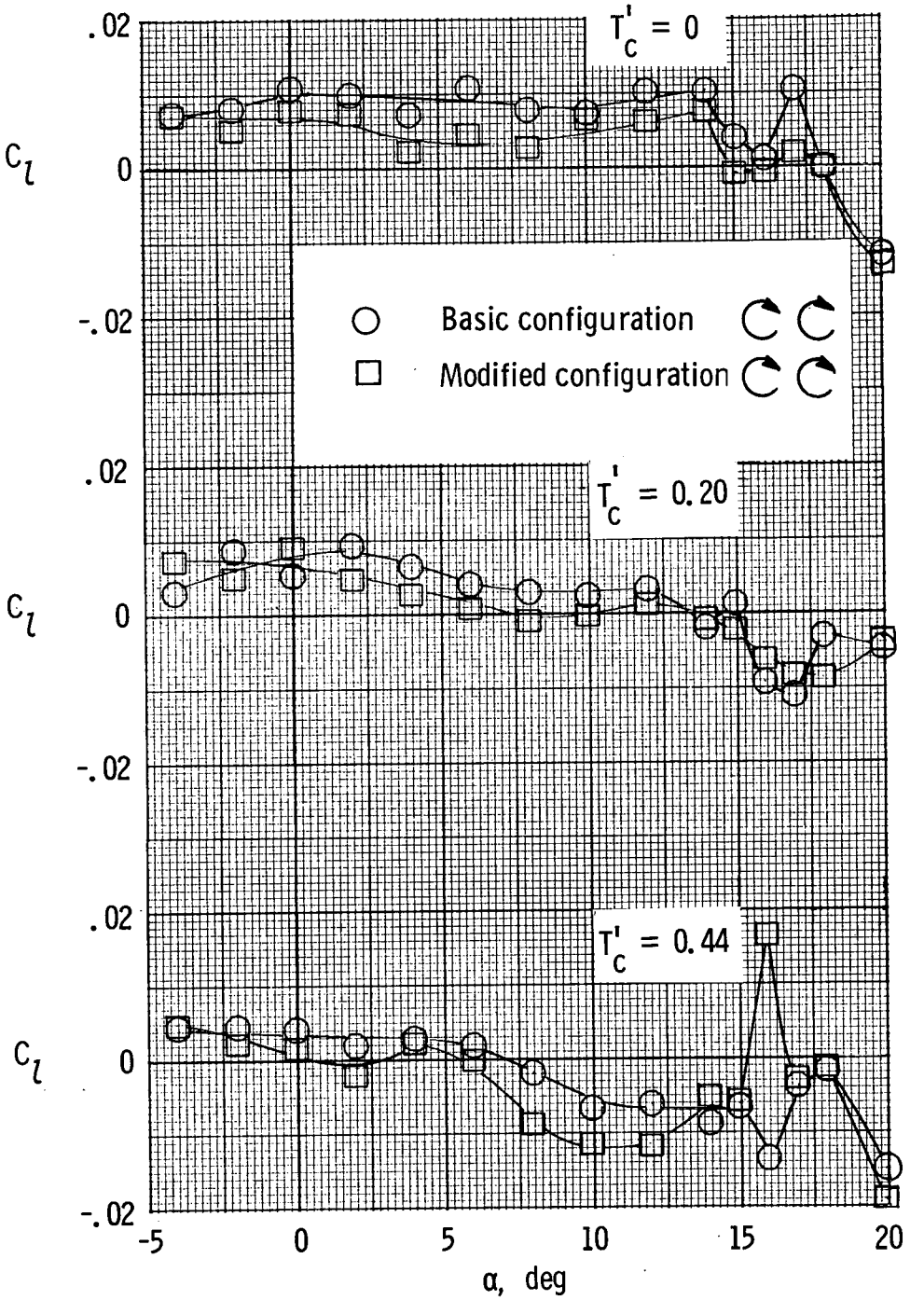

Figure 96.- Comparison of rolling-moment coefficients of the modified afterbody and modified cowl with the basic afterbody and cowl configuration. $\beta = 0^o$; $\delta_f = 0^o$.

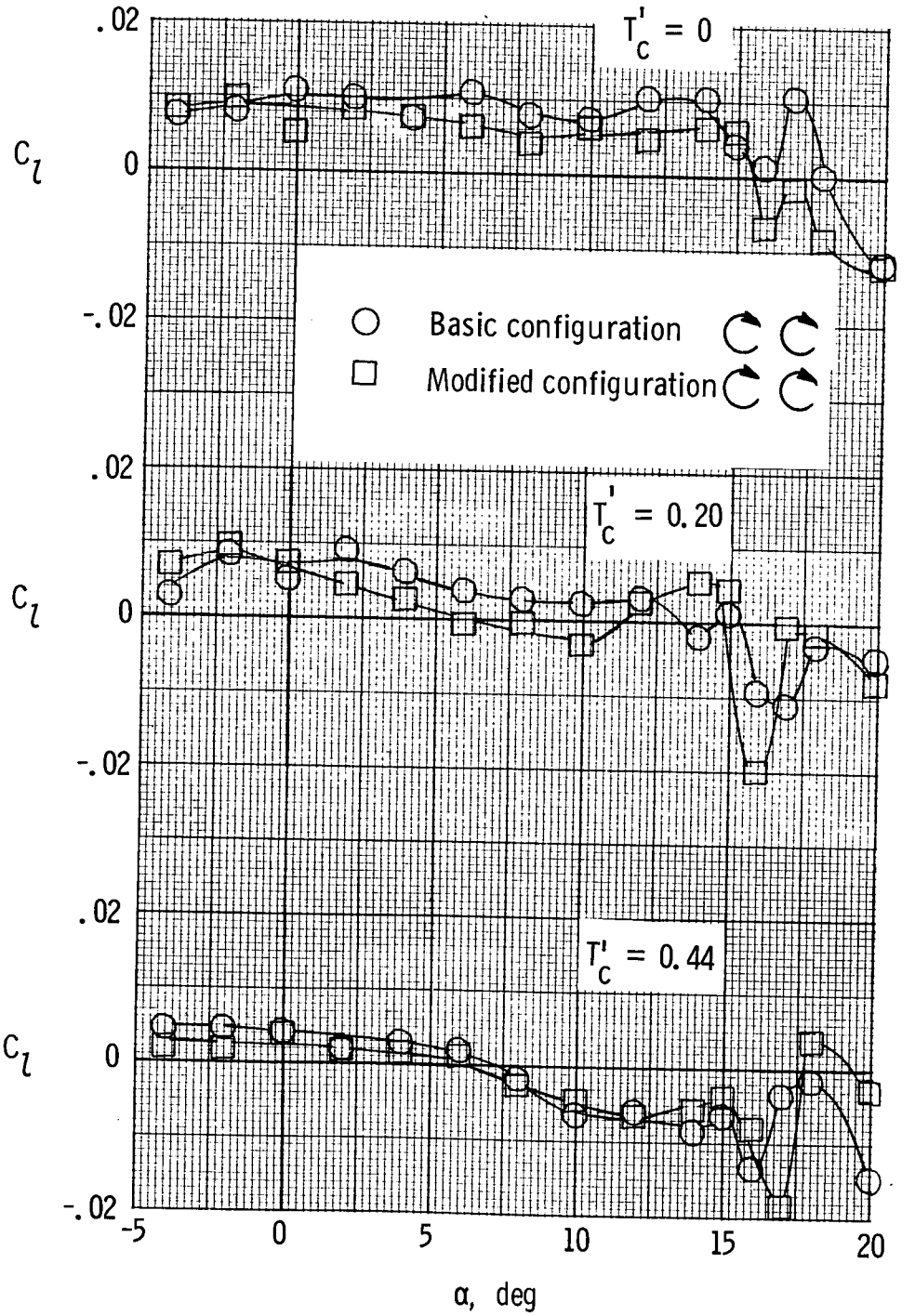

Figure 97.- Comparison of rolling-moment coefficients of the modified airfoil section and cowl configuration with the basic configuration. $\beta = 0^o$; $\delta_f = 0^o$.

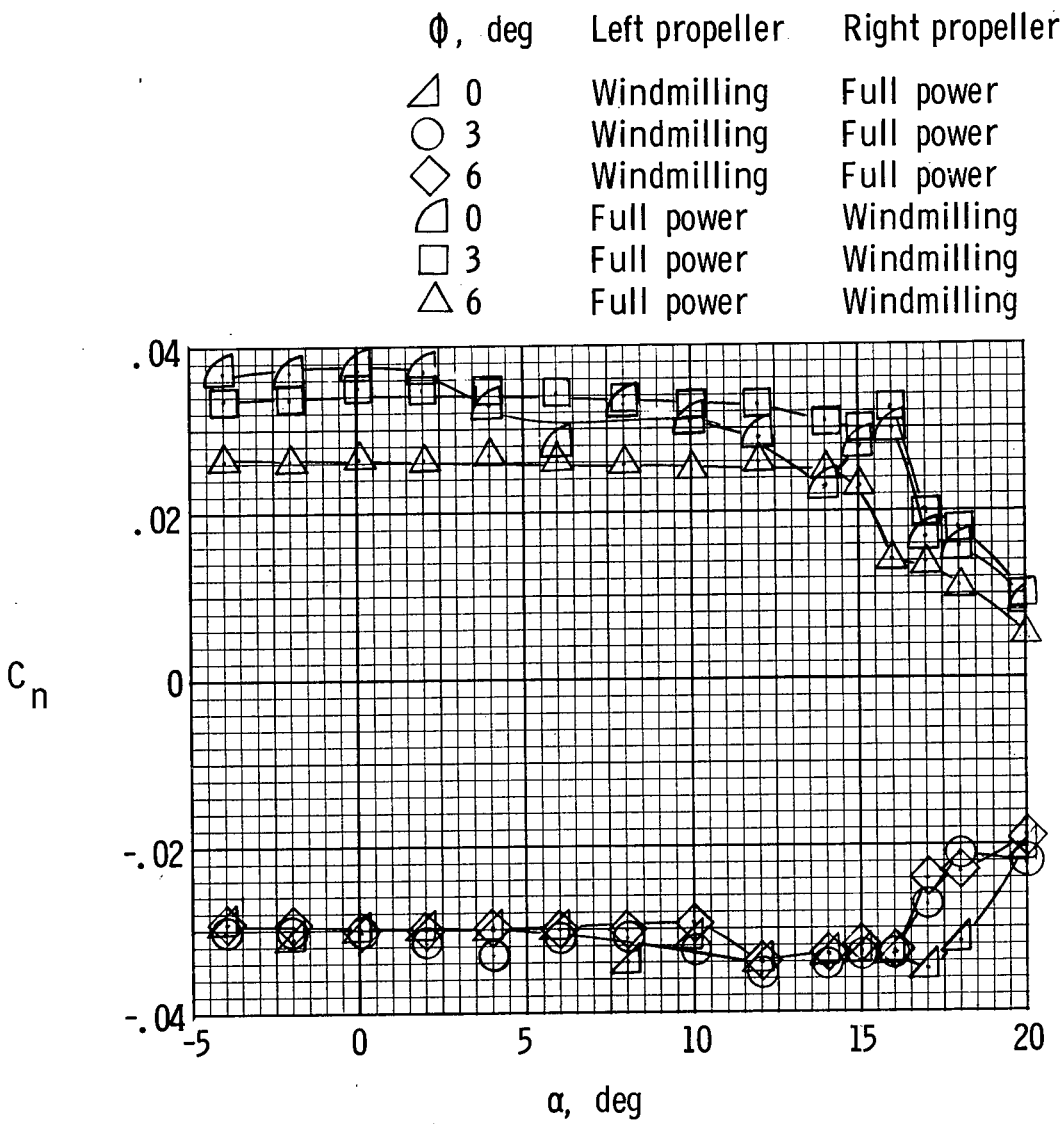

Figure 98.- Effect of toed-out thrust axes on yawing-moment coefficient with asymmetric power. $\beta = 0^{\circ}$; $\delta_f = 0^{\circ}$.